

Chapter 5

Control Systems and Valves

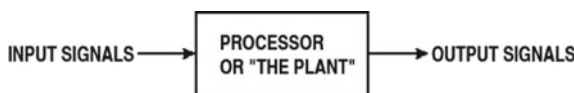


5.1 Fundamental Concepts on Control Systems

The engine of a rocket vehicle is a particular case of a dynamical system. By system we mean a collection of parts or elements or components which work together to attain an object. By dynamical system we mean a system whose behaviour changes with time in response to an external stimulus or force. In case of an engine of a rocket vehicle, the object of the system is the generation of a thrust vector having the desired magnitude and direction.

A dynamical system has inputs (or signals coming in), outputs (or signals going out), and an internal processor which transforms inputs into outputs. The part of a dynamical system which transforms inputs into outputs, that is, the processor of signals, is also known as the plant. The plant is the part of a dynamical system which fulfils the function of receiving, handling, and emitting signals.

A dynamical system is usually represented graphically by means of a block diagram, in which lines indicate input or output signals, and boxes indicate the plant or other components of the system, as shown in the following figure.

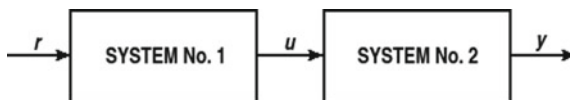


In case of a rocket vehicle, the success or the failure of the mission of the vehicle depends on the outputs of the various components or subsystems of which the system is made. Therefore, a rocket vehicle belongs to a particular class of dynamical systems, which are called controlled systems.

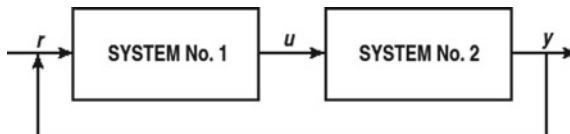
Controlled systems exist in several fields of engineering. Controlling a dynamical system means regulating, or commanding, or governing that system in order to reach

a desired goal. A control system is an arrangement of components connected one to another for the purpose of regulating the system itself or another system to be controlled by the first.

A control system which cannot adjust itself or another system to input signals received is called an open-loop system. An open-loop system is shown in the following figure, re-drawn from [1], which illustrates two systems which are connected between them, because the output signals u of the first (controller) are also the input signals of the second, which is the controlled system. Therefore, the first system controls the second system, but is not controlled by it. There is no mutual control of one system over the other. In other words, a system whose output signal y has no effect upon the input to the control process is called an open-loop control system.



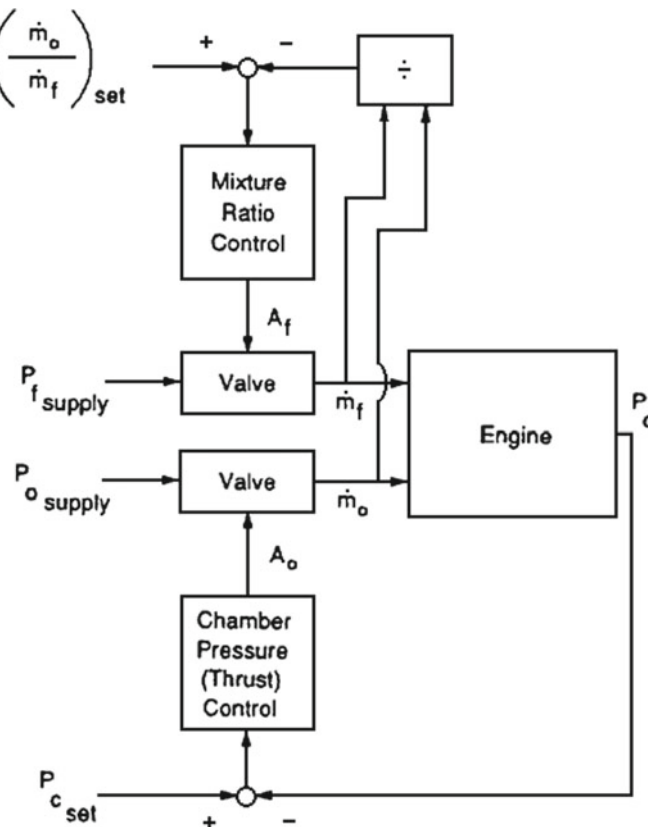
A control system which can adjust itself or another system to input signals is called a closed-loop or feedback system. A closed-loop system is shown in the following figure, re-drawn from [1], which illustrates two systems which have mutual control one over the other.



In other words, a closed-loop control system is a control system in which some function of the output y of some part of the system is fed back as a secondary input which adds to the primary input r to the system, so as to affect the response of the system itself. As an example of a control system for a rocket vehicle, Lorenzo and Musgrave [2] describe a pressure-fed bi-propellant engine, in which the propellants are kept under pressure in their respective tanks and then supplied to the main combustion chamber through appropriate feed lines, control valves, and injector elements, as has been shown in Chap. 3. The propellants are to be delivered to the main combustion chamber in a determined mixture ratio

$$\frac{o}{f} = \frac{\dot{m}_o}{\dot{m}_f}$$

where \dot{m}_o and \dot{m}_f are the mass flow rates of respectively the oxidiser and the fuel, and at a total mass flow rate $\dot{m}_t = \dot{m}_o + \dot{m}_f$ related to the desired thrust. The control system of this rocket engine regulates the thrust by controlling the pressure p_c of the gas in the combustion chamber and the mixture ratio o/f of the two propellants, as shown in the following figure, adapted from [2].



The preceding scheme has two control loops. One of them controls the mixture ratio *of* of the propellants, and the other controls the pressure p_c of the gas in the combustion chamber. The first loop operates usually, but not necessarily, on the propellant supplied at higher mass flow rate than the other. This loop is tuned to be the fast loop. This reduces excursions in the mixture ratio away from the set point, which in turn keeps the temperatures of the gas and of the metal at the design conditions. The second loop, which controls the pressure of the gas in the combustion chamber, is the slow loop, and its bandwidth is set by thrust response requirements. The type of control shown above requires three measurements (p_c , \dot{m}_o and \dot{m}_f) and two control inputs for the valve areas A_o and A_f [2].

An open-loop control system for a rocket engine is calibrated to a fixed set of conditions, and uses orifices and on-off command devices to correct deviations of some parameters from their design values. For example, orifices of proper size are inserted into the flow lines to command pressure drops, and the mass flow rates of the propellants are controlled by opening or closing valves. An open-loop control system is simple, but is also limited to a specific set of parameters, and cannot compensate for variable conditions. The sequence times in an open-loop control system are often established by means of interlocks.

A closed-loop control system uses sensors, computers to detect errors (which are differences between a given reference signal r and the output y of the system), and actuation commands u generated by the computers to correct the errors. Therefore, a closed-loop control system does not require calibration for a specific set of conditions. It requires sensors and computers to detect errors and take appropriate steps to correct them. A closed-loop control system is often used in a rocket engine to control the mixture ratio o/f of the propellants, and the thrust vector \mathbf{F} in magnitude and direction.

A closed-loop control system in a rocket engine may operate in one of the modes indicated below.

- (1) On-off control, which can be described as follows:

$$u = \begin{cases} u_{\max} & \text{if } e > 0 \\ u_{\min} & \text{if } e < 0 \end{cases}$$

where the control error $e = r - y$ is the difference between the reference signal r and the output y of the system, and u is the actuation command. The preceding equation does not define a value of the actuation command u when the control error e is equal to zero. In practice, u is taken equal to zero ($u = 0$) when the control error e is in a narrow band centred around $e = 0$. The on-off control is used for a rocket engine, for example, when a pressure switch opens or closes a valve which regulates the pressure in a tank.

- (2) Proportional-integral-derivative (PID) control, which can be described as follows:

$$u = \begin{cases} u_{\max} & \text{if } e \geq e_{\max} \\ k_p e & \text{if } e_{\min} < e < e_{\max} \\ u_{\min} & \text{if } e \leq e_{\min} \end{cases}$$

where k_p is the controller gain, $e_{\min} = u_{\min}/k_p$, and $e_{\max} = u_{\max}/k_p$.

The interval (e_{\min}, e_{\max}) is called the proportional band, because the behaviour of the controller is linear when the error $e = r - y$ is in this interval, as follows

$$u = k_p(r - y) = k_p e \quad \text{if } e_{\min} < e < e_{\max}$$

In a proportional control, the process variable often deviates from a reference value. When some level of the control signal u is required for the system to maintain a desired value, then the control error e must be other than zero to generate the required value. For this purpose, the control signal u is made proportional to the integral of the error over a given time interval, as follows

$$u(t) = k_i \int_0^t e(\tau) d\tau$$

where k_i is the integral gain. This type of control is called integral control. A controller with integral control has zero steady-state error [1].

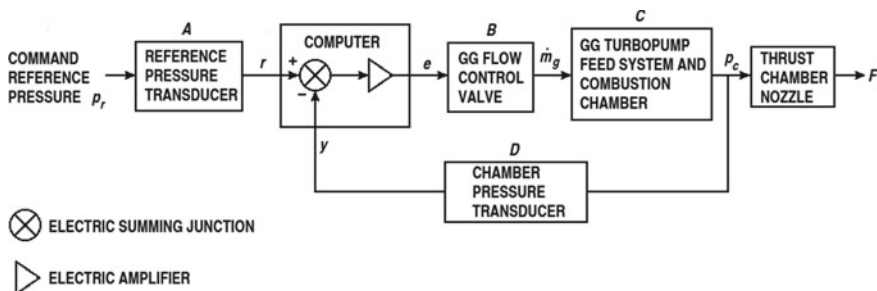
Unfortunately, there may not always be a steady state, because the system may be subject to oscillations. In this case, a controller can be made able to predict the error e some time T_d ahead of the present time t , by using the following linear extrapolation

$$e(t + T_d) \approx e(t) + T_d \frac{de}{dt}$$

By combining proportional, integral, and derivative control, it is possible to obtain a PID controller based on the following equation

$$u(t) = k_p e(t) + k_i \int_0^t e(\tau) d\tau + k_d \frac{de}{dt}$$

By so doing, the control signal $u(t)$ results from the sum of three terms: the term relating to the present time is proportional, through the coefficient k_p , to the error at the present time; the term relating to the past time is proportional, through the coefficient k_i , to the error cumulated over an interval before the present time; and the term relating to the future time is proportional, through the coefficient k_d , to the error resulting from a linear extrapolation of the error at some time ahead of the present time [1]. The proportional-integral-derivative control is used for a rocket engine in several cases, for example, to control the pressure in the combustion chamber (proportional term), or the mixture ratio of the propellants (integral term), or the direction of the thrust vector with phase lead (derivative term). An example of a closed-loop control system for a rocket engine has been given by Huzel and Huang [3] by means of the following scheme, re-drawn from [3].



This control system illustrated above has the purpose of maintaining the value p_c of the pressure in the combustion chamber equal to a desired value p_r of reference, by using a valve which controls the value \dot{m}_g of the mass flow rate in the gas generator (GG). The magnitude F of the thrust vector is controlled indirectly, by regulating the pressure p_c in the combustion chamber.

This control system consists of a sensor (chamber pressure transducer), a computer containing an electric summing junction and an electric amplifier, and a controller (gas generator flow control valve) which regulates the value of the mass flow rate \dot{m}_g in the gas generator. The computer compares the reference input signal r with the input signal y coming from the sensor (chamber pressure transducer). The signal r is related to the reference pressure p_r , and the signal y is related to the actual pressure p_c in the combustion chamber through differential equations, which describe the behaviour of the components of the system.

The letters A , B , C , and D in the preceding figure indicate the relations existing between the input and the output of the respective components. The equations which govern this control systems can be written symbolically as follows

$$r = Ap_r$$

$$e = r - y$$

$$\dot{m}_g = Be$$

$$p_c = C\dot{m}_g$$

$$y = Dp_c$$

The behaviour of this control system results from the solution of the preceding equations. These equations are usually solved by using the method of the Laplace transformation (see, for example, [4]). The values to be given to the gains and to the response lags of a control system are to be chosen carefully, sometimes by trial and error, in order not to introduce overshoots or other causes of instability, which could give rise to large oscillations.

5.2 Control Systems for Rocket Engines

The control systems described in general terms in the preceding section are used in liquid-propellant rocket engines to perform some or all of the following tasks:

- engine start;
- engine shutdown;
- engine restart, in case of engines having restart capability;
- execution of a given plan of operation;
- change of the given plan of operation, or even engine shutdown, in the presence of a malfunction;
- propellant tank filling up;

- draining excess of propellants after filling;
- in case of cryogenic propellants, chilling pipes, pumps, cooling jackets, injectors, and valves by bleeding the cold propellants through them;
- check-out the proper operation of critical components before flight; and
- in case of recoverable and reusable engines, recycling and refurbishing the engines to put them in conditions of readiness for a new use.

In the specific case of liquid-propellant rocket engines, most of the actuators used for control functions are valves, regulators, pressure switches, and flow controls. Special computers for automatic control in large engines are also commonly used [5].

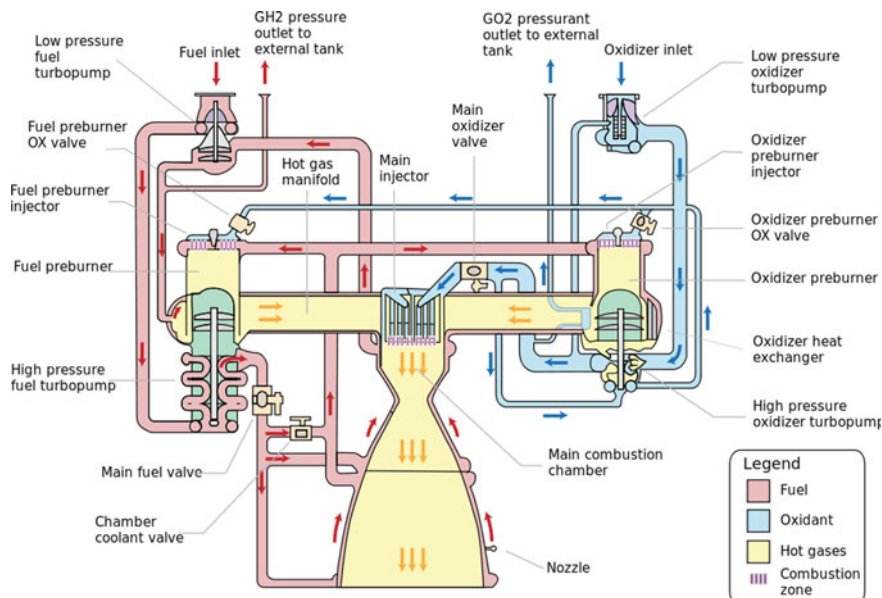
In addition, safety controls are used to protect personnel and equipment in case of malfunctions, and check-out controls make it possible to test the operation of critical components of a rocket engine without actually firing the engine.

The start sequence of a rocket engine has the purpose of controlling the engine from the moment in which the start signal is given to the full operation of the main stage. This sequence includes the steps of preparation (thrust chamber purging and chill-down of propellant transfer lines), application of start energy (start tanks and turbine spinner), and introduction followed by ignition of the propellants in the main combustion chamber. Secondary start sequences may be needed for some subsystems, as is the case with a gas generator or a pre-burner. A start sequence is regulated by means of interlocks, and by monitoring each step of the sequence. The opening sequence of the propellant valves may perform either an oxidiser-lead or a fuel-lead start, depending on the combination of propellants chosen, on the method used to ignite the propellants, and on the method used to cool the thrust chamber. The start delay time is the time necessary to purge the engine, open the valves, initiate the combustion, and increase the pressure in the combustion chamber to the rated value. This time is usually small (from 0.003 to 0.015 s in small thrusters) for an engine fed by gas under pressure, in which the pressurisation system has to be activated and the ullage volume has to be put under pressure before the start. An engine fed by turbo-pumps requires more time to start (from 1 to 5 s), because it is necessary not only to execute the operations indicated above for a pressure-fed engine, but also to start a gas generator or a pre-burner, and to increase the speed of the turbo-pumps to a level in which the combustion can be firstly self-sustained and then brought to its full extent. When the combination of propellants used in a rocket engine is not hypergolic, additional time is necessary for the igniter to work and for the control function to confirm the proper operation of the igniter. The ignition methods used for liquid-propellant rocket engines have been discussed in Chap. 2, Sects. 2.7 and 2.8.

The shutdown sequence is executed either in normal operating conditions or in cases of emergency. This is done by shutting off the flow to the gas generator (or to the pre-burner) and to the main combustion chamber. In case of test firings, the shutdown sequence also includes purges and flushes for post-firing safety. The control system regulates the valve closing sequence in such a way as to provide a fuel-rich cut-off in the main combustion chamber. This prevents high peaks of temperature and

results in a smooth and rapid termination of the thrust. The valves close in a fixed sequence. The valve controlling the gas generator or the pre-burner closes first. The pressurisation in the propellant tanks is stopped. The pumps slow down, as a result of the decrease in the gas flow through the turbine. The pressures and the mass flow rates of the propellants decrease quickly and reduce to zero.

In the three main engines (RS-25) of the Space Shuttle, the characteristics of start, run, and shutdown are established by the combined actions of the main fuel valve, the main oxidiser valve, the oxidiser pre-burner oxidiser valve, the fuel pre-burner oxidiser valve, and the chamber coolant valve. These valves are powered by hydraulic actuators which receive positioning signals from the engine controller, which in turn uses performance data gathered by sensors located throughout the engine. A functional scheme showing the propellant flow through the RS-25 engine and the valves named above is shown in the following figure, due to the courtesy of Wikimedia [6].



With reference to the preceding figure, the main oxidiser valve, the main fuel valve, and the chamber coolant valve are switched to run schedules during the engine run phase, while the oxidiser pre-burner oxidiser valve and the fuel pre-burner oxidiser valve are switched to closed-loop operations. The run schedule for the main oxidiser valve and for the main fuel valve cause them to simply remain fully open, whereas the run schedule for the chamber coolant valve drives it between half open at 67% thrust (minimum power level) and fully open at 100% thrust and above (in the Space Shuttle main engine, the thrust is variable between the minimum power level or 67% to the full power level or 109%, the rated or 100% value being 2.094×10^6 N in vacuo and 1.667×10^6 N at sea level). This action maintains the appropriate

flow relationships among the several parallel fuel flow paths, as the high-pressure fuel turbo-pump output pressure varies with thrust. During engine run, the oxidiser pre-burner oxidiser valve and the fuel pre-burner oxidiser valve are used as control devices for thrust and mixture ratio. Manipulating the valves affects the output of the pre-burners, the speed of the turbo-pumps, and therefore the propellant flow rates. The fuel pre-burner oxidiser valve is driven alone to maintain mixture ratio in the main combustion chamber, while the oxidiser pre-burner oxidiser valve is driven with the fuel pre-burner oxidiser valve to increase or decrease thrust while maintaining the mixture ratio. The control loops include the controller, the valve actuators, and the transducers which sense the flow rates and the pressure in the main combustion chamber, and therefore the thrust. During the engine shutdown phase, all five valves are switched to shutdown schedules. These schedules ensure a smooth and safe shutdown by establishing a fuel lag. In other words, the oxidiser leaves the combustion chambers ahead of the fuel. This lag creates a fuel-rich and cool shutdown environment [7].

The controller of the RS-25 engine provides complete and continuous monitoring and control of engine operation. In addition, it performs maintenance and start preparation checks, and collects data for historical and maintenance purposes. The controller of the RS-25 engine is shown in the following figure, due to the courtesy of Boeing-Rocketdyne [7].



The controller is an electronic package which contains five principal sections:

- power supply section;
- input electronics section;
- output electronics section;
- computer interface section; and
- digital computer unit.

Pressure, temperature, pump speed, flow rate, and position sensors supply the input signals. Output signals operate spark igniters, solenoid valves, and hydraulic

actuators. The controller is dual-redundant, which gives it normal, fail-operate, and fail-safe operational mode capability. Fail-operate mode follows a first failure, and is similar to normal mode, but with a loss of some redundancy. Fail-safe mode follows a second failure. In this mode, engine throttling and mixture ratio control are suspended, the main propellant valves are held fixed in their last commanded position, and the engine is subsequently shutdown pneumatically. The controller provides active and continuous control of the engine thrust and of the mixture ratio in the main combustion chamber through closed-loop control. The controller reads the pressure (equivalent to the thrust) in the main combustion chamber, and compares it to the existing thrust reference signal. It uses the error to drive the oxidiser pre-burner oxidiser valve, which adjusts the thrust and eliminates the error. For the mixture ratio in the main combustion chamber, the controller reads the fuel flow-meter and drives the fuel pre-burner oxidiser valve to adjust the fuel flowing to the main combustion chamber, thus maintaining a mixture ratio $o/f = 6$. In addition to these primary functions, the controller performs engine checkout, limit monitoring, start readiness verification, and engine start and shutdown sequencing. The controller instructions to the engine control elements are updated 50 times per second (every 20 ms). The electronics are mounted on modular boards inside a sealed and pressurised chassis, which is cooled by heat convection through pin fins [7].

5.3 Control of Thrust Magnitude

The thrust of a rocket engine is controlled in magnitude by regulating the pressure in the main combustion chamber. Sometimes, a reduction of the thrust magnitude, also known as throttling, is necessary in the last part of the propelled flight of a rocket vehicle. This reduction can be performed by decreasing, either stepwise or continuously, the pressure in the main combustion chamber.

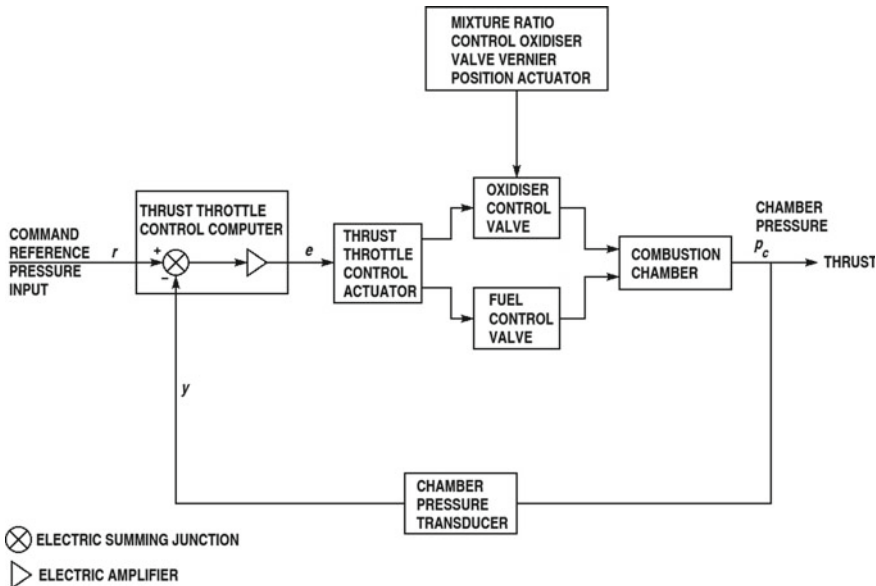
In case of rocket engines fed by turbo-pumps, the pressure in the main combustion chamber can be reduced by regulating either the mass flow rate of the propellants through the gas generator or the mass flow rate of the hot gas through the turbine. When the first method is used, it is also possible to vary the mixture ratio of the propellants.

In case of rocket engines fed by gases under pressure, the pressure in the combustion chamber can be reduced by regulating the pressures in the main tanks of the propellants.

In case of multiple engines arranged in a cluster, thrust control can be performed by shutting off one or more engines of the cluster.

The examples of thrust regulation considered in Sect. 5.1 concern the case of a rocket engine fed by gases under pressure and the case of a rocket engine fed by turbo-pumps. In the second case, the thrust has been controlled in magnitude by using a valve regulating the value of the mass flow rate in the gas generator, and therefore the power delivered by the turbine.

The example given below concerns thrust regulation performed by varying the flow of the propellants. The following, figure, re-drawn from [3], illustrates the scheme of a closed-loop control system based on flow variation.



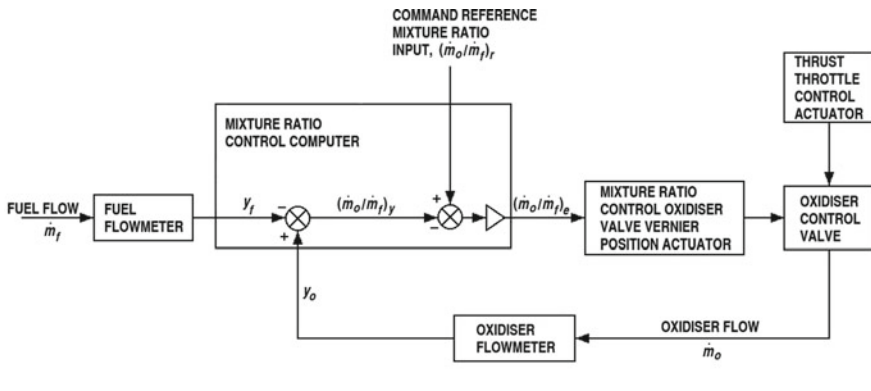
In the present case, the regulation is based on two valves which determine the resistances encountered by the two different propellants in their respective lines towards the combustion chamber. A chamber pressure transducer senses the pressure p_c in the combustion chamber, which is used as an indicator of the thrust magnitude. The output signal y of the chamber pressure transducer is fed back as a secondary input to the thrust throttle control computer, which compares the signal y with its primary input, which is the reference signal r . The error $e = r - y$ is used to drive the thrust throttle control actuator, which in turn regulates the control valves of the propellants in such a way as to reduce the error.

In the RS-25 engine, throttling is accomplished by varying the output of the pre-burners, thus varying the speed of the high-pressure turbo-pumps, and therefore the mass flow rates of the propellants (liquid oxygen and liquid hydrogen). The mixture ratio of the propellants in the main combustion chamber is $o/f = 6.032$. This value is maintained by varying the fuel flow rate around the oxidiser flow rate [7]. In other words, restricting the oxidiser flow to the pre-burners causes the turbine inlet temperature to decrease.

5.4 Control of Propellant Mixture Ratio

An open-loop control system of the mixture ratio of the propellants in a rocket engine can be obtained by installing calibration orifices of proper size in the propellant lines. Further refinements are possible by weighing accurately the propellants loaded in the tanks, by using orifices of adjustable (rather than fixed) size in case of storable fluids, in order to regulate the size of the orifices just before take-off, and by installing valves at the pump inlet of engines fed by turbo-pumps, in order to compensate for effects induced by accelerations acting on the fluid mass. In the last manner, an increase or decrease in pressure in the fluids due to variable accelerations is sensed and fed back to a closed-loop control system, which regulates gradually the valves and also protects the pumps.

In certain cases, it is necessary to perform a continuous control of the mixture ratio by using a closed-loop system. In such cases, Huzel and Huang [3] suggest the control scheme shown in the following figure.



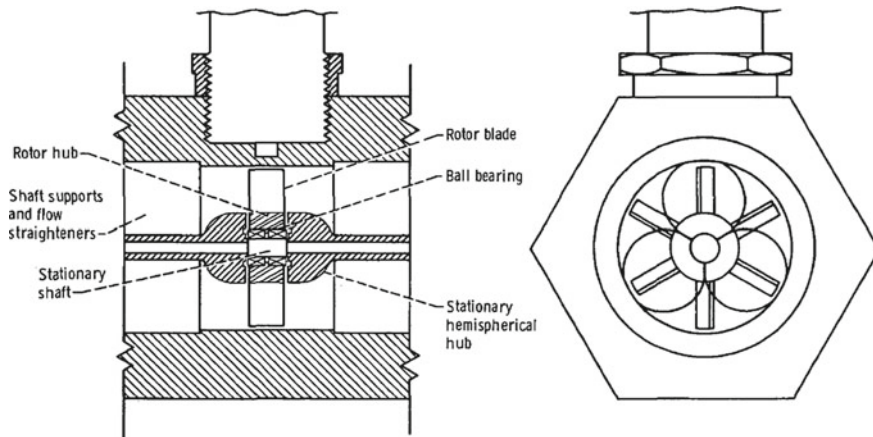
ELECTRIC SUMMING JUNCTION
 ELECTRIC AMPLIFIER

The control system illustrated in the preceding figure has two flow-meters which sense continuously the mass flow rates \dot{m}_o and \dot{m}_f of the propellants. The mixture ratio feedback signal $(\dot{m}_o/\dot{m}_f)_y$ is compared in a computer with a reference command signal $(\dot{m}_o/\dot{m}_f)_r$, and the resulting error $(\dot{m}_o/\dot{m}_f)_e$ is fed to a mixture ratio control oxidiser valve Vernier position actuator. This actuator, in turn, commands the oxidiser control valve, which varies the mass flow rate \dot{m}_o of the oxidiser, in such a way as to correct the error.

A flow-meter is a device which measures either the volume flow rate q (m^3/s) or the mass flow rate \dot{m} (kg/s) of a fluid which passes through it. A volumetric flow-meter (such as a positive displacement flow-meter) measures the volume flow rate $q = Av$ of a fluid stream which passes through a cross-sectional area A (m^2) at a velocity v (m/s). A velocity flow meter (such as a magnetic, turbine, ultrasonic, and

vortex shedding and fluidic flow-meter) measures the velocity v of a fluid stream to determine the volume flow rate q . When the volume flow rate q is known, the mass flow rate \dot{m} results from $\dot{m} = \rho q$, where ρ (kg/m^3) is the density of the fluid in the given conditions.

A turbine-type flow-meter having a hemispherical hub is illustrated in the following figure, due to the courtesy of NASA [8].

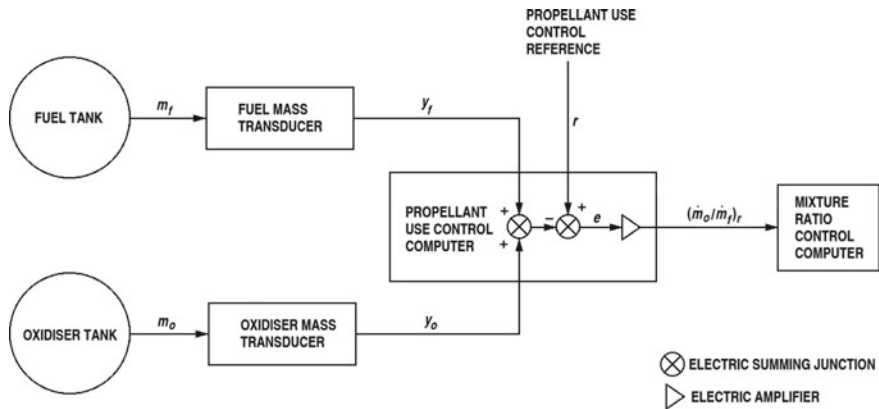


A turbine-type flow-meter is a device in which the entire flow stream turns a bladed rotor at a speed proportional to the volume flow rate of the fluid, and which generates or modulates an output signal, whose frequency is proportional to the angular velocity of the rotor. As shown in the preceding figure, the fluid passing through the flow-meter impinges on the blades of a turbine, which are free to rotate about an axis along the central line of the turbine housing. A permanent magnet placed within the windings of a pickoff coil generates a magnetic field. An electrical cycle is generated by each blade which sweeps through the magnetic field present in the fluid passage.

Another flow-meter, based on the Venturi tube, will be described in Sect. 5.7. Further information on several types of flow-meters can be found in [9].

5.5 Control of Propellant Consumption

This type of control is performed by sensors which measure the amount of propellant remaining in the tanks and the unbalance of one of the two propellants with respect to the other. A closed-loop scheme indicated by Huzel and Huang [3] is shown in the following figure.



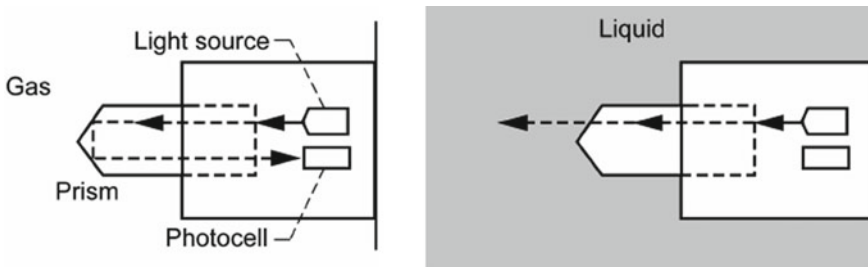
This control system measures continuously the residual masses m_f and m_o of the two propellants by using sensors placed in the respective tanks. The transducer output signals y_f and y_o corresponding to these masses are summed, and the signal resulting from the sum $y_f + y_o$ is compared with a propellant use control reference signal r which is fed to the propellant use control computer.

The error signal $e = r - (y_f + y_o)$ is amplified and then used to modify the command reference mixture ratio signal $(\dot{m}_o/\dot{m}_f)_r$ which is fed to the mixture ratio control computer.

A survey on the sensors used to determine the amount of propellant contained in a tank has been performed by Dodge [10]. A brief account is given below.

Sensors detecting the presence of fluids of a given type at given locations in a tank are usually called wet-dry sensors. Most wet-dry sensors are based on a hot wire or an electrical resistance or an electrical impedance element which carries a small current. The presence of a given type of fluid at the sensor location is detected by a change in the electrical impedance of the sensor, which in turn depends on the type of fluid (gas or liquid) around the sensor. This is because the sensor impedance depends on the amount of heat transfer from the sensor to the surrounding medium, due to the heating caused by the passage of the electric current. The heat transfer is greater when the sensor is surrounded by a liquid. Thus, by measuring a change in current for a constant applied voltage or a change in voltage for a constant applied current, it is possible to detect whether the sensor is in a liquid or in a gas.

Another type of sensor is based on a laser light source incorporated in a prism-like capsule, whose index of refraction is matched to the index of refraction of the liquid contained in a tank. A scheme of this optical sensor is shown in the following figure, due to the courtesy of NASA [10].



When the sensor is immersed in a gas, as shown on the left-hand side of the preceding figure, the light is reflected off the end of the prism back to a photocell at the light source. By contrast, when the sensor is immersed in a liquid, as shown on the right-hand side of the preceding figure, the light is transmitted through the liquid without reflection off the prism. Thus, the presence or absence of a reflection indicates whether the sensor is dry or wet.

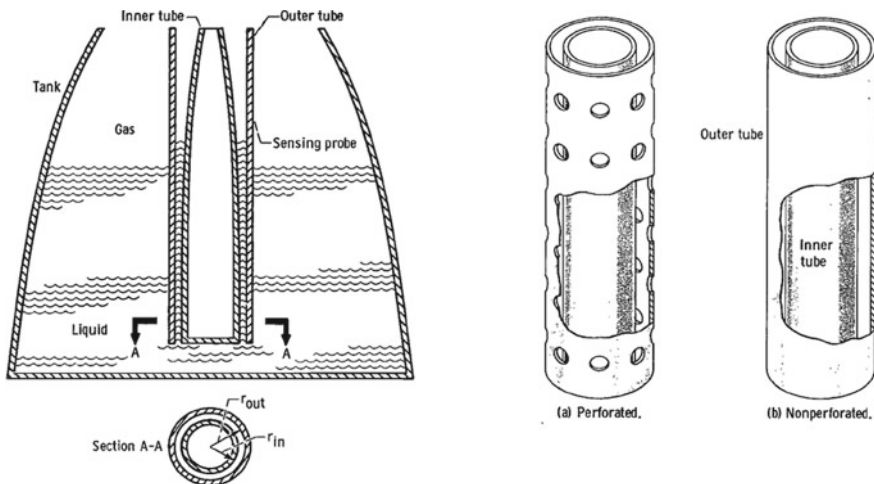
Sensors which detect the location of the surface of a liquid in a tank or the depth of this liquid above the sensor are called level sensors. In this category are pressure sensors, ultrasonic sensors, and electrical capacity sensors.

Pressure sensors cannot be used in weightless conditions, because they measure the pressure head $p/(\rho g_0)$ of the liquid placed above the location of the sensor. A pressure transducer is inserted at the bottom of a gauge line going from the bottom to the top of a tank. A pressure sensor detects the difference of pressure existing between the gas at the top and the liquid at the bottom of the tank. This difference is related to the depth of the liquid when the pressure and the temperature of the substance (liquid or gas) are known.

Ultrasonic sensors generate an ultrasonic pulse which is transmitted through the liquid propellant contained in a tank. A mismatch of acoustic impedance at the liquid-gas interface generates an echo, which is transmitted back through the liquid to an ultrasonic receiver at the transducer location. The time elapsed between the emission of the pulse and the reception of the echo is related to the depth of liquid above the transducer by the sonic velocity in the liquid. A sensor of this type can be used in low-gravity conditions, but the liquid must be maintained in a known configuration above the sensor by a propellant management device based on the principle of capillarity.

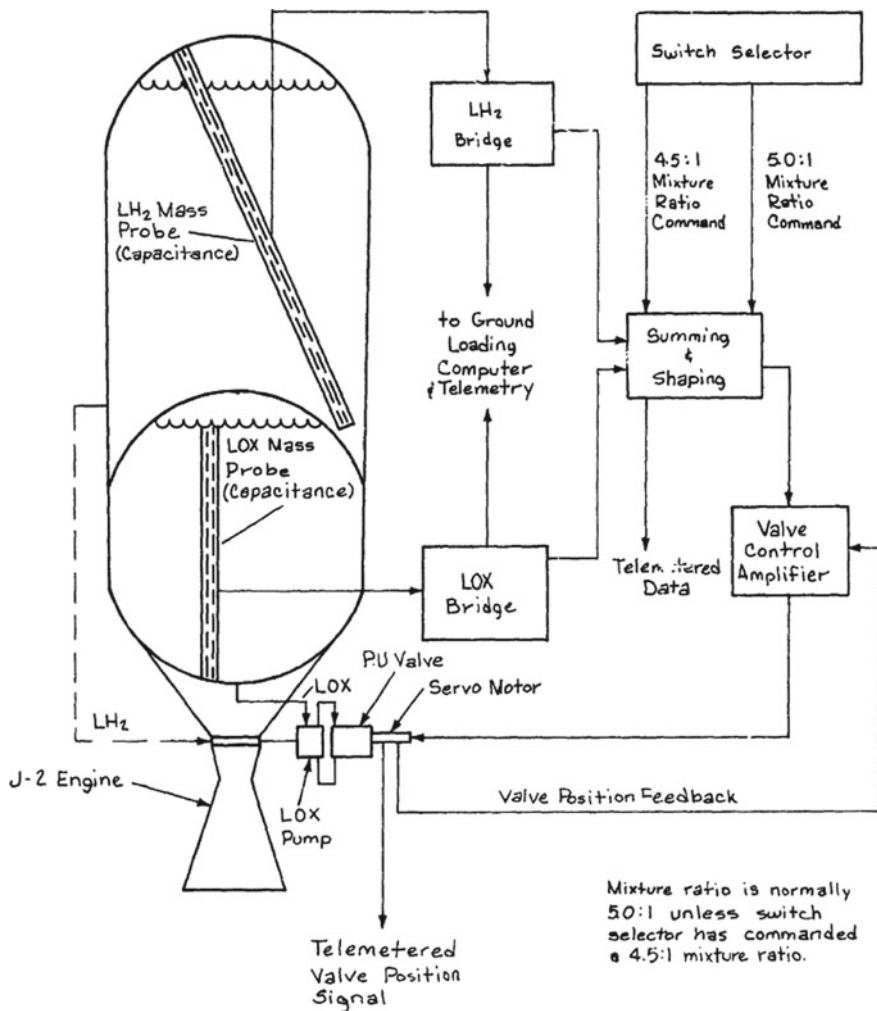
An ultrasonic sensor of another type is a torsional wave guide. In this sensor, the speed of a torsional wave propagating along a wave guide, such as a rod, depends on whether the wave guide is immersed in a liquid or in a gas. The impedance mismatch at the liquid-gas interface generates an echo, which is detected to provide information on the length of the wave guide which is immersed in the liquid. However, some tests executed in conditions of zero gravity have shown that the adherence of liquid to portions of the wave guide supposed to be dry degraded seriously the accuracy of the sensor.

A capacity sensor contained in a propellant tank is shown in the following figure, due to the courtesy of NASA [11].



A capacity probe senses mass directly. The sensing probe consists essentially of two coaxial tubes contained in a tank. These tubes, when a voltage is applied to them, act as the plates of an electric condenser, whose capacity changes when the proportion between liquid and gas changes. This is because the liquid and the gas contained in the tank have different values of dielectric constant. In other words, the dielectric medium between the two tubes of the probe is the propellant, in liquid and gaseous state, contained in the tank. The total electrical capacity of the probe depends on the level of the liquid which fills it. Thus, the measured electrical capacity of the probe provides information on the mass of liquid in the tank. With a suitable electronic apparatus, the mass of the residual propellant in the tank can be measured continuously. The outer tube of the capacity probe may be perforated or not, as shown in the preceding figure. A non-perforated probe was chosen for the Centaur launch vehicle, because it provided a better measurement [11].

A propellant management system using electrical capacity probes was also chosen for the J-2 engine in the S-IVB stage, as shown in the following figure, due to the courtesy of NASA [12].



In the S-IVB stage, the propellant management system, in conjunction with the switch selector, controls the mass propellant loading ratio and the engine mixture ratio (liquid oxygen to liquid hydrogen) to ensure balanced consumption of propellant. The electrical capacity probes, located in the two tanks, monitor the mass of the propellants. During flight, the electrical capacity probes are not used to control the propellant mixture ratio. The mixture ratio is controlled by switch selector outputs, which are used to operate the propellant utilisation (PU) valve. The PU valve is a rotary valve which controls the quantity of liquid oxygen flowing to the engine. The PU valve is commanded to its null position to obtain an engine mixture ratio (EMR) of 5.0:1 prior to engine start. The PU valve remains at the 5.0:1 position during the first burn. Prior to engine restart (first opportunity), the PU valve is commanded by the switch selector to an EMR of 4.5:1 and remain at this position until approximately

2 min of S-IVB burn. Then the PU valve is commanded to its null position (5.0:1) by the switch selector. However, if the S-IVB restart is delayed to the second opportunity, the EMR is shifted from 4.5:1 to 5.0:1 by the switch selector at about the time in which the engine reaches 90% thrust [12].

An electrical capacity probe depends on the liquid being settled, and therefore can only be used for gauging during periods of thrusting [10]. In principle, an electrical capacity probe might be used in low-gravity conditions if the liquid configuration is controlled by propellant management devices. However, in such conditions, capillary forces in the annular gap between the walls of the probe would cause the liquid meniscus location to differ from the liquid level in the tank, and thus cause an inaccurate reading, which may be small and could be compensated for. Depending on the design, the probe can also be sensitive to liquid motions such as occurred with the first landing of the Lunar Module on the Moon, for which non-linear sloshing lowered the effective level of the liquid within the gauge to the point that a premature low liquid level warning was given [10].

In the absence of a specific measurement system, the quantity of propellant remaining in a tank can be estimated by determining the consumption of the propellants which have already been used in comparison with the quantity initially loaded in the tanks. This method is commonly called bookkeeping. Some sensors and devices are used in the bookkeeping method, either separately or in conjunction. They are:

- flow-meters or Venturi-meters in the lines between the tanks and the main combustion chamber or the gas generator to measure the flow rates of the propellants;
- sensors which determine the flow rates of the propellants by measuring their pressures in the pumps in conjunction with the performance curves of the pumps; and
- calibrations of engine thrust versus propellant flow rate and tank pressure.

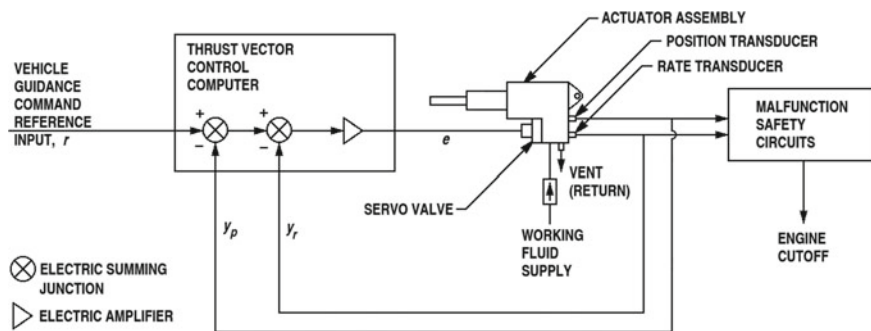
Various types of flow-meters, turbine-meters, accelerometers, and pressure sensors are required for the bookkeeping method. This method can only be used during periods of engine thrusting, and its accuracy is limited by the accumulation over time of the errors committed in estimating the propellant consumption, in particular near the point of propellant depletion. In addition, the bookkeeping method cannot detect leaks.

Other methods indicated by Dodge [10] to evaluate propellant consumption are:

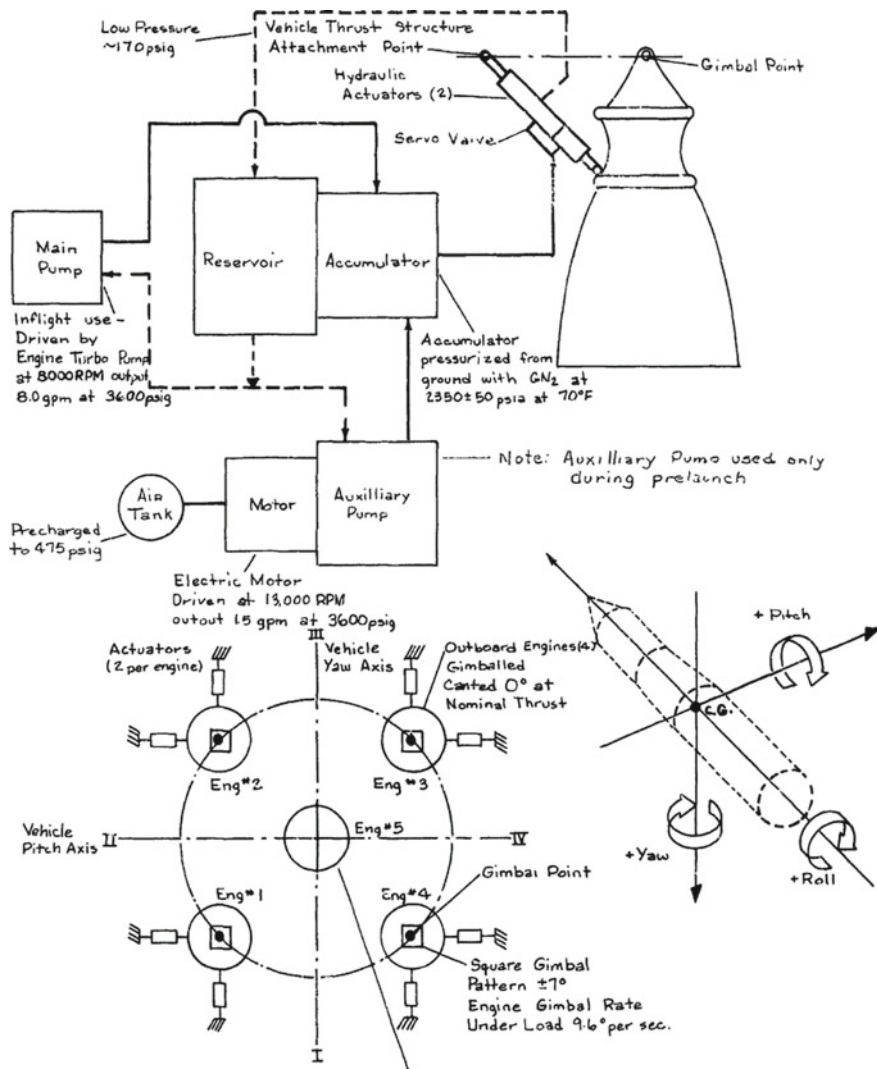
- measuring the acceleration of the vehicle and the thrust of the engine, in order to determine the mass of the vehicle at any given time in comparison with the mass of the empty vehicle; and
- measuring the decay of pressure in the ullage spaces, in case of tanks which are initially pressurised, as the liquids are drained from their tanks and the ullage spaces increase.

5.6 Control of Thrust Direction

Several methods used to control the direction of the thrust vector in a rocket vehicle have been discussed in Chap. 2, Sect. 2.2, as far as they can affect the design of the thrust chamber of a rocket engine. The present section is meant to describe in further depth the method of controlling the thrust vector by using a gimbal mechanism acting on either the nozzle or the engine assembly. This method is the most used in liquid-propellant rocket engines, due to its reliability and performance. The following figure, re-drawn from [3], shows a control scheme for thrust vector control using hydraulic actuators.



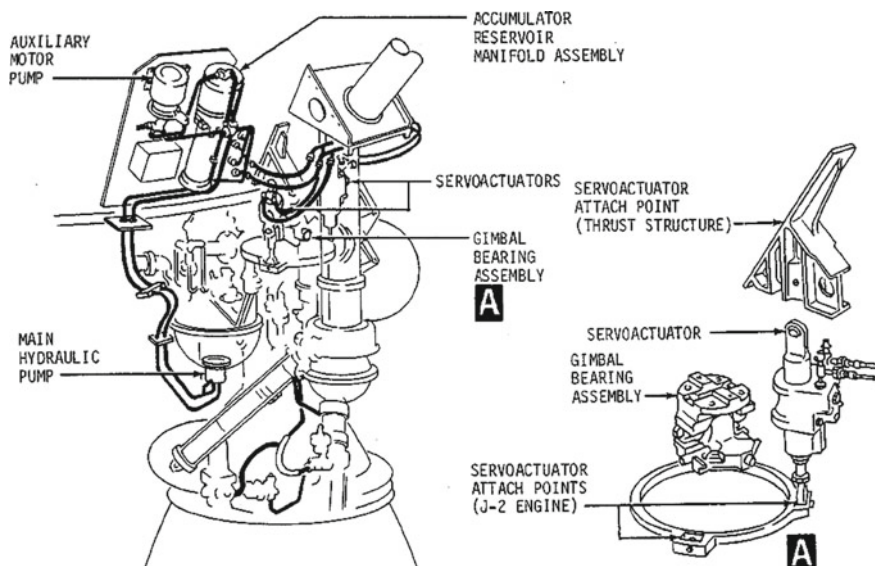
An example of a closed-loop control system using hydraulic actuators for thrust vector control is provided by the S-II, which is the second stage of the Saturn V rocket vehicle. A functional scheme of the control system of the S-II is shown in the following figure, due to the courtesy of NASA [12].



With reference to the preceding figure, the S-II has five J-2 engines arranged in a quincunx pattern (that is, one at the barycentre and four at the vertices of a square). The four outboard engines (No. 1, 2, 3, and 4 in the figure) are gimbal-mounted to provide thrust vector control during powered flight. Attitude control of the S-II stage is maintained by gimbaling the four outboard engines in conjunction with electrical control signals from the inertial unit flight control computer. The gimbaling system consists of four independent closed-loop hydraulic control subsystems, which provide power for engine gimbaling.

The primary components of each control subsystem, also shown in the preceding figure, are an auxiliary pump, a main pump, an accumulator/reservoir manifold

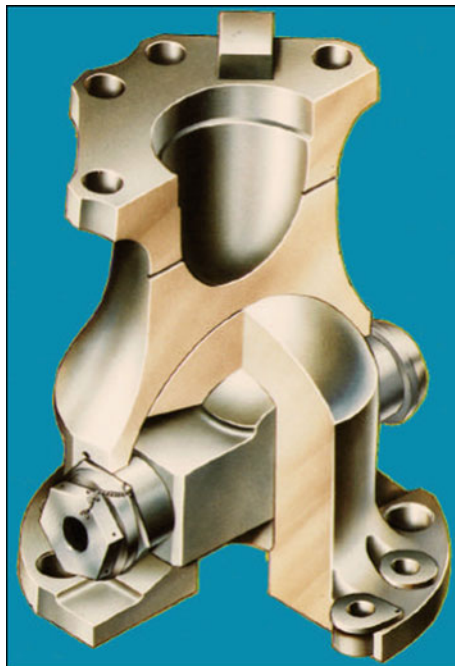
assembly, and two servo-actuators. The auxiliary pump is electrically driven from the ground support equipment to provide hydraulic fluid circulation prior to launch. The main pump is mounted to and driven by the engine liquid-oxygen turbo-pump. The accumulator/reservoir manifold assembly consists of a high-pressure accumulator, which receives high-pressure fluid from the pump, and a low-pressure reservoir, which receives return fluid from the servo-actuators. The servo-actuator is a power control unit, which converts electrical signals and hydraulic power into mechanical outputs which gimbal the engine. The components indicated in the preceding functional scheme are also shown in the following figure, due to the courtesy of NASA [13].



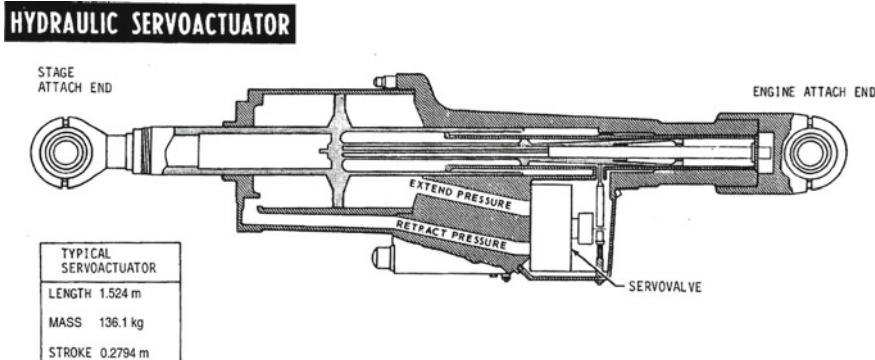
During the pre-launch period, the auxiliary pump circulates the hydraulic fluid to preclude fluid freezing during propellant loading. Circulation is not required during the first stage (S-IC) burn, due to the short duration of the burn. After separation of the second stage (S-II) from the first, a S-II switch selector command unlocks the accumulator lock-up valves, releasing high-pressure fluid to each of the servo-actuators. The accumulators provide gimbaling power prior to the main hydraulic pump operation, in the transient of separation of the two stages. During the S-II main-stage operation, the main hydraulic pump supplies high-pressure fluid to each of the servo-actuators. The return fluid from the actuators is routed to the reservoir, which stores hydraulic fluid at sufficient pressure to supply a positive pressure at the main pump inlet [11].

As has been shown in Chap. 2, Sect. 2.2, a gimballed engine is mounted on a spherical joint. In the three main engines (RS-25) of the Space Shuttle, the gimbal bearing is bolted to the vehicle by its upper flange and to the engine by its lower flange. It supports 33,271 N of engine weight and 2,224,000 N of thrust. It is a ball-and-socket

universal joint where concave and convex spherical surfaces are interconnected. Sliding contact occurs between these surfaces as the bearing is angulated. Fabroid® inserts located at the sliding contact surfaces reduce friction which occurs during gimbal bearing angulation. The bearing, which is installed during engine assembly, measures approximately 27.9 cm × 36.6 cm, weighs about 467 N, has an angular capability of ± 0.218 rad (± 12.5 deg) and is made of a titanium alloy (Ti-6Al-6 V-2Sn). It is shown in the following figure, due to the courtesy of Boeing-Rocketdyne [7].



The following figure, adapted from [13], illustrates a typical hydraulic servo-actuator, installed to gimbal the F-1 engine of the S-IC stage of the Saturn V rocket vehicle.



A detailed example of design of a control system for a rocket engine mounted on gimbals can be found, for example, in [14].

5.7 Principal Components of Flow Control Systems

Liquid-propellant rocket engines have several components which measure and control the motion of fluids through them. The principal components used for this purpose are valves, pressure regulators, and flow-meters. They are described here and in the following sections.

A simple analysis of flow control devices can be done by considering firstly the motion of an ideal fluid, and then the corrections which are necessary to take account of the behaviour of real fluids. For example, a liquid can be considered inviscid, incompressible, and moving in laminar flow (see below) through a tube. The Bernoulli principle, so called after the Swiss scientist Daniel Bernoulli, applies to this case. According to this principle, the total energy (potential energy plus pressure energy plus kinetic energy) possessed by an ideal fluid in steady motion between any two cross sections 1 and 2 of a tube is constant.

By considering the total energy per unit weight, the Bernoulli principle can be expressed as follows

$$z_1 + \frac{p_1}{\rho g_0} + \frac{v_1^2}{2g_0} = z_2 + \frac{p_2}{\rho g_0} + \frac{v_2^2}{2g_0}$$

where z (m) is the elevation of the chosen point with respect to a reference plane, p (N/m^2) is the absolute pressure in the fluid in the chosen point, ρ (kg/m^3) is the density of the fluid in all points at the given temperature, $g_0 = 9.80665 \text{ m/s}^2$ is the acceleration of gravity near the surface of the Earth, and v (m/s) is the velocity of the fluid in the chosen point along a stream line.

When the flow takes place at a constant elevation, then $z_1 = z_2$, and therefore the preceding equation may be written as follows

$$\frac{p_1 - p_2}{\rho g_0} = \frac{v_2^2 - v_1^2}{2g_0}$$

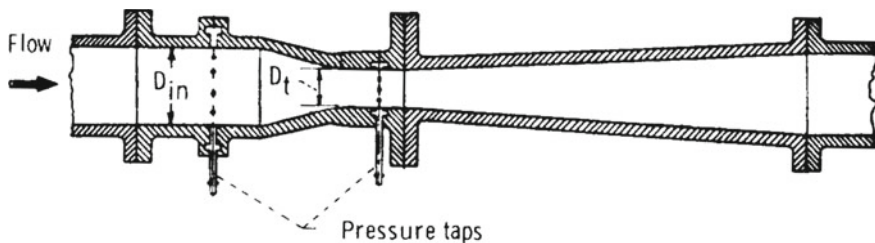
In addition, due to the continuity of the flow, the product $\rho v A$ has the same value at any cross section of area A along the tube, and therefore

$$\frac{v_1}{v_2} = \frac{A_2}{A_1}$$

where A_1 (m^2) and A_2 (m^2) are the areas of any two cross sections along the tube.

The preceding equations can be used to measure the volume flow rate q (m^3/s) of a fluid through a fluid control system, as will be shown below.

The following figure, due to the courtesy of NASA [15], shows a longitudinal section of a flow-meter based on the Venturi tube.



A Venturi-meter, so called after the Italian scientist Giovanni Battista Venturi, is a device which measures the volume flow rate of a liquid moving in a pipe.

It has three main parts, which are

- a convergent cone, whose diameter decreases from the value D_{in} of the pipe to the value D_t of the throat;
- a cylindrical throat, whose diameter D_t is usually one-fourth to one-half of the value D_{in} ; and
- a diffuser, whose diameter increases downstream of the throat and reaches again the value D_{in} at the outlet plane.

The included angle of the convergent cone is approximately 0.3665 rad (21°), and the included angle of the diffuser cone ranges from 0.1222 rad (7°) to 0.2618 rad (15°). Two pressure taps are placed one at the inlet of the convergent cone and the other at the throat. A Venturi-meter is based on the Bernoulli principle. When the cross-sectional area of the tube decreases from the inlet plane to the throat, then the pressure head $p/(\rho g_0)$ of the fluid is forced to decrease, and its velocity head $v^2/(2g_0)$ is forced to increase, in order for its total head to be constant. The decrease in static pressure is measurable at the two taps (usually, by reading the difference of head in open vertical tubes inserted through the wall of the tube under pressure), and the volume flow rate q can be expressed as a function of the decrease in static pressure $p_1 - p_2$, as will be shown below. The velocity head acquired by the fluid

in the convergent part is then converted back into pressure head (minus a loss due to friction) in the diffuser going from the throat to the outlet plane. The Bernoulli equation, written for $z_1 = z_2$, is

$$p_1 - p_2 = \frac{1}{2} \rho (v_2^2 - v_1^2)$$

This equation, solved for v_1^2 , yields

$$v_1^2 = v_2^2 - \frac{2(p_1 - p_2)}{\rho}$$

By substituting this value of v_1^2 into $v_2 = (A_1/A_2)v_1$, there results

$$v_2^2 = \frac{2(p_1 - p_2)}{\rho} \frac{1}{1 - \left(\frac{A_2}{A_1}\right)^2} = \frac{2g_0 \Delta H_p}{1 - \left(\frac{A_2}{A_1}\right)^2}$$

Therefore, the volume flow rate q (m^3/s) in ideal conditions results from

$$q = A_2 v_2 = A_2 \left[\frac{\frac{2(p_1 - p_2)}{\rho}}{1 - \left(\frac{A_2}{A_1}\right)^2} \right]^{\frac{1}{2}} = A_2 \left[\frac{2g_0 \Delta H_p}{1 - \left(\frac{A_2}{A_1}\right)^2} \right]^{\frac{1}{2}}$$

where ΔH_p (m) is the difference of pressure head measured between the inlet plane and the throat in the two open vertical tubes inserted through the wall of the Venturi-meter.

In practice, some loss of total head occurs in a Venturi-meter due to friction, and therefore the actual value of the volume flow rate q is slightly lower than the theoretical value resulting from the preceding equation. This loss can be taken into account by means of a discharge coefficient C_d , whose value is determined experimentally and is always less than unity, as follows

$$q = C_d A_2 \left[\frac{\frac{2(p_1 - p_2)}{\rho}}{1 - \left(\frac{A_2}{A_1}\right)^2} \right]^{\frac{1}{2}} = C_d A_2 \left[\frac{2g_0 \Delta H_p}{1 - \left(\frac{A_2}{A_1}\right)^2} \right]^{\frac{1}{2}}$$

When the volume flow rate q (m^3/s) of a given fluid has been determined by means of a Venturi-meter, as has been shown above, then the mass flow rate \dot{m} (kg/s) of the same fluid results by multiplying the volume flow rate q by the density ρ (kg/m^3) of the fluid at the temperature of interest.

As an example of application of the concepts exposed above, it is required to calculate the mass flow rate of liquid oxygen flowing through an horizontal Venturi-meter which has the following properties: diameter at the inlet plane $D_{in} = 0.1524$ m, diameter at the throat plane $D_t = 0.0762$ m, and discharge coefficient $C_d = 0.92$. The difference of pressure head measured between the inlet and the throat is $\Delta H_p = 13.86$ m, and the density of liquid oxygen at its boiling point is $\rho = 1141$ kg/m³ [16].

By substituting these data in the preceding equation, the volume flow rate results

$$q = 0.92 \times \frac{3.1416 \times 0.0762^2}{4} \times \left[\frac{2 \times 9.807 \times 13.86}{1 - \left(\frac{0.0762}{0.1524} \right)^4} \right]^{\frac{1}{2}} = 0.07144 \text{ m}^3/\text{s}$$

and the mass flow rate results

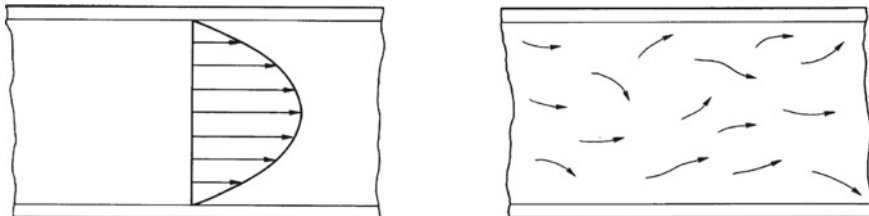
$$\dot{m} = \rho q = 1141 \times 0.07144 = 81.52 \text{ kg/s}$$

All real fluids are viscous in various degrees. As has been shown in Chap. 4, Sect. 4.7, viscosity is a physical property which measures the degree of internal resistance opposed by a fluid to motion. The fluids for which the rate of deformation is proportional to the shear stress applied to them are called Newtonian fluids, after Isaac Newton. In case of a one-dimensional motion of a Newtonian fluid along a direction x (planar Couette flow), this linear relationship can be expressed as follows

$$\tau_{xy} = \mu \frac{dv}{dy}$$

where τ_{xy} (N/m²) is the shear stress, dv/dy (s⁻¹) is the rate of shear strain, that is, the velocity gradient in the direction y perpendicular to the direction x of motion, $v \equiv v(y)$ (m/s) is the velocity of motion in the direction x , and μ (Ns/m²) is the coefficient of dynamic viscosity of the fluid.

The motion of a viscous fluid in a cylindrical tube may be either laminar or turbulent or transitional. The first two types of flow are shown in the following figure, due to the courtesy of NASA [17].



A viscous fluid in laminar flow regime (left) moves smoothly in thin layers, called laminae, which do not mix together. The layers in contact with the walls of the tube

are stationary, whereas the internal layers move by sliding one over another. The velocity of the layers increases from the walls to the central line of the tube with a parabolic profile.

By contrast, a viscous fluid in turbulent flow regime (right) moves irregularly with eddies and swirls which mix the layers of fluid together. The mean velocity profile for turbulent flow is approximately elliptic (blunt nose) and is characterised by a much higher shear stress, due to the slope of the velocity profile at the walls [17]. Even in conditions of turbulent flow, a thin layer (called boundary layer) exist near each wall of the tube where the fluid moves in laminar flow regime.

A transitional flow fluctuates between laminar flow and turbulent flow. When this happens, a laminar flow is on the verge of becoming turbulent.

A criterion to indicate whether the motion of a fluid occurs in laminar or turbulent flow is provided by the value of the Reynolds number. As has been shown in Chap. 2, Sect. 2.5, the Reynolds number Re is defined as follows

$$Re = \frac{\rho v d}{\mu}$$

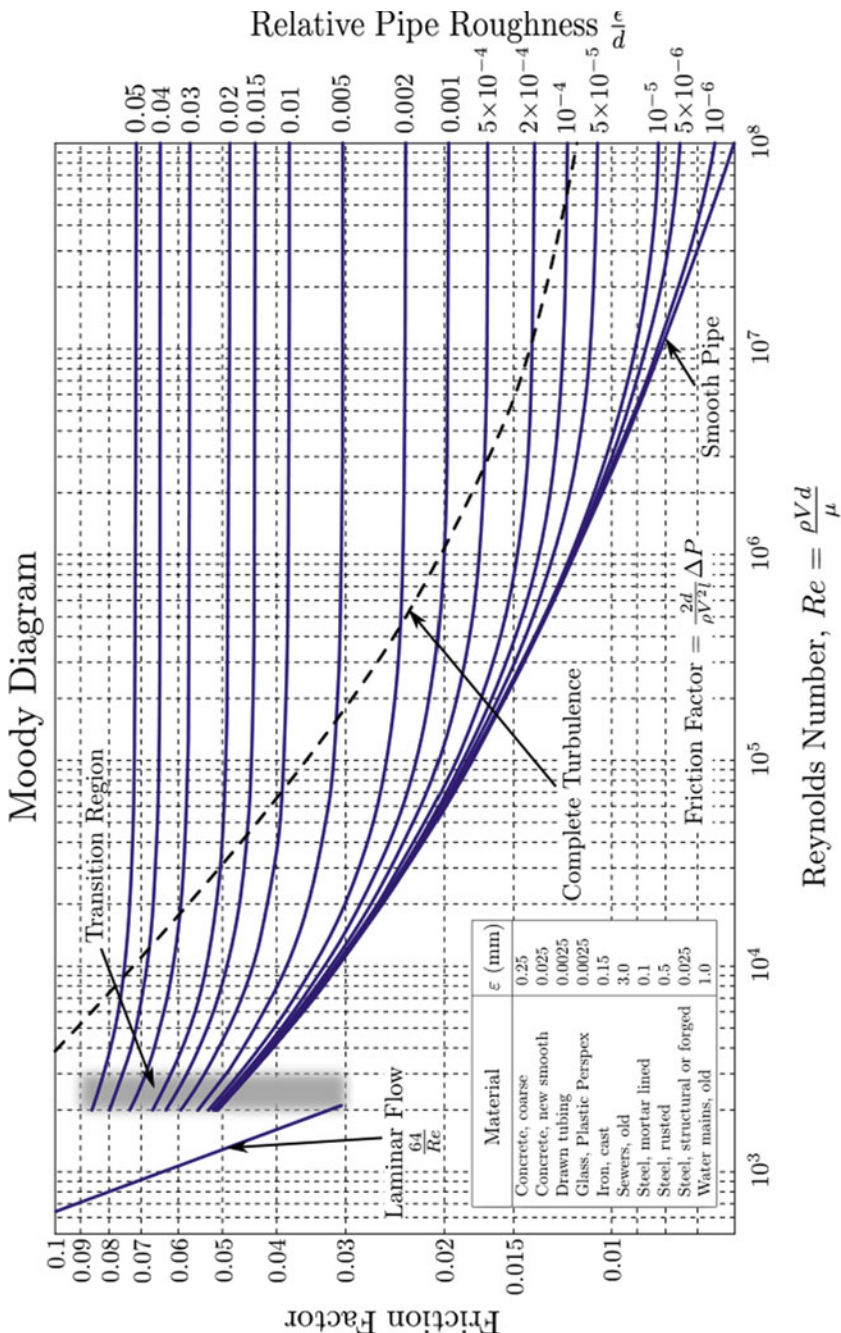
where ρ (kg/m^3) is the density of the fluid at the given temperature, v (m/s) is the mean velocity of the fluid in the tube, d (m) is the hydraulic diameter of the tube, and μ (N s m^{-2}) is the coefficient of dynamic viscosity of the fluid at the given temperature. The Reynolds number is the ratio of the inertial forces to the viscous forces which act on a unit volume of fluid moving in a tube. For low values of the Reynolds number, the viscous forces are sufficiently high to keep the fluid particles in parallel layers, and consequently the flow is laminar. For high values of the Reynolds number, the inertial forces prevail over the viscous forces, and consequently the flow is turbulent. For practical purposes, when the value of the Reynolds number is less than 2000, then the flow is laminar. The transition value for a fluid moving in a tube of circular cross section is $Re = 2300$. When the value of the Reynolds number ranges from about 2300 and 4000, then the flow is unstable, due to an incipient turbulence. When the value of Re is greater than 4000, then the flow is turbulent.

The friction forces acting on the particles of a fluid moving in a tube are due to the rubbing of the particles one against another and also against the walls of the tube. As a result of these forces, part of the kinetic energy possessed by the fluid is converted into heat. This heat may either remain into the fluid or be transferred to the external environment through the walls.

As has also been shown in Chap. 2, Sect. 2.5, the drop of pressure head ΔH_p (m) due to friction in a tube of length L (m) and hydraulic diameter d (m) is expressed as a function of the Darcy friction factor f_D (dimensionless) of the tube by means of the Darcy-Weisbach equation, as follows

$$\Delta H_p = f_D \frac{L}{d} \left(\frac{v^2}{2g_0} \right)$$

where v (m/s) is the average velocity of the fluid, and $g_0 = 9.80665 \text{ m/s}^2$ is the acceleration of gravity near the surface of the Earth. The Darcy friction factor f_D depends on the Reynolds number Re defined above and also on the shape and smoothness of the tube. This factor can be determined as a function of the Reynolds number Re and of the relative roughness ε/d of the tube not only by means of the Colebrook-White relation (see Chap. 2, Sect. 2.5), but also by means of the Moody diagram (so called after the American scientist Lewis Ferry Moody) shown in the following figure, due to the courtesy of Beck and Collins, through Wikimedia [18].



The presence of fittings, such as valves, elbows, T's, sudden expansions or contractions, et c., which may be present in a piping system, causes further losses due to friction. These losses can be taken into account by means of a fictitious term L_e (m), called equivalent length, which adds to the actual length L (m) of the pipe. By so doing, the Darcy-Weisbach equation written above becomes

$$\Delta H_p = f_D \left(\frac{L + L_e}{d} \right) \left(\frac{v^2}{2g_0} \right)$$

In other words, the actual length L of a tube and its equivalent length L_e , which takes account of all the fittings placed along the tube, are summed up to form a total length $L + L_e$, which in turn is introduced in the Darcy-Weisbach equation instead of the actual length L . The equivalent lengths L_e for a range of sizes of a given type of fitting have been found experimentally to be in an approximately constant ratio to the diameters d of the fittings. In other words, $L_e/d \approx \text{constant}$. Therefore, a single value is sufficient to cover all sizes of each fitting. A table, which can be found in [19], gives the values of the L_e/d ratio for many valves and other typical fittings.

Another method, called K-method, takes account of the pressure drop due to the fittings by means of a resistance coefficient k assigned to each type of fitting. When this method is used, the total drop of pressure head can be computed by using the Darcy-Weisbach equation, as follows

$$\Delta H_p = \left(\frac{f_D L}{d} + \sum_{i=1}^N k_i \right) \left(\frac{v^2}{2g_0} \right)$$

Values of the coefficient k for several fittings can be found in [20]. Other methods are those called the 2-K (Hooper) method and the 3-K (Darby) method. They are refinements of the K method described above. Particulars and values of the coefficients to be used in the 2-K method and in the 3-K method can be found in [21, 22].

As an application of the concepts discussed above, it is required to compute the drop of pressure head for the discharge flexible duct of the oxidiser pump of a rocket engine and also for the main oxidiser valve, which is of the butterfly type, fully open. The following data are known: volume flow rate of liquid oxygen in the flexible duct $q = 0.7836 \text{ m}^3/\text{s}$, inside diameter of the flexible duct $d = 0.2032 \text{ m}$, actual length of the flexible duct $L = 0.4064 \text{ m}$, equivalent length of the flexible duct (due to the resistance arising from flow deviation) $L_e = 6d = 6 \times 0.2032 = 1.219 \text{ m}$, absolute roughness $\epsilon = 1.524 \times 10^{-5} \text{ m}$, and characteristic flow area of the main oxidiser valve $A_2 = 0.78A_1$, where $A_1 = \pi d^2/4$ is the area of the cross section of the flexible duct.

The density and the dynamic viscosity of liquid oxygen at its boiling point are respectively $\rho = 1141 \text{ kg/m}^3$ and $\mu = 1.95 \times 10^{-4} \text{ Ns/m}^2$ [16].

The mean velocity of liquid oxygen in the flexible duct is computed as follows

$$v_1 = \frac{4q}{\pi d^2} = \frac{4 \times 0.7836}{3.1416 \times 0.2032^2} = 24.16 \text{ m/s}$$

The Reynolds number results from

$$Re = \frac{\rho v_1 d}{\mu} = \frac{1141 \times 24.16 \times 0.2032}{0.000195} = 2.873 \times 10^7$$

By inserting $\varepsilon = 1.524 \times 10^{-5}$ m, $d = 0.2032$ m, and $Re = 2.873 \times 10^7$ in the on-line calculator of [23], we find $f_D = 0.01143$, which is the Darcy friction factor.

After substituting $f_D = 0.01143$, $L = 0.4064$ m, $L_e = 1.219$ m, $d = 0.2032$ m, $v_1 = 24.16$ m/s, and $g_0 = 9.807$ m/s² in the following equation

$$\Delta H_{p1} = f_D \left(\frac{L + L_e}{d} \right) \left(\frac{v_1^2}{2g_0} \right)$$

we compute the drop of pressure head due to the discharge flexible duct

$$\Delta H_{p1} = 0.01143 \times \left(\frac{0.4064 + 1.219}{0.2032} \right) \times \left(\frac{24.16^2}{2 \times 9.807} \right) = 2.721 \text{ m}$$

This value corresponds to a drop of pressure in the flexible duct

$$\Delta p_1 = \rho g_0 \Delta H_{p1} = 1141 \times 9.807 \times 2.721 = 3.045 \times 10^4 \text{ N/m}^2$$

As to the drop of pressure head due only to the butterfly valve, the continuity equation $\rho v_1 A_1 = \rho v_2 A_2$ implies an increase in velocity, from v_1 to a higher value v_2 , for the fluid moving through the valve. In the present case, the velocity v_2 is

$$v_2 = \frac{A_1}{A_2} v_1 = \frac{24.16}{0.78} = 30.97 \text{ m/s}$$

The value of the resistance coefficient k for each valve is specified by its manufacturer. In [24], we find the value $k = 0.3$ for a butterfly valve fully open. As a check, we use the following formula (relating to the 2-K method) indicated in [21] to compute the resistance coefficient k for a butterfly valve in a duct of inner diameter d (m):

$$k = \frac{800}{Re} + 0.25 \times \left(1 + \frac{0.0254}{d} \right)$$

After substituting $Re = 2.873 \times 10^7$ and $d = 0.2032$ m in the preceding equation, we find $k = 0.2813$. This confirms the value $k = 0.3$ found in [24].

Therefore, the drop of pressure head, due only to the butterfly valve, is

$$\Delta H_{p2} = k \frac{v_2^2}{2g_0} = 0.3 \times \frac{30.97^2}{2 \times 9.807} = 14.67 \text{ m}$$

This value corresponds to a drop of pressure in the butterfly valve

$$\Delta p_2 = \rho g_0 \Delta H_{p2} = 1141 \times 9.807 \times 14.67 = 1.642 \times 10^5 \text{ N/m}^2$$

5.8 Static and Dynamic Seals for Leakage Control in Valves

The dynamic seals considered here are mechanical devices used to prevent or reduce to an acceptable level the leakage of a fluid from one region of a valve in which flow occurs to another, when the surfaces to be protected from leakage are in relative motion. Static seals (such as O-ring seals and gaskets) for stationary surfaces are also considered here. The dynamic seals used for turbo-pumps of rocket engines have been described in Chap. 4, Sect. 4.13.

The leakage from a valve may be either internal leakage, which occurs in the direction of the flow, or external leakage, which occurs from a valve to the external environment, in a direction which differs from the normal direction of the flow. According to Howell and Weathers [25], the factors affecting the leakage requirements for valves are:

- loss of pressure or loss of propellant, to be prevented or kept below an acceptable value in order to avoid system failure due to premature depletion of fluid;
- damage to the system, such as corrosion or fire, which might occur as a result of leakage of propellants;
- damage to personnel, which may occur in case of leakage of fluids which are toxic for inhalation or exposure; and
- interference with experiments, which might occur in case of gases under pressure or propellants enveloping a spacecraft whose mission is to sample the atmosphere of a planet.

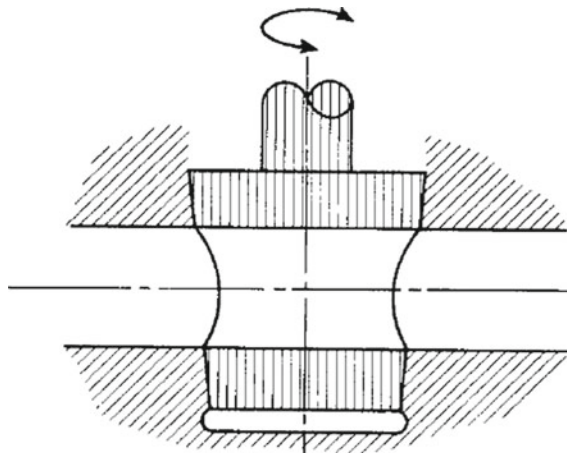
The following seals are considered here:

- seals for valves operating at high pressures and temperatures; and
- seals for valves operating at cryogenic temperatures.

Burmeister et al. [26] have made a survey on the matter. A brief account of this survey is given below. Valves for rocket engines operate at pressures ranging from zero to $6.895 \times 10^8 \text{ N/m}^2$, and at temperatures ranging from cryogenic values to over 1366 K. They can be classified into three principal categories, which are

- plug valves;
- gate valves; and
- globe valves.

All of these valves can be used at high pressures and temperatures. Valves of other types, such as butterfly or vane valves, fall into one of these categories or into some combination of them. A tapered plug valve is shown in the following figure, due to the courtesy of NASA [26].



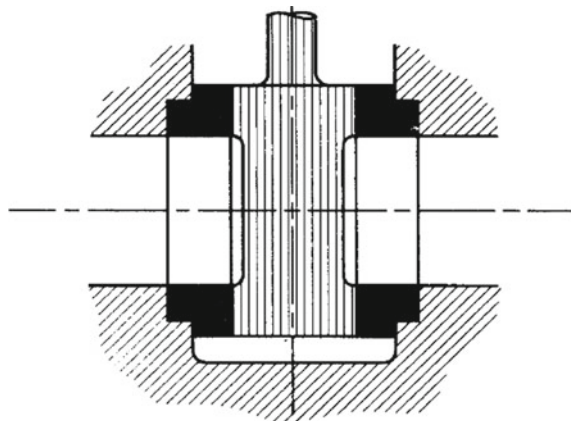
A plug valve has a tapered or cylindrical plug with a hole drilled in the middle. When this plug is rotated, the position of the hole opens, or restricts, or closes the passage of a fluid through the valve. A plug valve can be operated in an intermediate position, in order to throttle the flow. Simple quarter-turn valves, such as the one shown in the preceding figure, are limited in high-pressure application by the rapid increase in operating torque with increasing difference of pressure. When the fluid has access to either the large end or the small end of a tapered plug, then a force unbalance arises into or out of the valve body.

The operating torque depends on the plug taper. The purpose of a tapered plug valve is to shut off flow in a leak-tight manner. When the thickness of the lubricant film is not uniform, then leakage occurs. The lubricant may be washed away by the fluid when unseating the plug, or may also be extruded by the difference of pressure. The three functions fulfilled by the lubricant (lubrication, plug unseating, and viscous sealing) are combined in plug valves of the Nordstrom type, such as the valve shown in the following figure, due to the courtesy of NASA [26].



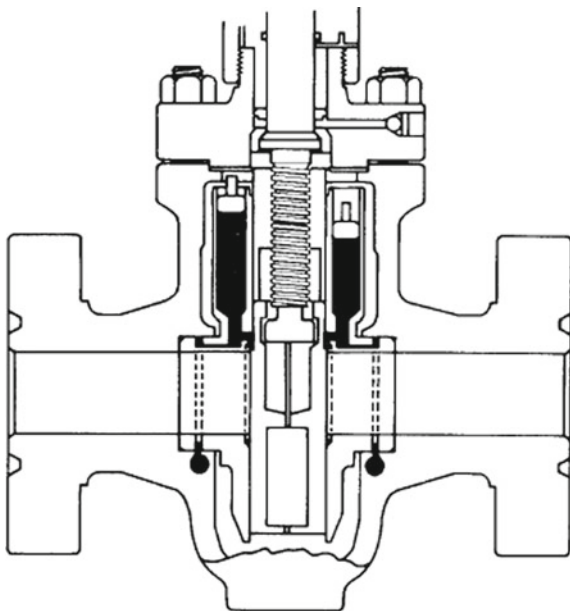
A valve of this type can bear a higher pressure than the maximum pressure bearable by an ordinary tapered plug valve. An increase in temperature degrades the properties of the lubricant-sealant. Maximum temperatures bearable by this type of valve are about 700 K or 800 K. The high viscosity of the lubricant-sealant at very low temperatures precludes application of grease at cryogenic temperatures.

A gate valve opens or closes the passage of fluid in a pipe by raising or lowering a flat plate across the pipe. This plate slides over sealing surfaces in a direction perpendicular to the fluid stream in the pipe, as shown in the following figure, due to the courtesy of NASA [26].

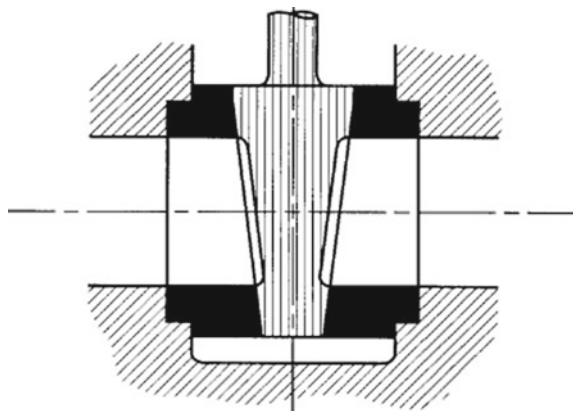


The sealing surfaces of a gate valve must bear the stresses induced by moving the plate from the fully open to the fully closed position. Therefore, the galling properties of the materials used and their ability to withstand stresses are very important. As a general rule, the galling tendency increases and the strength decreases with increasing temperature. To provide good sealing surfaces, the gate and the seat must be flat. Therefore, a gate valve must be thick, especially in large valves subject to high pressures.

Gate valves and tapered plug valves can be protected from leakage by using viscous sealing. For this purpose, a sealant is injected into grooves located around the flow passage in the gate or in the seat, as shown in the following figure, due to the courtesy of NASA [26].



In the valve shown in the preceding figure, the injection pressure of the sealant is proportional to the pressure of the fluid which moves in the pipe. Gate valves using viscous sealants have lower operating torques than conventional parallel slide gate valves. The following figure, due to the courtesy of NASA [26], shows a tapered gate valve, which makes it unnecessary to slide the gate across the entire sealing surface.

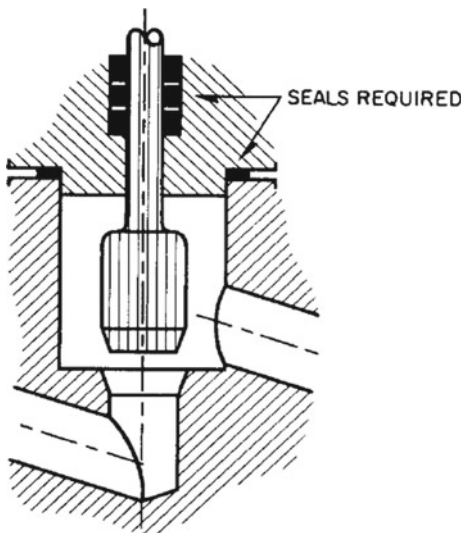


The seat and the gate are not in mutual contact when the gate has been lifted by part of its total travel. Side ribs on a tapered gate valve resist the action exerted by the flow impingement and by the difference of pressure, which tends to move the gate toward the downstream seat, and keep the sealing surfaces from sliding contact.

When a tapered gate valve is closed at a high temperature and then cools down, then the gate tends to bind, because the gate and the body parts have different coefficients of thermal expansion. This can be avoided by using flexible tapered gates for valves operating at high temperatures.

Gate valves not using viscous sealants are subject to leakage, and therefore are not used in case of high pressures. Gate valves using viscous sealants can bear gas and petroleum pressures as high as $1.034 \times 10^8 \text{ N/m}^2$. Gate valves sealed by inserts made of elastomers or fluorocarbons are used when contamination of the fluid is to be avoided. However, the pressure which these valves can bear is limited by plastic flow of these inserts.

Globe valves are those used in water taps to start or stop or regulate the flow in a pipe. They have a moving member which is pushed into the flow passage, as a cork is pushed into the neck of a bottle, and a stationary member, which is a ring seat. The moving member is shaped as a cone frustum, which fits into the mating body seat, as shown in the following figure, due to the courtesy of NASA [26]. The included angle of this cone frustum is much greater than that of a plug used in a tapered plug valve.

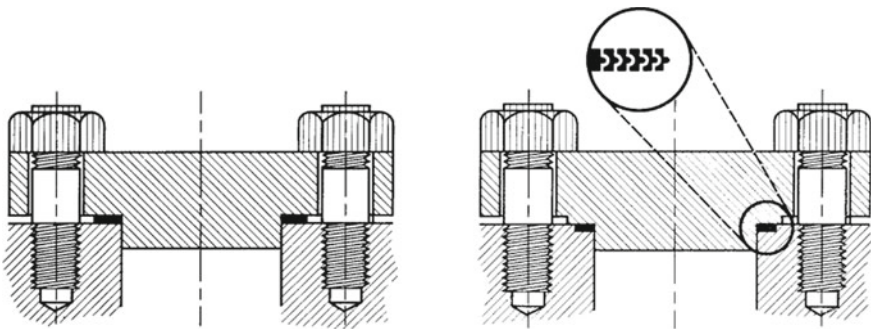


A seat shaped as a cone frustum is very resistant to distortions of the valve body due to the pressure exerted by the fluid. In addition, should such distortions occur, the elastic deformation in the seat tends to maintain satisfactory sealing contact. Globe valves lend themselves to be used in cases of high pressures and temperatures. Of course, the materials used in such cases must be carefully selected. The sealing surfaces of these valves are made of cobalt-chromium alloys, such as the Stellites®, or of other materials such as carbides and ceramics. However, these materials have low resistance to impact. Globe valves are widely used for high-pressure and high-temperature applications. Commercial valves of this type are available for pressures up to 1.034×10^8 N/m² at atmospheric temperatures, and also for pressures of 0.3447×10^8 N/m² at a temperature of 922 K [26].

Since the inner parts of a valve must be contained into the body of the valve, which also contains the fluid under pressure, then it is necessary to provide some means of closure or cover. In addition, an operating mechanism for flow control must be contained into the valve body. Therefore, at least two seals are necessary to a valve. These seals are illustrated in the preceding figure, with reference to a globe valve. However, they are also necessary with valves of other types.

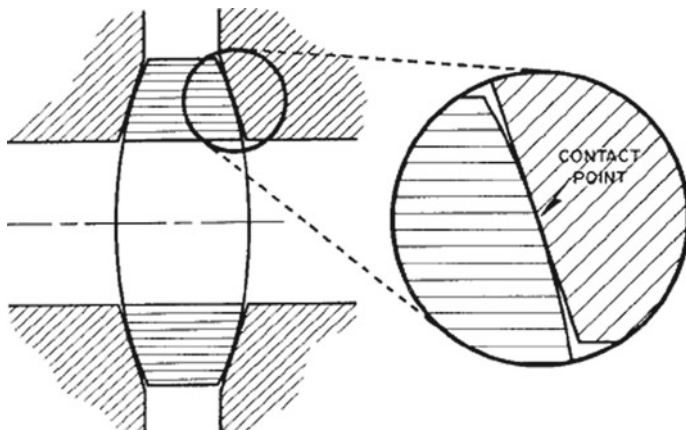
Cover sealing can be obtained in several ways, each of which has its maximum level of pressure and its cost.

A flat gasket for cover sealing, shown on the left-hand side of the following figure, is not suited to either high-pressure or high-temperature applications, because it requires large surfaces. Other types of gaskets which are better suited to these applications are the spiral-wound gaskets and the lens ring gasket. A spiral-wound gasket is shown (right), in comparison with a flat gasket (left), in the following figure, due to the courtesy of NASA [26].



A spiral-wound gasket is made of a V-shaped metallic strip or ribbon mixed with a non-metallic filler material. The metal (usually stainless steel) is wound outwards in a circular spiral, and the filler material (usually graphite or poly-tetra-fluoro-ethylene, whose commercial name is Teflon[®]) is wound in the same manner, but starting on the opposite side. This results in alternating layers of filler and metal. The filler is the sealing element, and the metal provides structural strength to the gasket. For temperatures above 811 K, ceramic fibre fillers have been used [25]. An inner ring and an outer ring made of steel are used on the gasket for centring and controlling compression.

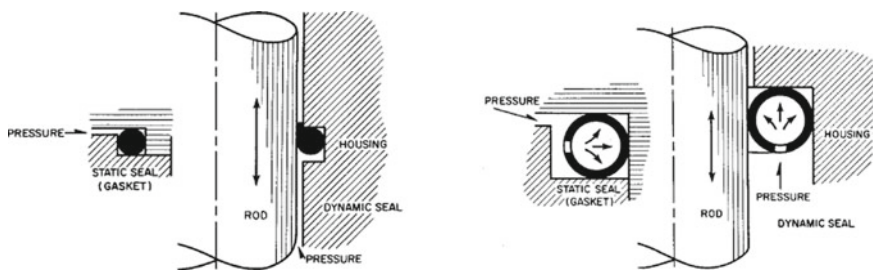
A lens ring gasket is shown in the following figure, due to the courtesy of NASA [26].



A lens ring gasket is made of a sealing metal of lenticular shape which fits into the recesses or grooves of a flange. Since the metallic ring is designed to be softer than the flange grooves, then the gasket deforms plastically under compressive loads instead of the flange. This deformation spreads the gasket faces, and therefore protects the gasket from overstresses.

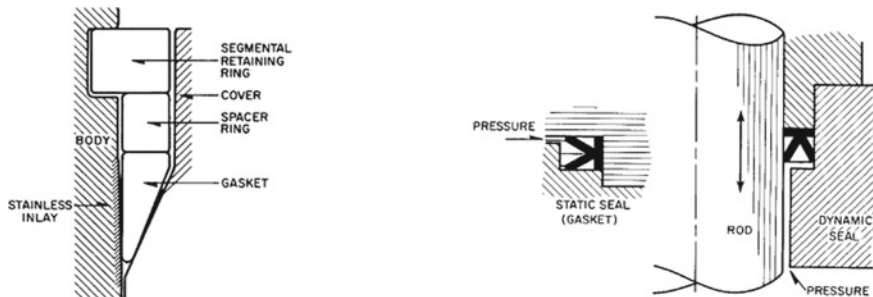
In a spiral-wound gasket and in a lens ring gasket, the sealing stress is proportional to the internal pressure. Lens ring gaskets are suitable for pressures of 6.895×10^8 N/m² and above [26].

The O-ring is another type of static or dynamic seal, in which the sealing stress is proportional to the internal pressure. An O-ring is placed in a groove which is designed to provide a radial or lateral containment, depending upon the specific application. As pressure increases, an O-ring deforms as shown on the left-hand side of the following figure, due to the courtesy of NASA [26]. The same figure also shows, on the right-hand side, a metallic O-ring having holes to admit the fluid under pressure into the ring, in order to make the sealing stress proportional to the pressure exerted by the fluid contained in the valve.



Metallic O-rings may also be coated with elastomers or fluorocarbons to provide better sealing. They are suitable for high pressures, but are also easily damaged, and therefore must be installed in specially designed split grooves [26].

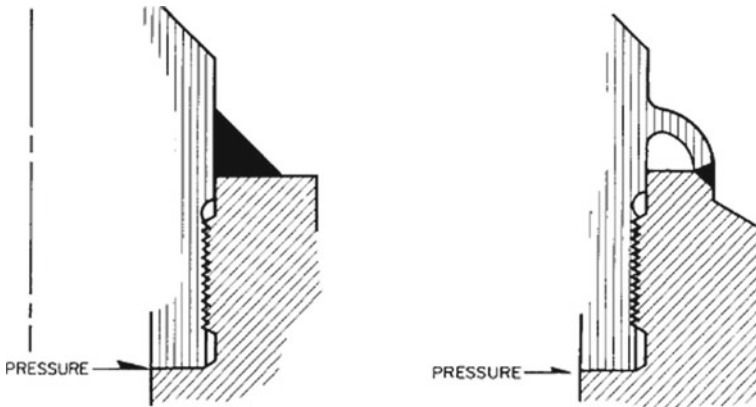
Two further types of seals are the pressure sealing ring and the lapped seal, which are shown on respectively the left-hand side and the right-hand side of the following figure, due to the courtesy of NASA [26].



A pressure sealing ring (left) consists of a segmented retaining ring, a spacer ring, and a gasket. A pressure sealing ring uses the displacement of one of its members to develop the sealing stresses. The gasket is initially wedged against the surface of the body by means of bolts. When the internal pressure exerted by the fluid in the body increases, then the gasket is wedged more and more tightly against its constraints. A lapped seal (right) has a very smooth mating surface whose sealing capability is

reinforced by lapping. This type of seal is suited to either radial or axial installation, as shown in the preceding figure.

Body-cover joints can also be sealed by using a fillet-weld seal or a canopy seal, which are shown on respectively the left-hand side and the right-hand side of the following figure, due to the courtesy of NASA [26].



A fillet-weld seal (left) is performed by depositing a fillet weld bead at the interface of the mating parts. A canopy seal (right) is similar to a fillet-weld seal and is used where a slight movement of the mating parts is expected.

Other types of seals for valves used in high-pressure and high-temperature applications are described in [25, 26].

Valves operating at cryogenic temperatures and seals used for them also require a careful design. As has been shown in Chap. 1, Sect. 1.4, by cryogenic fluids we mean gases which can be liquefied at or below 122 K [27].

Permanent gases, such as methane, oxygen, nitrogen, hydrogen, and helium, change from gas to liquid at atmospheric pressure at the temperatures shown in the following table (due to the courtesy of NIST [28]), called the normal boiling point (NBP). Such liquids are known as cryogenic liquids or cryogens. Liquid helium, when cooled further to 2.17 K or below, becomes a superfluid with very unusual properties associated with being in the quantum mechanical ground state.

Cryogen	Temperature (K)
Methane	111.7
Oxygen	90.2
Nitrogen	77.4
Hydrogen	20.3
Helium	4.2

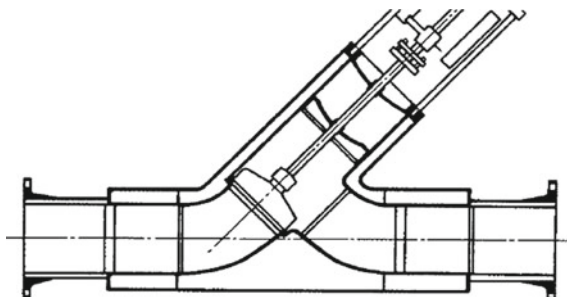
According to Howell and Weathers [25], in the design of valves operating at cryogenic temperatures, the following requirements are to be taken into account:

- reduction of heat transfer from the external environment to the valve, in order to prevent excessive losses of cryogenic fluid by evaporation; and
- reduction of heat transfer between temperature-sensitive parts of valves in cryogenic fluids.

A method often used to thermally insulate temperature-sensitive parts of valves (for example, actuators) from the valve body which contains the cryogenic fluid consists in placing a thermal barrier made of a non-metallic material having a low thermal conductivity (for example, Teflon[®]) between the valve body and the part to be insulated. Ductile metals of low conductivity which are often used for cryogenic valves are austenitic stainless steels (usually the lower-carbon 304, also known as 18/8, and the ever lower-carbon 304L), aluminium alloys, copper, ASTM B-61 and B-62 bronzes, and nickel [26]. In addition to using materials of low thermal conductivity, other methods are also used for the same purpose. These methods are:

- breaking completely the path of heat conduction, by separating the parts which operate at different temperatures by an insulating space (for example, in a broken stem valve, the valve actuator is thermally insulated from the valve body by means of radial bars on the upper stem which drive against axial pins on the lower stem) and enclosing the entire valve in an evacuated chamber;
- using vacuum-jacketed valves;
- increasing the path of heat conduction, by using extended stems and bonnets including long gaseous columns, in order to keep the stem seal packings exposed only to insulating vapour, and not to the cold liquid;
- providing bonnets with integral black-coated fins, to direct heat away through radiation from the packing to the external environment;
- using plastiform insulating foams, made of polystyrene, polyurethane, rubber, silica, and glass, around the valve body; and
- using low-density materials, such as powders and fibres, with gas at atmospheric pressure in the interstitial spaces.

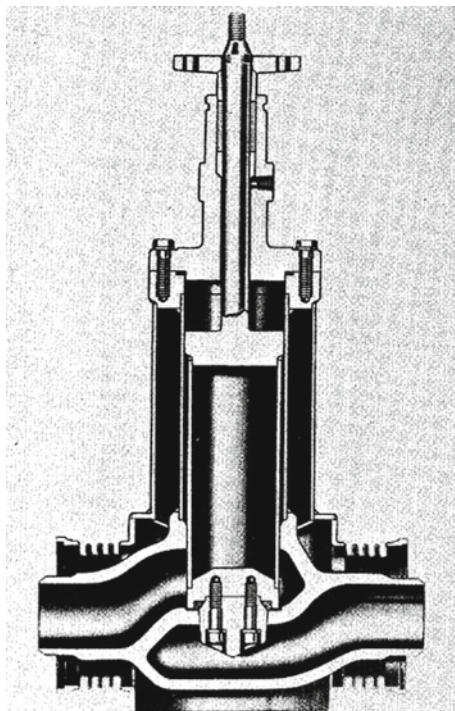
The following figure, due to the courtesy of NASA [26], shows a vacuum-jacketed valve used for cryogenic fluids, where the inner wall surrounds the primary pressure vessel, and the outer wall is of light construction to reduce cool-down mass.



Brightly finished interior surfaces may be used to reduce radiative heat transfer.

In some cases, especially when the cryogenic fluid is liquid helium, a valve is surrounded with a vacuum-jacket, then another cryogenic fluid (usually liquid nitrogen) is circulated in the interstitial space between the two walls to act as a thermal radiation shield, and finally an insulating foam is placed as an outside covering [26]. It is possible to have insulating foam bonded to the surface of the insulation cavity. This type of insulation, usually called “foamed in place” is quite adaptable to valves and other components having irregular surfaces [25]. Trim parts, such as plugs and stems, of valves for cryogenic fluids are often made of stainless steel or Monel®, which is a nickel-copper alloy. Teflon® and Kel-F®/Neoflon® are commonly used for seats. Valves for fluorine have often seats made of copper. Bushings made of Ampco® (aluminium bronze) have been successfully used with stems made of stainless steel. Bushings are also made of Teflon® or glass-impregnated Teflon®. Packing is made of pure or filled Teflon® and Kel-F®/Neoflon®. Welded bellows are sometimes used instead of packings. Gaskets are made of Teflon® or metal-clad Teflon®. Rings made of stainless steel are used in ring-type joint flanges. Fluorine requires soft copper, aluminium 25, or stainless steel for gaskets [26].

The following figure, due to the courtesy of NASA [26], shows a cryogenic fluid valve whose vacuum-insulating jacket encloses the entire body. An expansion bellows for attachment to a piping jacket is provided to prevent the transmission of strains. Air is sealed in the stem cylinder to achieve long, poorly conductive path, and a vapour space is provided between the cylinder and the body extension. Heat transfer is also reduced by the absence of bolts or studs in the valve body [26].



Most of the principal seals considered above for high-pressure and high-temperature applications may also be used for cryogenic fluids. However, special care is necessary because of the different properties of the materials.

The use of soft plastic gaskets is limited to reinforced or laminated Teflon®. Thin gaskets made of hard plastics, such as polyethylene terephthalate (PET), whose trade name is Mylar®, may be used in case of high stress loading. Soft metals, such as copper and aluminium, may be used in case of high shear-stress loading. The following figure, re-drawn from [25], shows two gasket gland designs used for cryogenic service. They are: (left) a rounded-edge seal ring, and (right) a knife-edge shear seal.

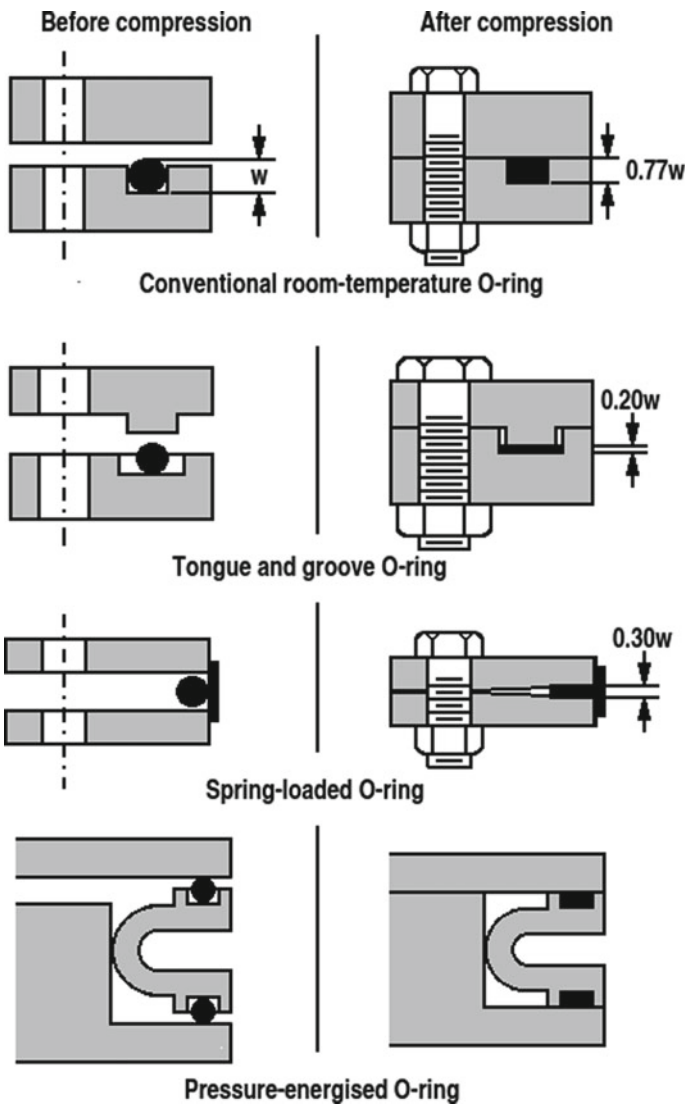


Rounded-edge rings for plastics



Knife-edge shear seal

The following figure, re-drawn from [25], shows some installation techniques for using elastomeric O-rings in cryogenic applications.



Metallic O-rings, either solid or hollow, may be used as seals for cryogenic fluids. In particular, solid rings made of soft metals such as copper, indium, or lead have given the best results. When using indium, care must be taken to confine the gland because of the cold-flow tendency of this metal [25].

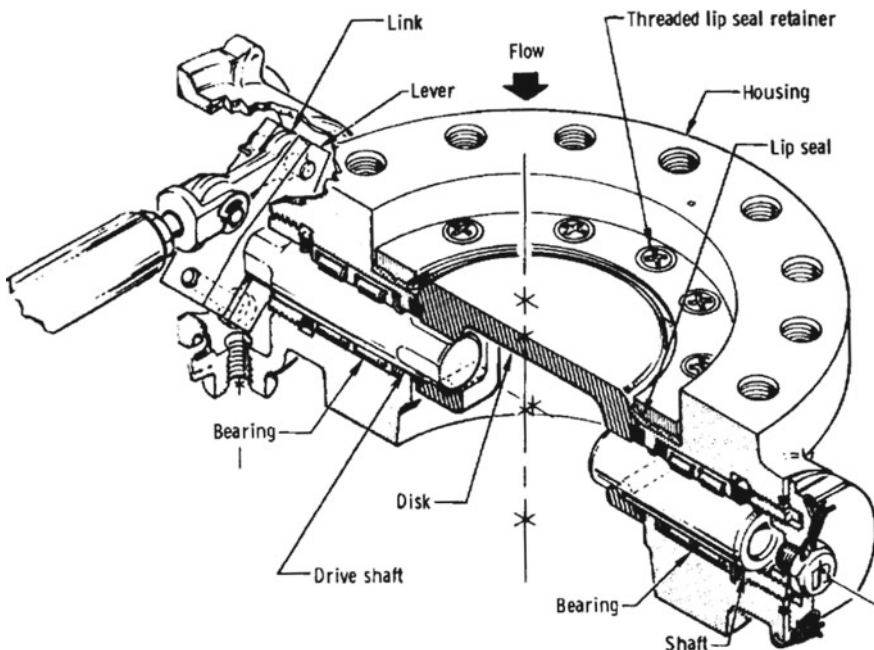
5.9 Design of Propellant Valves

The valves described in the present section are principally used to initiate and terminate the flow of propellants from the tanks to the main combustion chamber and to the gas generator of a rocket engine. Therefore, these valves are often of the open-closed, two-position, normally closed type. However, some valves are also required to control the flow rate of propellants by means of a restriction of variable area. Valves of the latter type are used for thrust-throttle and propellant-mixture-ratio control, because they can continuously vary their operating position, in contrast to shut-off valves, which are either fully open or fully closed.

Requirements for propellant valves are compatibility with propellants, structural strength, absence of leakage in closed position, proper actuation time when opening or closing, and minimum pressure loss.

Apart from the general classification considered in Sect. 5.8, we describe here in particular the most used types of propellant valves, which are butterfly valves, ball valves, poppet valves, Venturi valves, gate valves, and needle valves.

An isometric cross section of a butterfly valve is shown in the following figure, due to the courtesy of NASA [29].

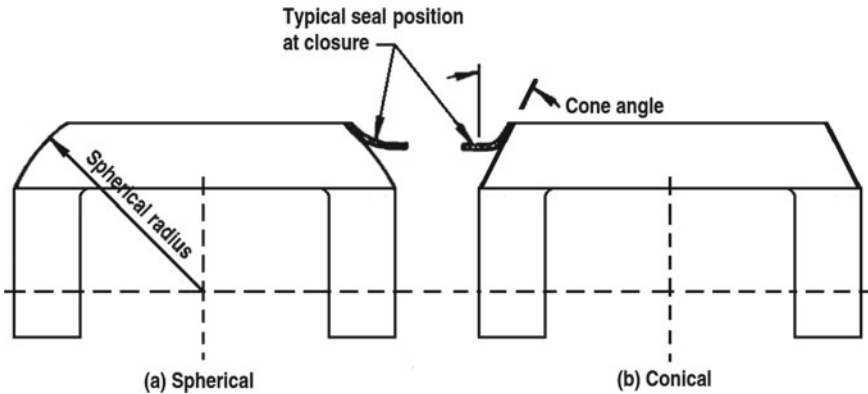


A butterfly valve is used to start, regulate, or stop the motion of a fluid in a duct. With reference to the preceding figure, the movable part of a butterfly valve is a flat element, called the disc, which may be rotated to control the flow through the valve body. The disc can rotate on a single-piece shaft or on a two-piece shaft, which

extends across the diameter of an orifice and supports the disc on both sides. The internal diameter of existing butterfly valves ranges from 50 to 400 mm. These valves are used for propellants at absolute pressures ranging from 1.4×10^5 to 1×10^7 N/m² [3].

For greater rigidity, the shaft may be integral with the disc. The centre of rotation of the disc is usually offset, as shown in the preceding figure, in order to allow the disc to rotate off the primary seal. For low leakage, a plastic lip seal (described in Chap. 4, Sect. 4.13) is usually employed in the valve housing.

The discs of butterfly valves have spherical or conical shapes, as shown in the following figure, re-drawn from [29]. A disc of spherical shape (left) has better performance, but is more expensive to fabricate. A disc of conical shape (right) is more subject to leakage because of greater wear [29].



A butterfly valve is operated by an actuator of the piston type, through a connecting link and shaft crank arm. The actuating power is the pressure exerted by either a non-cryogenic liquid propellant or an inert gas, and is controlled by a pilot valve. The shaft and the pins are made of stainless steel, whereas most of the other parts are made of aluminium alloys. Butterfly valves oppose low resistance to the motion of propellants flowing through them.

The characteristic area A_c (m²) of a butterfly valve results from

$$A_c = \pi \frac{d_s^2}{4} - A_g$$

where d_s (m) is the inside diameter of the valve seat lip seal, and A_g (m²) is the projected valve disc area at the fully open position. The values of A_c range from $0.65 \times (\pi d_s^2/4)$ for a 50 mm diameter valve to about $0.87 \times (\pi d_s^2/4)$ for a 300 mm diameter valve [3].

A butterfly valve maintains a smooth flow over a wide range of angular positions of the valve disc. The values of the resistance coefficient k as a function of the opening angle are given by the manufacturer of the valve or can be found, for example, in [30, 31].

RP-1 is used sometimes as the actuating fluid for liquid-oxygen valves in rocket engines burning RP-1 with liquid oxygen. In this case, it is necessary to prevent RP-1 from freezing at the actuator by using a heater. A potentiometer is often attached to the drive shaft of a butterfly valve to indicate continuously the position of the valve disc.

The torque required to rotate the shaft and the disc of a butterfly valve depends on the hydraulic torque T_h (Nm) and on the frictional torque T_f (Nm) acting on the valve. The frictional torque opposes always rotation. The hydraulic torque (in spite of the offset of the disc, which is always placed on the side opposite to the direction of the flow, as shown in the preceding figures) acts in the closing direction for most angular positions (from $\pi/20$ to $4\pi/9$ rad) of the disc.

The opening torque T_o (Nm) and the closing torque T_c (Nm) required to operate a butterfly valve can be expressed as follows

$$\begin{aligned} T_o &= T_f + T_h \\ T_c &= T_f - T_h \end{aligned}$$

where the hydraulic torque T_h is supposed to act on the disc of the valve in the closing direction.

The frictional torque T_f depends on the difference of pressure on the two faces of the disc and also on the projected area of the disc, which in turn depends on the angular position of the disc in the valve. The value of the frictional torque can be estimated as follows

$$T_f = k_f r_s f_m d_s^2 \Delta p$$

where k_f is the friction factor coefficient whose value is determined experimentally, r_s (m) is the radius of the shaft at the bearing section, f_m is the coefficient of friction between the shaft and the bearing, d_s (m) is the inside diameter of the valve seat lip seal, and Δp (N/m²) is the difference of pressure across the disc.

The value of the hydraulic torque can be estimated as follows

$$T_h = k_h d_s^3 \Delta p$$

where k_h is the hydraulic coefficient whose value is determined experimentally and depends on the angular position of the disc in the valve.

In the practical design of a butterfly valve, the actuator is required to provide a torque whose value ranges from two to three times the maximum estimated value necessary to open or close the valve. In addition, at the start of the opening stroke, the actuator must overcome the static friction forces due to all seals. The opening and closing times of butterfly valves range from 0.02 to 0.2 s [3].

As an application of the concepts discussed above, it is required to determine the torques necessary to open and close a butterfly valve having the following data: radius of the valve shaft at the bearing section $r_s = 0.02032$ m, inside diameter of

the valve seat lip seal $d_s = 0.1956$ m, coefficient of friction between the shaft and the bearing $f_m = 0.05$. The data found experimentally are given below.

Disc angle (rad)	Δp (N/m ²)	k_f	k_h
$\pi/36$	7.295×10^6	0.78	0.00111
$\pi/12$	5.302×10^6	0.78	0.00255
$2\pi/9$	6.033×10^5	1.57	0.0125
$17\pi/36$	1.724×10^5	3.61	-0.01164

By substituting these data in the equation $T_f = k_f r_s f_m d_s^2 \Delta p$ we find the following values of the frictional torque T_f at the given angles:

$$(\pi/36) \quad T_f = 0.78 \times 0.02032 \times 0.05 \times 0.1956^2 \times 7.295 \times 10^6 = 221.2 \text{ Nm}$$

$$(\pi/12) \quad T_f = 0.78 \times 0.02032 \times 0.05 \times 0.1956^2 \times 5.302 \times 10^6 = 160.8 \text{ Nm}$$

$$(2\pi/9) \quad T_f = 1.57 \times 0.02032 \times 0.05 \times 0.1956^2 \times 6.033 \times 10^5 = 36.82 \text{ Nm}$$

$$(17\pi/36) \quad T_f = 3.61 \times 0.02032 \times 0.05 \times 0.1956^2 \times 1.724 \times 10^5 = 24.19 \text{ Nm}$$

Likewise, by substituting these data in the equation $T_h = k_h d_s^3 \Delta p$ we find the following values of the hydraulic torque T_h at the given angles:

$$(\pi/36) \quad T_h = 0.00111 \times 0.1956^3 \times 7.295 \times 10^6 = 60.60 \text{ Nm}$$

$$(\pi/12) \quad T_h = 0.00255 \times 0.1956^3 \times 5.302 \times 10^6 = 101.2 \text{ Nm}$$

$$(2\pi/9) \quad T_h = 0.0125 \times 0.1956^3 \times 6.033 \times 10^5 = 56.44 \text{ Nm}$$

$$(17\pi/36) \quad T_h = -0.01164 \times 0.1956^3 \times 1.724 \times 10^5 = -15.02 \text{ Nm}$$

The torques T_o required to open the butterfly valve at the given angles result from the equation $T_o = T_f + T_h$ as follows

$$(\pi/36) \quad T_o = 221.2 + 60.60 = 281.8 \text{ Nm}$$

$$(\pi/12) \quad T_o = 160.8 + 101.2 = 262.0 \text{ Nm}$$

$$(2\pi/9) \quad T_o = 36.82 + 56.44 = 93.26 \text{ Nm}$$

$$(17\pi/36) \quad T_o = 24.19 + (-15.02) = 9.17 \text{ Nm}$$

Likewise, the torques T_c required to close the butterfly valve at the given angles result from the equation $T_c = T_f - T_h$ as follows

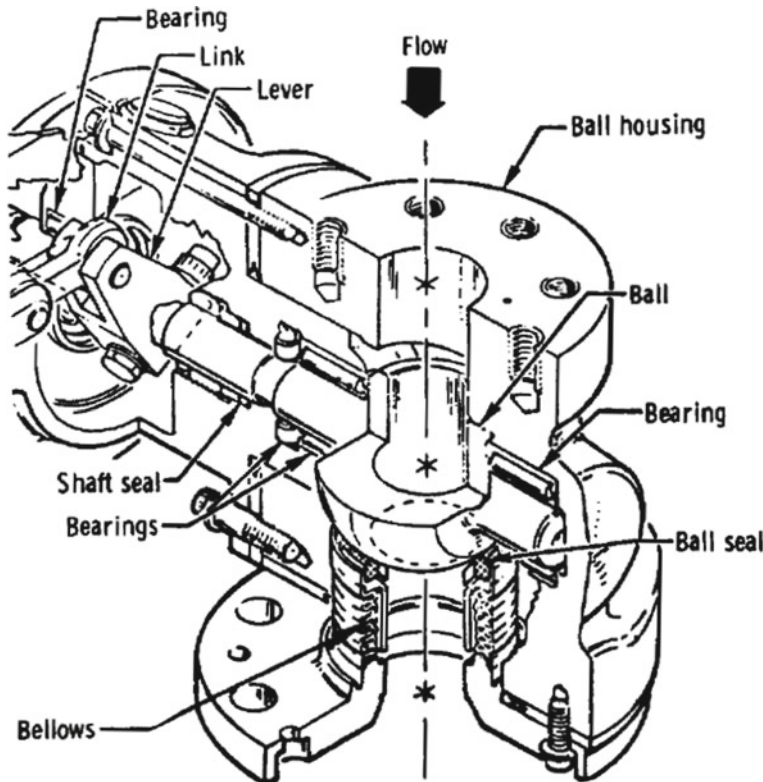
$$(\pi/36) \quad T_c = 221.2 - 60.60 = 160.6 \text{ Nm}$$

$$(\pi/12) \quad T_c = 160.8 - 101.2 = 59.6 \text{ Nm}$$

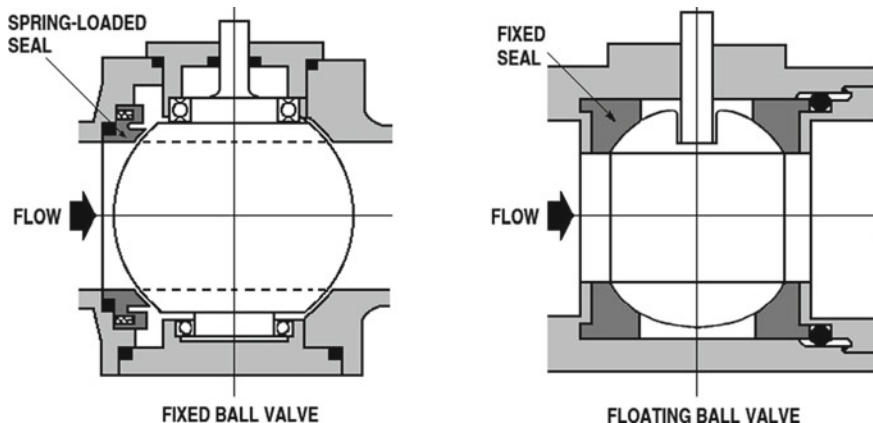
$$(2\pi/9) \quad T_c = 36.82 - 56.44 = -19.62 \text{ Nm}$$

$$(17\pi/36) \quad T_c = 24.19 - (-15.02) = 39.21 \text{ Nm}$$

An isometric cross section of a ball valve is shown in the following figure, due to the courtesy of NASA [29].



A ball valve is substantially a sphere provided with a port and fitting into a cup-shaped housing, such that a rotation of this sphere through a right angle changes the position of the valve from open to closed. In other words, when the valve is turned to the open position, the ball rotates to a point in which the hole through the ball is aligned with the flow openings (inlet and outlet) of the valve body. When the valve is turned to the closed position, the ball rotates to a point in which the hole through the ball is perpendicular to the flow openings of the valve body, and therefore the flow is stopped. There are two common types of this valve. They are the fixed ball valve and the floating ball valve, which are shown in the following figure, re-drawn from [25].



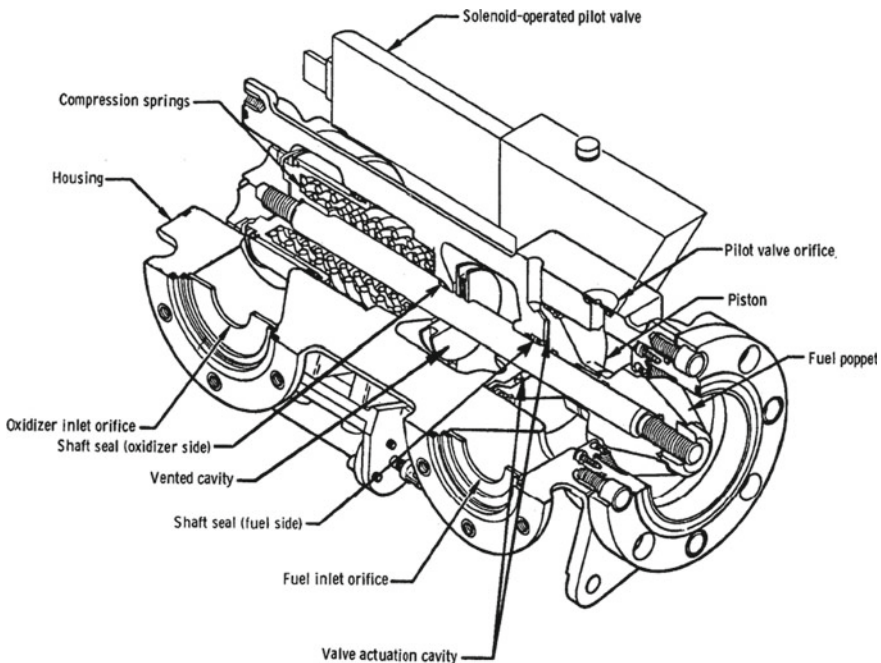
In a fixed ball valve (left), the ball is supported by fixed bearings, and the seal is spring-loaded against the ball. The seal is mounted on the upstream side of the ball, and is usually designed to act in one direction only. However, another spring-loaded seal may also be mounted on the downstream side of the ball, in order to obtain a bi-directional sealing.

In a floating ball valve (right), the ball is supported by fixed seals, and the seating force is provided by the fluid under pressure, which pushes the ball against the seat. In a floating ball valve, the seals are placed both upstream and downstream of the ball, and therefore the valve may be used in either direction. The use of floating ball valves is confined to low-pressure applications.

The materials used for the body of a ball valve may be metals or plastics, such as Unplasticised Polyvinyl Chloride (UPVC). The ball may be made of metal or plastic. Metallic balls have highly polished, hard chrome surfaces. Seal materials may be plastics or elastomers. Teflon® is the most commonly used material for seals, due to its properties of high resistance to corrosion and low friction.

The principal advantage of ball valves is a low pressure drop. They also have a very good leakage control, and can be designed to operate equally well with the flow in either direction. On the other hand, the actuating forces required by them are high, because these valves cannot be pressure-balanced [25].

An isometric cross section of a poppet valve, used for the AJ10-138 rocket engine, is shown in the following figure, due to the courtesy of NASA [32].

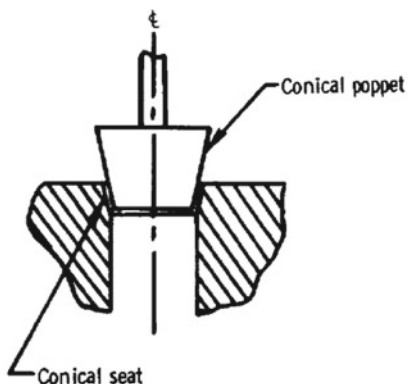


Poppet valves are those used in cylinders of car engines. They are similar to globe valves (described in Sect. 5.8), because for both of them the movable part of the valve travels perpendicularly to a plane through the seating surface. According to Howell and Weathers [25], the term poppet valve is used synonymously with globe valve.

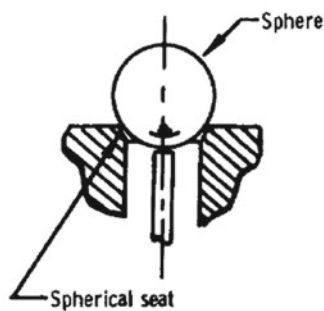
The designer of a poppet valve chooses the types of sealing surfaces, either hard or soft, which are best suited for the poppet and for the seat. These surfaces are said to be hard or soft depending on the type of material used. A hard sealing surface is made of a material (metal, ceramic, or cermet, the last being a composite material made of ceramic and metallic materials) which does not permanently yield or deform except with wear. By the way, flexible metallic discs are a special type of hard sealing surface. A soft sealing surface is made of plastic or elastomeric materials. Possible configurations for combinations of hard and soft sealing surfaces are indicated below.

Poppet sealing surface	Seat sealing surface	Configuration designation
Hard	Hard	Hard-on-hard
Hard	Soft	Hard-on-soft
Soft	Hard	Hard-on-soft

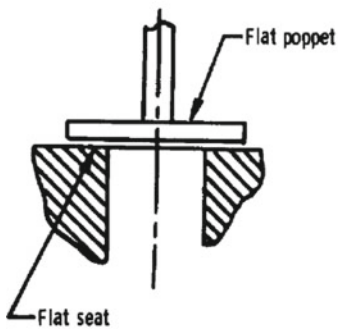
The following figure, due to the courtesy of NASA [29] shows four examples of hard-on-hard sealing configurations.



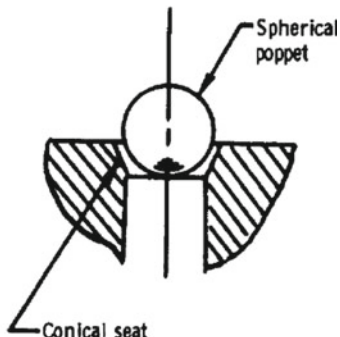
(a) Conical on conical.



(b) Spherical on spherical.



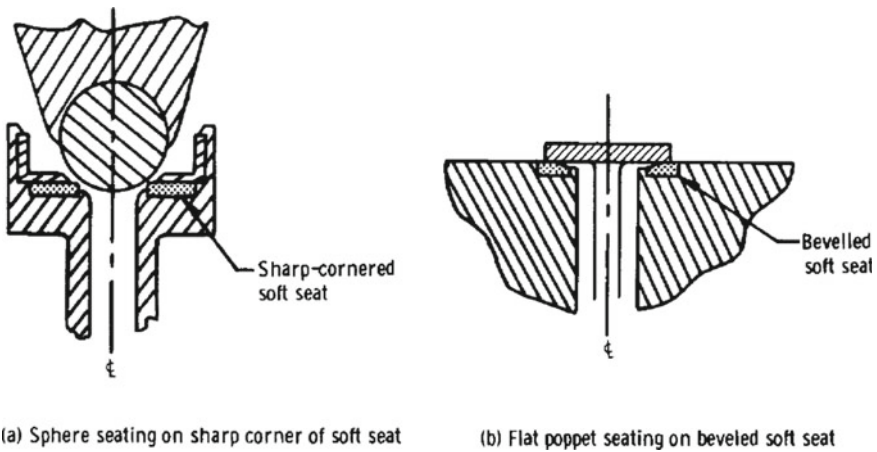
(c) Flat on flat.



(d) Spherical on conical.

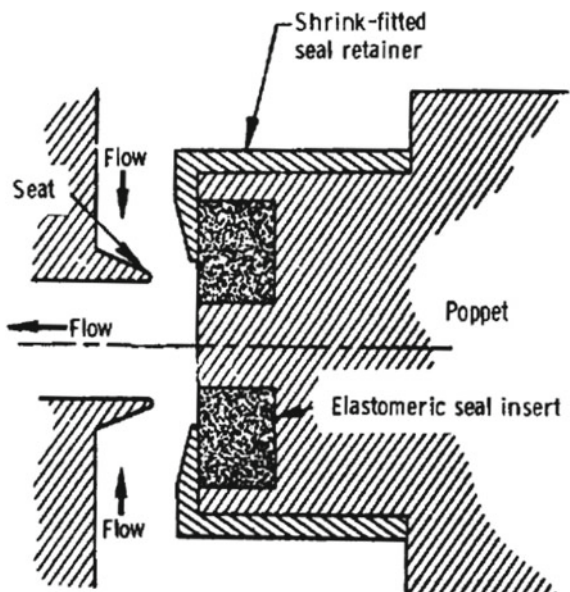
A poppet valve in which the hard sealing surface meets a soft sealing surface may incorporate the soft sealing surface as an insert of elastomer or plastic in the housing. This type of design is known as a soft-seat poppet.

The following figure, due to the courtesy of NASA [29] shows typical configurations for a soft-seat poppet.



It is also possible to incorporate the soft sealing surface either as an integral part of the poppet (for example, of a plastic poppet) or as an insert of elastomer or plastic in the poppet. This type of design is known as a soft poppet. In either location, the soft sealing insert is designated as a seal.

The following figure, due to the courtesy of NASA [29] shows an elastomeric seal insert retained in a poppet by a shrink-fit mechanical retainer.



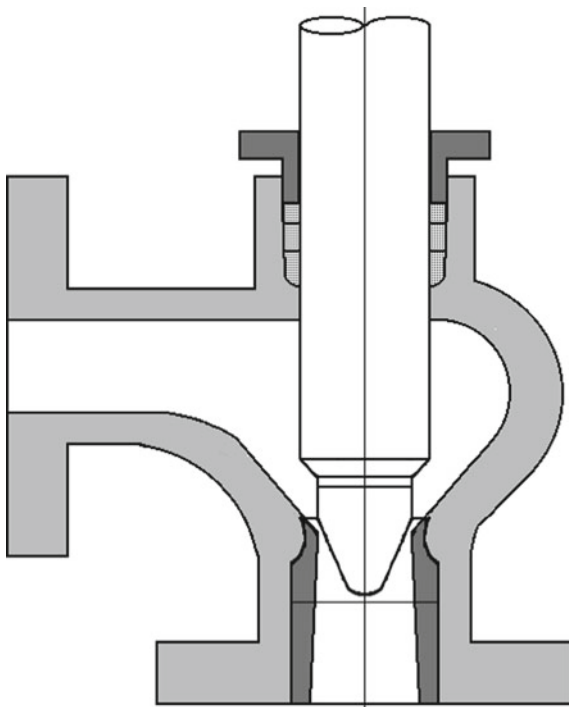
A large flow area in a poppet valve is provided with short travel of the poppet. This makes it possible to use actuators such as solenoids or diaphragms, which are short-stroke devices. A very good leakage control can be achieved by using hard or

soft seals, as has been shown above. When hard seals are used, great care must be taken to eliminate contamination from the fluid and from the duct upstream of the valves.

A poppet valve can be pressure-balanced by using two poppets which are on the same stem and seat on separate seats. By so doing, the pressure acting on the top of one poppet provides the counterbalancing force acting on the bottom of the other poppet. The same result can also be obtained by providing the poppet stem with a pressure-balancing piston area, or by making the poppet stem diameter equal to the seating diameter. However, it is practically impossible to obtain complete pressure balance under both shut-off and flow conditions.

A poppet valve is lighter than valves of other types for many applications, due to the small stroke of its actuator. For example, ball and butterfly valves require a rotation through a right angle for full stroke, and therefore need a larger associated mechanism. A poppet valve is used when the valve is desired to open rapidly from zero to full flow with a short travel of its movable element. Of all types of poppet valve, the in-line valve is the one which has the best flow properties. The body of a poppet valve may be either cast on one piece or split. In the latter case, the body halves are joined by bolts [25].

A cross section of a cavitating Venturi valve is shown in the following figure, re-drawn from [25].



A cavitating Venturi valve is used to control the flow rate of a propellant in a rocket engine as a function of the pressure upstream of the valve and of the throat area. When the minimum pressure of a liquid propellant is made to decrease below its vapour pressure at the throat of a Venturi tube, then cavitation occurs and the propellant evaporates. In case of cavitation, the propellant flow rate is independent of the downstream pressure. Cavitation occurs by decreasing the pressure of a liquid propellant at the throat of a Venturi tube to such an extent that nearly all of the upstream pressure head of the fluid is converted into velocity head. When this occurs, the only static pressure remaining in the fluid at the throat is equal to the vapour pressure of the fluid itself. In such conditions, when the upstream pressure of the fluid is kept constant, a further decrease in downstream pressure does not result in increased flow rate, because cavitation at the throat maintains the pressure equal to the vapour pressure of the fluid.

In other words, the flow rate through the valve remains constant for a given throat area and for a given upstream pressure, independently of the downstream pressure, provided that the downstream pressure does not increase above the level in which cavitation occurs. In practice, the downstream pressure must be less than 85% of the upstream pressure in order for cavitation to occur [25].

Cavitating Venturi valves are used in rocket engines when it is desired to prevent variations of propellant flow rate caused by variable back pressure on the control valve. In the design of a cavitating Venturi valve used to control flow rates, it is necessary to know the total pressure p_T (N/m^2) and the vapour pressure p_v (N/m^2) of the propellant whose flow rate is to be controlled. The ratio

$$\frac{p_T - p_v}{\rho g_0}$$

is the total pressure head available for conversion to velocity head in the Venturi tube. In the preceding equation, ρ (kg/m^3) is the density of the propellant at the given temperature, and $g_0 = 9.80665 \text{ m/s}^2$ is the acceleration of gravity on the surface of the Earth. The total pressure head $(p_T - p_v)/(\rho g_0)$ is used to determine the theoretical value v_t (m/s) of the propellant velocity at the throat of the Venturi tube, as follows

$$\frac{p_T - p_v}{\rho g_0} = \frac{v_t^2}{2g_0}$$

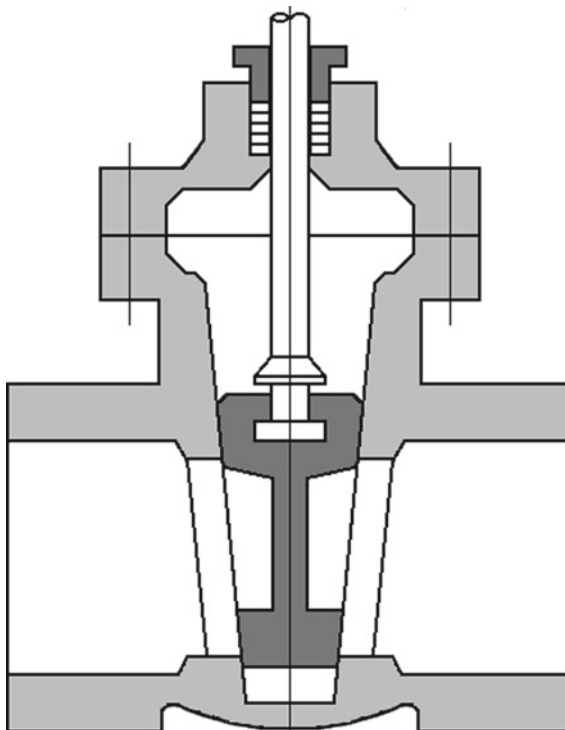
The actual volume flow rate q (m^3/s) of propellant through the Venturi tube can be determined by assuming a discharge coefficient of 0.93 [25]. Therefore, the actual volume flow rate is

$$q = 0.93 A_t v_t = 0.93 A_t \left[\frac{2(p_T - p_v)}{\rho} \right]^{\frac{1}{2}}$$

where A_t (m^2) is the area of the throat of the Venturi tube.

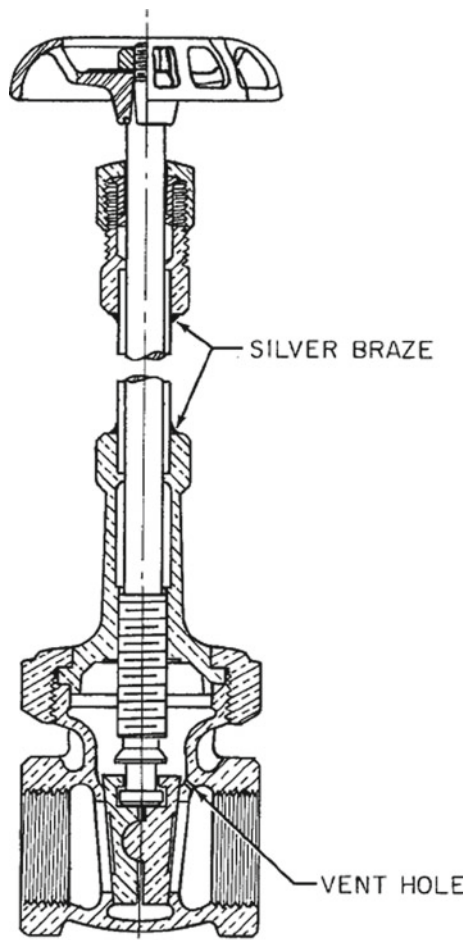
It has been found experimentally [25] that the best pressure recovery through a cavitating Venturi valve is obtained when the included angle of the diffuser cone is in the range going from $\pi/36$ rad (5°) to $\pi/30$ rad (6°). Venturi valves have been used successfully in rocket engines for cryogenic and storable propellants [3].

A cross section of a gate valve is shown in the following figure, re-drawn from [25].

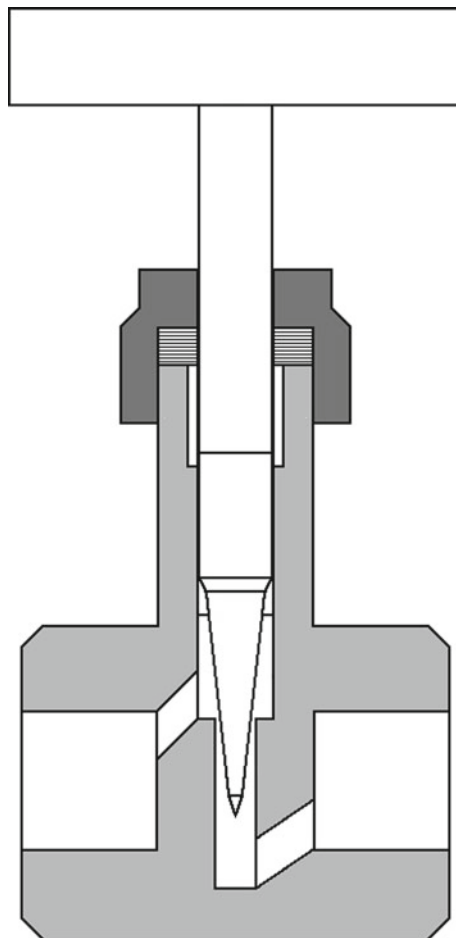


Gate valves have been considered in Sect. 5.8 from the point of view of sealing and leakage control. Their use as propellant valves is discussed below. Gate valves have a flat plate which moves perpendicularly to the fluid stream in a duct in order to open or close the passage of the fluid through them. They may be operated by any of the usual actuators used for this purpose. Quick-return mechanisms have been used when it was desired to open or close such valves at different flow rates. When the plate is completely removed from the fluid stream, a gate valve opposes little or no resistance to the flow. Consequently, the principal advantage of a gate valve is unrestricted fluid stream, and therefore low pressure drop when the valve is in the wide open position. When a gate valve is in the closed position, the contact surface between the plate and the seal extends along the whole circumference of the tube cross section, and therefore this valve provides good sealing, which results in little or no leakage across the plate.

A gate valve has a short distance between the sections of inlet and outlet in the direction of the flow. On the other hand, it has poor throttling properties and is also subject to erosion when it is in the near closed position. Its response is slow, because of the large travel and the high actuation forces due to friction. Consequently, gate valves are normally used as on-off mechanisms. They have been designed for propellant line pressures up to $2 \times 10^7 \text{ N/m}^2$ [3] and for low propellant flow applications (for example, for gas generator control and ground support services). In ground support systems, they are used as shut-off or block valves in systems subject to moderate pressures. This is because they cannot be balanced. Gate valves have also been used for cryogenic propellants. An example is shown in the following figure, due to the courtesy of NASA [26]. The vent hole on the inlet end of this gate valve is necessary to avoid trapping liquid in the bonnet [26].



A cross section of a needle valve is shown in the following figure, re-drawn from [25].



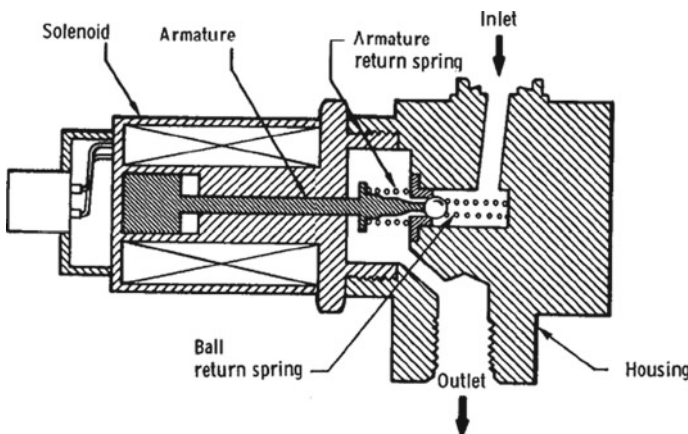
A needle valve is a variation of a globe valve. In comparison with the latter, a needle valve has a control orifice of smaller diameter, and a longer and slimmer movable element, in order to permit throttling. A needle valve is used for regulating the flow of small quantities of fluid, for blending carefully a fluid with another, and for speed control of pumps and actuators. The construction property of a needle valve which makes it apt to be used for a fine flow control is the plug of the valve, which moves inside the seat ring and has long tapered slots milled and ground into its surface. The plug remains inside the seat ring at all times, even when the valve is in the wide-open position, in order for the flow through the valve to be closely controllable by the relative position of the long plug and its gradually tapering grooves. A tight shut-off of a needle valve depends on the concentric position of the plug with the seat at the

point of closure. In case of need for a repeated shut-off of a needle valve, a good sealing is obtained by using a disc made of rubber or plastic which closes against a metallic seat. When a non-metallic seal cannot be used due to high temperatures or to the necessity of handling a corrosive fluid, then a non-rotating plug may be designed for closing against the seat, or a device may be used to limit the closing force applied to the stem to the amount strictly necessary for a tight shut-off. Needle valves are used in lines whose diameter is less than 20 mm, a typical value being 6.35 mm. They are used for temperatures ranging from cryogenic values to 811 K and above, and for pressures ranging from vacuum to 2×10^8 N/m² and above [25].

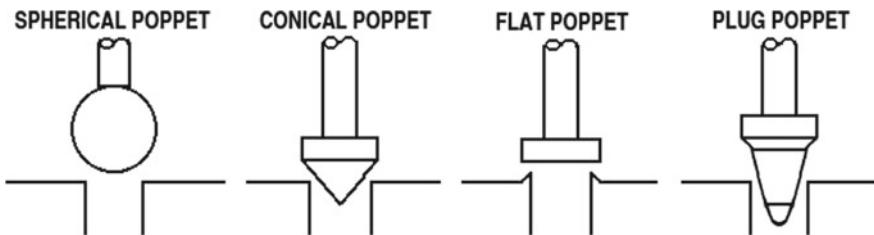
5.10 Design of Pilot Valves

Pilot valves are used to control fluids, which in turn control other components of hydraulic circuits (for example, valves for propellants) or a sequence of events occurring in a rocket engine (for example, the admission of fuel for ignition purposes). The control action performed by a pilot valve is of the on-off, open-loop type. The most common types of pilot valves are solenoid valves, pressure-actuated valves, and position-actuated valves in two-way, three-way, and four-way configurations.

A solenoid valve is an electromagnetic device having a solenoid, which is a helically wound coil of wire, a movable cylindrical core of ferromagnetic material mounted coaxially within the coil, a poppet, and a return spring. This core is called the plunger. When the coil conducts no electric current, the compressed spring closes a small orifice by means of the poppet. When a voltage is applied to the ends of the coil, the electric current flowing through the coil generates a magnetic field, which exerts a force on the plunger. This force pulls the plunger toward the centre of the coil, thereby opening the orifice. The following figure, due to the courtesy of NASA [32], shows a cross section of a solenoid valve having a spherical poppet.



The following figure, re-drawn from [25], shows various shapes of poppets which can be actuated by a solenoid in a pilot valve.



Solenoid actuators can be used not only for simple, two-port, on-off valves, but also for multi-passage valves, in which the flow is directed to three or four ports, as required, as the sequel will show. Solenoid on-off valves are either normally open or normally closed, where the normal position of a valve is the position of its movable element with respect to the upstream pressure when no electric power is applied to the solenoid. In the presence of an electric power, the solenoid places the valve to the desired position by attracting a magnetic core attached to the valve stem. When the electric power is removed, a spring pushes back the magnetic core to its normal position.

Directly acting solenoid valves have response times ranging from 5 to 50 ms [25]. A large opening can be obtained through a short stroke of the movable element. The electric current required to operate these valves depends on their size, on the difference of pressure, and on the response required. Their leakage control is very good, particularly when a soft seat is used. When a hard seat is used, it is advisable to lap the seat parts. Solenoid valves do not require external dynamic seals, and have a very long operating life, of the order of magnitude of hundreds of thousands of cycles without degradation of performance [25].

According to Huzel and Huang [3], the following equations apply to the case of a flat-faced, plunger-type magnetic core

$$F = \frac{B^2 A}{C}$$

$$B = \frac{f P N i}{G}$$

where F (N) is the attracting force which acts on the plunger in its normal position, B (Wb/m^2) is the magnetic flux density in the air gap, A (m^2) is the cross-sectional area of the plunger, C is a factor comprising constants and allowances for stray flux (a value of 2.505×10^{-6} is applicable to round, flat-faced, plunger-type magnets), f is a leakage factor of the magnetic flux, whose value is less than unity and depends on the magnetic circuit, P is a factor comprising constants and the permeability of the fluid in the gap G (m) between the core and the armature (a value $P = 1.255 \times$

10^{-6} applies to an air gap), N is the number of coil turns, and i (A) is the electric current applied to the coil.

The radiating surface of a solenoid valve should be sufficiently large to prevent an overheating of the coil. For this purpose, the resistance of the conductor should be designed according to the maximum allowable temperature. It is necessary to use appropriate seals in order to prevent the propellants from contaminating the coil. When the plunger of a solenoid valve is designed to be in contact with the core in the absence of electric power, then it is also necessary to cover the face of the plunger with a layer of non-magnetic material to avoid sticking [3].

As an application of the concepts discussed above, it is required to determine the electric resistance of the coil for a solenoid valve to be used in a rocket engine.

The following data are known: the required actuating force at the start of the stroke is $F = 120.1$ N, the electric supply has a voltage of 28 V direct current, the maximum current is $i_{\max} = 2$ A, the air gap between the solenoid core and the plunger of the valve is $G = 0.00127$ m, the diameter of the plunger is $d = 0.01422$ m, and the leakage factor of the magnetic flux is $f = 0.7$.

The area of the plunger results from

$$A = \frac{1}{4}\pi d^2 = 0.25 \times 3.1416 \times 0.01422^2 = 0.0001588 \text{ m}^2$$

By substituting the value of A found above, $F = 120.1$ N, and $C = 2.505 \times 10^{-6}$ in the equation

$$F = \frac{B^2 A}{C}$$

and solving for B , we find

$$B = \left(\frac{FC}{A} \right)^{\frac{1}{2}} = \left(\frac{120.1 \times 2.505 \times 10^{-6}}{0.0001588} \right)^{\frac{1}{2}} = 1.376 \text{ Wb/m}^2$$

By substituting the value of B found above, $f = 0.7$, $P = 1.255 \times 10^{-6}$, and $G = 0.00127$ m in the following equation

$$B = \frac{f P N i}{G}$$

and solving for Ni , we find

$$Ni = \frac{BG}{fP} = \frac{1.376 \times 0.00127}{0.7 \times 1.255 \times 10^{-6}} = 1989 \text{ turns A}$$

Taking the value $i = 1.4$ A for the current in the coil, the corresponding number of turns is

$$N = \frac{Ni}{i} = \frac{1989}{1.4} = 1421$$

The resistance of the conductor used for the coil is

$$R = \frac{V}{i} = \frac{28}{1.4} = 20 \Omega$$

We use a copper wire AWG No. 26 for the coil. In [33], we find the following data, at a temperature $T = 293$ K, for this wire: diameter $d = 0.4049$ mm, area $A = \frac{1}{4}\pi d^2 = 0.1288$ mm 2 , and resistance per metre $R = 0.1336$ Ω/m.

In order for the coil to have a resistance of 20 Ω, the length L of the wire must be

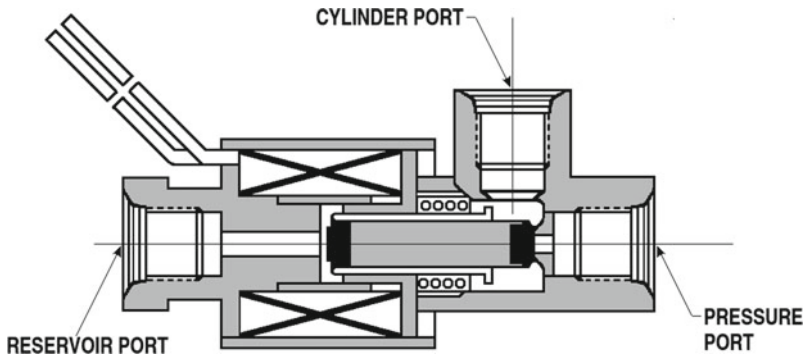
$$L = \frac{20}{0.1336} = 149.7 \text{ m}$$

Since the wire has $N = 1421$ turns, then the average diameter D of each turn results from

$$D = \frac{L}{N\pi} = \frac{149.7}{1421 \times 3.1416} = 0.03353 \text{ m}$$

The pilot valve described above is a two-way valve, which can be either fully open or fully closed. Other pilot valves are multiple-passage valves, which can start, stop, and divert the motion of a fluid between three or more alternate paths. These valves are described below.

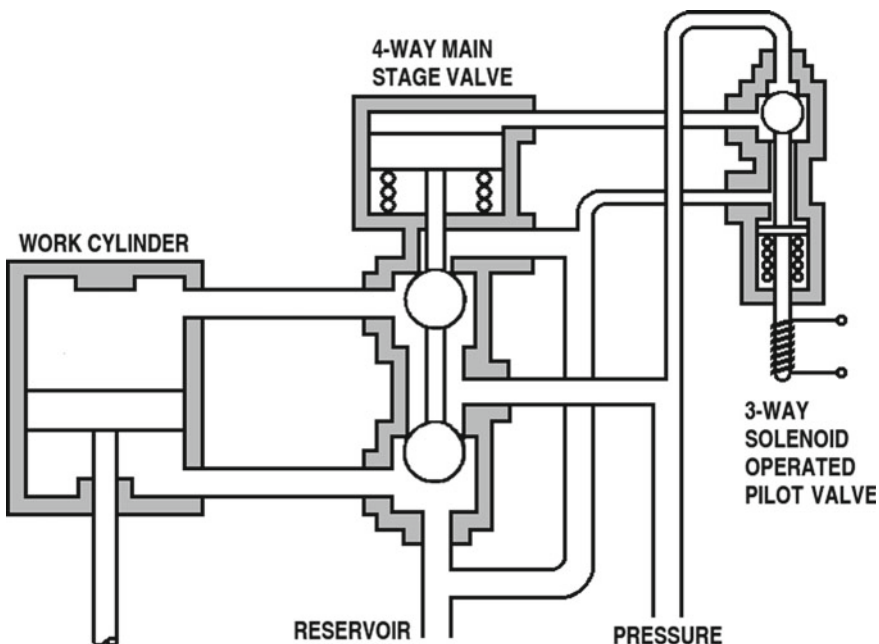
Multiple-passage valves are used to control fluids moving to and from actuating cylinders. They are also used to control the direction of flow when it is necessary to switch or direct it between various paths. These valves are known as three-way valves, four-way valves, diversion valves, selection valves, sequence valves, and shuttle valves. Their method of actuation may be manual, mechanical, hydraulic, pneumatic, or electrical. They operate in two or more discrete positions, which change only when these valves are shifted. Their mode of operation is only of the on-off type. Therefore, they cannot be used in proportional or throttling mode. The name three-way valve or four-way valve specifies the number of ports in a valve. The following figure, re-drawn from [25], shows a three-way valve (designed by Valcor Engineering Corporation) of the poppet type, which is actuated by a solenoid.



The valve illustrated above has a common port (the cylinder port), which can be connected to either one of two alternate ports (the pressure port and the reservoir port) when the non-connected port is closed. The poppet, when actuated in one direction, opens the cylinder port to the pressure port and closes it to the reservoir port. The same poppet, when actuated in the other direction, opens the cylinder port to the reservoir port and closes it to the pressure port. The cylinder port of a three-way valve is used to control a single-acting cylinder.

A four-way valve is a valve having four external ports arranged so that there are two simultaneous flow paths in the valve. The ports of a four-way valve are identified as pressure port, reservoir port, and two cylinder ports. A four-way valve is used to actuate a double-acting cylinder. For this purpose, the valve is connected so that, when pressure is applied to one of the two cylinder ports, then the other cylinder port is connected to the reservoir, and vice versa. Four-way valves are normally two-position or three-position valves. In a three-position, four-way valve, there is a central position in which all ports are closed.

The following figure, re-drawn from [25], shows how multiple-passage valves can be used to control the position of a pneumatic piston-cylinder.



The pilot stage valve (right) is a three-way, solenoid-operated, ball-type poppet valve. The main stage valve (centre) is a four-way, two position, ball-type poppet valve operated by means of a single-acting cylinder, which in turn is actuated by the pilot stage valve. When the solenoid carries no current, then the actuation cylinder of the main stage is not connected with the pressure port, and the work cylinder (left) is in the down position. When the solenoid carries a current, then the actuation cylinder of the main stage is connected with the pressure port and therefore moves down, thereby connecting the upper end of the work cylinder with the reservoir port and the shaft end of the work cylinder with the pressure port, and therefore the work cylinder moves up.

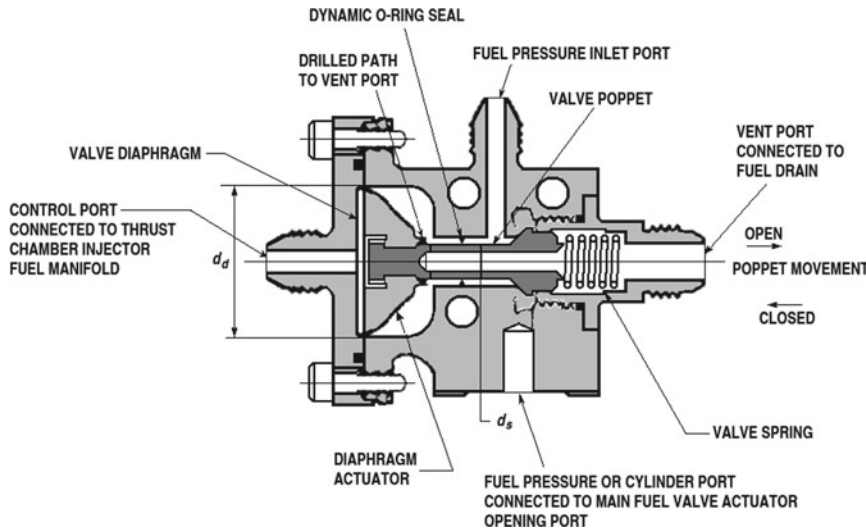
A diversion valve is a three-way valve, such that the common port is the pressure port. A flow can be diverted by a diversion valve to either one of two alternate paths.

A selection valve is similar to a diversion valve, but the number of alternate paths to which the flow from the pressure port can be diverted is unlimited.

A sequence valve is a valve which directs a flow in a pre-determined sequence between two or more paths.

A shuttle valve is a sequence valve which is actuated by pressure, so that, when a desired pressure has been reached, the valve is automatically actuated, directing a flow to two or more paths.

Huzel and Huang [3] describe two examples of multiple-passage valves used for rocket engines. The first example concerns a pressure-actuated, three-way pilot valve, which may be used as an ignition monitor valve. This valve is shown in the following figure, re-drawn from [3].



The valve illustrated above is held normally closed by a spring, and has a diaphragm at its control port, which is connected to the thrust chamber injector fuel manifold. By the way, a diaphragm is a thin dividing membrane which is used as a seal to prevent fluid leakage and also as a pressure-sensing element having small (less than 1.5 mm) displacements. During engine start and when a satisfactory ignition has been achieved in the main thrust chamber, the increase in pressure sensed at the thrust chamber injector fuel manifold causes the ignition monitor valve to open, because the diaphragm of the valve is put under pressure. This opening, in turn, directs the fuel pressure to the cylinder port connected to the main fuel valve actuator opening port. The valve spring can be calibrated to correspond to the effective area of the diaphragm, so that the valve opens at a preset sensed pressure. During engine cut-off, the decreasing pressure of the fuel causes the ignition monitor valve to close. This closure, in turn, vents the opening side of the main fuel valve actuator, thereby closing the valve.

The poppet of the valve is balanced by the internal pressure of the fluid which acts on a dynamic O-ring seal having the same diameter d_s (m) as the poppet. The valve diaphragm is made of a several layers of thin Mylar® sheets, which are pressure-formed with heat added. The effective area of the diaphragm can be determined experimentally. The required preload of the valve spring may be estimated as follows

$$\frac{1}{4}\pi d_d^2 p_s = F_f + S_p$$

where d_d (m) is the effective diameter of the diaphragm, p_s (N/m^2) is the rated sensed threshold pressure to open the valve, F_f (N) is the static friction force of the valve poppet, and S_p (N) is the required preload of the valve spring.

For example, we want to determine the required preload S_p (N) and the output power P (W) for a pressure-actuated, three-way ignition monitor valve of the type

described above, which has the following properties: characteristic flow area of the valve at the fully open position $A_c = 1.226 \times 10^{-4} \text{ m}^2$, diameter of the diaphragm $d_d = 0.05334 \text{ m}$, sensed threshold pressure to open the valve $p_s = 1.379 \times 10^5 \text{ N/m}^2$, static friction force of the poppet $F_f = 62.28 \text{ N}$, resistance coefficient at the fully open position $k = 3.5$, required volume flow rate $q = 0.003277 \text{ m}^3/\text{s}$, fuel pressure at the inlet port $p_f = 2.413 \times 10^6 \text{ N/m}^2$. From [34], we also know the density of the fuel (RP-1) to be $\rho = 824 \text{ kg/m}^3$ at a temperature of 283 K.

By substituting $d_d = 0.05334 \text{ m}$, $p_s = 1.379 \times 10^5 \text{ N/m}^2$, $F_f = 62.28 \text{ N}$ into the preceding equation and solving for S_p , we find

$$S_p = \frac{\pi d_d^2 p_s}{4} - F_f = \frac{3.1416 \times 0.05334^2 \times 1.379 \times 10^5}{4} - 62.28 = 245.9 \text{ N}$$

The characteristic velocity of flow in the valve is

$$v = \frac{q}{A_c} = \frac{0.003277}{1.226 \times 10^{-4}} = 26.73 \text{ m/s}$$

The pressure loss through the valve in the design conditions is

$$\Delta p = k \left(\frac{1}{2} \rho v^2 \right) = 3.5 \times 0.5 \times 824 \times 26.73^2 = 1.03 \times 10^6 \text{ N/m}^2$$

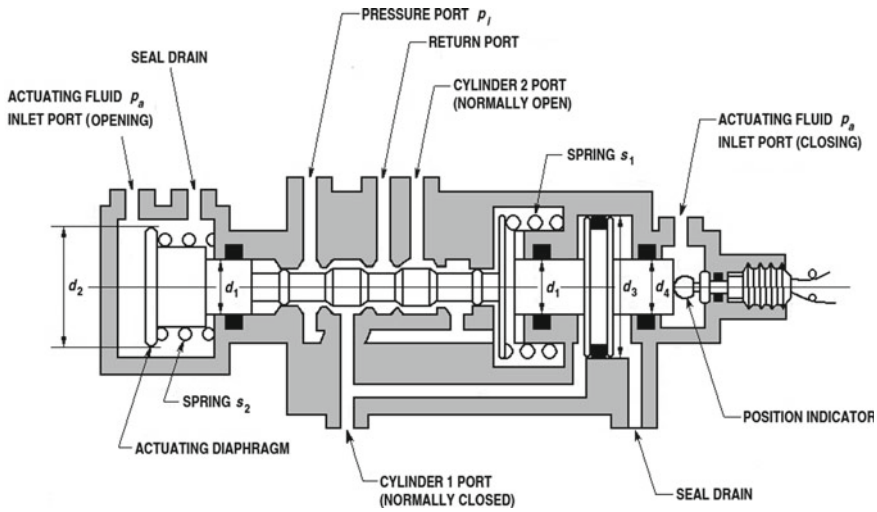
The pressure of the fuel at the point of discharge of the valve is

$$p_d = 2.413 \times 10^6 - 1.03 \times 10^6 = 1.383 \times 10^6 \text{ N/m}^2$$

The output power of the valve results from the product of the pressure of the fluid at the point of discharge by the volume flow rate, as follows

$$P = p_d q = 1.383 \times 10^6 \times 0.003277 = 4531 \text{ W}$$

The second example concerns a four-way pilot valve of the self-locking type. A scheme of this valve is shown in the following figure, re-drawn from [3].



The valve illustrated above is held normally closed at the cylinder 1 port by two springs s_1 and s_2 . The actuating pressure p_a is applied to the inlet port (opening) of the valve. The pressure p_a causes the translating shaft to move, and consequently the pressure port is connected to the cylinder 1 port, and the cylinder 2 port is connected to the return port. An unbalanced self-locking force $\frac{1}{4}\pi(d_3^2 - d_1^2)p_i$ acts in the opening direction and causes the valve to remain open, even after the actuating pressure p_a is removed from the opening port. The valve can be closed only by applying the actuating pressure p_a to the inlet port (closing) and venting the inlet port (opening).

As an application of the concepts discussed above, it is required to determine the diameters d_2 , d_3 , and d_4 for the four-way pilot valve shown in the preceding figure, with a contingency factor $c = 1.5$, knowing the following data: pre-load $F_1 = 155.7$ N and elastic constant $k_1 = 3.678 \times 10^4$ N/m of the spring s_1 , pre-load $F_2 = 111.2$ N and elastic constant $k_2 = 4.378 \times 10^4$ N/m of the spring s_2 , static friction $F_f = 106.8$ N of the poppet, relative pressure $p_i = 2.758 \times 10^6$ N/m² at the pressure port, relative pressure $p_a = 1.724 \times 10^6$ N/m² of the actuating fluid, ambient pressure (that is, relative pressure equal to zero) at the return port, diameter $d_1 = 0.0127$ m of the poppet guide, and total travel $x = 0.00127$ m of the poppet in the valve.

In order for the valve to be opened, the pressure p_a , which the actuating fluid exerts on the diaphragm area $\frac{1}{4}\pi d_2^2$, must be sufficient to counterbalance the pre-loads F_1 and F_2 of the springs s_1 and s_2 and the static friction force F_f . Therefore, the diameter d_2 of the diaphragm which opens the valve results from the following equation

$$\frac{\pi d_2^2}{4} p_a = c(F_1 + F_2 + F_f)$$

where $c = 1.5$ is the contingency factor. Solving for d_2 , we find

$$d_2 = \left[\frac{4c(F_1 + F_2 + F_f)}{\pi p_a} \right]^{\frac{1}{2}} = \left[\frac{4 \times 1.5 \times (155.7 + 111.2 + 106.8)}{3.1416 \times 1.724 \times 10^6} \right]^{\frac{1}{2}} \\ = 0.02035 \text{ m}$$

The diameter d_3 of the piston depends on the value of the force to be applied in order to lock the valve in the open position even when the actuating pressure p_a is removed from the pressure port. This force is

$$\frac{\pi(d_3^2 - d_1^2)}{4} p_i = c(F_1 + F_2 + k_1 x + k_2 x - F_f)$$

By substituting $d_1 = 0.0127 \text{ m}$, $p_i = 2.758 \times 10^6 \text{ N/m}^2$, $c = 1.5$, $F_1 = 155.7 \text{ N}$, $F_2 = 111.2 \text{ N}$, $k_1 = 3.678 \times 10^4 \text{ N/m}$, $k_2 = 4.378 \times 10^4 \text{ N/m}$, $x = 0.00127 \text{ m}$, and $F_f = 106.8 \text{ N}$ in the preceding equation and solving for d_3 , we find

$$d_3 = \left[\frac{4 \times 1.5 \times (155.7 + 111.2 + 36780 \times 0.00127 + 43780 \times 0.00127 - 106.8)}{3.1416 \times 2.758 \times 10^6} \right. \\ \left. + 0.0127^2 \right]^{\frac{1}{2}} = 0.01852 \text{ m}$$

The diameter d_4 needed for the actuating pressure p_a to close the valve results from the following equation

$$\frac{\pi d_4^2}{4} p_a = c \left[\frac{\pi(d_3^2 - d_1^2)}{4} p_i + F_f - F_1 - F_2 - k_1 x - k_2 x \right]$$

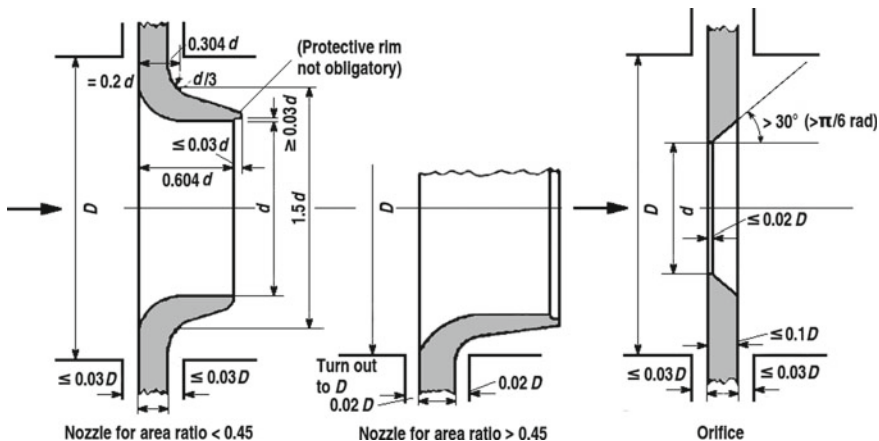
By substituting $p_a = 1.724 \times 10^6 \text{ N/m}^2$, $d_3 = 0.01852 \text{ m}$, $d_1 = 0.0127 \text{ m}$, $p_i = 2.758 \times 10^6 \text{ N/m}^2$, $F_f = 106.8 \text{ N}$, $F_1 = 155.7 \text{ N}$, $F_2 = 111.2 \text{ N}$, $k_1 = 3.678 \times 10^4 \text{ N/m}$, $k_2 = 4.378 \times 10^4 \text{ N/m}$, and $x = 0.00127 \text{ m}$ in the preceding equation and solving for d_4 , we find

$$d_4 = \left\{ \frac{4 \times 1.5}{3.1416 \times 1.724 \times 10^6} \left[\frac{3.1416 \times (0.01852^2 - 0.0127^2)}{4} \times 2.758 \times 10^6 \right. \right. \\ \left. \left. + 106.8 - 155.7 - 36780 \times 0.00127 - 43780 \times 0.00127 \right] \right\}^{\frac{1}{2}} = 0.01205 \text{ m}$$

5.11 Design of Flow Regulating Devices of the Fixed-Area Type

The flow regulating devices described in the present section are nozzles and orifices. Venturi tubes and valves used for the same purpose have been described in Sects. 5.7 and 5.9.

A nozzle is a convergent device inserted coaxially in a conduit and having a curved profile without discontinuities. An orifice is a circular aperture in a thin plate which restricts the cross-sectional area of a conduit in which this plate is inserted coaxially. According to the principle of Bernoulli, a fluid moving through a nozzle or an orifice increases its velocity and decreases its pressure in the direction of flow. These devices can be used in liquid-propellant rocket engines as flow regulators, as will be shown below. Typical shapes used for nozzles and orifices are shown in the following figure, re-drawn from [35].



The small turned-out part (protective rim at the discharge of the nozzle) shown in the preceding figure serves to protect the discharge edge, and consequently may be omitted when no damage is to be feared [35].

In Europe, the matter is regulated by the standards ISO 5167 [36]. In the United States of America, it is regulated by the standards of the American Gas Association [37].

The fundamental equation which governs the flow of liquids or gases through nozzles or orifices is the same as that which was shown in Sect. 5.7. This equation is re-written below for convenience of the reader

$$q = C_d A_0 \varepsilon \left[\frac{2\Delta p}{\rho(1 - \beta^4)} \right]^{\frac{1}{2}} = C_d A_0 \varepsilon \left[\frac{2\Delta H}{1 - \beta^4} \right]^{\frac{1}{2}}$$

where q (m^3/s) is the volume flow rate of the fluid, C_d is the coefficient of discharge, $A_0 = \pi d^2/4$ (m^2) is the area of the throat section, ε is the expansion coefficient (whose value can be taken equal to unity for incompressible fluids) of the fluid, Δp (N/m^2) and ΔH (m) are the differences of respectively pressure and pressure head measured upstream and downstream of the device, ρ (kg/m^3) is the density of the fluid in the operating conditions, and $\beta = d/D$ is the ratio of the diameter d of the throat to the diameter D of the conduit.

In case of gaseous substances, the value of the expansion coefficient ε can be computed by using the following empirical formula, which holds for $p_2/p_1 \geq 0.75$ [36]:

$$\varepsilon = 1 - (0.351 + 0.256\beta^4 + 0.92\beta^8) \left[1 - \left(\frac{p_2}{p_1} \right)^{\frac{1}{\gamma}} \right]$$

where $\beta = d/D$ is the ratio of the diameter d of the throat to the diameter D of the conduit, p_1 and p_2 (N/m^2) are the static pressures of the gas respectively upstream and downstream of the device, and $\gamma = c_p/c_v$ is the specific heat ratio of the gas.

In addition, [38] gives the following equations for the mass flow rate \dot{m} (kg/s) of a gas through an orifice:

$$\dot{m} = C_d \frac{\pi d^2}{4} \left\{ \frac{2\gamma p_1 \rho_1}{\gamma - 1} \left[\left(\frac{p_2}{p_1} \right)^{\frac{2}{\gamma}} - \left(\frac{p_2}{p_1} \right)^{\frac{\gamma+1}{\gamma}} \right] \right\}^{\frac{1}{2}}$$

which holds under non-chocked flow conditions, and

$$\dot{m} = C_d \frac{\pi d^2}{4} \left[\gamma p_1 \rho_1 \left(\frac{2}{\gamma + 1} \right)^{\frac{\gamma+1}{\gamma-1}} \right]^{\frac{1}{2}}$$

which holds under choked (that is, maximum) flow conditions. In the preceding equations, p_1 (N/m^2) and ρ_1 (kg/m^3) are respectively the static absolute pressure and the density of the gas upstream of the orifice, and p_2 (N/m^2) is the static absolute pressure of the gas downstream of the orifice.

The value of the coefficient of discharge C_d depends on the type of device, on the manner in which it is inserted in the conduit, and on the Reynolds number computed upstream of the device

$$Re = \frac{\rho v D}{\mu}$$

where v (m/s) is the stream velocity and μ (Ns/m^2) is the coefficient of dynamic viscosity of the fluid.

The coefficient of discharge C_d may be computed by using the Reader-Harris/Gallagher equation, as indicated in [36, 37]. According to [39], in most

practical cases, the coefficient of discharge may be computed as follows

$$C_d = C_{d\infty} + \frac{b}{Re^n}$$

where $C_{d\infty}$ (discharge coefficient at infinite Reynolds number), b , and n are three terms whose values can be determined as indicated in [39], depending on the particular case. For example, in case of a nozzle ISA 1932, [39] indicates the following values to be substituted in the preceding equation

$$\begin{aligned} C_{d\infty} &= 0.99 - 0.2262\beta^{4.1} \\ b &= 1708 - 8936\beta + 19779\beta^{4.7} \\ n &= 1.15 \end{aligned}$$

As an application of the concepts discussed above, the discharge duct of the fuel pump of a rocket engine burning liquid oxygen with RP-1 has a diameter $D = 0.1778$ m and a mass flow rate $\dot{m} = 404.6$ kg/s. We want to regulate the pressure in the duct by inserting a plate having an orifice, in order to obtain a pressure drop $\Delta p = 8.895 \times 10^5$ N/m² downstream of the plate. From [34], we know the density and the coefficient of dynamic viscosity of RP-1 to be respectively $\rho = 824$ kg/m³ and $\mu = 2.451 \times 10^{-3}$ Ns/m² at 283 K. It is required to estimate the diameter d of the throat of the orifice.

Since RP-1 is liquid at 283 K, then its expansion coefficient ε can be taken equal to unity. The volume flow rate q of RP-1 in the duct results from

$$q = \frac{\dot{m}}{\rho} = \frac{404.6}{824} = 0.491 \text{ m}^3/\text{s}$$

The velocity of the fluid upstream of the orifice is

$$v = \frac{4q}{\pi D^2} = \frac{4 \times 0.491}{3.1416 \times 0.1778^2} = 19.78 \text{ m/s}$$

The Reynolds number upstream of the orifice is

$$Re = \frac{\rho v D}{\mu} = \frac{824 \times 19.78 \times 0.1778}{2.451 \times 10^{-3}} = 1.182 \times 10^6$$

In [39], we find the following expressions

$$\begin{aligned} C_{d\infty} &= 0.5959 + 0.0312\beta^{2.1} - 0.184\beta^6 \\ b &= 91.71\beta^{2.5} \\ n &= 0.75 \end{aligned}$$

for the terms of the equation

$$C_d = C_{d\infty} + \frac{b}{Re^n}$$

which expresses the coefficient of discharge C_d for an orifice with corner taps as a function of β . Since $d = \beta D$, we use the following equation

$$q = C_d \frac{\pi \beta^2 D^2}{4} \varepsilon \left[\frac{2 \Delta p}{\rho(1 - \beta^4)} \right]^{\frac{1}{2}}$$

and solve this equation iteratively for β . To this end, we define the following function of β

$$f(\beta) = q - C_d \frac{\pi \beta^2 D^2}{4} \varepsilon \left[\frac{2 \Delta p}{\rho(1 - \beta^4)} \right]^{\frac{1}{2}}$$

and search the value of β for which the function $f(\beta)$ is equal to zero within a fixed tolerance. Since $\beta = d/D$, then we search the unknown value of β in some interval $0 < \beta < 1$ such that the value of the function $f(\beta)$ changes sign in that interval. We search the value of β in the interval $0.7 \leq \beta \leq 0.8$.

For $\beta = 0.7$, we find

$$C_{d\infty} = 0.5959 + 0.0312 \times 0.7^{2.1} - 0.184 \times 0.7^6 = 0.5890$$

$$b = 91.71 \times 0.7^{2.5} = 37.60$$

$$n = 0.75$$

$$C_d = 0.5890 + 37.60 / (1.182 \times 10^6)^{0.75} = 0.5900$$

$$\begin{aligned} f(0.7) &= 0.491 - 0.25 \times 0.5900 \times 3.1416 \times 0.7^2 \times 0.1778^2 \times 1 \\ &\quad \times \{2 \times 8.895 \times 10^5 / [824 \times (1 - 0.7^4)]\}^{\frac{1}{2}} = 0.1084 \end{aligned}$$

For $\beta = 0.8$, we find

$$C_{d\infty} = 0.5959 + 0.0312 \times 0.8^{2.1} - 0.184 \times 0.8^6 = 0.5672$$

$$b = 91.71 \times 0.8^{2.5} = 52.50$$

$$n = 0.75$$

$$C_d = 0.5672 + 52.50 / (1.182 \times 10^6)^{0.75} = 0.5697$$

$$\begin{aligned} f(0.8) &= 0.491 - 0.25 \times 0.5687 \times 3.1416 \times 0.8^2 \times 0.1778^2 \times 1 \\ &\quad \times \{2 \times 8.895 \times 10^5 / [824 \times (1 - 0.8^4)]\}^{\frac{1}{2}} = -0.05547 \end{aligned}$$

Since the value of the function $f(\beta)$ changes sign in the interval $0.7 \leq \beta \leq 0.8$, then the unknown value of β for which $f(\beta) = 0$ falls within this interval. By using repeatedly the numerical method described in Chap. 1, Sect. 1.2, we find $\beta = 0.7706$ with four significant figures. As is easy to verify, for $\beta = 0.7706$ there results $C_{d\infty} = 0.5754$, $b = 47.81$, $n = 0.75$, $C_d = 0.5768$, and $f(\beta) = -7.743 \times 10^{-5}$. Therefore, the diameter of the orifice necessary to obtain the desired pressure drop $\Delta p = 8.895 \times 10^5 \text{ N/m}^2$ is

$$d = \beta D = 0.7706 \times 0.1778 = 0.137 \text{ m}$$

The following example concerns the flow of a gas (helium) through an orifice. Knowing the diameter $d = 0.001524 \text{ m}$ and the discharge coefficient $C_d = 0.6$ of the orifice, and the static absolute pressure $p_1 = 3.548 \times 10^6 \text{ N/m}^2$ and the temperature $T_1 = 311 \text{ K}$ of helium upstream of the orifice, it is required to calculate the mass flow rates of helium through the orifice for the static absolute pressures $p_2 = 0.1013 \times 10^6 \text{ N/m}^2$ (atmospheric pressure) and $p_2 = 2.514 \times 10^6 \text{ N/m}^2$ downstream of the orifice.

From [40], we know the specific heat ratio and the density of helium to be respectively $\gamma = 1.663$ and $\rho_1 = 5.408 \text{ kg/m}^3$ in the given conditions.

The critical pressure ratio of helium is

$$\frac{p_c}{p_1} = \left(\frac{2}{\gamma + 1} \right)^{\frac{\gamma}{\gamma-1}} = \left(\frac{2}{1.663 + 1} \right)^{\frac{1.663}{1.663-1}} = 0.4877$$

When the static absolute pressure downstream of the orifice is $p_2 = 0.1013 \times 10^6 \text{ N/m}^2$ (atmospheric pressure), then the pressure ratio is

$$\frac{p_2}{p_1} = \frac{0.1013 \times 10^6}{3.548 \times 10^6} = 0.02855$$

and therefore the pressure ratio p_2/p_1 is less than the critical pressure ratio p_c/p_1 (choked flow). By substituting $\rho_1 = 5.408 \text{ kg/m}^3$, $C_d = 0.6$, $d = 0.001524 \text{ m}$, $\gamma = 1.663$, and $p_1 = 3.548 \times 10^6 \text{ N/m}^2$ in the following equation

$$\dot{m} = C_d \frac{\pi d^2}{4} \left[\gamma p_1 \rho_1 \left(\frac{2}{\gamma + 1} \right)^{\frac{\gamma+1}{\gamma-1}} \right]^{\frac{1}{2}}$$

we find

$$\begin{aligned} \dot{m} &= 0.6 \times \frac{3.1416 \times 0.001524^2}{4} \times [1.663 \times 3.548 \times 10^6 \times 5.408 \\ &\quad \times \left(\frac{2}{1.663 + 1} \right)^{\frac{1.663+1}{1.663-1}}]^{\frac{1}{2}} = 0.003479 \text{ kg/s} \end{aligned}$$

When the static absolute pressure downstream of the orifice is $p_2 = 2.514 \times 10^6$ N/m², then the pressure ratio is

$$\frac{p_2}{p_1} = \frac{2.514 \times 10^6}{3.548 \times 10^6} = 0.7086$$

and therefore the pressure ratio p_2/p_1 is greater than the critical pressure ratio p_c/p_1 (non-choked flow). By substituting $C_d = 0.6$, $d = 0.001524$ m, $\gamma = 1.663$, $p_1 = 3.548 \times 10^6$ N/m², $\rho_1 = 5.408$ kg/m³, and $p_2/p_1 = 0.7086$ in the following equation

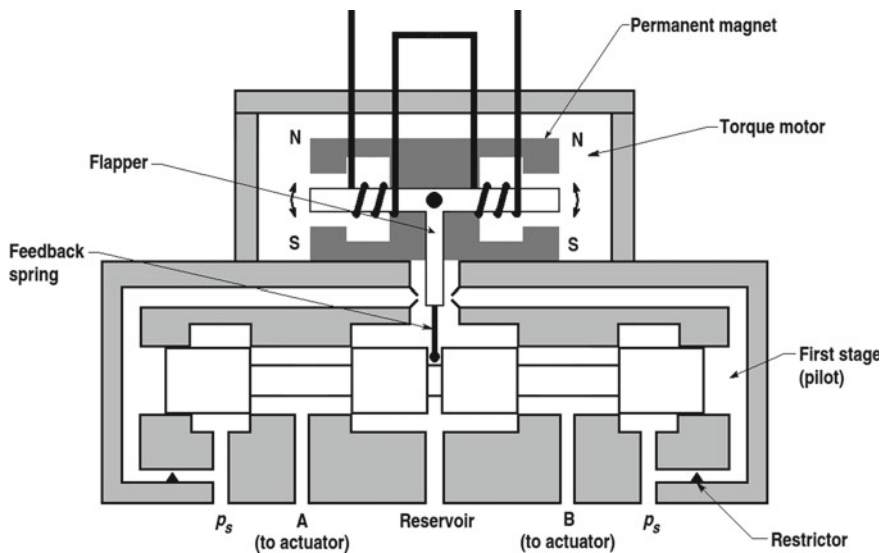
$$\dot{m} = C_d \frac{\pi d^2}{4} \left\{ \frac{2\gamma p_1 \rho_1}{\gamma - 1} \left[\left(\frac{p_2}{p_1} \right)^{\frac{2}{\gamma}} - \left(\frac{p_2}{p_1} \right)^{\frac{\gamma+1}{\gamma}} \right] \right\}^{\frac{1}{2}}$$

we find

$$\begin{aligned} \dot{m} &= 0.6 \times \frac{3.1416 \times 0.001524^2}{4} \times \left[\frac{2 \times 1.663 \times 3.548 \times 10^6 \times 5.408}{1.663 - 1} \right. \\ &\quad \left. \times \left(0.7086^{\frac{2}{1.663}} - 0.7086^{\frac{1.663+1}{1.663}} \right) \right]^{\frac{1}{2}} = 0.003127 \text{ kg/s} \end{aligned}$$

5.12 Design of Servo-Valves

According to the definition given in [41], a servo-valve is a modulating operator that amplifies system signals for variable-displacement, closed-loop control of actuator position. There are two principal types of servo-valves. In a servo-valve of the nozzle-flapper type, the pressure exerted by the fluid on the actuator is controlled directly by a flapper, which restricts the flow through two nozzles of variable size, in response to an electrical input signal applied to a torque motor. In a servo-valve of the spool type, the pressure is controlled indirectly, by means of a sliding spool, whose position in the body of the valve depends on the angular position of the flapper. A spool is a solid cylindrical element having two or more recesses which fits closely in the bore of the valve body, such that the valve opens or closes by translating the spool within the bore. In other words, a servo-valve of the spool type is an electro-hydraulic valve having a spool, whose position in the valve body changes proportionally to an electrical input signal received by the valve. The translational motion of the spool in the valve is obtained by hydraulic pressure, and changes the size of two orifices in order for the valve to control flow. The control exerted by the valve depends on the difference of hydraulic pressure across the orifices, unless some form of compensation is used. A functional scheme of a servo-valve of the spool type is given in the following figure, re-drawn from [42].



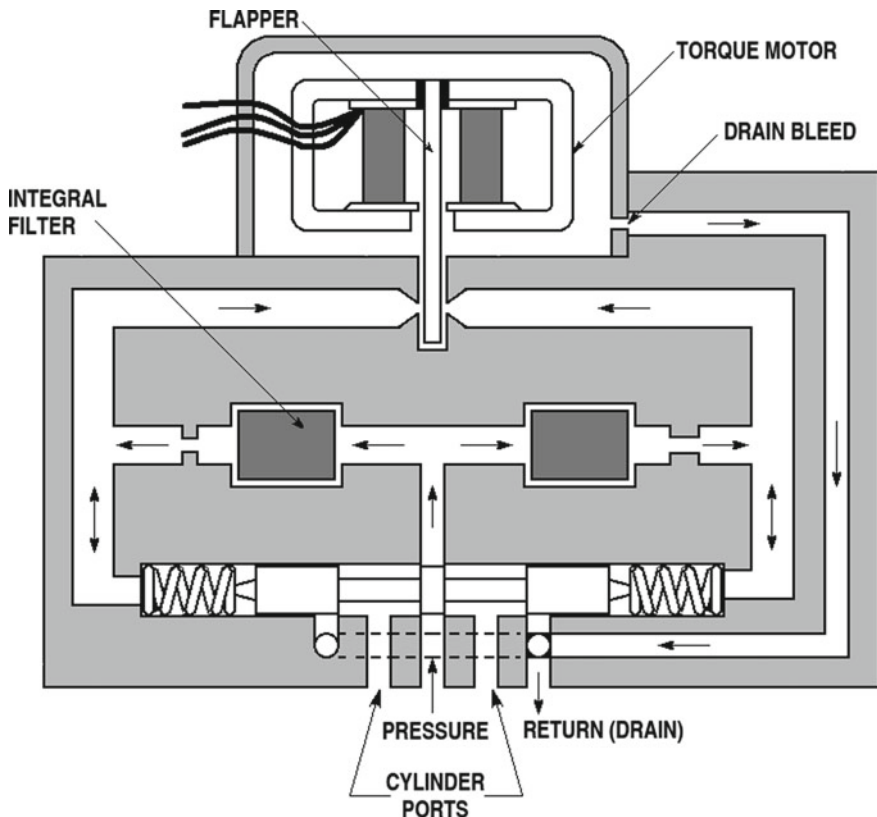
The principal components of the servo-valve shown above are:

- an electromagnetic torque motor, which acts as a transducer to convert an electrical input signal into a mechanical force;
- a flapper driven by the mechanical force generated by the torque motor, which restricts differentially the flow from a pair of nozzles, the flapper stroke being about 0.1 mm;
- a spool, whose translational motion within the valve body is due to the difference of hydraulic pressure when the flapper is off-centre; and
- a feedback spring, which allows the spool to move, the stroke of the spool being about 1 mm, until the restoring force acting on the flapper is in equilibrium with the force generated by the torque motor.

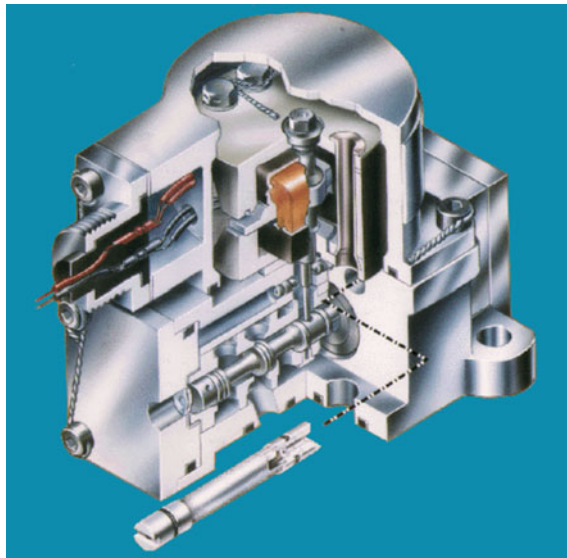
The direction and the magnitude of the displacement of the flapper caused by the torque motor depend on the input signal. The flapper is located between two opposed nozzles, and therefore its motion in one or in the other direction restricts the flow through one or the other of these nozzles. When no electrical signal is applied to the torque motor, then the flapper is located at an equal distance between the two nozzles (neutral position). The presence of an electrical signal causes the flapper to move toward one or the other nozzle, thereby producing an unbalance of hydraulic pressure across the spool. The set of components comprising the torque motor, the nozzles, and the flapper is known as the first stage of a servo-valve. The first stage pilots the second stage, which comprises the spool and the feedback spring. The spring makes the displacement of the spool proportional to the difference of pressure caused by the off-centre position of the flapper in the first stage. The position of the flapper, in turn, depends on the force generated by the torque motor in response to the input signal.

Therefore, the direction and the magnitude of the displacement of the spool are proportional to the direction and to the magnitude of the input signal, and are used to control the direction and the magnitude of flow to the actuator through the pressure at the cylinder ports of the valve. For example, with reference to the preceding figure, an electrical signal resulting in a displacement of the flapper to the right restricts the flow from the nozzle on the right hand side. This restriction increases the pressure upstream of the right nozzle circuit, and decreases the pressure upstream of the left circuit. This unbalance of pressure causes the spool to shift to the left, until the difference of pressure is balanced by the pressure exerted by the spring on the spool. The shift of the spool to the left opens a flow path from the pressure port placed on the left to the cylinder port A, and the returning fluid through the cylinder port B moves through the return line to the reservoir. A servo-valve is not only an electrical-to-hydraulic transducer, but also a power amplifier, because the electrical input power, whose order of magnitude is about 0.1 W, is amplified in the first stage to at least 10 W of hydraulic power, and then used to control, by means of the spool, an amount of about 10 kW of hydraulic power. Therefore, the power amplification factor in a two-stage servo-valve is 10^5 [42].

Another two-stage servo-valve of the spool type is illustrated in the following figure, re-drawn from [25]. In the servo-valve shown below, the spool is spring-loaded, in order for its position in the valve to be proportional to the input received from the first stage. The spool is centred by helical coil springs on each side. Integral filters are used to remove small particles, which would otherwise coalesce and obstruct orifices and nozzles. These filters are also used to protect the spool from contaminants. This servo-valve has also a drain bleed system to protect the torque motor from leakage fluid.



In the main engines (RS-25) of the Space Shuttle, two servo-valves (channel A and channel B) are mounted on each of the five actuators. These servo-valves convert the electrical command signal from the engine controller (described in Sect. 5.2) to hydraulic flow directed to the valve actuator. They convert the polarity and the amplitude of the electrical command signal into respectively the rotation direction and the rotation rate of the shaft. The two servo-valves are redundant, in order for the failure of one of them not to affect the performance of the actuators. An assembly of one of these servo-valves is shown in the following figure, due to the courtesy of Boeing-Rocketdyne [7]. When the torque motor of the servo-valve tilts in response to the polarity and to the amplitude of the input signal, the flow restriction is increased at one nozzle, and decreased at the other. These variable restrictors are paired with constant restrictors at the end of the filter, forming two matched pressure dividers. Therefore, the pressures applied to the ends of the spool in the second stage can be varied, being equal in the null position and not equal otherwise.



The resulting offset of the spool is opposite to the tilt of the torque motor, and is fed back to the torque motor via the springy connecting rod, thereby assuring proportional control. The spool offset in effect simultaneously moves one port toward the input (higher) pressure, and the other port toward the return (lower) pressure, driving the pistons. Therefore, the polarity of the signal determines the direction of rotation, and the amplitude of the signal determines the rotation rate in the valve [7].

The equations which can be used for the design of servo-valves of the flapper-nozzle type are those shown in Sect. 5.11 for the flow of liquid or gaseous substances through nozzles or orifices. These equations are re-written below for convenience of the reader. In case of liquid substances, the following equation can be used

$$\dot{m} = \rho q = \rho C_d A_0 \varepsilon \left[\frac{2\Delta p}{\rho(1 - \beta^4)} \right]^{\frac{1}{2}} = \rho C_d A_0 \varepsilon \left[\frac{2\Delta H}{1 - \beta^4} \right]^{\frac{1}{2}}$$

where \dot{m} (kg/s) and q (m³/s) are respectively the mass flow rate and the volume flow rate of the liquid, C_d is the coefficient of discharge of the valve, $A_0 = \pi d^2/4$ (m²) is the area of the throat section, ε is the expansion coefficient (whose value can be taken equal to unity) of the liquid, Δp (N/m²) and ΔH (m) are the differences of respectively pressure and pressure head measured upstream and downstream of the device, ρ (kg/m³) is the density of the liquid in the operating conditions, and $\beta = d/D$ is the ratio of the diameter d of the throat to the diameter D of the conduit.

In case of gaseous substances under non-chocked flow conditions, the following equation can be used

$$\dot{m} = C_d \frac{\pi d^2}{4} \left\{ \frac{2\gamma p_1 \rho_1}{\gamma - 1} \left[\left(\frac{p_2}{p_1} \right)^{\frac{2}{\gamma}} - \left(\frac{p_2}{p_1} \right)^{\frac{\gamma+1}{\gamma}} \right] \right\}^{\frac{1}{2}}$$

In case of gaseous substances under choked flow conditions, the following equation can be used

$$\dot{m} = C_d \frac{\pi d^2}{4} \left[\gamma p_1 \rho_1 \left(\frac{2}{\gamma + 1} \right)^{\frac{\gamma+1}{\gamma-1}} \right]^{\frac{1}{2}}$$

In the preceding equations, $\gamma = c_p/c_v$ is the specific heat ratio of the gas, p_1 (N/m^2) and ρ_1 (kg/m^3) are respectively the static pressure and the density of the gas upstream of the device, and p_2 (N/m^2) is the static pressure of the gas downstream of the device.

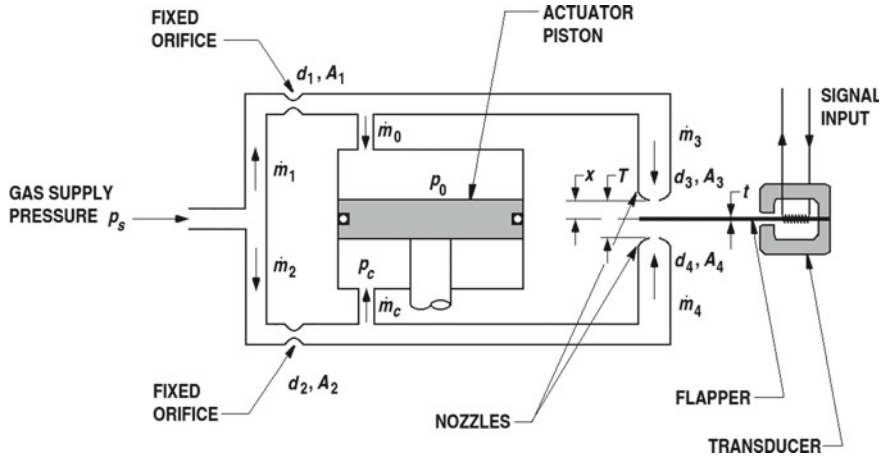
In addition, Huzel and Huang [3] indicate the following equation to compute the effective, ring-shaped flow area A_n (m^2) of a nozzle of diameter d_n (m) in the presence of a flapper displaced by x (m) from the nozzle

$$A_n = \pi d_n x$$

where the maximum value of the distance x should not exceed $d_n/5$.

The following example of application concerns a pneumatic servo-valve of the flapper-nozzle type. This servo-valve is used as a pilot valve of another valve, which in turn controls the propellant (oxidiser) utilisation in a rocket engine. A scheme of the pneumatic servo-valve, redrawn from [3], is shown below.

The following data are known. The gaseous substance flowing in the circuit is helium. The absolute pressure and the temperature of helium at the supply point are respectively $p_s = 3.447 \times 10^6 \text{ N/m}^2$ and $T_s = 311 \text{ K}$. The diameters of the ducts are such that $d_1 = d_2$, and $d_3 = d_4$. The coefficient of discharge for the orifices and for the nozzles is $C_d = 0.7$. The thickness of the flapper is $t = 0.1016 \text{ mm} = 1.016 \times 10^{-4} \text{ m}$. The distance between the nozzles is $T = d_3/4 + t$. At the neutral position of the flapper, the absolute pressures in the actuator are $p_c = p_0 = 3.103 \times 10^6 \text{ N/m}^2$. The mass flow rates through the nozzles are $\dot{m}_3 = \dot{m}_4 = 3.529 \times 10^{-4} \text{ kg/s}$. The gas is discharged downstream of the nozzles at atmospheric pressure ($p_2 = 0.1013 \times 10^6 \text{ N/m}^2$). It is required to determine the diameters d_1 and d_2 of the fixed orifices, the diameters d_3 and d_4 of the nozzles, and the distance T between the nozzles.



As has been shown in Sect. 5.11, the critical pressure ratio of helium is

$$\frac{p_c}{p_s} = \left(\frac{2}{\gamma + 1} \right)^{\frac{\gamma}{\gamma - 1}} = \left(\frac{2}{1.663 + 1} \right)^{\frac{1.663}{1.663 - 1}} = 0.4877$$

Since the static absolute pressure downstream of the nozzles is $p_2 = 0.1013 \times 10^6 \text{ N/m}^2$ (atmospheric pressure), then the pressure ratio for the nozzles is

$$\frac{p_2}{p_s} = \frac{0.1013 \times 10^6}{3.447 \times 10^6} = 0.02939$$

and therefore the pressure ratio p_2/p_s is less than the critical pressure ratio $p_c/p_s = 0.4877$ (choked flow). Therefore, the equations to be used to compute the mass flow rates \dot{m}_3 and \dot{m}_4 through the nozzles are

$$\begin{aligned} \dot{m}_3 &= C_d A_3 \left[\gamma p_0 \rho_s \left(\frac{2}{\gamma + 1} \right)^{\frac{\gamma+1}{\gamma-1}} \right]^{\frac{1}{2}} \\ \dot{m}_4 &= C_d A_4 \left[\gamma p_c \rho_s \left(\frac{2}{\gamma + 1} \right)^{\frac{\gamma+1}{\gamma-1}} \right]^{\frac{1}{2}} \end{aligned}$$

where p_0 and p_c are the static pressures upstream of the nozzles, and $\rho_s = 5.256 \text{ kg/m}^3$ [40] is the density of helium at $p_s = 3.447 \times 10^6 \text{ N/m}^2$ and $T_s = 311 \text{ K}$.

After substituting $\rho_s = 5.256 \text{ kg/m}^3$, $C_d = 0.7$, and $\gamma = 1.663$ in the two equations which express \dot{m}_3 and \dot{m}_4 we find

$$\dot{m}_3 = 1.165 A_3 p_0^{\frac{1}{2}}$$

$$\dot{m}_4 = 1.165 A_4 p_c^{\frac{1}{2}}$$

Since the static pressures p_0 and p_c are by far greater than the atmospheric pressure, then the equations to be used to compute the mass flow rates \dot{m}_1 and \dot{m}_2 through the fixed orifices are

$$\begin{aligned}\dot{m}_1 &= C_d A_1 \left\{ \frac{2\gamma p_s \rho_s}{\gamma - 1} \left[\left(\frac{p_0}{p_s} \right)^{\frac{2}{\gamma}} - \left(\frac{p_0}{p_s} \right)^{\frac{\gamma+1}{\gamma}} \right] \right\}^{\frac{1}{2}} \\ \dot{m}_2 &= C_d A_2 \left\{ \frac{2\gamma p_s \rho_s}{\gamma - 1} \left[\left(\frac{p_c}{p_s} \right)^{\frac{2}{\gamma}} - \left(\frac{p_c}{p_s} \right)^{\frac{\gamma+1}{\gamma}} \right] \right\}^{\frac{1}{2}}\end{aligned}$$

With reference to the preceding figure, the areas A_1 , A_2 , A_3 , and A_4 are

$$\begin{aligned}A_1 &= \frac{1}{4}\pi d_1^2 \\ A_2 &= \frac{1}{4}\pi d_2^2 \\ A_3 &= \pi d_3 x \\ A_4 &= \pi d_4(T - t - x)\end{aligned}$$

where x is the displacement of the flapper from the nozzle.

When the flapper is in its neutral position, then the actuator is at rest, and consequently the following equations hold

$$\dot{m}_c = \dot{m}_0 = 0$$

$$\dot{m}_1 = \dot{m}_2 = \dot{m}_3 = \dot{m}_4 = 3.529 \times 10^{-4} \text{ kg/s}$$

$$x = \frac{1}{2}(T - t) = \frac{1}{2} \left(\frac{d_3}{4} + t - t \right) = \frac{d_3}{8}$$

In addition, in the same conditions, the absolute pressures acting on the piston are $p_c = p_0 = 3.103 \times 10^6 \text{ N/m}^2$. Therefore, the pressure ratio for both of the fixed orifices is

$$\frac{p_c}{p_s} = \frac{p_0}{p_s} = \frac{3.103 \times 10^6}{3.447 \times 10^6} = 0.9002$$

By introducing this value, $p_s = 3.447 \times 10^6 \text{ N/m}^2$, $\rho_s = 5.256 \text{ kg/m}^3$, $C_d = 0.7$, and $\gamma = 1.663$ in the following equations

$$\dot{m}_1 = C_d A_1 \left\{ \frac{2\gamma p_0 \rho_s}{\gamma - 1} \left[\left(\frac{p_0}{p_s} \right)^{\frac{2}{\gamma}} - \left(\frac{p_0}{p_s} \right)^{\frac{\gamma+1}{\gamma}} \right] \right\}^{\frac{1}{2}}$$

$$\dot{m}_2 = C_d A_2 \left\{ \frac{2\gamma p_c \rho_s}{\gamma - 1} \left[\left(\frac{p_c}{p_s} \right)^{\frac{2}{\gamma}} - \left(\frac{p_c}{p_s} \right)^{\frac{\gamma+1}{\gamma}} \right] \right\}^{\frac{1}{2}}$$

we find

$$\dot{m}_1 = 0.6836 A_1 p_0^{\frac{1}{2}}$$

$$\dot{m}_2 = 0.6836 A_2 p_c^{\frac{1}{2}}$$

which in turn, for $p_0 = p_c = 3.103 \times 10^6 \text{ N/m}^2$, yield

$$\dot{m}_1 = 1204 A_1$$

$$\dot{m}_2 = 1204 A_2$$

By comparing these two equations with

$$\dot{m}_1 = \dot{m}_2 = \dot{m}_3 = \dot{m}_4 = 3.529 \times 10^{-4} \text{ kg/s}$$

there results

$$A_1 = \frac{\pi d_1^2}{4} = \frac{3.529 \times 10^{-4}}{1204} = 2.930 \times 10^{-7} \text{ m}^2$$

$$A_2 = \frac{\pi d_2^2}{4} = \frac{3.529 \times 10^{-4}}{1204} = 2.930 \times 10^{-7} \text{ m}^2$$

hence $d_1 = d_2 = 0.0006108 \text{ m} = 0.6108 \text{ mm}$.

By comparing the following equations found above

$$\dot{m}_3 = 1.165 A_3 p_0^{\frac{1}{2}}$$

$$\dot{m}_4 = 1.165 A_4 p_c^{\frac{1}{2}}$$

with

$$\dot{m}_1 = \dot{m}_2 = \dot{m}_3 = \dot{m}_4 = 3.529 \times 10^{-4} \text{ kg/s}$$

where $p_c = p_0 = 3.103 \times 10^6 \text{ N/m}^2$, there results

$$A_3 = A_4 = \frac{3.529 \times 10^{-4}}{1.165 \times (3.103 \times 10^6)^{\frac{1}{2}}} = 1.720 \times 10^{-7} \text{ m}^2$$

Since

$$A_3 = \pi d_3 x = \pi d_3 \left(\frac{d_3}{8} \right)$$

then

$$d_3 = d_4 = \left(\frac{8A_3}{\pi} \right)^{\frac{1}{2}} = \left(\frac{8 \times 1.720 \times 10^{-7}}{3.1416} \right)^{\frac{1}{2}} = 0.0006617 \text{ m} = 0.6617 \text{ mm}$$

$$T = \frac{d_3}{4} + t = \frac{0.0006617}{4} + 0.0001016 = 0.0002670 \text{ m} = 0.2670 \text{ mm}$$

Now, we suppose the flapper to be deflected $0.03635 \text{ mm} = 3.635 \times 10^{-5} \text{ m}$ below its neutral position, and the mass flow rates \dot{m}_0 and \dot{m}_c respectively to and from the actuator to be $9.525 \times 10^{-5} \text{ kg/s}$. We want to compute the difference of pressure across the actuator piston.

When the flapper is deflected $3.635 \times 10^{-5} \text{ m}$ below its neutral position, the distance between the flapper and the upper nozzle is

$$\begin{aligned} x &= \frac{T - t}{2} + 3.635 \times 10^{-5} = \frac{0.0002670 - 0.0001016}{2} + 0.00003635 \\ &= 0.0001191 \text{ m} \end{aligned}$$

In this position of the flapper, the flow area of the upper nozzle is

$$A_3 = \pi d_3 x = 3.1416 \times 0.0006617 \times 0.0001191 = 2.475 \times 10^{-7} \text{ m}^2$$

In these conditions, the mass flow rate \dot{m}_3 through the upper nozzle is equal to the mass flow rate \dot{m}_1 through the upper orifice plus the mass flow rate $\dot{m}_0 = 9.525 \times 10^{-5} \text{ kg/s}$ through the upper duct of the actuator, as follows

$$\dot{m}_3 = \dot{m}_1 + \dot{m}_0$$

Since \dot{m}_3 has been found above to be

$$\dot{m}_3 = 1.165 A_3 p_0^{\frac{1}{2}}$$

which, for $A_3 = 2.475 \times 10^{-7} \text{ m}^2$, yields

$$\dot{m}_3 = 2.884 \times 10^{-7} p_0^{\frac{1}{2}}$$

and since \dot{m}_1 depends on the unknown value of p_0 as follows

$$\begin{aligned}\dot{m}_1 &= C_d A_1 \left\{ \frac{2\gamma p_0 \rho_s}{\gamma - 1} \left[\left(\frac{p_0}{p_s} \right)^{\frac{2}{\gamma}} - \left(\frac{p_0}{p_s} \right)^{\frac{\gamma+1}{\gamma}} \right] \right\}^{\frac{1}{2}} \\ &= 1.053 \times 10^{-6} \times \left\{ p_0 \left[\left(\frac{p_0}{3.447 \times 10^6} \right)^{\frac{2}{1.663}} - \left(\frac{p_0}{3.447 \times 10^6} \right)^{\frac{2.663}{1.663}} \right] \right\}^{\frac{1}{2}}\end{aligned}$$

then the equation $\dot{m}_3 = \dot{m}_1 + \dot{m}_0$ becomes

$$\begin{aligned}&2.884 \times 10^{-7} p_0^{\frac{1}{2}} \\ &= 1.053 \times 10^{-6} \times \left\{ p_0 \left[\left(\frac{p_0}{3.447 \times 10^6} \right)^{\frac{2}{1.663}} - \left(\frac{p_0}{3.447 \times 10^6} \right)^{\frac{2.663}{1.663}} \right] \right\}^{\frac{1}{2}} \\ &\quad + 9.525 \times 10^{-5}\end{aligned}$$

The preceding equation can be solved numerically for p_0 . For this purpose, we define the following function

$$\begin{aligned}f(p_0) &\equiv 2.884 \times 10^{-7} p_0^{\frac{1}{2}} - 1.053 \times 10^{-6} \times \left\{ p_0 \left[\left(\frac{p_0}{3.447 \times 10^6} \right)^{\frac{2}{1.663}} \right. \right. \\ &\quad \left. \left. - \left(\frac{p_0}{3.447 \times 10^6} \right)^{\frac{2.663}{1.663}} \right] \right\}^{\frac{1}{2}} - 9.525 \times 10^{-5}\end{aligned}$$

and search the value of p_0 for which $f(p_0) = 0$ within an interval $p_{01} \leq p_0 \leq p_{02}$ such that $f(p_{01})f(p_{02}) < 0$. We choose $p_{01} = \frac{3}{4} p_s = 0.75 \times 3.447 \times 10^6 = 2.585 \times 10^6$ N/m² and $p_{02} = \frac{7}{8} p_s = 0.875 \times 3.447 \times 10^6 = 3.016 \times 10^6$ N/m².

We find $f(p_{01}) = -0.0001004$ and $f(p_{02}) = 0.00002130$, and therefore the condition $f(p_{01})f(p_{02}) < 0$ is satisfied. The unknown value of p_0 can be found in the interval indicated above by using a numerical method, for example, the method described in Chap. 1, Sect. 1.2. We find $p_0 = 2.961 \times 10^6$ N/m² with four significant figures (for this value, $f(p_0) = 4.471 \times 10^{-8}$).

Likewise, when the flapper is deflected 3.635×10^{-5} m below its neutral position, the flow area A_4 is

$$\begin{aligned}A_4 &= \pi d_4(T - t - x) = 3.1416 \times 6.617 \times 10^{-4} \\ &\quad \times (2.670 \times 10^{-4} - 1.016 \times 10^{-4} - 1.191 \times 10^{-4}) \\ &= 9.625 \times 10^{-8} \text{ m}^2\end{aligned}$$

In these conditions, the mass flow rate \dot{m}_4 through the lower nozzle is equal to the mass flow rate \dot{m}_2 through the lower orifice minus the mass flow rate $\dot{m}_c = 9.525 \times 10^{-5}$ kg/s through the lower duct of the actuator, as follows

$$\dot{m}_4 = \dot{m}_2 - \dot{m}_c$$

Since \dot{m}_4 has been found above to be

$$\dot{m}_4 = 1.165 A_4 p_c^{\frac{1}{2}}$$

which, for $A_4 = 9.625 \times 10^{-8}$ m², yields

$$\dot{m}_4 = 1.121 \times 10^{-7} p_c^{\frac{1}{2}}$$

and since \dot{m}_2 depends on the unknown value of p_c as follows

$$\begin{aligned}\dot{m}_2 &= C_d A_2 \left\{ \frac{2\gamma p_c \rho_s}{\gamma - 1} \left[\left(\frac{p_c}{p_s} \right)^{\frac{2}{\gamma}} - \left(\frac{p_c}{p_s} \right)^{\frac{\gamma+1}{\gamma}} \right] \right\}^{\frac{1}{2}} \\ &= 9.992 \times 10^{-7} \times \left\{ p_c \left[\left(\frac{p_c}{3.447 \times 10^6} \right)^{\frac{2}{1.663}} - \left(\frac{p_c}{3.447 \times 10^6} \right)^{\frac{2.663}{1.663}} \right] \right\}^{\frac{1}{2}}\end{aligned}$$

then the equation $\dot{m}_4 = \dot{m}_2 - \dot{m}_c$ becomes

$$\begin{aligned}&1.121 \times 10^{-7} p_c^{\frac{1}{2}} \\ &= 1.053 \times 10^{-6} \times \left\{ p_c \left[\left(\frac{p_c}{3.447 \times 10^6} \right)^{\frac{2}{1.663}} - \left(\frac{p_c}{3.447 \times 10^6} \right)^{\frac{2.663}{1.663}} \right] \right\}^{\frac{1}{2}} \\ &\quad - 9.525 \times 10^{-5}\end{aligned}$$

The preceding equation can be solved numerically for p_c . For this purpose, we define the following function

$$\begin{aligned}f(p_c) &\equiv 1.121 \times 10^{-7} p_c^{\frac{1}{2}} - 1.053 \times 10^{-6} \times \left\{ p_c \left[\left(\frac{p_c}{3.447 \times 10^6} \right)^{\frac{2}{1.663}} \right. \right. \\ &\quad \left. \left. - \left(\frac{p_c}{3.447 \times 10^6} \right)^{\frac{2.663}{1.663}} \right] \right\}^{\frac{1}{2}} + 9.525 \times 10^{-5}\end{aligned}$$

By operating as has been shown above, we find $p_c = 3.221 \times 10^6$ N/m² with four significant figures (for this value, $f(p_c) = 1.243 \times 10^{-7}$).

Therefore, the difference of pressure across the actuator piston is

$$p_c - p_0 = 3.221 \times 10^6 - 2.961 \times 10^6 = 0.26 \times 10^6 \text{ N/m}^2$$

5.13 Design of Pressure-Reducing Regulators

In general terms, a pressure regulator is a control valve which has no auxiliary source of power during operation. The pressure is controlled by varying the flow in the valve as a function of the sensed difference between the actual value and the desired value of pressure. Any unbalanced force resulting from this difference of pressure moves a metering element, which increases or decreases flow to reduce the pressure error to zero [25].

However, in the aerospace field, the name of pressure regulator indicates any device which maintains a desired value of upstream, downstream, or differential pressure by means of a pressure-reducing control element. For example, pressure regulators are used to maintain a constant pneumatic pressure in a tank for the storage of liquid propellants. In a pump-fed rocket engine, this constant pressure is used to protect the structure of the tank and to meet the requirements of pump suction head. A further protection is provided to the tank by a relief valve.

In control systems of large rocket engines, pressure regulators maintain the pressure of gas at a constant value to operate engine control valves, main propellant valves, gas-generator valves, and other control components [43].

In pneumatic control systems, variations of regulated pressure affect valve timing and sequencing in engine start and shutdown operations. In reaction-control systems, the source of energy for propellant feed is supplied by gas stored at high pressure [43].

Pressure regulators can be classified into the following categories:

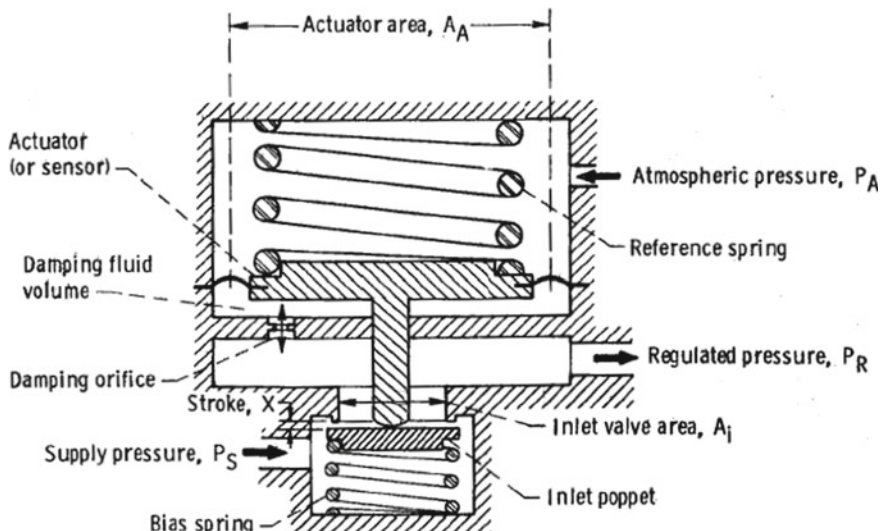
- pressure-reducing regulators, which are used to reduce the pressure upstream of them to a desired downstream pressure, independently of variations of upstream pressure;
- back pressure regulators, which measure and regulate the pressure upstream of them independently of variations of downstream pressure; and
- differential pressure regulators, which maintain a constant difference of pressure across a restrictor of constant area, for example, across an orifice, to maintain a constant desired value of flow rate.

The pressure regulators described in the present section are only those of the first type. The regulators of the other types (relief valves and differential pressure regulators) will be described in the following sections.

Pressure-reducing regulators may be modulating or non-modulating. A regulator of the modulating type is a device which maintains a constant regulated pressure in a tank. A regulator of the non-modulating type is an on-off device which maintains the pressure in a tank between chosen limits by means of a signal from a pressure switch, which senses variations of pressure in the tank, and consequently opens or

closes valves, which control the flow of pressurising gas to the tank. Modulating pressure-reducing regulators include, in turn, directly-operated, dome-loaded, and pilot-operated regulators.

A scheme of a directly-operated regulator is shown in the following figure, due to the courtesy of NASA [43].



It consists of three principal elements: a sensing element (for example, a diaphragm), an inlet valve (comprising a movable element and a seat), and a source of reference load, which is usually a spring. The reference load due to the spring acts on the sensing element in one direction, and the force due to the regulated pressure acts in the opposite direction. The combination comprising the sensing element, the inlet valve, and the stem, which connects the sensing element with the inlet valve, is called the metering element. The force exerted by the reference spring on the sensing element is called the load. The sensing element is also subject to the actual regulated pressure and compresses the reference spring, which is used to establish the desired pressure setting. The net force acting on the inlet valve controls the flow through the regulator.

The movable element of the inlet valve may, or may not, be pressure-balanced. When the movable element is not pressure-balanced, then the inlet pressure acts on the main seat and changes the force equilibrium within the inlet valve. Consequently, a loss of inlet pressure across the main seat results in an increase in outlet pressure. When the movable element is pressure-balanced, then there is no variation of outlet pressure resulting from changes of inlet pressure. A regulator having a pressure-balanced movable element requires a dynamic seal to pressure-balance the main seat of the inlet valve.

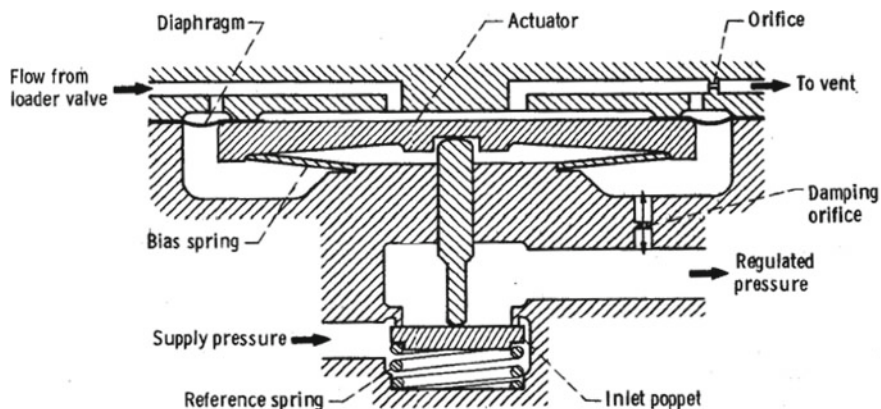
The set point of a direct-acting regulator can be adjusted by means of a screw (not shown in the figure) which lifts or lowers a plate located above the reference

spring, in order to extend or compress the spring. To a low value of the constant of the reference spring there corresponds a high value of the stroke of the movable element of the inlet valve which it is possible to achieve.

When a highly accurate regulation with small changes of outlet pressure is desired, then a large area of the sensing element is needed to achieve a high driving force. Therefore, a high force due to the reference spring is needed. Since a low value of the spring constant is desired, then it is necessary to use springs having a high number of coils. This, in turn, increases the size and the mass of the regulator.

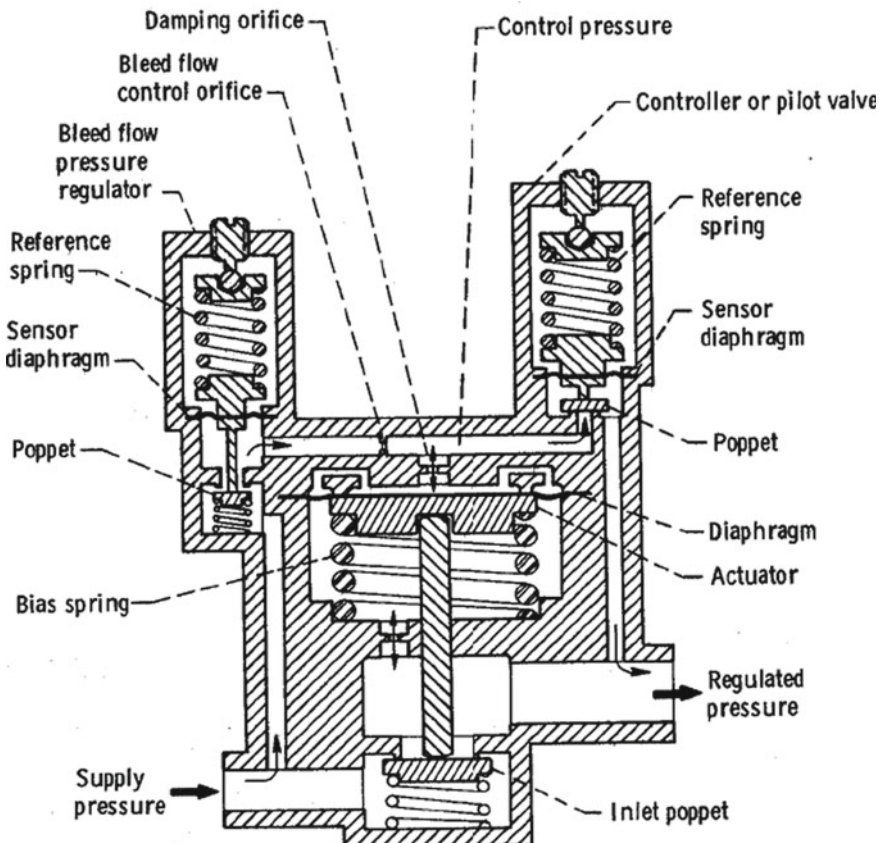
The principal disadvantage of a spring-loaded regulator is that any change in the spring length during the regulation cycle changes the load and the set point of the regulator. This undesirable effect can be counteracted by using a spring having low value of spring constant, or by decreasing the stroke of the movable element [25].

A dome-loaded regulator is a regulator in which the source of reference load is a force obtained by pressurising the dome above the sensing element with gas. A scheme of a dome-loaded regulator is shown in the following figure, due to the courtesy of NASA [43].



The source of load in a regulator of the dome-loaded type is not a spring. It is the reference pressure which a pilot gas exerts on the dome above the sensing element. The pilot gas, which may be the same as the gas whose pressure is to be regulated, is supplied to the dome through a small loader valve. The loader valve reduces the supply pressure to the desired reference pressure. The excess of pilot gas is directed to a vent side through an orifice. The poppet of the inlet valve is opened or closed by the pressure of the pilot gas and by the stroke of the diaphragm, which depends on the chosen pressure.

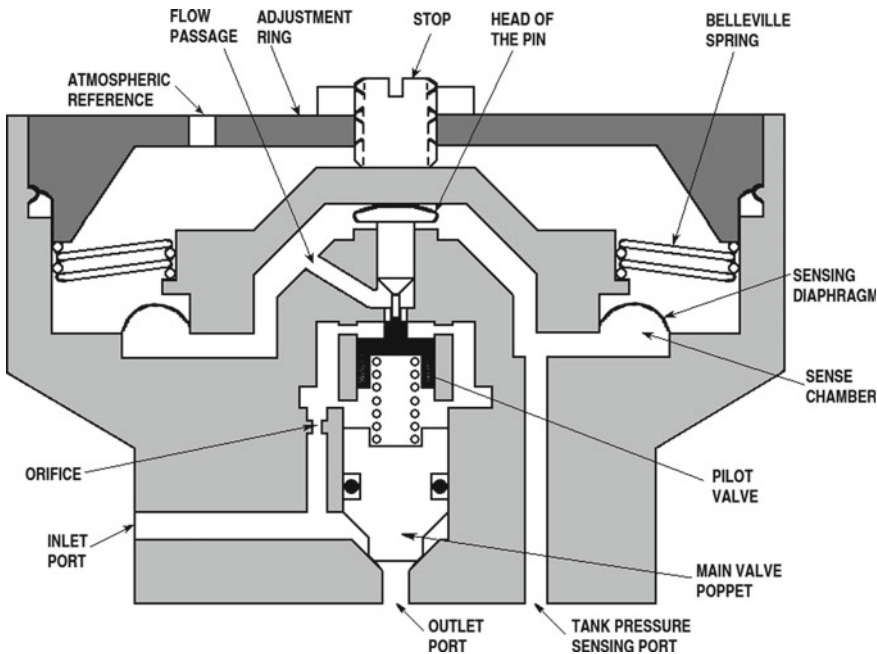
A pilot-operated regulator is a small flow control device operated by a small actuation force which controls indirectly a large flow requiring a large actuation force. A scheme of a pilot-operated regulator is shown in the following figure, due to the courtesy of NASA [43].



A non-modulating regulator consists principally of a pressure switch and an on-off solenoid valve. The pressure switch senses the pressure in a tank, and the on-off valve controls the flow of a pressurising gas to the tank. A pressure transducer with an amplifying circuit may be used instead of the pressure switch. When the pressure in the tank decreases below the minimum desired value, the electrical contacts of the pressure switch close, and an electrical signal opens the solenoid valve. This causes the pressurising gas to flow to the tank to increase the pressure in the tank. As the pressure in the tank approaches the desired maximum value, the contacts of the pressure switch open, the solenoid valve is not fed by current, and the flow of the pressurising gas stops. Therefore, the pressure in the tank oscillates between a minimum value and a maximum value. Since this regulator requires an external source of energy, then a failure of this source of energy or of any of its components can cause a failure of a system of pressurisation using the regulator [43].

Another example of non-modulating regulator is the device developed by the Frebank Company. This regulator is a single stage, pilot operated valve meant to control the pressure in the tank of a missile. The metering valve is closed until the pressure in the tank falls below the lower set point. When this happens, the metering

valve of the regulator opens to full flow until the pressure in the tank reaches the upper set point, at which time the valve closes. A scheme of this valve is shown in the following figure, re-drawn from [25].



The dead-band of a non-modulating regulator is the pressure range between the upper set point and the lower set point. In the regulator shown in the preceding figure, the two set points are determined by the pre-deflection point and the post-deflection point, which limit the travel of the Belleville springs. The pre-deflection point is determined by the adjustment ring, and the post-deflection point is determined by the stop. The regulated pressure exerts a force on the sensing diaphragm through the sensing port. The force acting on the diaphragm is transmitted by the diaphragm assembly to the Belleville springs. In the absence of pressure, no force acts on the diaphragm. In this condition, the actuator assembly (comprising the diaphragm and the Belleville springs) holds the head of the pin against the pre-deflection travel stop, and causes the pilot valve to be fully open. The adjustment ring provides the pre-deflection adjustment. Gas at high pressure, introduced into the inlet port, flows through an orifice, through the open pilot valve, and into the sense chamber through the flow passage. When the pilot valve is open, the pressure difference across the orifice causes the pressure in the chamber behind the poppet of the main valve to decrease, thereby creating a pressure difference across the poppet. This pressure difference creates a force unbalance, and the poppet opens until it bottoms on the shank of the seat of the pilot valve. Now, the gas flows directly through the main valve into the ullage space. When the pressure in the tank reaches the value corresponding

to the pre-deflection setting of the Belleville springs, the actuator assembly snaps to the post-deflection stop. Now, the pilot valve, which is no longer held open by the actuator assembly, is closed by the spring between the poppets. When the pilot valve is closed, the pressure increases in the chamber between the poppets, and reaches a value where the poppet of the main valve closes. The pressure in the chamber continues to increase, until it becomes equal to the inlet pressure, and then both poppets are held on their seats by the pressure difference between the inlet and the outlet, and also by the spring force of the poppet. When the actuator assembly is at the post-deflection stop and both poppets are closed, the regulator is in lock-up. In this condition, any demand on the system decreases the pressure in the ullage space. As the pressure drops to a value of the post-deflection setting, the actuator assembly snaps to the pre-deflection point. The pin moves the poppet of the pilot valve to the full open position, and the chamber between the poppets evacuates to create the pressure difference to cause the poppet of the main valve to open. This cycle is repeated to hold the regulated pressure in the dead-band [25].

For the pressure regulators described above, the characteristic flow area A_c (m^2) of the regulator, that is, the area of the valve in fully open position, can be determined as a function of the required mass flow rate \dot{m} (kg/s) and of the regulated outlet pressure p_r (N/m^2) at the minimum allowable inlet pressure p_i (N/m^2) of the pressurising gas, by using the equations of Sect. 5.11, which govern the flow of gases through orifices. These equations are

$$\dot{m} = C_d A_c \left\{ \frac{2\gamma p_i \rho_i}{\gamma - 1} \left[\left(\frac{p_r}{p_i} \right)^{\frac{2}{\gamma}} - \left(\frac{p_r}{p_i} \right)^{\frac{\gamma+1}{\gamma}} \right] \right\}^{\frac{1}{2}}$$

which holds under non-choked flow conditions, and

$$\dot{m} = C_d A_c \left[\gamma p_i \rho_i \left(\frac{2}{\gamma + 1} \right)^{\frac{\gamma+1}{\gamma-1}} \right]^{\frac{1}{2}}$$

which holds under choked (that is, maximum) flow conditions. In the preceding equations, C_d is the coefficient of discharge, and ρ_i (kg/m^3) is the density of the gas upstream of the regulator. The design values of C_d range from 0.6 to 0.7 [3].

As an example of application, the following data are known for the gas (helium) pressure regulator used in a rocket engine: design mass flow rate $\dot{m} = 0.02177 \text{ kg/s}$, minimum allowable inlet pressure $p_i = 1.689 \times 10^6 \text{ N/m}^2$, inlet temperature $T = 572 \text{ K}$ at the minimum inlet pressure, required regulated outlet pressure $p_r = 1.158 \times 10^6 \text{ N/m}^2$, and flow discharge coefficient $C_d = 0.65$ of the regulator.

It is required to calculate the characteristic area A_c of the pressure regulator.

From [40] we take the following data for helium in the inlet conditions: specific heat ratio $\gamma = 1.666$, and density $\rho_i = 1.416 \text{ kg/m}^3$.

As has been shown in Sect. 5.11, the critical pressure ratio of helium is

$$\frac{p_c}{p_i} = \left(\frac{2}{\gamma + 1} \right)^{\frac{\gamma}{\gamma-1}} = \left(\frac{2}{1.666 + 1} \right)^{\frac{1.666}{1.666-1}} = 0.4873$$

Since

$$\frac{p_r}{p_i} = \frac{1.158 \times 10^6}{1.689 \times 10^6} = 0.6856$$

then the value of the pressure ratio p_r/p_i is greater than the critical value (non-choked flow conditions).

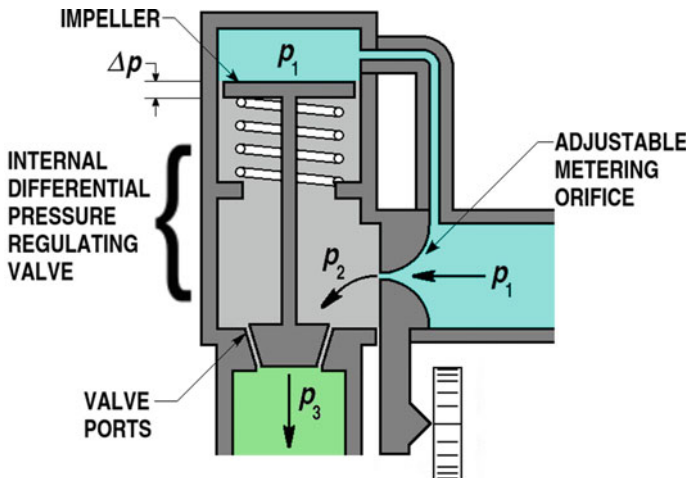
After introducing $\dot{m} = 0.02177 \text{ kg/s}$, $C_d = 0.65$, $\gamma = 1.666$, $p_i = 1.689 \times 10^6 \text{ N/m}^2$, $\rho_i = 1.416 \text{ kg/m}^3$, and $p_r/p_i = 0.6856$ in the equation written above of gas flow through orifices and solving for A_c , we find

$$A_c = \frac{0.02177}{0.65 \times \left[\frac{2 \times 1.666 \times 1.689 \times 10^6 \times 1.416}{1.666 - 1} \times \left(0.6856^{\frac{2}{1.666}} - 0.6856^{\frac{1.666+1}{1.666}} \right) \right]^{\frac{1}{2}}} \\ = 3.245 \times 10^{-5} \text{ m}^2$$

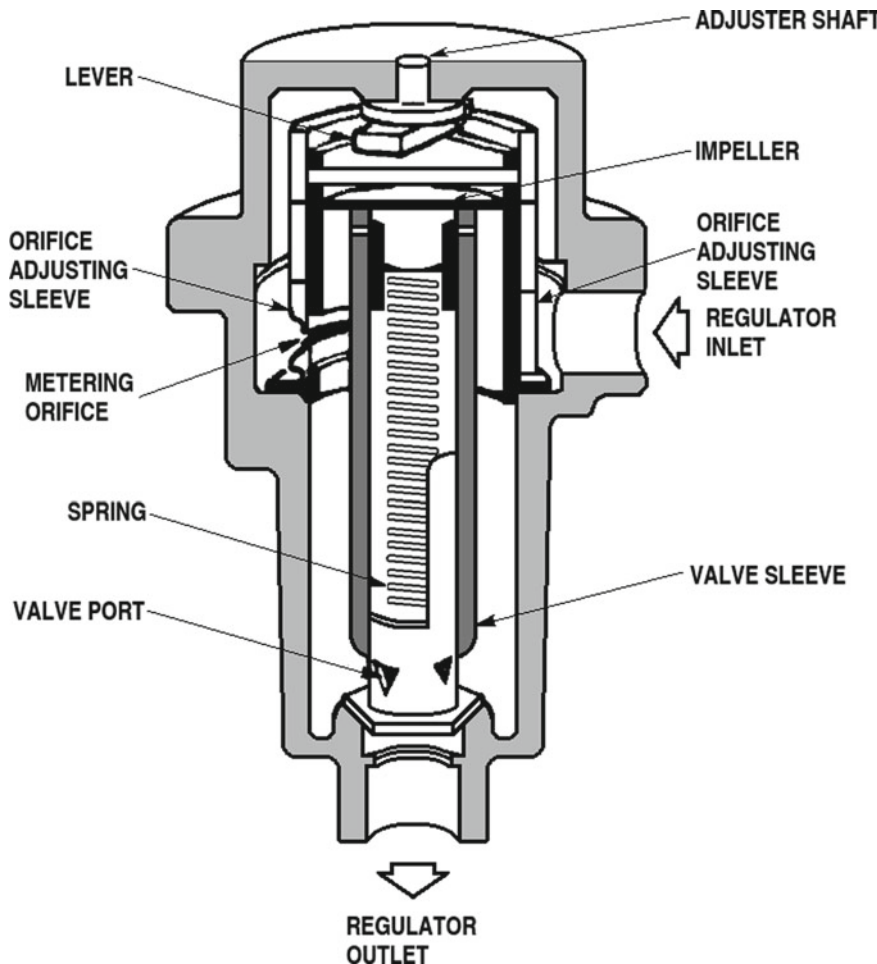
5.14 Design of Differential Pressure Regulators

A differential pressure regulator is used to measure the volume flow rate q (m^3/s) of a liquid in a line, and to maintain it at a desired constant value.

The measurement can be performed by using a variable head flow-meter (for example, an orifice, or a nozzle, or a Venturi tube) installed in the main line. The flow-meter has static pressure taps placed at two points along the fluid stream, as has been shown in Sect. 5.7, for the Venturi tube. In Sect. 5.7, it has also been shown how the volume flow rate depends on the pressure drop. When the pressure drop across a flow-meter is kept constant, then the volume flow rate will also be constant. The pressure drop is kept constant by using a pressure-reducing regulator. The static pressures are impressed to the fluid on opposite sides of the sensing element of the regulator. These pressures can be adjusted by means of a spring placed on one side of the sensing element. The force provided by the spring can be regulated so as to balance the lower value of static pressure against the upper value. The working principle of a direct-acting differential pressure regulator, designed by the W.A. Kates Company, is illustrated in the following figure, re-drawn from [44].



In this regulator, the internal differential pressure regulating valve maintains a constant pressure drop across the adjustable metering orifice to provide the set flow rate, independently of pressure variations which may occur upstream or downstream of the device. The supply pressure p_1 upstream of the valve is balanced by the pressure p_2 within the valve plus the force provided by the spring. When the pressure p_1 upstream of the regulator increases above the desired pressure drop, then the instantaneous imbalance of pressure moves the impeller downward. This movement restricts the valve ports and therefore increases the orifice back-pressure p_2 , so as to restore the difference of pressure and the flow rate at the previous settings. The valve works oppositely in case of an increase in the outlet pressure p_3 . A direct-acting differential pressure regulator, designed by the W.A. Kates Company, is shown in the following figure, re-drawn from [25].



5.15 Design of Relief Valves

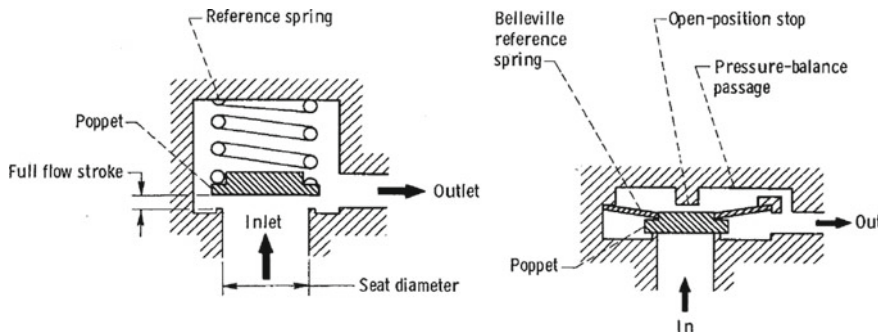
Relief valves are devices which measure and regulate the pressure of a fluid in a tank by discharging fluid above the permitted limits to another tank, where the pressure is lower. They open automatically when a pre-set level of pressure is reached in the tank under control, and are used primarily in hydraulic systems. Safety valves are particular relief valves which control the pressure in pneumatic systems by discharging the excessive gas or vapour to the atmosphere.

In aerospace airborne systems, relief valves are used for both liquid and gaseous substances, and differ one from another depending on the fluids for which they are

used. For example, there are relief valves for liquid oxygen, and relief valves for gaseous helium. The fluid in excess is discharged overboard.

An excess of pressure can occur in a tank due to thermal changes or to leaking valves. Relief valves differ from other valves, because their operation creates a high pressure drop during flow [43].

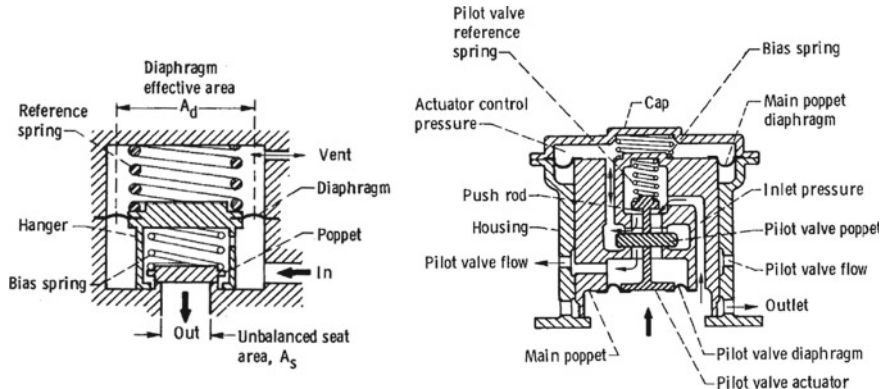
A relief valve consists of a valve body, a source of reference load (such as a spring), and a control element (such as a poppet) which matches with a seat. The following figure, due to the courtesy of NASA [43], shows a modulating (left) and a non-modulating (right) directly-operated relief valve.



In a direct-operating relief valve, the reference load due to the spring is applied at all times to the control element. The reference load acts on the control element against the pressure in the tank or in the circuit under control. The intensity of the load determines the set point of the relief pressure. When the pressure of the fluid in the tank rises to the level necessary to balance the reference load, then the control element moves from the seat so as to discharge the fluid in excess to a reservoir of lower pressure placed downstream of the valve. Likewise, when the pressure of the fluid in the tank decreases below the set point, then the reference load acting against the pressure closes the valve.

A relief valve has good operating characteristics when the pressure p_f for rated flow and the pressure p_r for reseat closely approach the cracking pressure p_c . The cracking pressure is the relief setting of the valve, that is, the pressure level at which the leakage flow reaches some specified value. The cracking pressure is always less than the allowable working pressure of the tank, and is usually less than 110% of the normal operating pressure. The rated flow is usually established for pressures 10% greater than the pressure setting of the relief valve. The reseat pressure is less than the cracking pressure, by an amount depending on the configuration of the closure (control element and seat). A reseat pressure of 95% of the cracking pressure is a common value [25].

A relief valve may be not only directly-operated, as shown in the preceding figure, but also inversely-operated or pilot-operated. The following figure, due to the courtesy of NASA [43], shows an inversely-operated (left) and a pilot-operated (right) relief valve.



In an inversely-operated relief valve, the reference load holding the poppet on the seat increases with increasing pressure. The diaphragm senses the increasing pressure in the tank and, at some value of pressure, strokes the hanger which comes in contact with the poppet and reduces the closing force applied to the poppet. When the forces applied to the poppet are equal, then the valve is at the cracking pressure. The bias spring applies a load to the poppet to place it in the initial position at low-pressure sealing [43]. It is desirable that the force which holds the poppet on the seat at a specified pressure p_t (where p_t is less than the cracking pressure p_c) should be as great as possible. For this purpose, the effective area A_d of the diaphragm is larger than the unbalanced seat area A_s , as follows

$$A_d \approx \frac{p_c}{p_c - p_t} A_s$$

The effective diameter of the diaphragm becomes increasingly larger than the diameter of the seat when the maximum closing pressure approaches the cracking pressure.

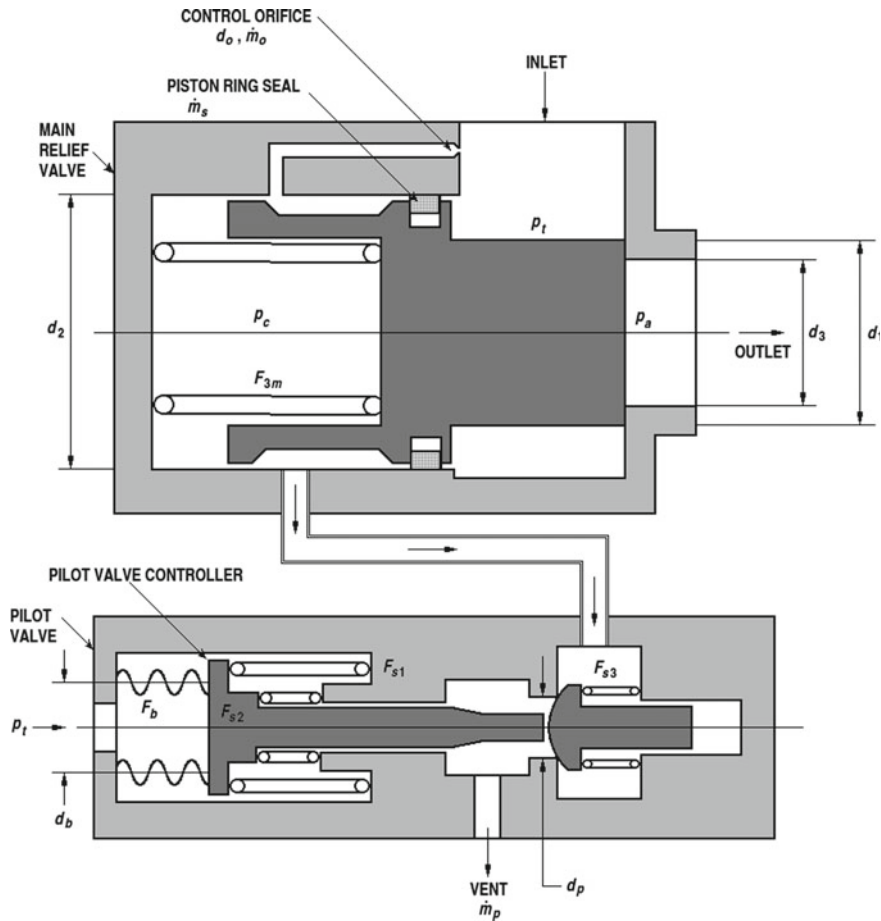
A pilot-operated relief valve is used when it is necessary to control large flows. When this valve is in the non-relieving conditions, the control pressure of the actuator is at the level of the inlet pressure, and the resulting force holds the main poppet in the position of closure. When the inlet pressure increases so as to reach the cracking value, the pilot valve partially strokes, the control pressure of the actuator is ported to the outlet cavity, the pressure in the actuator control-pressure is reduced so much that the resulting force is zero, and the main poppet is ready to open. As the inlet pressure continues to increase, the pilot valve stroke increases, the pressure in the control-pressure cavity decreases, and the resulting force opens the main poppet [43].

In airborne applications, lightweight materials, such as aluminium, are used for the valve body. The source of reference load is a force acting against an increase in pressure on the control element until the set point of pressure relief is reached. The most common element used for this purpose is a compressed spring.

The closure unit comprises a seat and a control element. The seat may have a flat, or spherical, or conical shape. The control element may be a ball, or a poppet (which in turn may be conical or V-shaped), or a piston.

Another type of pilot-operated relief valve, used to protect propellant tanks from overpressure, has been described by Huzel and Huang [3]. A scheme of this valve is illustrated in the following figure, re-drawn from [3]. Both the main valve and the pilot valve are normally held closed by the spring forces F_{sm} and F_{s3} and by the control pressure p_c . The controller of the pilot valve senses the pressure p_t in the tank. When the pressure in the tank reaches or exceeds the preset level, the pilot valve is actuated to crack. This vents the actuator control pressure p_c of the main relief valve and in turn permits the main valve to open. The position of the poppet of the main valve depends on the control pressure p_c , which in turn is controlled by the position of the poppet of the pilot valve and by the pressure p_t in the tank.

With reference to the following figure, it is required to determine the dimensions, in terms of diameters, for the main valve and for the pilot valve. The following data are known: temperature of the pressurising gas (helium) $T = 389$ K, set point for the absolute pressure of relief in the tank $p_t = 1.138 \times 10^6$ N/m², required maximum mass flow rate $\dot{m} = 1.361$ kg/s, discharge coefficient of the main valve $C_d = 0.75$, estimated leakage past the actuator piston seal of the main valve $\dot{m}_s = 0.001361$ kg/s, diameter of the control orifice $d_o = 2.032$ mm = 0.002032 m, discharge coefficient for the control orifice and for the pilot valve $C_{do} = 0.60$, and maximum value of the absolute ambient pressure $p_a = 1.031 \times 10^5$ N/m² (atmospheric pressure).



From [40] we take the following data for helium at $T = 389 \text{ K}$ and $p_t = 1.138 \times 10^6 \text{ N/m}^2$: specific heat ratio $\gamma = 1.666$, and density $\rho_t = 1.403 \text{ kg/m}^3$.

As has been shown in Sect. 5.11, the critical pressure ratio of helium is

$$\frac{p_c}{p_t} = \left(\frac{2}{\gamma + 1} \right)^{\frac{\gamma}{\gamma - 1}} = \left(\frac{2}{1.666 + 1} \right)^{\frac{1.666}{1.666 - 1}} = 0.4873$$

Since

$$\frac{p_a}{p_t} = \frac{0.1031 \times 10^6}{1.138 \times 10^6} = 0.09060$$

then the value of the pressure ratio p_a/p_t is less than the critical value (choked flow conditions). Therefore, the following equation holds for the mass flow rate \dot{m} through the main valve

$$\dot{m} = C_d \frac{\pi d_3^2}{4} \left[\gamma p_t \rho_t \left(\frac{2}{\gamma + 1} \right)^{\frac{\gamma+1}{\gamma-1}} \right]^{\frac{1}{2}}$$

where C_d is the coefficient of discharge, d_3 (m) is the diameter of the orifice, and p_t (N/m²) and ρ_t (kg/m³) are respectively the pressure and the density of the gas upstream of the orifice of the main valve.

After substituting $\dot{m}_o = 1.361$ kg/s, $C_d = 0.75$, $\gamma = 1.666$, $p_t = 1.138 \times 10^6$ N/m², and $\rho_t = 1.403$ kg/m³ in the preceding equation and solving for d_3 , we find

$$\begin{aligned} d_3 &= 2 \times \left(\frac{1.361}{3.1416 \times 0.75} \right)^{\frac{1}{2}} \\ &\times \left[1.666 \times 1.138 \times 10^6 \times 1.403 \times \left(\frac{2}{1.666 + 1} \right)^{\frac{1.666+1}{1.666-1}} \right]^{-\frac{1}{4}} \\ &= 0.05018 \text{ m} \approx 5 \text{ cm} \end{aligned}$$

The displacement x_{mo} (m) of the movable element of the main valve from the closed position to the fully opened position results from the following equation

$$A_3 = \frac{\pi d_3^2}{4} = \pi d_3 x_{mo}$$

Hence

$$x_{mo} = \frac{d_3}{4} = \frac{0.05018}{4} = 0.01255 \text{ m} = 1.255 \text{ cm}$$

The general equation which expresses the equilibrium of the forces acting in the main valve is

$$F_{sm} + p_c A_2 - p_t (A_2 - A_1) - p_a A_3 = F_{seat}$$

where F_{sm} (N) is the pre-load of the spring of the main valve, p_c (N/m²) is the control pressure, p_t (N/m²) is the pressure in the tank, $A_2 = \frac{1}{4}\pi d_2^2$ (m²), $A_1 = \frac{1}{4}\pi d_1^2$ (m²), $p_a = 1.031 \times 10^5$ N/m² is the atmospheric pressure, $A_3 = \frac{1}{4}\pi d_3^2$ (m²), and F_{seat} (N) is the seating force of the main valve.

In the cracking conditions, the general equation becomes

$$F_{sm} + p_{cc} A_2 - p_{tc} (A_2 - A_1) - p_a A_3 = 0$$

where p_{cc} (N/m²) is the value of the control pressure p_c in the cracking conditions and p_{tc} (N/m²) is the value of the tank pressure p_t in the cracking conditions.

For any displacement x_m (m) of the movable element of the main valve from the closed position (such that $x_m < x_{mo}$), the general equation becomes

$$F_{sm} + k_{sm}x_m + p_c A_2 - p_t(A_2 - A_1) - p_a A_3 = 0$$

where k_{sm} (N/m) is the constant of the spring of the main valve.

When the main valve is fully open ($x_m = x_{mo}$), the general equation becomes

$$F_{sm} + k_{sm}x_{mo} + p_{co}A_2 - p_{to}(A_2 - A_1) - p_a A_3 = 0$$

where p_{co} (N/m²) and p_{to} (N/m²) are respectively the control pressure p_c and the tank pressure p_t in the fully open conditions.

When the main valve is at the start to reseat ($x_m = x_{mo}$), the general equation becomes

$$F_{sm} + k_{sm}x_{mo} + p_{cr}A_2 - p_{ti}(A_2 - A_1) - p_a A_3 = 0$$

where p_{cr} (N/m²) and p_{tr} (N/m²) are respectively the control pressure p_c and the tank pressure p_t in the reseat conditions.

When the main valve is fully reseated ($x_m = 0$), the general equation becomes

$$F_{sm} + p_{cr}A_2 - p_{tr}(A_2 - A_1) - p_a A_3 = 0$$

The mass flow rate \dot{m}_p (kg/s) of the pilot valve must be greater than to the mass flow rate \dot{m}_o (kg/s) through the control orifice of the main valve summed to the leakage \dot{m}_s (kg/s) past the actuator piston seal of the main valve, in order for the control pressure p_c to be sufficiently vented.

The mass flow rate through the control orifice of the main valve results from

$$\dot{m}_o = C_{do} \frac{\pi d_o^2}{4} \left[\gamma p_t \rho_t \left(\frac{2}{\gamma + 1} \right)^{\frac{\gamma+1}{\gamma-1}} \right]^{\frac{1}{2}}$$

After substituting $C_{do} = 0.60$, $d_o = 0.002032$ m, $\gamma = 1.666$, $p_t = 1.138 \times 10^6$ N/m², and $\rho_t = 1.403$ kg/m³ in the preceding equation, we find

$$\begin{aligned} \dot{m}_o &= 0.60 \times \frac{3.1416 \times 0.002032^2}{4} \times [1.666 \times 1.138 \times 10^6 \times 1.403 \\ &\quad \times \left(\frac{2}{1.666 + 1} \right)^{\frac{1.666+1}{1.666-1}}]^{\frac{1}{2}} = 0.001785 \text{ kg/s} \end{aligned}$$

The total mass flow rate through the control cavity of the pilot valve results from

$$\dot{m}_o + \dot{m}_s = 0.001785 + 0.001361 = 0.003146 \text{ kg/s}$$

We set the mass flow rate \dot{m}_p of the pilot valve equal to the preceding value multiplied by 1.5, as follows

$$\dot{m}_p = 1.5 \times 0.003146 = 0.004719 \text{ kg/s}$$

In order for the flow through the restrictions to be maximum, the pressure ratio p_c/p_t of the control pressure to the tank pressure should be at least equal to the critical value

$$\frac{p_c}{p_t} = \left(\frac{2}{\gamma + 1} \right)^{\frac{\gamma}{\gamma - 1}}$$

After substituting $p_t = 1.138 \times 10^6 \text{ N/m}^2$ and $\gamma = 1.666$ in the preceding equation and solving for p_c , we find the maximum allowable value of the control pressure to be

$$p_c = 1.138 \times 10^6 \times \left(\frac{2}{1.666 + 1} \right)^{\frac{1.666}{1.666 - 1}} = 5.545 \times 10^5 \text{ N/m}^2$$

We substitute the value found above for p_c , $\dot{m}_p = 0.004719 \text{ kg/s}$, $C_{do} = 0.60$, $\gamma = 1.666$, and $\rho_t = 1.403 \text{ kg/m}^3$ in the following equation

$$\dot{m}_p = C_{do} \frac{\pi d_p^2}{4} \left[\gamma p_c \rho_t \left(\frac{2}{\gamma + 1} \right)^{\frac{\gamma+1}{\gamma-1}} \right]^{\frac{1}{2}}$$

and solve this equation for the unknown value of the diameter d_p of the port in the pilot valve. By so doing, we find

$$d_p = 2 \times \left(\frac{0.004719}{3.1416 \times 0.60} \right)^{\frac{1}{2}} \times \left[1.666 \times 5.545 \times 10^5 \times 1.403 \times \left(\frac{2}{1.666 + 1} \right)^{\frac{1.666+1}{1.666-1}} \right]^{-\frac{1}{4}} = 0.003954 \text{ m}$$

The displacement x_{po} (m) of the movable element of the pilot valve from the closed position to the fully opened position results from the following equation

$$A_p = \frac{\pi d_p^2}{4} = \pi d_p x_{po}$$

Hence

$$x_{po} = \frac{d_p}{4} = \frac{0.003954}{4} = 0.0009886 \text{ m} \approx 1 \text{ mm}$$

The equation which expresses the equilibrium of the forces acting on the poppet of the pilot valve is

$$(p_c - p_a)A_p + F_{s3} = F_p$$

where $p_c = 5.545 \times 10^5 \text{ N/m}^2$ is the control pressure, $p_a = 1.031 \times 10^5 \text{ N/m}^2$ is the ambient (atmospheric) pressure, $A_p = \frac{1}{4}\pi d_p^2 (\text{m}^2)$ is the area of the port in the pilot valve, $d_p = 0.003954 \text{ m}$ is the diameter of the port in the pilot valve, F_{s3} (N) is the force due to the spring acting on the poppet, and F_p (N) is the seating force of the poppet.

The equation which expresses the equilibrium of the forces acting on the actuator of the pilot valve is

$$(p_t - p_a)A_b - F_b - F_{s1} - F_{s2} = F_a$$

where $p_t = 1.138 \times 10^6 \text{ N/m}^2$ is the set point for the absolute pressure of relief in the tank, $p_a = 1.031 \times 10^5 \text{ N/m}^2$ is the ambient (atmospheric) pressure, $A_b = \frac{1}{4}\pi d_b^2 (\text{m}^2)$ is the area of the cross section of the sensor bellows, F_b (N) is the force due to the sensor bellows, F_{s1} (N) and F_{s2} (N) are the forces due to the springs acting on the sensor bellows, and F_a (N) is the actuating force of the pilot valve.

The pilot valve starts to open when $F_a > F_p$.

5.16 Design of Check Valves

A check valve is a device which prevents a moving fluid from reversing its direction of motion. A check valve allows a fluid to move freely in one direction, and stops the motion in case of a pressure reversal. A pressure reversal may occur in a fluid either normally or as a result of a failure. In the latter case, a flow reversal must be promptly stopped, in order to avoid an overflow or an overpressure in a tank, or an unwanted combination of reactive fluids, or other damages to components of a rocket engine.

A check valve operates automatically, because its movable element is actuated by the forces exerted by the moving fluid. In case of aerospace vehicles, the movable element of a check valve is spring-loaded, in order for the valve to be operated independently of either the gravitational force or the attitude of the vehicle. A check valve requires neither an actuation signal nor a source of power for its operation. Howell and Weathers [25] have identified some criteria to be considered in the design and in the choice of a particular type of check valve. These criteria are briefly indicated below.

The first of them concerns the pressure drop across a check valve. In valves used for aerospace applications, it is desirable to keep the increase in pressure drop with increasing volume flow rate as low as possible. The increase in pressure drop in a valve depends on the type (sphere or cone frustum or poppet having another shape) of its closing element.

Another criterion concerns the type of seal used in a check valve. This is because the sealing properties of a check valve depend on the sealing material, on the initial

load of the spring, and on the difference of pressure across the closing element of the valve. In case of a pressure reversal, a check valve leaks until the back pressure acting on it becomes as high as to provide a sufficient seating force. In order for the valve not to leak when the reversal pressure is null or very low, the initial load of the spring must be high, which fact implies a high value of pressure drop when the controlled fluid moves in its normal direction. The use of elastic materials for the seat makes it possible to reduce leakage at low values of the seating load.

Another criterion concerns the cracking and the reseating pressures of a check valve. As has been shown in Sect. 5.15, the cracking pressure of a valve is the minimum pressure which assures a given value of flow rate. The reseating pressure of a valve is the reverse differential pressure needed to keep leakage at or below a given value. A proper choice of the spring loading and of the seating properties can reduce the reseating pressure. The cracking and the reseating pressures of a check valve depend on its pressure drop and on its leakage properties.

Another criterion concerns the type of fluid moving through a check valve. The materials (including metals, seals, and coatings) of which a valve is made must be compatible with the fluid controlled by the valve. In particular, the choice of the materials depends on whether the fluid is a liquid or a gas. In the latter case, special care must be taken with gases of low molar mass, such as hydrogen and helium.

Another criterion concerns the operating pressure of a check valve. The body of a valve must be designed for the maximum pressure to which the valve is subject. In particular, when a valve is rapidly closed, a water hammer can arise in the valve. This phenomenon increases the level of pressure several times the normal operating pressure. When a valve is subject to a large number of pressure cycles, a failure due to fatigue must be taken into account.

Another criterion concerns the temperature at which the fluid and the valve operate. Special care must be taken of the non-metallic materials which are used for the seals. All materials used in a valve must be designed to withstand the worst thermal conditions in their operating environment. Since the mass of the valve acts as a heat sink, short-term excursions of temperature beyond the recommended limits are tolerable. Particular attention should be given to temperature gradients, which can give rise to binding effects due to the different coefficients of thermal expansion of the materials.

Another criterion concerns the sensitivity of either the fluid system or the fluid itself to contamination. Contamination can cause malfunction or internal leakage in a valve. Special care must be taken of the valve body and of the seals.

Another criterion concerns the operations of maintenance required by a valve. The maintenance requirements should be reduced as far as possible, and the need to use special tools should be avoided. Seals requiring periodic replacement should be readily available and easily accessible. Care must be taken to avoid contamination during disassembly and service.

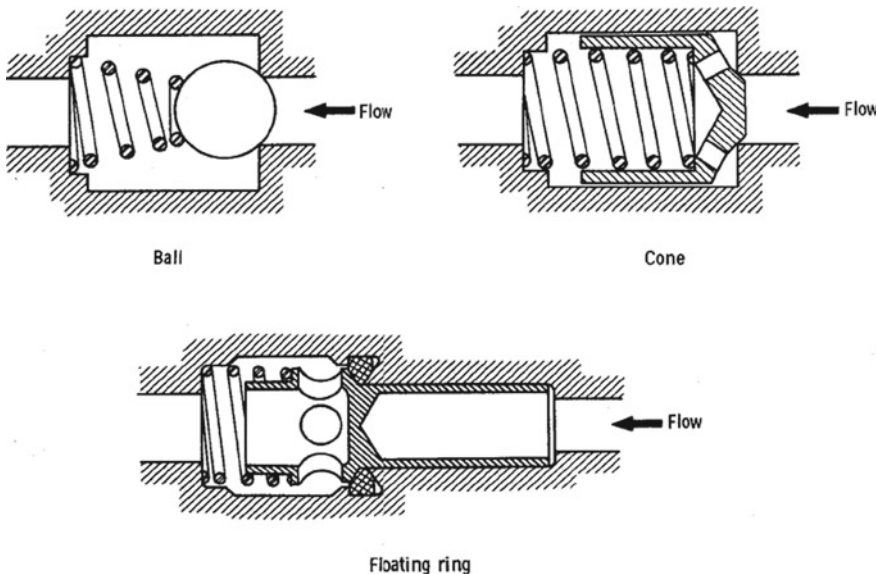
Another criterion concerns the mass and the size of a valve, which are aspects of primary importance in valves used for aerospace applications. For example, in a check valve of the ball type, the mass of the ball is proportional the cube of its radius; by contrast, in a check valve of the flapper type, the mass of the closing element is

nearly proportional to the square of its linear size. Therefore, check valves of the ball type are rarely used when the radius of the ball exceeds 1 cm. In this case, flapper-type or swing-type check valves are used.

Another aspect concerns the cost of a check valve. The cost depends on such factors as operating pressure, temperature, flow rate, leakage requirements, type of fluid, mass, reliability, and life-cycle requirements. In case of check valves used for aerospace applications, performance and reliability are factors of primary importance.

Another criterion concerns the operating life of a check valve. The operating life depends on such factors as type of fluid, contamination, operating temperature, stresses, number of cycles, type of seals, materials of construction, and procedures of maintenance. In order to increase the operating life of a valve, loads and stresses acting on the valve components should be reduced as far as possible. However, valves to be used for aerospace applications should not be over-designed for their life-cycle requirements.

According to Tomlinson and Keller [43], check valves can be classified in two categories: poppet valves and flapper valves. Three different valves (ball, cone, and floating ring) of the poppet type are shown in the following figure, due to the courtesy of NASA [43].



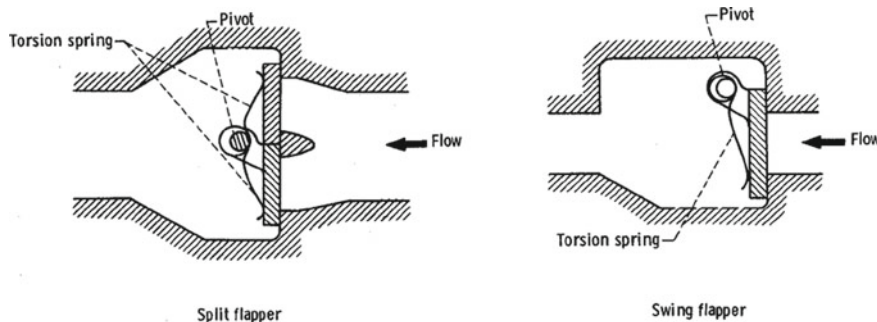
A check valve of the poppet type has a poppet as its closing element. This poppet translates axially in the valve body and a compressed spring of the coil type forces the poppet against the seat. Valves of this type are used in applications requiring low leakage in the direction of the checked flow and low pressure drop in the direction of the free flow. The cracking pressure is low (in the range going from 21000 to 103000 N/m², according to [43], and the full-flow pressure is as close to the cracking

pressure as possible. The cracking pressure of check valves of the poppet type can be increased by increasing the load of the return spring. In these conditions, a check valve can be used as a relief valve or a back-pressure regulator [43]. A check valve of the ball type is illustrated in the preceding figure. This valve has a hard ball as its closing element. The ball is spring-loaded against a circular, conical, or spherical seat. In order to reduce leakage, a soft seal is sometimes used. This soft seat is made of Teflon®, or of another plastic or elastomeric material. Otherwise, a combination of soft with hard materials is used for the seat. The force due to the fluid stream lifts the ball off the seat against the load provided by the spring, and the flow passes around the ball. Since the flow must surround the ball, then a check valve of the ball type has a tendency toward turbulence and a higher pressure drop than other types of check valves. In normal operating conditions, the ball may rotate slightly on the return spring, thereby causing wear on the ball and on the seat. A check valve of the ball type is prone to chatter when opened by a low flow which does not fully stroke and hold the ball in the full-open position. By chatter we mean an uncontrolled seating and reseating of the closing element of a valve. Check valves of the ball type are simple and cheap to manufacture, since the seat is the only costly detail. They are used in low-flow applications where the stroke is short and the ball will self-guide into the seat [43].

A check valve of the cone type is an improvement of the valve of the ball type described above. The improvement is obtained by guiding and aligning the closing element in a constant direction, in order for its contact with the seat to be continuous and even. For this purpose, the ball is replaced by a piston sliding in a hollow cylinder and having a conical seating surface at one end. This surface is spring-loaded to seat against a spherical or conical surface, which may be made of either a soft material or a hard material. A check valve of the cone type has a lower pressure drop than one of the ball type having the same size, and a lower tendency to chatter, because of the guided movement and the resultant damping of its closing element. The presence of contaminating particles in the seating area and between the piston and the body of the valve can cause sticking or cocking with consequent leakage between the piston and the seating area.

A check valve of the floating-ring type is also a valve having a closing element guided and aligned in a constant direction. It has a mushroom-shaped poppet, whose stem slides in the valve body and whose head seals through an O-ring against a circular flat or tapered seat. The force due to the fluid stream causes the head of the poppet to move off the seat in the flow direction, and the fluid passes through the stem of the poppet, around the head of the poppet, and through the body of the valve. A check valve of this type has a lower pressure drop at an equal flow rate than a ball or a cone check valve. Damping chambers may be incorporated in a floating-ring valve in order to eliminate chatter and hammering. The presence of contaminating particles between the poppet stem and the valve body can cause sticking and leakage. A check valve of the floating-ring type has more components and therefore is more costly than a ball or a cone check valve.

Two check valves of the flapper type, namely, a split-flapper (left) and a swing-flapper (right) valve, are shown in the following figure, due to the courtesy of NASA [43].



A check valve of the flapper type has a rotating flapper as its closing element. The loaded spring acting on the flapper is of the torsion type, and the flapper may be either a split element which pivots across the centre of the flow path or a single element which pivots from the side.

Flapper check valves are used in applications requiring low pressure drop with large flow rates. They are often smaller and lighter than those of the poppet type. However, when subject to high pressures, flapper check valves may become excessively heavy [43].

A swing-flapper check valve has a hinged disc which seats against a flat or tapered surface, or a circular sharp edge. A fluid stream moving through the valve in the free-flow direction swings the hinged disc from the seat and out of the flow path, thereby permitting a substantially unrestricted passage with very low pressure drop. When the flow through the valve stops or reverses its direction, the disc swings rapidly to its seat, thereby closing the valve against the reverse flow.

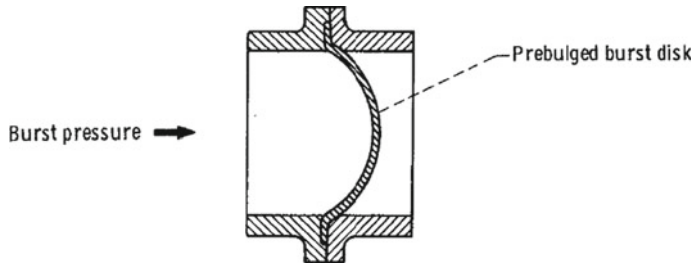
Very low pressure drops can be obtained with swing-flapper check valves, because small opening forces are required, and also because their disc swings out of the flow path. The presence of contaminating particles in the fluid has little effect on their performance. On the other hand, they are particularly subject to water hammer in case of sudden reversal of flow. This is because their disc rotates through a large angle from the open position to the closed position, and consequently the velocity of the reverse flow increases significantly before the complete closure of the disc. For this reason, their performance in eliminating a reverse flow is poor. Check valves of the swing-flapper type are used for applications requiring the minimum value of pressure drop and scarce control of fluid contamination. They are not used for applications having a high tendency toward sudden flow reversal.

Check valves of the split-flapper type have two or more hinged elements instead of one hinged disc. This makes it possible to reduce the moment of inertia of each hinged element. A typical split-flapper valve has two semi-circular elements which are open when the fluid stream moves through the valve in the free-flow direction

and closed otherwise. A pressure drop in a split-flapper valve can be reduced to a minimum value, as is also the case with a swing-flapper valve. For two valves of the same size, the flapper is lighter in a split-flapper valve than is in a swing-flapper valve. In addition, a split-flapper valve can bear a heavier life cycle and has a better performance in case of water hammer than a valve of the other type. Split-flapper valves are used principally in pneumatic systems. Their principal advantage is the minimum pressure drop for a given diameter. They are also scarcely sensitive to fluid contamination and have better performance than swing-flapper valves when a sudden flow reversal may occur.

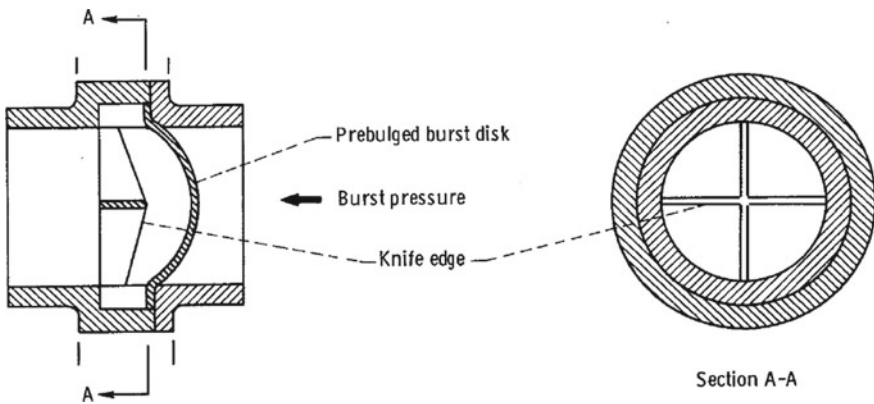
5.17 Design of Burst Discs

A burst disc, also known as a safety disc or a rupture disc or a frangible disc, is a thin metallic diaphragm designed to burst when the pressure in a tank or in a line exceeds a pre-set value. For example, a burst disc is used in a flow-carrying line to initiate flow when ruptured by sufficient pressure in the line. A burst disc commonly used is one of the pre-bulged type, which is shown in the following figure, due to the courtesy of NASA [43].



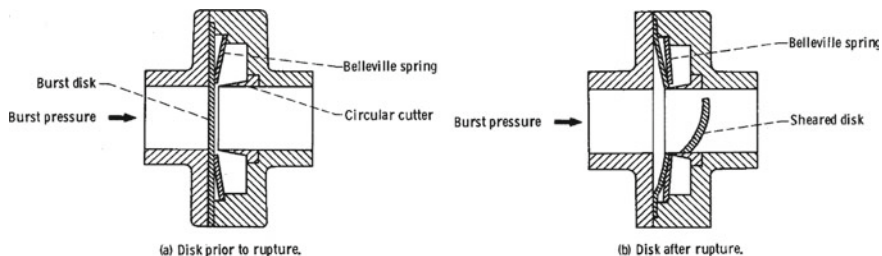
The burst disc shown in the preceding figure bursts due to tension induced by pressure, without the use of local weakening such as coined or machined grooves to initiate and control the bursting.

Another type of burst disc commonly used is the reverse-action knife-blade burst disc, shown in the following figure, due to the courtesy of NASA [43].



The burst disc illustrated in the preceding figure reverses its form under pressure and buckles onto a knife edge, thus requiring a lower pressure to burst than one of the pre-bulged type.

A burst disc of the shear type is shown in the following figure, due to the courtesy of NASA [43].



The burst disc shown above, before rupture (left) and after rupture (right), is pressure-loaded on a circular cutter by means of a Belleville spring, which is compressed into the negative-spring-rate region of the spring stroke. The Belleville spring supports a portion of the pressure acting on the burst disc up to a pre-set burst pressure. When this value of pressure is exceeded, the spring washer starts to stroke, its supporting force decreases rapidly, and the pressure causes the disc to be sheared by the sharp circular cutter. A catch screen may be required to keep the cut disc from moving downstream. The burst pressure of the disc can be pre-set by replacing the cutter with a flat plug and adjusting the Belleville spring washer until the desired burst pressure is indicated by the motion of the burst disc [43].

Burst discs are used for many components of rocket engines, such as hypergolic-start cartridges, repeat-start turbine spinner assemblies, pump-seal drain lines, and some instrumentation. They are also used to seal a cavity against downstream pressure or temperature, or to contain a liquid until a rise of pressure to a desired level ruptures the disc.

The burst pressure is the primary element to be considered in the design of a burst disc. This is because a burst disc must remain intact in all conditions of storage,

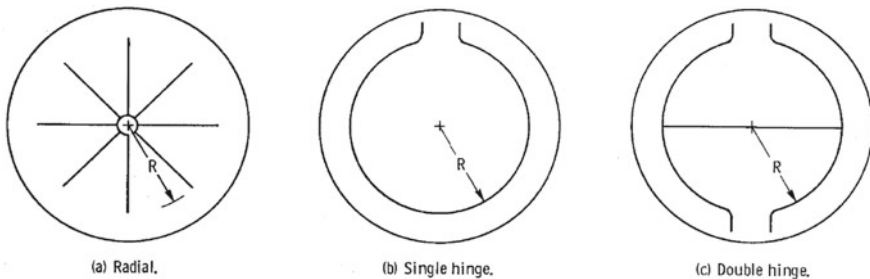
handling, and use of storable or cryogenic fluids, until the desired burst pressure is reached. The value of the burst pressure usually ranges from 6.895×10^3 to 6.895×10^7 N/m² [43], depending on the application.

Low values of burst pressure are desired for a cartridge containing an ignition aid for the thrust chamber of a rocket engine, in order to burst the cartridge discs, release the ignition aid, and establish ignition as soon as possible. Of course, the burst pressure must not be so low as to cause premature rupture in the discs due to the vapour pressure or to the thermal expansion of the propellants, or to handling loads. High values of burst pressure are desired for a burst disc used for the ignition of a pyrotechnic device, so long as the burning rate of the charge does not become excessive and the pressure level remains below the allowable operating pressure of the container [43].

Burst discs are made of aluminium alloys, mild steel, stainless steel, nickel, Monel®, Inconel®, copper, silver, gold, and platinum. Aluminium is used because of its low physical properties and good forming and machining properties. However, since the properties of this material vary widely with temperature, the upper temperature limit is only about 394 K [43]. Mild steel requires protection from corrosion. This material has low cost and good formability. Stainless steel and Inconel® are difficult to tool. Inconel® can be used over a wide range of temperatures. Silver, gold, and platinum resist corrosion and have good physical properties.

Burst discs can be attached mechanically or by welding. They must not be corroded by the fluid, and the materials of which they are made must not cause decomposition in the fluid.

The thickness of burst discs ranges from 0.05 to 3.18 mm [43], in case of coined-groove discs, for the material remaining under the groove. In this type of disc, the material is weakened locally by grooves which are stamped into the metal. The following figure, due to the courtesy of NASA [43], shows three patterns (radial, single hinge, and double hinge) used for these grooves.



5.18 Design of Explosive Valves

Explosive valves, also known as squib valves, are shut-off devices actuated by a very compact source of energy only once in a given mission.

The source of energy used by them is an explosive charge which generates high pressure on an actuator. It is possible to actuate repeatedly an explosive valve by using multiple squibs. However, most explosive valves are designed to operate only once, and are either replaced or refurbished after use. Since the explosive charge is expendable, the remaining part of the valve is often designed to be also expendable. This makes it possible to reduce mass and obtain very good sealing.

These valves cannot be tested non-destructively. Therefore, their reliability for a specific mission must be evaluated statistically, by purchasing a large number of them for qualification.

Explosive valves are actuated by mechanical energy resulting from conversion of chemical energy contained in explosive charges. This chemical energy can be released by the charges either by deflagration, which is the rapid combustion of the explosive material, or by detonation, which is the propagation of a shock wave through the explosive material. In case of deflagration, the mechanical energy obtained is the work done by the combusted gases acting on a piston. In case of detonation, the mechanical energy obtained is due to the momentum of the shock wave propagating through the explosive charge. This momentum is transferred to a piston, as if the end of the piston were subject to a sharp blow.

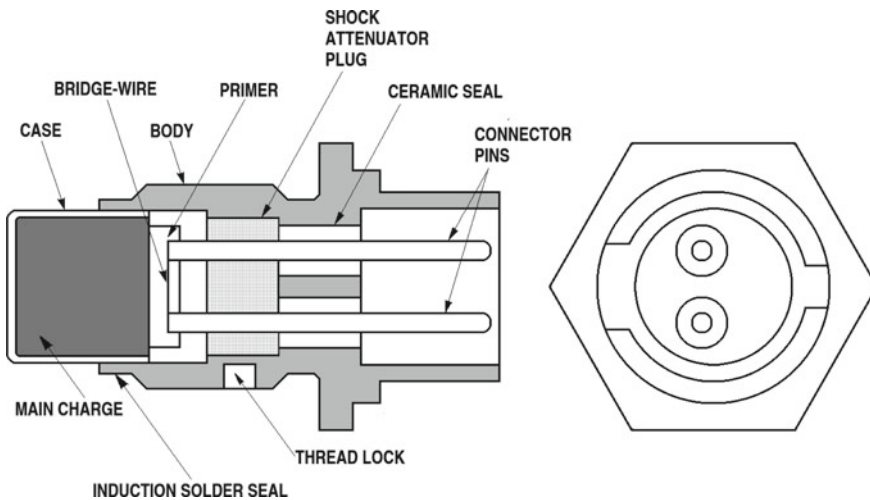
In either case, a small amount of explosive material is necessary to actuate a valve. For example, a typical normally-closed valve, 19.05 mm in diameter, whose working pressure is 2.759×10^7 N/m², uses 140 mg of explosive material. The explosive pressure of this valve is about 1.724×10^7 N/m⁸ [25].

A deflagrating charge used for explosive valves consists of small flake-like particles of powder similar to shotgun powder. A valve of typical design has a disc 0.254 mm in thickness and 1.27 mm in diameter. A detonating charge uses explosive materials such as PETN (pentaerythritol tetranitrate), or DDNP (diazodinitrophenol), or RDX (1,3,5-trinitroperhydro-1,3,5-triazine).

The explosion of a charge is obtained by a transfer of mechanical or electrical energy to a sensitive primer, such as lead styphnate. For this purpose, the charge is ignited by striking a sharp blow to the primer through a metallic barrier, like the firing pin of a gun, or by piercing abruptly the container of the primer by means of a sharp probe, or by heating electrically the primer by means of a bridge-wire.

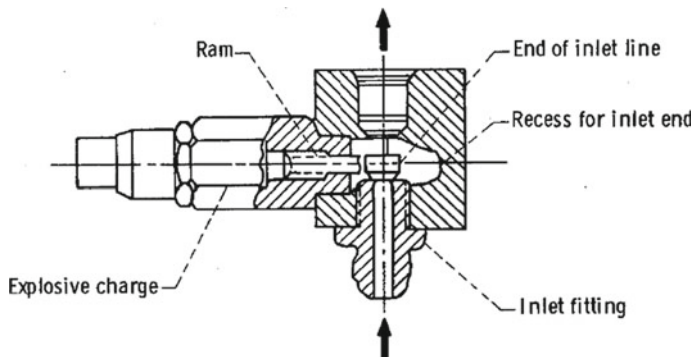
The ignition of a detonating or deflagrating charge may also be obtained without the primer, by using an exploding bridge-wire (EBW). In this case, it is necessary to use a firing pulse of several thousand volts, in comparison with a conventional firing pulse of about 28 V or even less. An exploding bridge-wire is extremely insensitive to accidental firing, but requires a high voltage obtained by discharging a condenser contained in a firing circuit.

A typical explosive cartridge (designed by Holex, Inc.), commonly used for explosive valves and having a low-voltage bridge-wire, is shown in the following figure, re-drawn from [25].



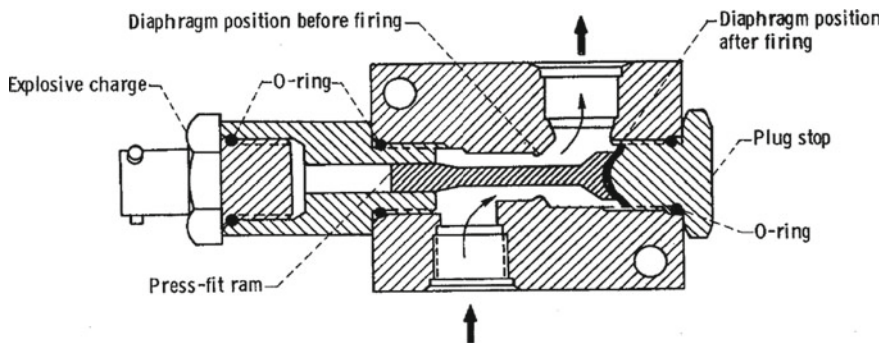
The charge in the cartridge shown above is ignited by means of an electrical connector incorporated in the cartridge. The charge is hermetically sealed to be protected from moisture and damage. The cartridge contains 188 mg of deflagrating charge, and the pressure generated by the ignition can be as high as $4.137 \times 10^8 \text{ N/m}^2$. The shock attenuator plug incorporated in the cartridge weakens the shock waves before they reach the ceramic seals. The electrical conductors are two connector pins made of stainless steel, and the case is made of the same material. The pins are locked into the case by fused ceramic seals. The current necessary to ignite a cartridge like this ranges from 1 to 5 A, and the firing time ranges from 1 to 20 ms [25].

Some explosive valves are illustrated below. The following figure, due to the courtesy of NASA [43], shows a normally closed valve which opens when the explosive charge actuates a pin (ram) which shears the end from the inlet fitting and retains it in a recess of the body.

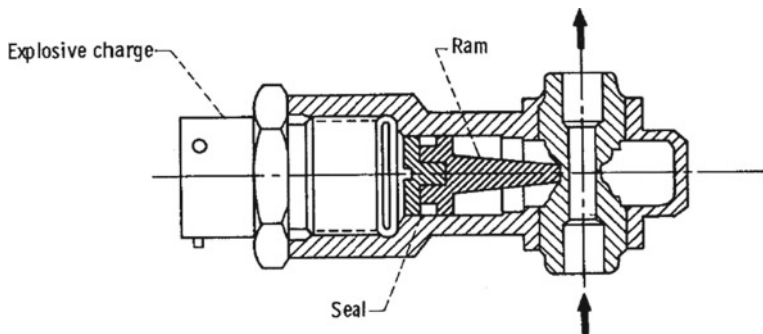


The valve shown above can be made reusable by replacing the explosive charge and the inlet fitting. A reusable valve must be cleaned immediately after firing.

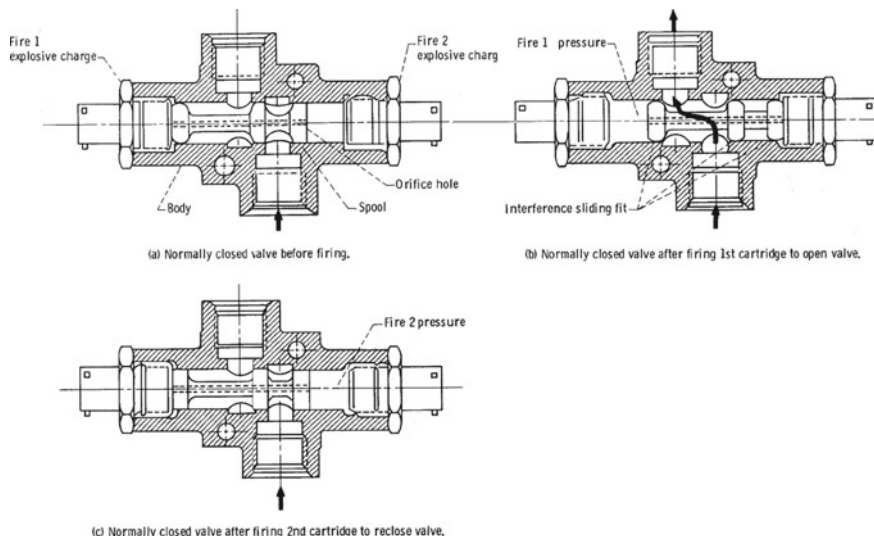
The following figure, due to the courtesy of NASA [43], shows a normally closed non-reusable valve, as it appears after firing. In this valve, a diaphragm is sheared from the body by the ram and is clamped by the ram to be retained within the body.



A normally open valve, as it appears before firing, is shown in the following figure, due to the courtesy of NASA [43]. In this valve, the explosive charge actuates the ram, which shears through the flow passage and wedges between the openings to close the flow passage.

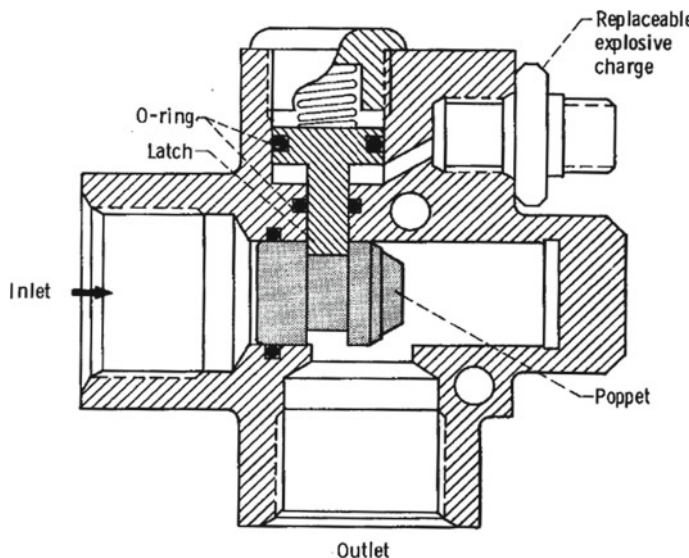


A dual function explosive valve (U.S. Patent No. 3,122,154) is shown in the following figure, due to the courtesy of NASA [43].



The valve shown above is normally closed (a), is opened (b) by firing the first explosive charge, and is re-opened (c) by firing the second explosive charge. Sealing is provided by interference sliding fits between the lands on the spool and the body. A hole balances the actuation pressure on each end of the spool after the spool travel.

Explosive valves are usually employed in lines of small diameters (less than 25 mm). However, explosive valves for lines of greater diameters can be obtained by using the energy of the fluid to open and close the valve, in which case the ram is used only as a latch, as shown for the valve (U.S. Patent No. 3,017,894) illustrated in the following figure, due to the courtesy of NASA [43].



Explosive valves are highly reliable components, when used properly. However, redundant explosive valves have also been used for some critical applications.

References

- Åström KJ, Murray RM (2008) Feedback systems: an introduction for scientists and engineers. Princeton University Press, Princeton, NJ, USA. ISBN 978-0-691-13576-2
- Lorenzo CF, Musgrave JL (1992) Overview of rocket engine control. NASA Technical Memorandum 105318, Jan 1992, 13pp. <https://ntrs.nasa.gov/archive/nasa/casi.ntrs.nasa.gov/1992004056.pdf>
- Huzel DK, Huang DH (1967) Design of liquid propellant rocket engines. 2nd edn. NASA SP-125, NASA, Washington, D.C., 472pp. <https://ntrs.nasa.gov/archive/nasa/casi.ntrs.nasa.gov/19710019929.pdf>
- Thomson WT (1960) Laplace transformation, 2nd edn. Prentice-Hall, Englewood Cliffs, NJ, USA
- Sutton GP, Biblarz O (2001) Rocket propulsion elements, 7th edn. Wiley, New York. ISBN 0-471-32642-9
- Wikimedia. [https://commons.wikimedia.org/wiki/File:Ssme_schematic_\(updated\).svg](https://commons.wikimedia.org/wiki/File:Ssme_schematic_(updated).svg). Attribution: Jkwchui with minor adjustments from Chouser [Public domain], via Wikimedia Commons
- Anonymous (1998) Space Shuttle main engine orientation, Boeing-Rocketdyne Propulsion & Power, Presentation BC98-04, June 1998, 105pp. http://large.stanford.edu/courses/2011/ph240/nguyen1/docs/SSME_PRESENTATION.pdf
- Hobart HF, Minkin HL, Warshawsky I (1973) Life tests of small turbine-type flowmeters in liquid hydrogen. NASA TN D-7323, 16 p, June 1973. <https://www.ntrs.nasa.gov/archive/nasa/casi.ntrs.nasa.gov/19730016551.pdf>
- France JT (1972) The measurement of fuel flow. AGARD-AG-160-Vol. 3, Mar 1972. <https://apps.dtic.mil/dtic/tr/fulltext/u2/741610.pdf>

10. Dodge FT (2008) Propellant mass gauging: database of vehicle applications and research and development studies. NASA/CR-2008-215281, Aug 2008, 43pp. <https://ntrs.nasa.gov/archive/nasa/casi.ntrs.nasa.gov/20080034885.pdf>
11. Szabo SV Jr, Berns JA, Stofan AJ (1968) Centaur launch vehicle propellant utilization system. NASA TN D-4848, Oct 1968, 35pp. <https://ntrs.nasa.gov/archive/nasa/casi.ntrs.nasa.gov/19680027035.pdf>
12. Anonymous (1969) Technical information summary on Apollo-10 (AS-505), Apollo Saturn V space vehicle, NASA, S&E-ASTR-S-69-24, 1 May 1969, 95pp. https://history.nasa.gov/afj/ap10fj/pdf/19700015780_as-505-a10-saturn-v-technical-info-summary.pdf
13. Anonymous (1969) Saturn V flight manual, SA 507, NASA MSFC-MAN-507, Oct 1969. https://www.history.nasa.gov/afj/ap12fj/pdf/a12_sa507-flightmanual.pdf
14. McGlinchey LF (1974) Viking orbiter 1975 thrust vector control system accuracy, NASA-CR-140705, JPL Technical Memorandum 33-703, 15 Oct 1974. <https://ntrs.nasa.gov/archive/nasa/casi.ntrs.nasa.gov/19750002097.pdf>
15. Glassman AJ (ed) (1994) Turbine design and application, vols 1, 2, and 3, NASA SP-290, NASA Lewis Research Centre, June 1994, 390pp. <https://ntrs.nasa.gov/archive/nasa/casi.ntrs.nasa.gov/19950015924.pdf>
16. Hands BA. Cryogenic fluids, thermopedia. <http://www.thermopedia.com/content/676/>
17. Zuk J (1976) Fundamentals of fluid sealing, NASA TN D-8151, Mar 1976. <https://ntrs.nasa.gov/archive/nasa/casi.ntrs.nasa.gov/19760012374.pdf>
18. Wikimedia, Attribution: Original diagram: S Beck and R Collins, University of Sheffield (Donebythesecondlaw at English Wikipedia) Conversion to SVG: Marc.derumaux [CC BY-SA 4.0 (<https://creativecommons.org/licenses/by-sa/4.0/>)]. https://commons.wikimedia.org/wiki/File:Moody_EN.svg
19. New Jersey Institute of Technology, Newark, NJ, USA. https://web.njit.edu/~barat/ChE396_Spring2011/EquivLengths.pdf
20. Queen's University, Kingston, Ontario, Canada, Faculty of Engineering and Applied Sciences, Mechanical and Materials Engineering, Losses in Pipes. <https://me.queensu.ca/People/Sellens/LossesinPipes.html>
21. Neutrium. https://neutrium.net/fluid_flow/pressure-loss-from-fittings-2k-method/
22. Neutrium. https://neutrium.net/fluid_flow/pressure-loss-from-fittings-3k-method/
23. AJ Design Software, Colebrook Equations Formulas Calculator. https://www.ajdesigner.com/php_colebrook/colebrook_equation.php
24. Tomoe Valve Co. Ltd., Osaka, Japan. <https://www.tomoevalve.com/english/pdf/ValveRelatedData.pdf>
25. Howell GW, Weathers TM (eds) (1970) Aerospace fluid component designers' handbook, vol I, Revision D, Report No. RPL-TDR-64-25, TRW Systems Group, One Space Park, Redondo Beach, CA, USA, Feb 1970. <https://apps.dtic.mil/dtic/tr/fulltext/u2/874542.pdf>
26. Burmeister LC, Loser JB, Sneegas EC (1967) NASA contributions to advanced valve technology, NASA SP-5019, 1967. <https://apps.dtic.mil/dtic/tr/fulltext/u2/a306561.pdf>
27. Davis ML, Allgeier RK Jr, Rogers ThG, Rysavy G (1970) The development of cryogenic storage systems for space flight, NASA SP-247, 132pp. <https://ntrs.nasa.gov/search.jsp?R=19710021434>
28. Radabaugh R. Cryogenics, National Institute of Standards and Technology (NIST), US Department of Commerce, Boulder, CO, USA. <https://www.nist.gov/sites/default/files/documents/2016/09/08/cryogenicsii.pdf>
29. Ellis HJ, Spring TR, Keller RB Jr (eds) (1973) Liquid rocket valve components, NASA SP-8094, Aug 1973. NASA Lewis Research Centre, Cleveland, OH, USA, 150pp. <https://ntrs.nasa.gov/archive/nasa/casi.ntrs.nasa.gov/19740019163.pdf>
30. Neutrium. https://neutrium.net/fluid_flow/pressure-loss-from-fittings-excess-head-k-method/
31. Suez degremont® water handbook <https://www.suezwaterhandbook.com/formulas-and-tools/formulary/hydraulics/minor-losses-in-the-pipelines-fittings-valves-for-water>
32. Spring TR, Keller RB Jr (eds) (1973) Liquid rocket valve assemblies, NASA SP-8097, Nov 1973. NASA Lewis Research Centre, Cleveland, OH, USA, 154pp. <https://ntrs.nasa.gov/archive/nasa/casi.ntrs.nasa.gov/19740018866.pdf>

33. AWG to Metric Converter. <https://technick.net/tools/awg-to-metric-converter/>
34. Giovanetti AJ, Spadaccini LJ, Szetela EJ (1983) Deposit formation and heat transfer in hydrocarbon rocket fuels, NASA-CR-168277, 168pp. <https://ntrs.nasa.gov/archive/nasa/casi.ntrs.nasa.gov/19840004157.pdf>
35. Anonymous (1940) Standards for discharge measurement with standardized nozzles and orifices, German industrial standard 1952, 4th edn. NACA Technical Memorandum No. 952, 78pp. <https://ntrs.nasa.gov/archive/nasa/casi.ntrs.nasa.gov/19930094464.pdf>
36. EN ISO 5167, Measurement of fluid flow by means of pressure differential devices inserted in circular cross-section conduits running full. <https://www.iso.org/obp/ui/#iso:std:iso:5167:-1:ed-2:v1:en>
37. AGA 3.1, Orifice metering of natural gas and other related hydrocarbon fluid. <https://law.resource.org/pub/us/cfr/ibr/001/aga.3.1.1990.pdf>
38. Anonymous, Risk management program guidance for offsite consequence analysis, United States Environmental Protection Agency, Appendix B. <https://www.epa.gov/sites/production/files/2017-05/documents/oca-apds.pdf>
39. Neutrium. https://neutrium.net/fluid_flow/discharge-coefficient-for-nozzles-and-orifices/
40. National Institute of Standards and Technology (NIST), U.S. Department of Commerce, Thermophysical Properties of Fluid Systems. <https://webbook.nist.gov/chemistry/fluid/>
41. Absalom JG, Keller RB Jr (eds) (1973) Liquid rocket actuators and operators, NASA SP-8090, May 1973. NASA Lewis Research Centre, Cleveland, OH, USA, 158pp. <https://ntrs.nasa.gov/archive/nasa/casi.ntrs.nasa.gov/19740009672.pdf>
42. Plummer AR, Electrohydraulic servovalves—past, present, and future. In: Proceedings of the 10th international fluid power conference, IFK2016, Dresden, Germany, 8–16 Mar 2016. University of Bath, UK, pp 405–424. <http://tud.qucosa.de/api/qucosa%3A29369/attachment/ATT-0/>
43. Tomlinson LE, Keller RB Jr (eds) (1973) Liquid rocket pressure regulators, relief valves, check valves, burst disks, and explosive valves, NASA SP-8080, Mar 1973, 123pp. <https://ntrs.nasa.gov/archive/nasa/casi.ntrs.nasa.gov/19740002611.pdf>
44. Kates flow control valves, Custom Valves Concepts. <https://www.customvalveconcepts.com/products/kates-flow-controllers-2/kates-fc-valve-automatic-flow-rate-controller.html>

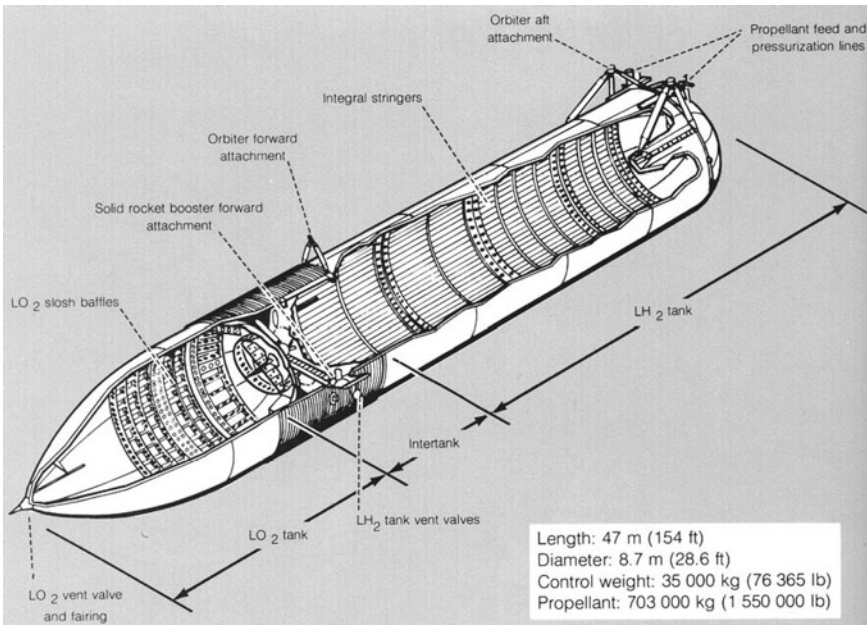
Chapter 6

Tanks for Propellants



6.1 Fundamental Concepts

Tanks containing liquid propellants for rocket engines can be considered as shells whose thin walls are surfaces of revolution. The following figure, due to the courtesy of NASA [1], shows the external tank of the Space Shuttle.



The word shell is used here because, at any point of a tank, the thickness of its wall is assumed to be constant and much smaller than the radii of curvature of its middle surface [2].

A surface of revolution results from rotating a plane curve about some straight line (called the axis of revolution) lying in the plane which contains the curve. A line resulting from the intersection of a surface of revolution with a plane containing the axis of revolution is called a meridian. A line resulting from the intersection of a surface of revolution with a plane perpendicular to the axis of revolution is called a circumference. Therefore, the meridian passing through any point of a surface of revolution is perpendicular to the circumference passing through the same point. The structural analysis of tanks which will be presented in this chapter is largely due to Roark's formulas for stress and strain [3].

When a shell is subject to distributed loads resulting from internal or external pressure, the predominant stresses acting on the shell are membrane stresses, which are stresses whose amount is constant through the thickness of the shell. Generally speaking, the stresses acting in a point of a shell are

- a meridian membrane stress σ_1 , whose direction is parallel to the local meridian;
- a circumferential membrane stress σ_2 , whose direction is parallel to the local circumference; and
- a small radial stress σ_3 , which varies through the thickness of the shell.

In addition to these stresses, there may be bending or shear stresses due to loading, or to physical properties of the shell, or to the supporting structure. The stresses considered above cause meridian, circumferential, and radial strains in a shell, and therefore changes in the slopes of its meridians. The circumferences of a shell may also deviate from their circular form when buckling occurs.

When a thin shell (one whose thickness is less than one tenth of its smaller radius of curvature) has no abrupt changes in thickness, slope, or curvature, and is subject to a loading uniformly distributed or smoothly varying and axisymmetric, then the meridian σ_1 and circumferential σ_2 membrane stresses are practically uniform through the thickness of the wall, and are also the most important stresses acting on the shell. The radial stress σ_3 and stresses induced by bending moments are negligible. In this case, the formulae of [3, Table 13.1] can be used to compute stresses and strains such as those described above for shells of cylindrical, conical, spherical, and toroidal shapes. Examples of application will be given in the following sections.

6.2 Tanks Subject Only to Membrane Stresses

Two thin shells can be joined together to form a tank. When it is desired to have no bending stresses at the junction in case of uniformly distributed or smoothly varying loads, then it is necessary to choose shells such that the radial deformations ΔR and the rotations ψ of the meridians be the same for each of them at the point of junction.

For example, a cylindrical shell of radius R (m) and thickness t (m), subject to uniform internal pressure q (N/m^2), see [3, Table 13.1, case 1c], has a radial deformation ΔR (m)

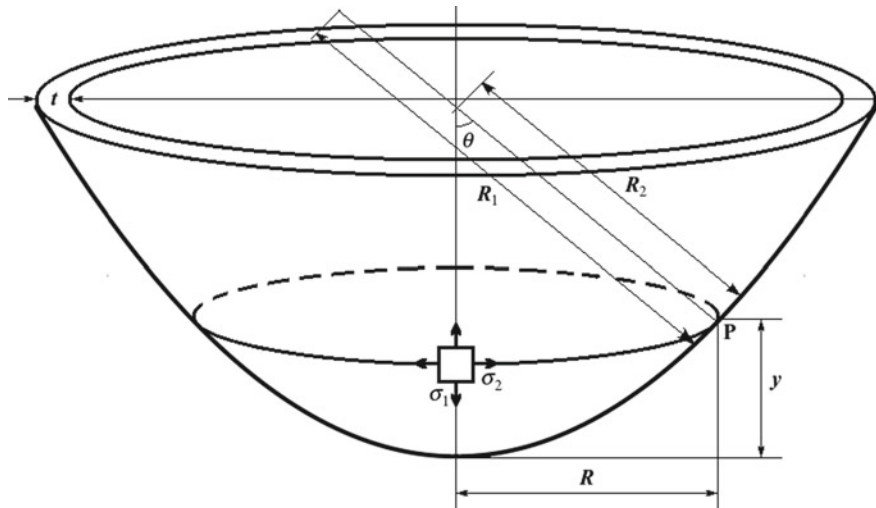
$$\Delta R = \frac{qR^2}{Et} \left(1 - \frac{\nu}{2}\right)$$

where E (N/m^2) and ν are respectively the Young modulus and the Poisson ratio of the material, whereas a hemispherical shell of equal radius and thickness, subject to the same pressure, see [3, Table 13.1, case 3a], has a radial deformation ΔR (m)

$$\Delta R = \frac{qR^2(1-\nu)}{2Et}$$

The rotations ψ of the meridians are the same in both cases. The different radial deformations ΔR cause bending and shear stresses in the vicinity of the junction.

The following figure shows a shell, whose middle surface is a smooth surface of revolution, not necessarily a hemisphere, subject to a uniform internal pressure q [3, Table 13.1, case 4a].



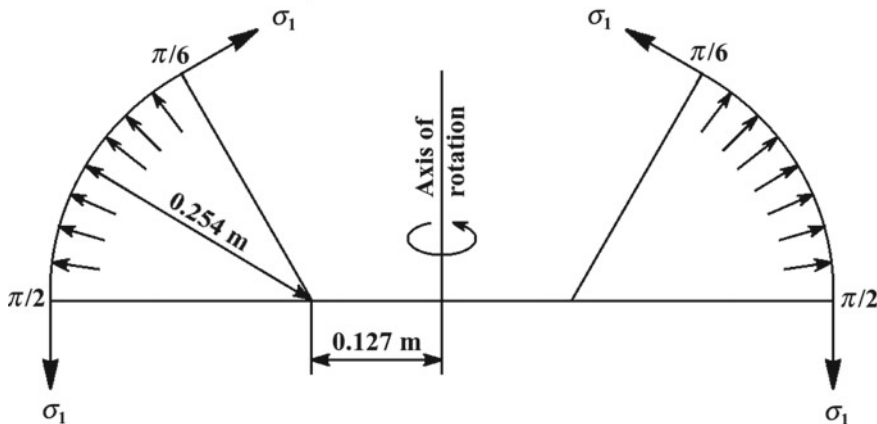
Roark's formulae cited above give the following expressions of respectively ΔR and ψ for this smooth surface of revolution

$$\Delta R = \frac{qR_2^2 \sin \theta}{2Et} \left(2 - \frac{R_2}{R_1} - \nu\right)$$

$$\psi = \frac{qR_2^2}{2EtR_1 \tan \theta} \left[3 \frac{R_1}{R_2} - 5 + \frac{R_2}{R_1} \left(2 + \frac{1}{R_1} \frac{dR_1}{d\theta} \tan \theta \right) \right]$$

These formulae show that, when the radius of curvature R_1 of a meridian is infinite at $\theta = \pi/2$, then the radial deformations ΔR and the rotations ψ of the meridians are the same as those of the cylindrical shell of [3, Table 13.1, case 1c]. In the preceding figure, R_1 (m) is the radius of curvature of a meridian in the point P of the shell, R_2 (m) is the length of the normal between the point P of the shell and the axis of rotation, and θ (rad) is the angle between the normal to the surface and the axis of rotation. Flügge [4] has shown that the family of the Cassinian curves (illustrated in Sect. 6.9) has the property indicated above.

As an application (from [3]) of the concepts discussed above, it is required to compute the radial deformations ΔR and the rotations ψ of the meridians at both ends of a segment of toroidal shell used as a transition between a cylinder and a head closure in a tank subject to an internal pressure $q = 1.379 \times 10^6$ N/m².



As shown in the preceding figure, the two ends of each toroidal segment are defined by the angles $\theta = \pi/6$ and $\theta = \pi/2$ which the normal to the toroidal surface forms with the axis of rotation. The Young modulus and the Poisson ratio of the material of which the tank is made are respectively $E = 2.068 \times 10^{11}$ N/m² and $\nu = 0.3$. The thickness of the wall of the tank is $t = 0.00254$ m = 2.54 mm. At the upper end (subscript U) of the toroidal surface, there results

$$\theta_U = \frac{\pi}{6}$$

$$R_1 = 0.254 \text{ m}$$

$$R_{2U} = 0.254 + \frac{0.127}{\sin(\pi/6)} = 0.508 \text{ m}$$

where R_1 is the constant radius of curvature of the meridians, and R_{2U} is the length of the normal between the upper end of the toroidal surface and the axis of rotation.

At the upper end, the formulae of [3, Table 13.1, case 4a] give the following results for respectively the radial deformations ΔR_U and the rotations ψ_U of the meridians, taking account that $dR_1/d\theta = 0$, because R_1 is constant

$$\begin{aligned}\Delta R_U &= \frac{q R_{2U}^2 \sin \theta_U}{2Et} \left(2 - \frac{R_{2U}}{R_1} - v \right) \\ &= \frac{1.379 \times 10^6 \times 0.508^2 \times \sin(\pi/6)}{2 \times 2.068 \times 10^{11} \times 2.54 \times 10^{-3}} \times \left(2 - \frac{0.508}{0.254} - 0.3 \right) \\ &= -5.081 \times 10^{-5} \text{ m} = -0.05081 \text{ mm}\end{aligned}$$

$$\begin{aligned}\psi_U &= \frac{q R_{2U}^2}{2Et R_1 \tan \theta_U} \left(3 \frac{R_1}{R_{2U}} - 5 + \frac{R_{2U}}{R_1} 2 \right) \\ &= \frac{1.379 \times 10^6 \times 0.508^2}{2 \times 2.068 \times 10^{11} \times 0.00254 \times 0.254 \times \tan(\pi/6)} \times \left(\frac{3 \times 0.254}{0.508} - 5 + \frac{2 \times 0.508}{0.254} \right) \\ &= 0.001155 \text{ rad}\end{aligned}$$

At the lower end (subscript L) of the toroidal surface, there results

$$\theta_L = \frac{\pi}{2}$$

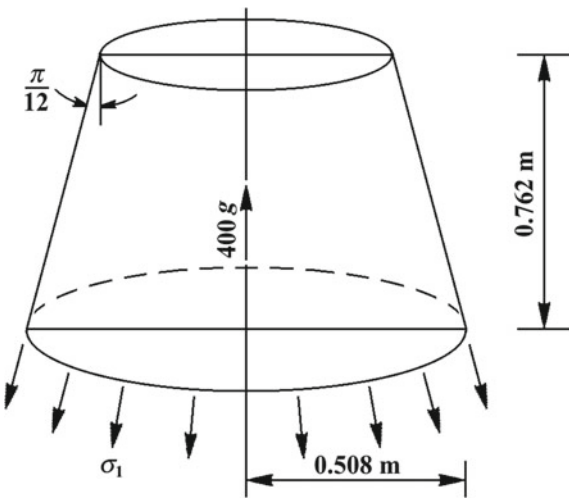
$$R_1 = 0.254 \text{ m}$$

$$R_{2L} = 0.254 + 0.127 = 0.381 \text{ m}$$

At the lower end, the formulae cited above lead to the following results for respectively the radial deformations ΔR_L and the rotations ψ_L of the meridians

$$\begin{aligned}\Delta R_L &= \frac{q R_{2L}^2 \sin \theta_L}{2Et} \left(2 - \frac{R_{2L}}{R_1} - v \right) \\ &= \frac{1.379 \times 10^6 \times 0.381^2 \times \sin(\pi/2)}{2 \times 2.068 \times 10^{11} \times 2.54 \times 10^{-3}} \times \left(2 - \frac{0.381}{0.254} - 0.3 \right) \\ &= 3.811 \times 10^{-5} \text{ m} = 0.03811 \text{ mm} \\ \psi_L &= 0 \quad \text{because } \tan \theta_L = \tan\left(\frac{\pi}{2}\right) = \infty\end{aligned}$$

Another example of application (also due to [3]) concerns a shell shaped as a cone frustum of semi-aperture angle $\alpha = \pi/12$ rad, supported at its base by the membrane stress σ_1 , as shown in the following figure.



The thickness of the shell is $t = 0.00635 \text{ m} = 6.35 \text{ mm}$. The density, the Young modulus, and the Poisson ratio of the material (aluminium) of which the shell is made are respectively $\rho = 2700 \text{ kg/m}^3$, $E = 6.9 \times 10^{10} \text{ N/m}^2$, and $\nu = 0.3$.

It is required to find the membrane stress σ_1 at the base, the radial deformation ΔR , and the height deformation Δy , supposing the shell to be subject to an acceleration of $400 g_0 = 400 \times 9.807 \text{ m/s}^2$ acting in the vertical direction.

The formulae of [3, Table 13.1, case 2c] concern a complete cone loaded by its own weight $\rho V g_0 \text{ N}$. Since the cone considered here is truncated, then the principle of superposition of effects applies, as will be shown below. For this purpose, we consider firstly a complete cone loaded by its own weight. The specific weight $\rho g_0 (\text{N/m}^3)$ of this cone is taken with the minus sign, because the vertex of the cone is up instead of down, and this value is multiplied by 400, in order to take account of the acceleration. We use the formulae of [3, Table 13.1, case 2c] with $\alpha = \pi/12 \text{ rad}$, $R = 0.508 \text{ m}$, $E = 6.9 \times 10^{10} \text{ N/m}^2$, $\nu = 0.3$, and $\rho g_0 = -2700 \times 400 \times 9.807 \text{ N/m}^3$. By so doing, we find

$$\sigma_1 = \frac{\rho g_0 R}{\sin(2\alpha)} = \frac{-2700 \times 400 \times 9.807 \times 0.508}{\sin(\pi/6)} = -1.076 \times 10^7 \text{ N/m}^2$$

$$\begin{aligned} \Delta R &= \frac{\rho g_0 R^2}{E \cos \alpha} \left(\sin \alpha - \frac{\nu}{2 \sin \alpha} \right) \\ &= \frac{-400 \times 2700 \times 9.807 \times 0.508^2}{6.9 \times 10^{10} \times \cos(\pi/12)} \times \left[\sin\left(\frac{\pi}{12}\right) - \frac{0.3}{2 \times \sin(\pi/12)} \right] \\ &= 1.315 \times 10^{-5} \text{ m} = 0.01315 \text{ mm} \end{aligned}$$

$$\Delta y = \frac{\rho g_0 R^2}{E \cos^2 \alpha} \left(\frac{1}{4 \sin^2 \alpha} - \sin^2 \alpha \right)$$

$$\begin{aligned}
 &= \frac{-400 \times 2700 \times 9.807 \times 0.508^2}{6.9 \times 10^{10} \times \cos^2(\pi/12)} \times \left[\frac{1}{4 \sin^2(\pi/12)} - \sin^2\left(\frac{\pi}{12}\right) \right] \\
 &= -1.556 \times 10^{-4} \text{ m} = -0.1556 \text{ mm}
 \end{aligned}$$

The radius of the circular base at the top of the cone frustum is

$$r = 0.508 - \frac{0.762}{\tan\left(\frac{5\pi}{12}\right)} = 0.3038 \text{ m}$$

The change in length of the upper conical shell to be removed is

$$\Delta y = -1.556 \times 10^{-4} \times \left(\frac{0.3038}{0.508} \right)^2 = -5.565 \times 10^{-5} \text{ m} = -0.05565 \text{ mm}$$

The slant side of the upper conical shell to be removed is

$$L = \frac{r}{\sin\left(\frac{\pi}{12}\right)}$$

The lateral surface of the upper conical shell to be removed is

$$S = \pi r L = \frac{\pi r^2}{\sin\left(\frac{\pi}{12}\right)}$$

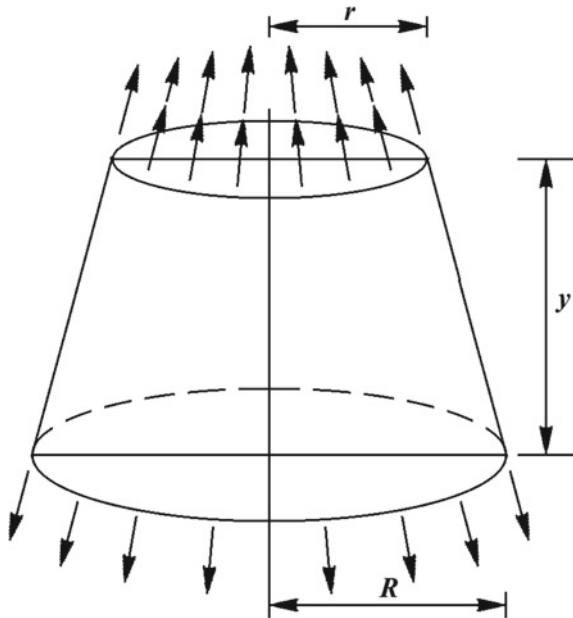
The volume of the upper conical shell to be removed is

$$V = St = \frac{\pi r^2 t}{\sin\left(\frac{\pi}{12}\right)} = \frac{3.1416 \times 0.3038^2 \times 0.00635}{\sin\left(\frac{\pi}{12}\right)} = 0.007114 \text{ m}^3$$

The effective weight of the upper conical shell to be removed is

$$P = 400 \rho g_0 V = 400 \times 2700 \times 9.807 \times 0.007114 = 7.535 \times 10^4 \text{ N}$$

In order to remove the effective weight P from the truncated conical shell, we substitute $P = 7.535 \times 10^4 \text{ N}$, $R = 0.508 \text{ m}$, $r = 0.3038 \text{ m}$, $h = 0.762 \text{ m}$, $t = 0.00635 \text{ m}$, $\alpha = \pi/12 \text{ rad}$, $E = 6.9 \times 10^{10} \text{ N/m}^2$, and $\nu = 0.3$ in the following formulae of [3, Table 13.1, case 2d], which concern a truncated conical shell subject to tangential loading only, with resultant load P , as shown in the following figure.



By so doing, we find

$$\begin{aligned}\sigma_1 &= \frac{P}{2\pi Rt \cos \alpha} = \frac{7.535 \times 10^4}{2 \times 3.1416 \times 0.508 \times 0.00635 \times \cos(\pi/12)} \\ &= 3.849 \times 10^6 \text{ N/m}^2\end{aligned}$$

$$\begin{aligned}\Delta R &= \frac{-vP}{2\pi Et \cos \alpha} = \frac{-0.3 \times 7.535 \times 10^4}{2 \times 3.1416 \times 6.9 \times 10^{10} \times 0.00635 \times \cos(\pi/12)} \\ &= -8.500 \times 10^{-6} \text{ m} = -0.008500 \text{ mm}\end{aligned}$$

$$\begin{aligned}\Delta h &= \frac{P}{2\pi Et \sin \alpha \cos^2 \alpha} \ln\left(\frac{R}{r}\right) \\ &= \frac{7.535 \times 10^4}{2 \times 3.1416 \times 6.9 \times 10^{10} \times 0.00635 \times \sin(\pi/12) \times \cos^2(\pi/12)} \times \ln\left(\frac{0.508}{0.3038}\right) \\ &= 5.827 \times 10^{-5} \text{ m} = 0.05827 \text{ mm}\end{aligned}$$

Therefore, for the original truncated conical shell, there results

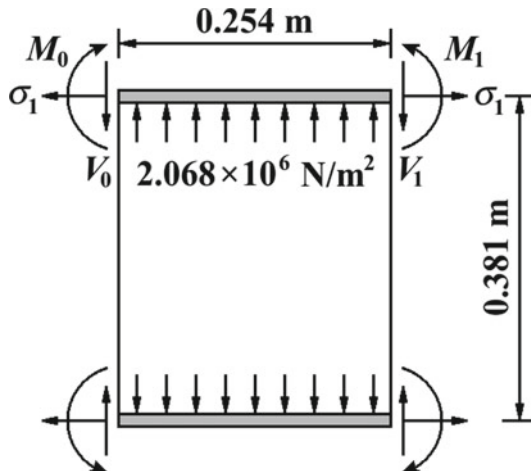
$$\sigma_1 = (-10.76 + 3.849) \times 10^6 \text{ N/m}^2 = -6.911 \times 10^6 \text{ N/m}^2$$

$$\Delta R = (13.15 - 8.500) \times 10^{-6} \text{ m} = 4.65 \times 10^{-6} \text{ m} = 0.00465 \text{ mm}$$

$$\begin{aligned}\Delta y &= [-15.56 - (-5.565) + 5.827] \times 10^{-5} \text{ m} \\ &= -4.168 \times 10^{-5} \text{ m} = -0.04168 \text{ mm}\end{aligned}$$

6.3 Tanks Subject to Membrane and Bending Stresses

Forces, moments, and displacements for cylindrical tanks can be computed by using the formulae of [3, Table 13.2]. These formulae concern thin-walled cylindrical shells having free ends and subject to axisymmetric loadings. The radial deformations of these shells are assumed to be small in comparison with the thickness of their walls. An example of calculation, from [3], is given below.



A cylindrical tank of aluminium, shown in the preceding figure, is 0.254 m in length and 0.381 m in diameter. This tank is desired to bear an internal pressure of $2.068 \times 10^6 \text{ N/m}^2$ with a maximum tensile stress of $8.274 \times 10^7 \text{ N/m}^2$. The ends of the tank are capped with flanges, which are sufficiently clamped to the tank to resist any radial or rotational deformations at their ends. Given the Young modulus $E = 6.9 \times 10^{10} \text{ N/m}^2$ and the Poisson ratio $\nu = 0.3$ of aluminium, it is required to determine the thickness t (m) of the wall of the tank.

The value of t may be computed by superposing the effects given in [3, Table 13.1, case 1c, and Table 13.2, cases 8 and 10]. For this purpose, it is necessary to determine the mean radius of the tank

$$R = \frac{0.381}{2} = 0.1905 \text{ m}$$

the length of the tank

$$l = 0.254 \text{ m}$$

the bending stiffness of the tank

$$D = \frac{Et^3}{12(1-\nu^2)} = \frac{6.9 \times 10^{10} t^3}{12 \times (1 - 0.3^2)} = 6.319 \times 10^9 t^3 \text{ Nm}$$

and the following quantities

$$\lambda = \left[\frac{3(1-\nu^2)}{R^2 t^2} \right]^{\frac{1}{4}} = \left[\frac{3 \times (1 - 0.3^2)}{0.1905^2 t^2} \right]^{\frac{1}{4}} = 2.945 t^{-\frac{1}{2}} \text{ m}^{-1}$$

$$\lambda l = 2.945 t^{-\frac{1}{2}} \times 0.254 = 0.748 t^{-\frac{1}{2}}$$

Since the value of t is still unknown, it is necessary to determine whether the loads at one end of the cylindrical shell have (short shell) or have not (long shell) any influence on the deformations at the other end. To this end, we determine approximately the value of t by using the formulae for membrane stresses and deformations given in [3, Table 13.1, case 1c], which concern a cylindrical shell subject to internal pressure q , with ends capped. These formulae are

$$\sigma_1 = \frac{qR}{2t}$$

$$\sigma_2 = \frac{qR}{t}$$

for respectively the meridian stress and the circumferential stress in the shell.

By equating σ_2 to the maximum allowable stress $8.274 \times 10^7 \text{ N/m}^2$, there results

$$8.274 \times 10^7 = \frac{2.068 \times 10^6 \times 0.1905}{t}$$

The preceding equation, solved for t , yields

$$t = \frac{2.068 \times 0.1905}{82.74} = 0.004769 \text{ m}$$

Since

$$\lambda l = 0.748 t^{-\frac{1}{2}} = 0.748 \times 0.004769^{-\frac{1}{2}} = 10.83$$

then the cylindrical shell considered here is very long.

A preliminary solution may be found by assuming the deformation at the left end of the cylindrical shell to be independent of the radial load and of the bending moment at the right end. Since the end caps are rigid, the radial deformation and the angular rotation of the left end are set to zero. The formulae of [3, Table 13.1, case 1c], which concern a cylindrical shell subject to internal pressure q , with ends capped, give the following values for respectively the meridional stress, the circumferential stress, the radial deformation, and the angular rotation

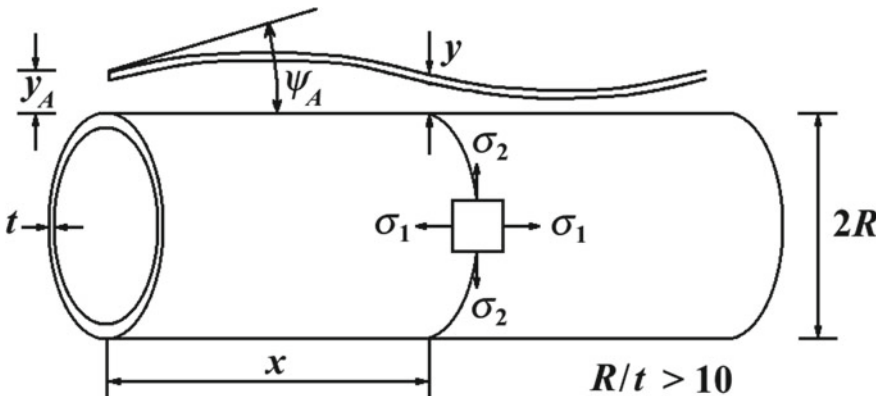
$$\sigma_1 = \frac{qR}{2t} = \frac{2.068 \times 10^6 \times 0.1905}{2t} = \frac{0.1970 \times 10^6}{t} \text{ N/m}^2$$

$$\sigma_2 = \frac{qR}{t} = \frac{2.068 \times 10^6 \times 0.1905}{t} = \frac{0.3940 \times 10^6}{t} \text{ N/m}^2$$

$$\Delta R = \frac{qR^2}{Et} \left(1 - \frac{\nu}{2}\right) = \frac{2.068 \times 10^6 \times 0.1905^2}{6.9 \times 10^{10}t} \times \left(1 - \frac{0.3}{2}\right) = \frac{9.245 \times 10^{-7}}{t} \text{ m}$$

$$\psi = 0 \text{ rad}$$

On the other hand, the formulae of [3, Table 13.2, case 8 and case 10] concern a long shell with the left end free and the right end more than $6/\lambda$ units of length from the closest load, as shown in the following figure.



In particular, case 8 concerns the angular rotation ψ_A (rad) and the radial deformation y_A (m) due to the radial load per unit length V_0 (N/m) at the end section A of the cylindrical shell, as follows

$$\psi_A = \frac{V_0}{2D\lambda^2}$$

$$y_A = \frac{-V_0}{2D\lambda^3}$$

After substituting the values of D and λ found above in the preceding equations, we find the following angular rotation and radial deformation for case 8

$$\psi_A = \frac{V_0}{t^2} \times 9.123 \times 10^{-12} \text{ rad}$$

$$y_A = -\frac{V_0}{t^{\frac{3}{2}}} \times 3.098 \times 10^{-12} \text{ m}$$

Case 10 concerns the angular rotation ψ_A and the radial deformation y_A due to the end moment per unit length M_0 (Nm/m) at the end section A of the cylindrical shell, as follows

$$\psi_A = \frac{-M_0}{D\lambda}$$

$$y_A = \frac{M_0}{2D\lambda^2}$$

After substituting the values of D and λ found above in the preceding equations, we find the following angular rotations and radial deformations for case 10

$$\psi_A = -\frac{M_0}{t^{\frac{5}{2}}} \times 53.74 \times 10^{-12} \text{ rad}$$

$$y_A = \frac{M_0}{t^2} \times 9.123 \times 10^{-12} \text{ m}$$

By summing all the radial deformations found above and equating the sum to zero, we find

$$\frac{9.245 \times 10^{-7}}{t} - \frac{V_0}{t^{\frac{3}{2}}} \times 3.098 \times 10^{-12} + \frac{M_0}{t^2} \times 9.123 \times 10^{-12} = 0$$

By summing all the angular rotations found above and equating the sum to zero, we find

$$0 + \frac{V_0}{t^2} \times 9.123 \times 10^{-12} - \frac{M_0}{t^{\frac{5}{2}}} \times 53.74 \times 10^{-12} = 0$$

By solving the two preceding equations for V_0 and M_0 , we find

$$V_0 = t^{\frac{1}{2}} \times 5.968 \times 10^5 \text{ N/m}$$

$$M_0 = t \times 1.013 \times 10^5 \text{ Nm/m}$$

Since the maximum bending stress occurs at the ends of the cylindrical shell, then the following stresses must be combined:

- (1) the meridian and circumferential membrane stresses computed above

$$\sigma_1 = \frac{qR}{2t} = \frac{2.068 \times 10^6 \times 0.1905}{2t} = \frac{0.1970 \times 10^6}{t} \text{ N/m}^2$$

$$\sigma_2 = \frac{qR}{t} = \frac{2.068 \times 10^6 \times 0.1905}{t} = \frac{0.3940 \times 10^6}{t} \text{ N/m}^2$$

- (2) the meridian and circumferential membrane and bending stresses given by [3, Table 13.2, case 8]

$$\sigma_1 = 0 \text{ N/m}^2$$

$$\begin{aligned}\sigma_2 &= \frac{-2V_0\lambda R}{t} = \frac{-2 \times (t^{\frac{1}{2}} \times 5.968 \times 10^5) \times (t^{-\frac{1}{2}} \times 2.945) \times 0.1905}{t} \\ &= \frac{-6.696 \times 10^5}{t} \text{ N/m}^2\end{aligned}$$

$$\sigma'_1 = 0 \text{ N/m}^2$$

$$\sigma'_2 = 0 \text{ N/m}^2$$

- (3) the meridian and circumferential membrane and bending stresses given by [3, Table 13.2, case 10]

$$\sigma_1 = 0 \text{ N/m}^2$$

$$\begin{aligned}\sigma_2 &= \frac{2M_0\lambda^2 R}{t} = \frac{2 \times (t \times 1.013 \times 10^5) \times (t^{-\frac{1}{2}} \times 2.945)^2 \times 0.1905}{t} \\ &= \frac{3.347 \times 10^5}{t} \text{ N/m}^2\end{aligned}$$

$$\sigma'_1 = \frac{6M_0}{t^2} = \frac{6 \times (t \times 1.013 \times 10^5)}{t^2} = \frac{6.078 \times 10^5}{t} \text{ N/m}^2$$

$$\sigma'_2 = \nu\sigma'_1 = \frac{0.3 \times 6.078 \times 10^5}{t} = \frac{1.823 \times 10^5}{t} \text{ N/m}^2$$

At the end of the cylindrical shell, the maximum meridian tensile stress is

$$\frac{0.1970 \times 10^6}{t} + \frac{6.078 \times 10^5}{t} = \frac{8.048 \times 10^5}{t} \text{ N/m}^2$$

Likewise, at the end of the cylindrical shell, the maximum circumferential tensile stress is

$$\begin{aligned} & \frac{0.3940 \times 10^6}{t} - \frac{6.696 \times 10^5}{t} + \frac{3.347 \times 10^5}{t} + \frac{1.823 \times 10^5}{t} \\ &= \frac{2.414 \times 10^5}{t} \text{ N/m}^2 \end{aligned}$$

Since the maximum allowable stress is $8.274 \times 10^7 \text{ N/m}^2$, then the thickness of the cylindrical shell results from

$$\frac{8.048 \times 10^5}{t} = 8.274 \times 10^7 \text{ N/m}^2$$

The preceding equation, solved for t , yields

$$t = \frac{8.048}{827.4} = 0.009727 \text{ m} = 9.727 \text{ mm}$$

This value of t , substituted in the equation derived above $\lambda l = 0.748 \times t^{-\frac{1}{2}}$, yields

$$\lambda l = 0.748 \times 0.009727^{-\frac{1}{2}} = 7.584$$

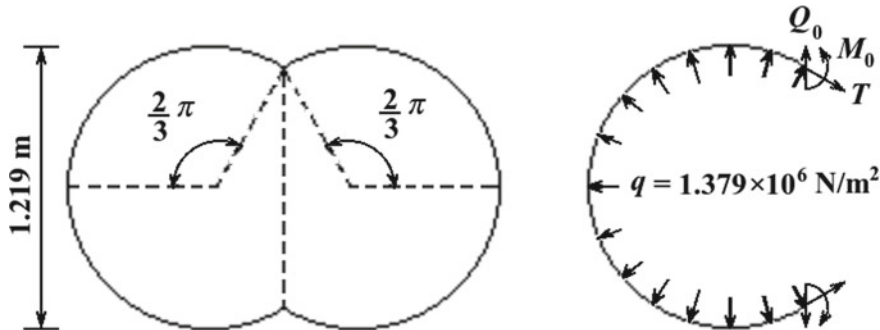
This value of λl justifies the assumption made above of having to do with a long cylindrical shell.

Forces, moments, and displacements for tanks of spherical, conical, or toroidal shapes can also be computed by using the formulae of [3], as will be shown below. The following example, from [3], concerns two spherical segments of aluminium ($E = 6.895 \times 10^{10} \text{ N/m}^2$, $\nu = 0.33$) welded together to form a symmetrical tank, which is subject to an internal pressure $q = 1.379 \times 10^6 \text{ N/m}^2$. The angle subtended by each spherical segment is $4\pi/3$ rad. The mean diameter of each spherical segment is 1.219 m, and the thickness of the wall is $t = 0.0127 \text{ m}$. It is required to compute the stresses at the junction.

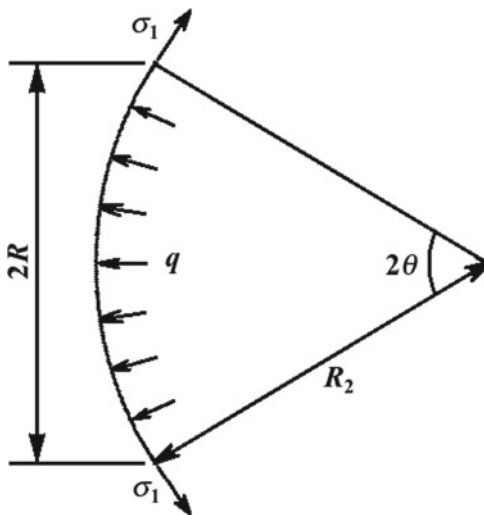
Since this tank is symmetrical and symmetrically loaded, then it is possible to consider only one of the two spherical segments. The effects due to the other segment are taken into account by adding the following loads to the internal pressure q :

- a tangential force T , which balances the force due to the internal pressure, and causes only membrane stresses and consequent radial deformations ΔR in the circumferences and no rotations in the meridians;
- a vertical force Q_0 , which is added to eliminate the radial component of T ; and
- a moment M_0 , which is added in order to prevent the edges of the spherical segment from rotating.

The whole tank, the spherical segment considered above, and the loads acting on it are shown in the following figure.



The formulae of [3, Table 13.1, case 3a] concern membrane stresses and deformations in a segment of spherical thin-walled shell of mean radius R_2 subject to an internal or external pressure q with tangential support at the edges, as shown in the following figure.



These formulae are

$$\sigma_1 = \sigma_2 = \frac{q R_2}{2t} = \frac{1.379 \times 10^6 \times 0.5 \times 1.219}{2 \times 0.0127} = 3.309 \times 10^7 \text{ N/m}^2$$

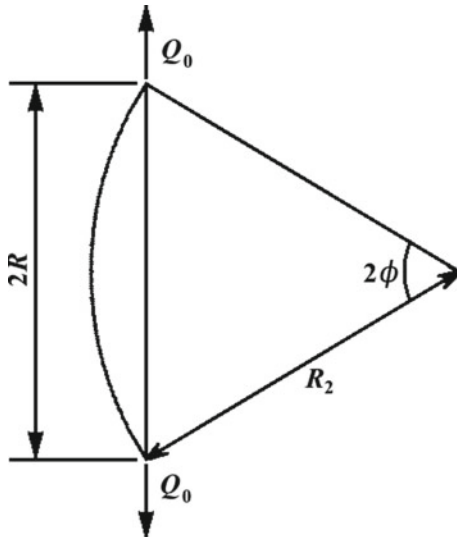
$$\Delta R = \frac{q R_2^2 (1 - \nu) \sin \theta}{2Et} = \frac{1.379 \times 10^6 \times (0.5 \times 1.219)^2 \times (1 - 0.33) \times \sin(2\pi/3)}{2 \times 6.895 \times 10^{10} \times 0.0127}$$

$$= 1.697 \times 10^{-4} \text{ m} = 0.1697 \text{ mm}$$

$$T = \sigma_1 t = 3.309 \times 10^7 \times 0.0127 = 4.203 \times 10^5 \text{ N/m}$$

$$\psi = 0 \text{ rad}$$

Now we apply the formulae of [3, Table 13.3, case 1a], which concern the membrane and bending stresses and strains in a segment of spherical shell with vertical forces Q_0 applied at the edges, as shown in the following figure.



These formulae, applied to the present case, are

$$Q_0 = T \cos\left(\frac{\pi}{3}\right) = 4.203 \times 10^5 \times 0.5 = 2.101 \times 10^5 \text{ N/m}$$

$$\phi = \frac{2}{3}\pi \text{ rad}$$

$$\beta = \left[3(1 - \nu^2) \left(\frac{R_2}{t} \right)^2 \right]^{\frac{1}{4}} = \left[3 \times (1 - 0.33^2) \times \left(\frac{0.5 \times 1.219}{0.0127} \right)^2 \right]^{\frac{1}{4}} = 8.858$$

$$K_1 = 1 - \frac{1 - 2\nu}{2\beta \tan \phi} = 1 - \frac{1 - 2 \times 0.33}{2 \times 8.858 \times \tan(2\pi/3)} = 1.011$$

$$K_2 = 1 - \frac{1 + 2\nu}{2\beta \tan \phi} = 1 - \frac{1 + 2 \times 0.33}{2 \times 8.858 \times \tan(2\pi/3)} = 1.054$$

$$\begin{aligned}\Delta R &= \frac{Q_0 R_2 \beta \sin^2 \phi}{E t K_1} (1 + K_1 K_2) \\ &= \frac{2.101 \times 10^5 \times 0.5 \times 1.219 \times 8.858 \times \sin^2(2/3\pi)}{6.895 \times 10^{10} \times 0.0127 \times 1.011} \times (1 + 1.011 \times 1.054) \\ &= 0.001985 \text{ m} = 1.985 \text{ mm}\end{aligned}$$

$$\psi = \frac{2Q_0\beta^2 \sin \phi}{E t K_1} = \frac{2 \times 2.101 \times 10^5 \times 8.858^2 \times \sin(2\pi/3)}{6.895 \times 10^{10} \times 0.0127 \times 1.011} = 0.03225 \text{ rad}$$

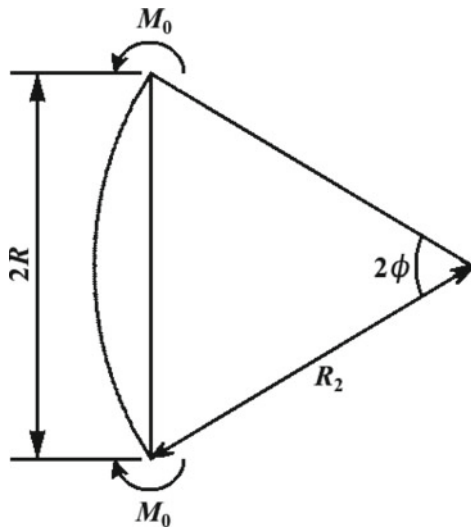
$$\sigma_1 = \frac{Q_0 \cos \phi}{t} = \frac{2.101 \times 10^5 \times \cos(2\pi/3)}{0.0127} = -8.272 \times 10^6 \text{ N/m}^2$$

$$\sigma'_1 = 0 \text{ N/m}^2$$

$$\begin{aligned}\sigma_2 &= \frac{Q_0 \beta \sin \phi}{2t} \left(\frac{2}{K_1} + K_1 + K_2 \right) \\ &= \frac{2.101 \times 10^5 \times 8.858 \times \sin(2\pi/3)}{2 \times 0.0127} \times \left(\frac{2}{1.011} + 1.011 + 1.054 \right) \\ &= 2.566 \times 10^8 \text{ N/m}^2\end{aligned}$$

$$\begin{aligned}\sigma'_2 &= \frac{-Q_0 \beta^2 \cos \phi}{K_1 R_2} = \frac{-2.101 \times 10^5 \times 8.858^2 \times \cos(2\pi/3)}{1.011 \times 0.5 \times 1.219} \\ &= 1.338 \times 10^7 \text{ N/m}^2\end{aligned}$$

Now we apply the formulae of [3, Table 13.3. case 1b], which concern the membrane and bending stresses and strains in a segment of spherical shell with moments M_0 applied at the edges, as shown in the following figure.



These formulae, applied to the present case, are

$$\begin{aligned}\Delta R &= \frac{2M_0\beta^2 \sin \phi}{EtK_1} = \frac{2 \times 8.858^2 \times \sin(2\pi/3)}{6.895 \times 10^{10} \times 0.0127 \times 1.011} M_0 = 1.535 \times 10^{-7} M_0 \text{ m} \\ \psi &= \frac{4M_0\beta^3}{EtR_2K_1} \\ &= \frac{4 \times 8.858^3}{6.895 \times 10^{10} \times 0.0127 \times 0.5 \times 1.219 \times 1.011} M_0 \\ &= 5.152 \times 10^{-6} M_0 \text{ rad}\end{aligned}$$

Since the total rotation ψ at the edges of the spherical segment must be equal to zero, then

$$0 + 0.03225 + 5.152 \times 10^{-6} M_0 = 0$$

The preceding equation, solved for M_0 , yields

$$M_0 = -6.259 \times 10^3 \text{ N/m/m}$$

and therefore the preceding expression of ΔR becomes

$$\Delta R = 1.535 \times 10^{-7} \times (-6.259 \times 10^3) = -9.608 \times 10^{-4} \text{ m}$$

The total radial deformation results from

$$\Delta R = (1.697 + 19.85 - 9.608) \times 10^{-4} = 11.94 \times 10^{-4} \text{ m} = 1.194 \text{ mm}$$

Since the value of M_0 is known, we can also use the following formulae of [3, Table 13.3, case 1b]

$$\sigma_1 = 0 \text{ N/m}^2$$

$$\sigma'_1 = \frac{-6M_0}{t^2} = \frac{-6 \times (-6.259 \times 10^3)}{0.0127^2} = 2.328 \times 10^8 \text{ N/m}^2$$

$$\sigma_2 = \frac{2M_0\beta^2}{R_2 K_1 t} = \frac{2 \times (-6.259 \times 10^3) \times 8.858^2}{0.5 \times 1.219 \times 1.011 \times 0.0127} = -1.255 \times 10^8 \text{ N/m}^2$$

$$M_2 = \frac{M_0}{2\nu K_1} [(1 + \nu^2)(K_1 + K_2) - 2K_2] = \frac{-6.259 \times 10^3}{2 \times 0.33 \times 1.011} \\ \times [(1 + 0.33^2) \times (1.011 + 1.054) - 2 \times 1.054] = -1.706 \times 10^3 \text{ Nm/m}$$

$$\sigma'_2 = \frac{-6M_2}{t^2} = \frac{-6 \times (-1.706 \times 10^3)}{0.0127^2} = 0.6347 \times 10^8 \text{ N/m}^2$$

Therefore, the total stresses at the junction are

$$\sigma_1 = (3.309 - 0.8272 + 0) \times 10^7 = 2.482 \times 10^7 \text{ N/m}^2$$

$$\sigma'_1 = (0 + 0 + 23.28) \times 10^7 = 23.28 \times 10^7 \text{ N/m}^2$$

$$\sigma_2 = (3.309 + 25.66 - 12.55) \times 10^7 = 16.42 \times 10^7 \text{ N/m}^2$$

$$\sigma'_2 = (0 + 1.338 + 6.347) \times 10^7 = 7.685 \times 10^7 \text{ N/m}^2$$

The maximum stress at the junction is a tensile meridian stress

$$\sigma_1 + \sigma'_1 = (2.482 + 23.28) \times 10^7 = 25.76 \times 10^7 \text{ N/m}^2$$

This value is greater than the yield stress of aluminium, which is $9.5 \times 10^7 \text{ N/m}^2$ [5]. In order to reduce the tensile stress at the junction between the two spherical segments, it is possible to add a reinforcing ring of aluminium. We want to compute the cross-sectional area A (m^2) of the reinforcing ring.

If the radial deformation ΔR (m) of the ring were equal to the radial deformation at the edge of each of the two spherical segments due only to membrane stresses, then the bending stresses would be eliminated. The radial deformation at the edge of one of the two spherical segments due only to membrane stresses has been found above to be $\Delta R = 1.697 \times 10^{-4} \text{ m}$. Therefore, let the reinforcing ring be subject to a load per unit length $2Q_0$ (N/m) (that is, to a load $F = 2Q_0R$) and have a radial

deformation $\Delta R = 1.697 \times 10^{-4}$ m. From Hooke's law, there results

$$\sigma = \varepsilon E$$

By substituting $\sigma = F/A = 2Q_0R/A$ and $\varepsilon = \Delta R/R$ in the preceding equation and solving for A , there results

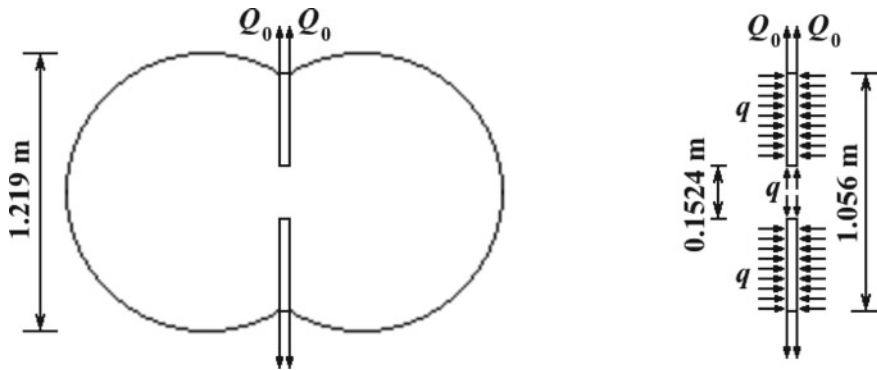
$$A = \frac{2Q_0R^2}{E\Delta R}$$

In the present case, as has been shown above, $Q_0 = 2.101 \times 10^5$ N/m, $R = R_2 \sin \phi = 0.5 \times 1.129 \times \sin(2\pi/3)$ m, $E = 6.895 \times 10^{10}$ N/m², and $\Delta R = 1.697 \times 10^{-4}$ m.

By substituting these values in the preceding equation, there results

$$A = \frac{2 \times 2.101 \times 10^5 \times [0.5 \times \sin(\frac{2}{3}\pi)]^2}{6.895 \times 10^{10} \times 1.697 \times 10^{-4}} = 0.01 \text{ m}^2$$

Since this value of A is considerable with respect to $R = 0.5278$ m, then the simple expression of $\Delta R/R$ given above (which is based on a thin ring) is not applicable. In addition, the reinforcing ring is too big to be placed outside the tank. Therefore, we place it inside the tank, as shown in the following figure.



In other words, the two spherical segments of the tank are put together by means of an internal reinforcing disc, which is $2a = 1.219 \times \sin(2\pi/3) = 1.056$ m in diameter. This disc has a coaxial orifice, whose diameter $2b$ is set arbitrarily to 0.1524 m, for the passage of the liquid contained in the tank, and a thickness t_1 (m), whose value is to be determined.

For this purpose, we use the formulae of [3, Table 13.5, case 1a], which concern the stresses and strains in a thick-walled disc subject to a uniform internal radial pressure q (N/m²) and to zero, or externally balanced, longitudinal pressure. According to the formulae indicated above, the radial deformation Δa (m) of the disc is

$$\Delta a = \frac{q}{E} \frac{2ab^2}{a^2 - b^2}$$

By substituting $q = 1.379 \times 10^6 \text{ N/m}^2$, $E = 6.895 \times 10^{10} \text{ N/m}^2$, $a = 0.5 \times 1.056 \text{ m}$, and $b = 0.5 \times 0.1524 \text{ m}$ in the preceding equation, we find

$$\Delta a = \frac{1.379 \times 10^6}{6.895 \times 10^{10}} \times \frac{1.056 \times 0.1524^2}{1.056^2 - 0.1524^2} = 4.492 \times 10^{-7} \text{ m}$$

The effect of the force per unit length $2Q_0$ on the disc can be evaluated by means of an external negative pressure $-2Q_0/t_1$. We use the formulae of [3, Table 13.5, case 1c], which concern the stresses and strains in a thick-walled disc subject to a uniform external radial pressure q (N/m^2) and to zero, or externally balanced, longitudinal pressure. According to the formulae indicated above, the radial deformation Δa (m) of the disc is

$$\Delta a = \frac{-qa}{E} \left(\frac{a^2 + b^2}{a^2 - b^2} - \nu \right)$$

By substituting the values indicated above, $q = -2 \times 2.101 \times 10^5/t_1$, and $\nu = 0.33$ in the preceding equation, we find

$$\Delta a = \frac{2.101 \times 10^5 \times 1.056}{6.895 \times 10^{10} t_1} \times \left(\frac{1.056^2 + 0.1524^2}{1.056^2 - 0.1524^2} - 0.33 \right) = \frac{2.293 \times 10^{-6}}{t_1} \text{ m}$$

In addition, the longitudinal pressure $q = 1.379 \times 10^6 \text{ N/m}^2$ causes a radial deformation of the disc

$$\Delta a = \frac{q\nu R}{E} = \frac{1.379 \times 10^6 \times 0.33 \times 0.5 \times 1.056}{6.895 \times 10^{10}} = 3.485 \times 10^{-6} \text{ m}$$

By summing the three values of the radial deformation Δa found above and equating the result to the desired value $1.697 \times 10^{-4} \text{ m}$, we find

$$0.004492 + \frac{0.02293}{t_1} + 0.03485 = 1.697 \text{ m}$$

The preceding equation, solved for t_1 , yields

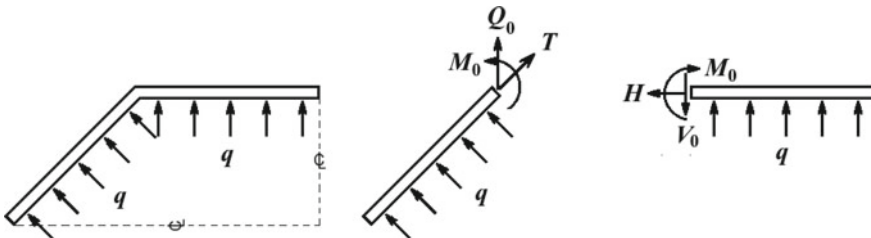
$$t_1 = \frac{0.02293}{1.697 - 0.004492 - 0.03485} = 0.01383 \text{ m} = 13.83 \text{ mm}$$

Further refinements are possible by varying the diameter $2b$ of the orifice in the reinforcing ring or the thickness t of the wall near the junction.

6.4 Multi-element Tanks

Stresses due to changes in thickness or in shape occur at the junctions of tanks made of shell elements. They are particularly important in case of tanks subject to cyclic or fatigue loads. The following examples show how the tables of [3] can be used to determine the stresses at the junctions of multi-element tanks.

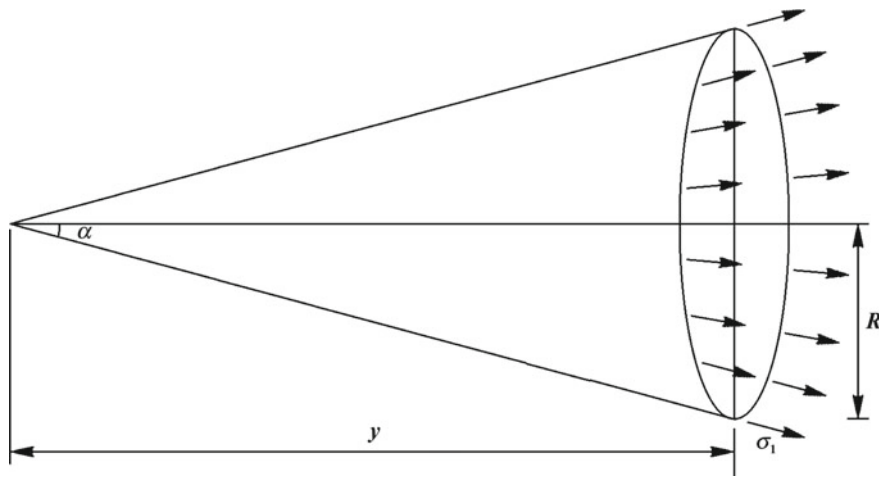
The tank shown in the following figure, in quarter longitudinal section, has a cylindrical shell and two conical shells at its ends.



The radius and the thickness of the cylindrical shell are respectively $R = 0.6096$ m and $t = 0.01608$ m. The semi-aperture angle and the thickness of the conical shells are respectively $\alpha = \pi/4$ rad and thickness $t = 0.01918$ m. The cylinder and the cones are welded together. The material of which the tank is made is steel, with Young's modulus $E = 2.068 \times 10^{11}$ N/m² and Poisson's ratio $\nu = 0.25$. The tank is subject to an internal pressure $q = 2.068 \times 10^6$ N/m². It is required to determine the maximum stress at the junction.

We apply once again the principle of superposition of effects first to the conical shell and then to the cylindrical shell, as will be shown below.

The stresses σ_1 (N/m²) and σ_2 (N/m²), the radial deformation ΔR (m), the angular rotation ψ (rad), and the force per unit length T (N/m) at the end of the cone can be determined by using the formulae of [3, Table 13.1, case 2a], which concern the membrane stresses and strains in a conical shell of radius R (m) at the base, thickness t (m) and semi-aperture angle α (rad), subject to a uniform internal or external pressure q (N/m²), with a tangential support at the edge, as shown in the following figure.



These formulae, applied to the present case, are

$$\sigma_1 = \frac{qR}{2t \cos \alpha} = \frac{2.068 \times 10^6 \times 0.6096}{2 \times 0.01918 \times \cos(\pi/4)} = 4.648 \times 10^7 \text{ N/m}^2$$

$$T = \sigma_1 t = 4.648 \times 10^7 \times 0.01918 = 8.914 \times 10^5 \text{ N/m}$$

$$\sigma_2 = \frac{qR}{t \cos \alpha} = 2\sigma_1 = 2 \times 4.648 \times 10^7 = 9.295 \times 10^7 \text{ N/m}^2$$

$$\sigma'_1 = \sigma'_2 = 0 \text{ N/m}^2$$

$$\begin{aligned} \Delta R &= \frac{qR^2}{Et \cos \alpha} \left(1 - \frac{\nu}{2}\right) = \frac{2.068 \times 10^6 \times 0.6096^2}{2.068 \times 10^{11} \times 0.01918 \times \cos(\pi/4)} \times \left(1 - \frac{0.25}{2}\right) \\ &= 0.0002398 \text{ m} = 0.2398 \text{ mm} \end{aligned}$$

$$\psi = \frac{3qR \tan \alpha}{2Et \cos \alpha} = \frac{3 \times 2.068 \times 10^6 \times 0.6096 \times \tan(\pi/4)}{2 \times 2.068 \times 10^{11} \times 0.01918 \times \cos(\pi/4)} = 0.0006742 \text{ rad}$$

Now we determine the radial force per unit length Q_0 (N/m) at the edge of the cone by using the formulae of [3, Table 13.3, case 4a]. These formulae concern the membrane and bending stresses and strains for a thin-walled cone of radius R_A (m) at its base and semi-aperture angle α , subject to a uniform radial force per unit length Q_0 at its base. These formulae, applied to the present case ($R_A = 0.6096$ m), are

$$k_A = \frac{2}{\sin \alpha} \left[\frac{12(1 - \nu^2)R^2 \cos^2 \alpha}{t^2} \right]^{\frac{1}{4}}$$

$$\begin{aligned}
&= \frac{2}{\sin(\pi/4)} \times \left[\frac{12 \times (1 - 0.25^2) \times 0.6096^2 \times \cos^2(\pi/4)}{0.01918^2} \right]^{\frac{1}{4}} \\
&= 24.56
\end{aligned}$$

$$\beta = [12(1 - v^2)]^{\frac{1}{2}} = [12 \times (1 - 0.25^2)]^{\frac{1}{2}} = 3.354$$

$$F_{1A} = F_{3A} = 0$$

$$\begin{aligned}
F_{4A} &= 1 - \frac{3.359}{k_A} + \frac{5.641}{k_A^2} - \frac{9.737}{k_A^3} + \frac{14.716}{k_A^4} \\
&= 1 - \frac{3.359}{24.56} + \frac{5.641}{24.56^2} - \frac{9.737}{24.56^3} \\
&\quad + \frac{14.716}{24.56^4} = 0.8720
\end{aligned}$$

$$\begin{aligned}
F_{10A} = F_{7A} = F_{6A} &= 1 - \frac{2.652}{k_A} + \frac{1.641}{k_A^2} - \frac{0.290}{k_A^3} - \frac{2.211}{k_A^4} \\
&= 1 - \frac{2.652}{24.56} + \frac{1.641}{24.56^2} - \frac{0.290}{24.56^3} - \frac{2.211}{24.56^4} = 0.8947
\end{aligned}$$

$$\begin{aligned}
F_{2A} &= 1 - \frac{2.652}{k_A} + \frac{3.516}{k_A^2} - \frac{2.610}{k_A^3} + \frac{0.038}{k_A^4} \\
&= 1 - \frac{2.652}{24.56} + \frac{3.516}{24.56^2} - \frac{2.610}{24.56^3} + \frac{0.038}{24.56^4} \\
&= 0.8977
\end{aligned}$$

$$\begin{aligned}
F_{8A} = F_{5A} &= 1 - \frac{3.359}{k_A} + \frac{7.266}{k_A^2} - \frac{10.068}{k_A^3} + \frac{5.787}{k_A^4} \\
&= 1 - \frac{3.359}{24.56} + \frac{7.266}{24.56^2} - \frac{10.068}{24.56^3} + \frac{5.787}{24.56^4} = 0.8746
\end{aligned}$$

$$\begin{aligned}
F_{9A} = C_1 &= F_{5A} + \frac{2(2)^{\frac{1}{2}}v}{k_A} F_{2A} = 0.8746 + \frac{2 \times 2^{\frac{1}{2}} \times 0.25}{24.56} \times 0.8977 = 0.9005 \\
\Delta R_A &= \frac{Q_0 R_A \sin \alpha}{E_t} \frac{k_A}{2^{\frac{1}{2}} C_1} \left(F_{4A} - \frac{4v^2}{k_A^2} F_{2A} \right) \\
&= \frac{Q_0 \times 0.6096 \times \sin(\pi/4)}{2.068 \times 10^{11} \times 0.01918} \times \frac{24.56}{2^{\frac{1}{2}} \times 0.9005} \times \left(0.8720 - \frac{4 \times 0.25^2}{24.56^2} \times 0.8977 \right) \\
&= 1.827 \times 10^{-9} \times Q_0 \text{ m}
\end{aligned}$$

$$\begin{aligned}\psi_A &= \frac{Q_0 R_A \beta}{E t^2 C_1} F_{10A} = \frac{Q_0 \times 0.6096 \times 3.354}{2.068 \times 10^{11} \times 0.01918^2 \times 0.9005} \times 0.8947 \\ &= 2.670 \times 10^{-8} \times Q_0 \text{ rad}\end{aligned}$$

$$N_{1A} = Q_0 \sin \alpha = Q_0 \times \sin(\pi/4) = 0.7071 \times Q_0 \text{ N/m}$$

$$\sigma_{1A} = \frac{N_{1A}}{t} = \frac{0.7071 \times Q_0}{0.01918} = 36.87 \times Q_0 \text{ N/m}^2$$

$$M_{1A} = 0 \text{ Nm/m}$$

$$\sigma'_{1A} = \frac{-6M_{1A}}{t^2} = 0 \text{ N/m}^2$$

$$\begin{aligned}N_{2A} &= \frac{Q_0 k_A}{2^{\frac{1}{2}} C_1} \left(F_{4A} + \frac{2^{\frac{1}{2}} \nu}{k_A} \right) \sin \alpha \\ &= \frac{Q_0 \times 24.56}{2^{\frac{1}{2}} \times 0.9005} \times \left(0.8720 + \frac{2^{\frac{1}{2}} \times 0.25}{24.56} \right) \times \sin(\pi/4) \\ &= 12.09 \times Q_0 \text{ N/m}\end{aligned}$$

$$\sigma_{2A} = \frac{N_{2A}}{t} = \frac{12.09 \times Q_0}{0.01918} = 630.3 \times Q_0 \text{ N/m}^2$$

$$\begin{aligned}M_{2A} &= Q_0 (1 - \nu^2) \frac{t}{\beta C_1} F_{10A} \sin \alpha \\ &= Q_0 \times (1 - 0.25^2) \times \frac{0.01918}{3.354 \times 0.9005} \times 0.8947 \times \sin(\pi/4) \\ &= 0.003767 \times Q_0 \text{ Nm/m}\end{aligned}$$

$$\sigma'_{2A} = \frac{-6M_{2A}}{t^2} = \frac{-6 \times 0.003767 \times Q_0}{0.01918^2} = -61.44 \times Q_0$$

Now we determine the moment per unit length M_0 (Nm/m) at the edge of the cone by using the formulae of [3, Table 13.3, case 4b]. These formulae concern the membrane and bending stresses and strains for a thin-walled cone of radius R_A (m) at its base and semi-aperture angle α , subject to a uniform moment per unit length M_0 at its base. These formulae, applied to the present case ($R_A = 0.6096$ m), are

$$\begin{aligned}\Delta R_A &= M_0 \frac{\beta R_A}{E t^2 C_1} F_{7A} = M_0 \frac{3.354 \times 0.6096}{2.068 \times 10^{11} \times 0.01918^2 \times 0.9005} \times 0.8947 \\ &= 2.670 \times 10^{-8} \times M_0 \text{ m}\end{aligned}$$

$$\begin{aligned}\psi_A &= M_0 \frac{2(2)^{\frac{1}{2}} \beta^2 R_A}{Et^3 k_A C_1 \sin \alpha} F_{2A} \\ &= M_0 \times \frac{2 \times 2^{\frac{1}{2}} \times 3.354^2 \times 0.6096}{2.068 \times 10^{11} \times 0.01918^3 \times 24.56 \times 0.9005 \times \sin(\pi/4)} \times 0.8977 \\ &= 7.631 \times 10^{-7} \times M_0 \text{ rad}\end{aligned}$$

$$N_{1A} = 0 \text{ N/m}$$

$$\sigma_{1A} = \frac{N_{1A}}{t} = 0 \text{ N/m}^2$$

$$N_{2A} = M_0 \frac{\beta}{t C_1} F_{7A} = M_0 \times \frac{3.354}{0.01918 \times 0.9005} \times 0.8947 = 173.8 \times M_0 \text{ N/m}$$

$$\sigma_{2A} = \frac{N_{2A}}{t} = \frac{173.8 \times M_0}{0.01918} = 9062 \times M_0 \text{ N/m}^2$$

$$M_{1A} = M_0 \text{ Nm/m}$$

$$\sigma'_{1A} = \frac{-6M_{1A}}{t^2} = \frac{-6 \times M_0}{0.01918^2} = -1.631 \times 10^4 \times M_0$$

$$\begin{aligned}M_{2A} &= M_0 \left[\nu + \frac{2(2)^{\frac{1}{2}}(1-\nu^2)}{k_A C_1} F_{2A} \right] \\ &= M_0 \times \left[0.25 + \frac{2 \times 2^{\frac{1}{2}} \times (1-0.25^2)}{24.56 \times 0.9005} \times 0.8977 \right] \\ &= 0.3576 \times M_0 \text{ Nm/m}\end{aligned}$$

$$\sigma'_{2A} = \frac{-6M_{2A}}{t^2} = \frac{-6 \times 0.3576 \times M_0}{0.01918^2} = -5833 \times M_0$$

Now, we consider the cylindrical shell. We assume the initial section and the final section of this shell to be at a sufficient distance one from the other, that the stresses and the deformations of the material at one of them do not affect the stresses and the deformations at the other. The radius and the thickness of the cylindrical shell are respectively $R = 0.6096 \text{ m}$ and $t = 0.01608 \text{ m}$. By using these values and the mechanical properties of the material ($E = 2.068 \times 10^{11} \text{ N/m}^2$ and $\nu = 0.25$), we compute the following quantities

$$\lambda = \left[\frac{3(1-\nu^2)}{R^2 t^2} \right]^{\frac{1}{4}} = \left[\frac{3 \times (1-0.25^2)}{0.6096^2 \times 0.01608^2} \right]^{\frac{1}{4}} = 13.08 \text{ m}^{-1}$$

$$D = \frac{Et^3}{12(1-\nu^2)} = \frac{2.068 \times 10^{11} \times 0.01608^3}{12 \times (1 - 0.25^2)} = 7.643 \times 10^4 \text{ Nm}$$

Now we use the formulae of [3, Table 13.1, case 1c], which concern the membrane stresses and strains on a thin-walled cylindrical shell subject to a uniform internal or external pressure q (N/m²), with ends capped. These formulae, applied to the present case, are

$$\sigma_1 = \frac{qR}{2t} = \frac{2.068 \times 10^6 \times 0.6096}{2 \times 0.01608} = 3.920 \times 10^7 \text{ N/m}^2$$

$$H = \sigma_1 t = 3.920 \times 10^7 \times 0.01608 = 6.303 \times 10^5 \text{ N/m}$$

$$\sigma_2 = \frac{qR}{t} = 2\sigma_1 = 2 \times 3.920 \times 10^7 = 7.840 \times 10^7 \text{ N/m}^2$$

$$\sigma'_1 = \sigma'_2 = 0 \text{ N/m}^2$$

$$\begin{aligned} \Delta R &= \frac{qR^2}{Et} \left(1 - \frac{\nu}{2}\right) = \frac{2.068 \times 10^6 \times 0.6096^2}{2.068 \times 10^{11} \times 0.01608} \times \left(1 - \frac{0.25}{2}\right) \\ &= 0.0002022 \text{ m} = 0.2022 \text{ mm} \end{aligned}$$

$$\psi = 0 \text{ rad}$$

Now we use the formulae of [3, Table 13.2, case 8], which concern the membrane and bending stresses and strains on a long cylindrical shell, with the left end free and the right end more than $6/\lambda$ units of length, subject at its left end to a radial load per unit length V_0 (N/m). These formulae, applied to the present case, are

$$\psi_A = \frac{V_0}{2D\lambda^2} = \frac{V_0}{2 \times 7.643 \times 10^4 \times 13.08^2} = 3.824 \times 10^{-8} \times V_0 \text{ rad}$$

$$\Delta R_A = y_A = \frac{-V_0}{2D\lambda^3} = \frac{-V_0}{2 \times 7.643 \times 10^4 \times 13.08^3} = -2.923 \times 10^{-9} \times V_0 \text{ m}$$

$$\sigma_1 = 0 \text{ N/m}^2$$

$$\sigma_2 = \frac{y_A E}{R} + \nu \sigma_1 = \frac{-2.923 \times 10^{-9} \times V_0 \times 2.068 \times 10^{11}}{0.6096} = -991.6 \times V_0 \text{ N/m}^2$$

$$\sigma'_1 = 0 \text{ N/m}^2$$

$$\sigma'_2 = v\sigma'_1 = 0 \text{ N/m}^2$$

Now we use the formulae of [3, Table 13.2, case 10], which concern the membrane and bending stresses and strains on a long cylindrical shell, with the left end free and the right end more than $6/\lambda$ units of length, subject at its left end to a moment per unit length M_0 (Nm/m). These formulae, applied to the present case, are

$$\psi_A = \frac{-M_0}{D\lambda} = \frac{-M_0}{7.643 \times 10^4 \times 13.08} = -1.000 \times 10^{-6} \times M_0 \text{ rad}$$

$$\Delta R_A = y_A = \frac{M_0}{2D\lambda^2} = \frac{M_0}{2 \times 7.643 \times 10^4 \times 13.08^2} = 3.824 \times 10^{-8} \times M_0 \text{ m}$$

$$\sigma_1 = 0 \text{ N/m}^2$$

$$\sigma_2 = \frac{2M_0\lambda^2R}{t} = \frac{2 \times M_0 \times 13.08^2 \times 0.6096}{0.01608} = 1.297 \times 10^4 \times M_0 \text{ N/m}^2$$

$$\sigma'_1 = \frac{-6M_0}{t^2} = \frac{-6 \times M_0}{0.01608^2} = -2.320 \times 10^4 \times M_0 \text{ N/m}^2$$

$$\sigma'_2 = v\sigma'_1 = 0.25 \times (-2.320 \times 10^4 \times M_0) = -5.801 \times 10^3 \times M_0 \text{ N/m}^2$$

Now, we sum the radial deformations ΔR for the conical shell and equate the result to the sum of the radial deformations ΔR for the cylindrical shell. This yields

$$\begin{aligned} & 0.0002398 + 1.827 \times 10^{-9} \times Q_0 + 2.670 \times 10^{-8} \times M_0 \\ & = 0.0002022 - 2.923 \times 10^{-9} \times V_0 + 3.824 \times 10^{-8} \times M_0 \end{aligned}$$

Then, we do the same operation for the sums of the angular rotations ψ of the two shells. This yields

$$\begin{aligned} & 0.0006742 + 2.670 \times 10^{-8} \times Q_0 + 7.631 \times 10^{-7} \times M_0 \\ & = 0 + 3.824 \times 10^{-8} \times V_0 - 1.0 \times 10^{-6} \times M_0 \end{aligned}$$

Finally, we do the same operation for the radial forces per unit length acting on the two shells. This yields

$$Q_0 + T \cos(\pi/4) = V_0$$

Since $T = 8.914 \times 10^5 \text{ N/m}$, then

$$Q_0 + 8.914 \times 10^5 \times \cos(\pi/4) = V_0$$

By substituting this value of V_0 in the two preceding equations which express respectively the radial deformations ΔR and the angular rotations ψ , we find

$$\begin{aligned} 11.54 M_0 - 4.750 Q_0 &= 1.880 \times 10^6 \\ 176.3 M_0 - 1.154 Q_0 &= 2.343 \times 10^6 \end{aligned}$$

The preceding system of linear equations, solved for M_0 and Q_0 , yields

$$\begin{aligned} M_0 &= 1.087 \times 10^4 \text{ Nm/m} \\ Q_0 &= -3.694 \times 10^5 \text{ N/m} \end{aligned}$$

Substituting $Q_0 = -3.694 \times 10^5 \text{ N/m}$ into $V_0 = Q_0 + 8.914 \times 10^5 \times \cos(\pi/4)$ yields

$$V_0 = -3.694 \times 10^5 + 8.914 \times 10^5 \times \cos(\pi/4) = 2.609 \times 10^5 \text{ N/m}$$

Since M_0 , Q_0 , and V_0 have known values, we can also evaluate the membrane and bending stresses in the cylindrical shell. They are

$$\sigma_1 = 3.920 \times 10^7 + 0 + 0 = 3.920 \times 10^7 \text{ N/m}^2$$

$$\begin{aligned} \sigma_2 &= 7.840 \times 10^7 - 991.6 \times 2.609 \times 10^5 + 1.297 \times 10^4 \times 1.087 \times 10^4 \\ &= -3.930 \times 10^7 \text{ N/m}^2 \end{aligned}$$

$$\sigma'_1 = 0 + 0 - 2.320 \times 10^4 \times 1.087 \times 10^4 = -2.522 \times 10^8 \text{ N/m}^2$$

$$\sigma'_2 = 0 + 0 - 5.801 \times 10^3 \times 1.087 \times 10^4 = -6.306 \times 10^7 \text{ N/m}^2$$

The combined meridian and circumferential stresses in the cylindrical shell are computed as follows:

(1) Combined meridian stress on the outside of the cylindrical shell:

$$0.3920 \times 10^8 - 2.522 \times 10^8 = -2.13 \times 10^8 \text{ N/m}^2$$

(2) Combined meridian stress on the inside of the cylindrical shell:

$$0.3920 \times 10^8 + 2.522 \times 10^8 = 2.914 \times 10^8 \text{ N/m}^2$$

(3) Combined circumferential stress on the outside of the cylindrical shell:

$$-0.393 \times 10^8 - 0.6306 \times 10^8 = -1.024 \times 10^8 \text{ N/m}^2$$

- (4) Combined circumferential stress on the inside of the cylindrical shell:

$$-3.930 \times 10^7 + 6.306 \times 10^7 = 2.376 \times 10^7 \text{ N/m}^2$$

We evaluate likewise the membrane and bending stresses in the conical shell. They are

$$\sigma_1 = 4.648 \times 10^7 + 36.87 \times (-3.694 \times 10^5) + 0 = 3.286 \times 10^7 \text{ N/m}^2$$

$$\begin{aligned}\sigma_2 &= 9.295 \times 10^7 + 630.3 \times (-3.694 \times 10^5) + 9062 \times 1.087 \times 10^4 \\ &= -4.138 \times 10^7 \text{ N/m}^2\end{aligned}$$

$$\sigma'_1 = 0 + 0 - 1.631 \times 10^4 \times 1.087 \times 10^4 = -1.773 \times 10^8 \text{ N/m}^2$$

$$\begin{aligned}\sigma'_2 &= 0 - 61.44 \times (-3.694 \times 10^5) - 5833 \times 1.087 \times 10^4 \\ &= -4.07 \times 10^7 \text{ N/m}^2\end{aligned}$$

The combined meridian and circumferential stresses in the conical shell are computed as follows:

- (1) Combined meridian stress on the outside of the conical shell:

$$0.3286 \times 10^8 - 1.773 \times 10^8 = -1.444 \times 10^8 \text{ N/m}^2$$

- (2) Combined meridian stress on the inside of the conical shell:

$$0.3286 \times 10^8 + 1.773 \times 10^8 = 2.102 \times 10^8 \text{ N/m}^2$$

- (3) Combined circumferential stress on the outside of the conical shell:

$$-4.138 \times 10^7 - 4.07 \times 10^7 = -8.208 \times 10^7 \text{ N/m}^2$$

- (4) Combined circumferential stress on the inside of the conical shell:

$$-4.138 \times 10^7 + 4.07 \times 10^7 = -0.068 \times 10^7 \text{ N/m}^2$$

6.5 Tanks Subject to Loads Due to Propellant Sloshing

This section considers the loads acting on the tanks of large space vehicles partially filled with liquid propellants. Since the initial masses of these vehicles consist principally of liquid propellants, then the time-varying loads due to the motion of such masses in their tanks are very large. The control systems and the structures of launch vehicles are to be designed in such a way as to respectively counteract and resist such loads.

The dynamical systems which describe the motion of liquid masses into moving containers are very complex, because of couplings of the components of such systems. In particular, the natural frequencies of the control systems, of the elastic bodies, and of the liquid sloshing are to be kept separated as widely as possible, because large forces and moments can be generated by a liquid propellant oscillating at one of its natural frequencies in a partially filled tank. Unfortunately, such is not always the case, as shown in the following table, adapted from [6], which refers to some representative launch vehicles.

Characteristics of Some Representative Launch Vehicles

Vehicle	Length, m	Diameter, m	Thrust, N	Range, km	Control frequency, Hz	Fundamental slosh frequency at liftoff, Hz	Fundamental bending frequency at liftoff, Hz	Important missions
Redstone-----	21	1.78	1.432×10^8	370.4	0.5	0.8	10-12	Exploration.
Redstone-Mercury	25	1.78	1.432×10^8	370.4	.5	.8	10	Suborbital manned flights.
Jupiter-----	20	2.65	3.925×10^8	2778	.4	.6	9	Reentry, recovery of monkeys Able and Baker.
Juno II-----	25	2.65	3.925×10^8	-----	.4	.6	8	Moon try, Sun orbit.
Saturn I-----	60	6.5	3.047×10^9	-----	.3	.45	2	Manned space flight.
Saturn V-----	130	10	1.512×10^{12}	-----	.16	b 0.3-0.4	1	Manned space flight.

* Large slosh masses in unfavorable locations.

b Exceptionally large slosh masses because of the large tank diameter.

By sloshing we mean the periodic motion of the free surface of a liquid in a partially filled container [7]. This motion results from longitudinal and lateral displacements or angular rotations of the vehicle carrying the container.

In particular, lateral sloshing is the standing wave formed on the free surface of a liquid when a tank partially filled is caused to oscillate horizontally [8], that is,

in a plane parallel to the free surface of the quiescent liquid. Lateral sloshing is antisymmetric, and occurs primarily in response to translational or pitching motions of a tank. By contrast, vertical sloshing is symmetric, and occurs primarily in response to motions of a tank in the direction perpendicular to the free surface of the quiescent liquid. Rotational sloshing is a motion exhibiting an apparent swirling of a liquid about a normal axis, and arising as an instability of the antisymmetric lateral sloshing near resonance [6].

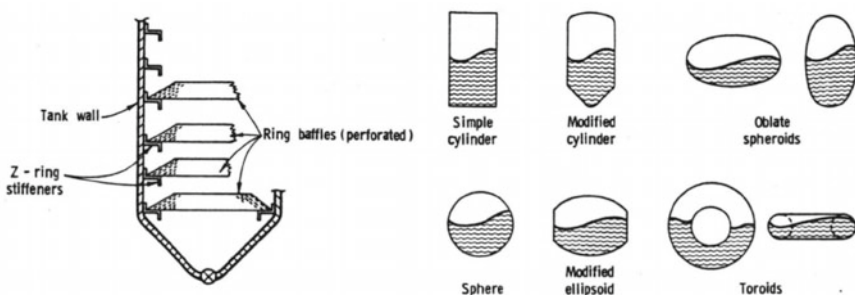
The tanks of space vehicles may be subject to oscillations for several causes, which act either separately or in combination. Some examples of these causes, identified by Abramson et al. [9], are

- wind gusts during powered flight;
- programmed changes of attitude of the vehicle;
- control pulses for attitude stabilisation;
- separation impulses; and
- elastic deformations of the vehicle.

The magnitude of the forces and moments due to sloshing depend upon

- shape of the tank;
- properties of the propellants;
- damping;
- height of the propellant in the tank;
- acceleration; and
- perturbing motion of the tank.

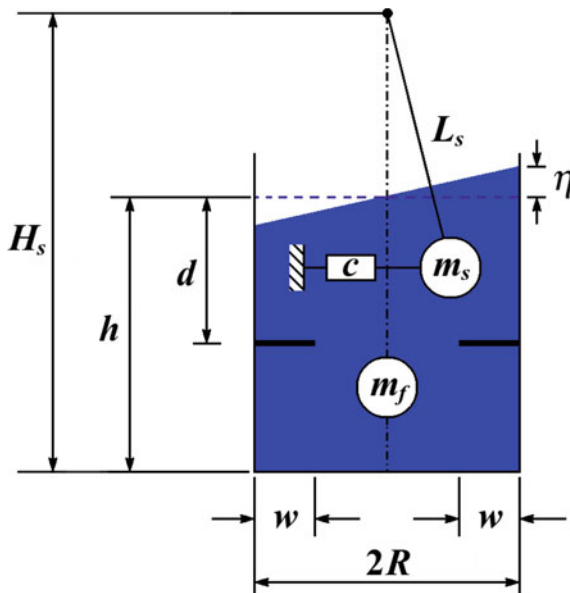
The sloshing phenomenon and its consequence on the stability of a space vehicle can be controlled by a proper design of the tank and by the addition of baffles, as will be shown in Sect. 6.6. The shape of the tank has an influence on the natural sloshing frequencies and modes, and on the response to the forced oscillations and to the forces and moments due to the presence of the propellant in the tank. The following figure, due to the courtesy of NASA [6], shows (left) ring baffles mounted on the wall of a circular cylindrical tank wall by means of Z-ring stiffeners, and (right) some typical shapes of tanks.



The number and the type of baffles depend on the damping requirements. The strength of the baffles depends on several factors, among which the strength and the rigidity required during manufacturing and handling, the mechanical and thermal stresses due to propellant loading, and the forces and moments due to propellant sloshing [9].

The coupling between a sloshing propellant and the elastic structure of its tank may have a large influence on the vibration frequencies and on the mode shapes of the tank. In addition, the system comprising a sloshing propellant and its tank may have dynamic instabilities either by itself or by coupling with some other components of a rocket engine subject to oscillations, as is the case with the combustion and feed-line systems.

The dynamic response of a space vehicle to sloshing loads can be determined by using an equivalent mechanical model which represents the behaviour of an oscillating tank partially filled with a liquid propellant. This mechanical model consists of fixed masses (m_f) and oscillating masses (m_s) connected to the tank by springs and dashpots or by pendulums and dashpots. The second case is shown in the following figure, re-drawn from [10].



Each mechanical model refers to a particular shape of tank, and is designed so as to have the same resultant force, moment, damping, and natural frequencies as the actual oscillating propellant. This model is then combined with other dynamic elements of the space vehicle being considered, and the dynamic behaviour of the whole system is studied by means of digital or analogue computers.

The number of slosh masses m_s included in an equivalent mechanical model corresponds to the number of slosh modes considered in the analysis. In case of a

circular cylindrical tank, the sloshing mass corresponding to the second mode has been found to be about 3% of the mass corresponding to the first node, and therefore the sloshing effects due to the second and higher modes are generally negligible for a tank of this shape. However, for a quarter tank, the sloshing mass corresponding to the second mode is 43% of the mass corresponding to the first mode, and therefore should be included in determining the total sloshing loads acting on the tank [9]. Sloshing effects in tanks having arbitrary shapes have been studied by various authors (see, for example, [6, 11]).

For lateral sloshing of a liquid propellant in a rigid circular cylindrical tank with a flat bottom, the frequencies f_n (Hz) of the oscillating free surface have been found [6, 9] to be

$$f_n = \frac{\omega_n}{2\pi} = \frac{1}{2\pi} \left[\varepsilon_n \frac{g}{R} \tanh\left(\varepsilon_n \frac{h}{R}\right) \right]^{\frac{1}{2}}$$

where ω_n (rad/s) are the angular frequencies, g (m/s²) is the vertical acceleration of the tank, ε_n are values determined from the roots of the following equation

$$\left(\frac{dJ_1(x)}{dx} \right)_{x=\varepsilon_n} = 0$$

$J_1(x)$ is the Bessel function of the first kind and order, R (m) is the radius of the circular cylindrical tank, and h (m) is the height of the free surface of the quiescent liquid propellant. Values of ε_n for the first four slosh modes are given in the following table (from [9]):

Slosh mode (n)	ε_n
1	1.841
2	5.331
3	8.536
4	11.706

Abramson et al. [9] point out that, when the height h of the liquid propellant is greater than the radius R of the circular cylindrical tank, then the equation expressing the frequencies f_n can be approximated as follows

$$f_n = \frac{1}{2\pi} \left(\varepsilon_n \frac{g}{R} \right)^{\frac{1}{2}}$$

A validation of the parameters of the equivalent mechanical model (pendulums and dashpots) illustrated in the preceding figure has been performed by Pérez et al. [10]. This linear (dashpot damping $c = \text{constant}$) model assumes the angles θ of oscillation of the pendulums to be within the interval $\pm\pi/12$ [12].

Since the dominant sloshing frequency f_1 corresponds to $n = 1$ and therefore to the root $\varepsilon_1 = 1.841$ of the equation $J'_1 = 0$, then Pérez et al. have considered only one sloshing mass m_s attached to a pendulum of length L_s .

A brief account of the results found by them is given below.

(1) Dominant sloshing frequency

$$f_1 = \frac{1}{2\pi} \left[1.841 \frac{g}{R} \tanh\left(1.841 \frac{h}{R}\right) \right]^{\frac{1}{2}}$$

(2) Sloshing mass

$$m_s = \frac{mR}{2.199h} \tanh\left(1.841 \frac{h}{R}\right)$$

where $m = m_s + m_f$ is the total mass of the propellant.

(3) Height of the suspension point of the pendulum

$$H_s = h - \frac{R}{1.841} \left[\tanh\left(0.9205 \frac{h}{R}\right) - \operatorname{csch}\left(1.841 \frac{h}{R}\right) \right]^{\frac{1}{2}}$$

(4) Dashpot damping

$$c = 4\pi f_1 m_s \zeta$$

where ζ is the damping ratio, which is defined in terms of the damping factor δ as follows

$$\zeta = \frac{\delta}{(4\pi^2 + \delta^2)^{\frac{1}{2}}}$$

and the damping factor δ is defined as follows

$$\delta = \frac{1}{k} \ln\left(\frac{A_0}{A_k}\right)$$

where A_0 (m) is the amplitude of the first wave, A_k (m) is the amplitude of the k th wave, and k is the number of cycles over which the decay is measured.

The magnitude of damping in smooth-wall and in baffled-wall tanks has been determined for several shapes. Generally speaking, the amount of damping due to the wiping action of a liquid propellant against the walls of a tank is insufficient, and therefore baffles must be added to provide the damping required to prevent instability. For example, a circular cylindrical tank having ring baffles of width w along its wall is shown in the preceding figure. The damping of liquid propellants in circular cylindrical tanks without baffles has been studied by Stephens et al. [13]. Viscous damping of liquid propellants in tanks of various shapes has been studied by several authors. By viscous damping we mean the damping produced by interaction between the liquid propellant and the wall of the tank. An account of empirical formulae for tanks of various shapes is given in [6, 8]. For example, for a circular cylindrical tank without baffles, the damping ratio ζ is expressed by the following experimental equation due to Mikishev and Dorozhkin [8]:

$$\zeta = 0.79 \left(\frac{\mu}{\rho} \right)^{\frac{1}{2}} R^{-\frac{3}{4}} g^{-\frac{1}{4}} \left\{ 1 + \frac{0.318}{\sinh(1.84h/R)} \left[\frac{1 - h/R}{\cosh(1.84h/R)} + 1 \right] \right\}$$

where μ/ρ is the kinematic viscosity of the liquid, R is the radius of the cross section of the tank, and g is the vertical acceleration. When the depth h of the liquid is greater than the diameter $2R$ of the tank cross section, then the preceding equation can be approximated as follows

$$\zeta = 0.79 \left(\frac{\mu}{\rho} \right)^{\frac{1}{2}} R^{-\frac{3}{4}} g^{-\frac{1}{4}}$$

Effective damping provided by baffles of various types has also been investigated by several authors. An account is given in [6, 8]. With reference to the preceding figure, Dodge [8] indicates the following equation, due to Miles [16], to estimate the damping ratio ζ for a flat ring rigid baffle in a circular cylindrical tank where the liquid depth h is considerably greater than the cross-sectional radius R ($h/R > 2$):

$$\zeta = 2.83 C_1^{\frac{3}{2}} \left(\frac{\eta}{R} \right)^{\frac{1}{2}} \exp \left(-4.6 \frac{d}{R} \right)$$

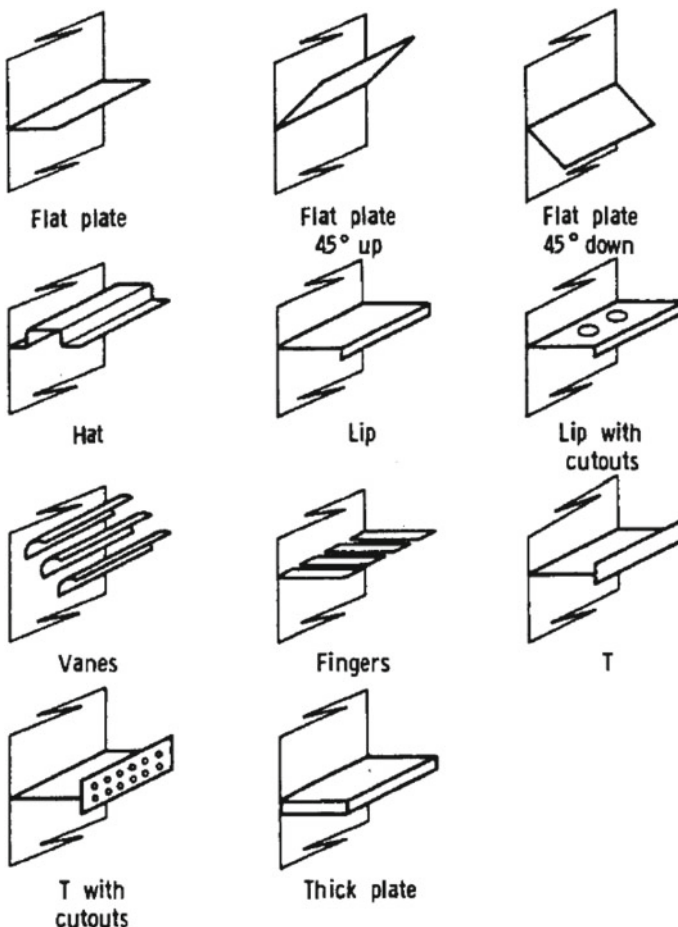
where C_1 is the ratio of the baffle area A_B to the tank cross-sectional area A_T , and therefore C_1 is for a circular cylindrical tank

$$C_1 = \frac{A_B}{A_T} = \frac{\pi R^2 - \pi(R-w)^2}{\pi R^2} = \frac{w}{R} \left(2 - \frac{w}{R} \right)$$

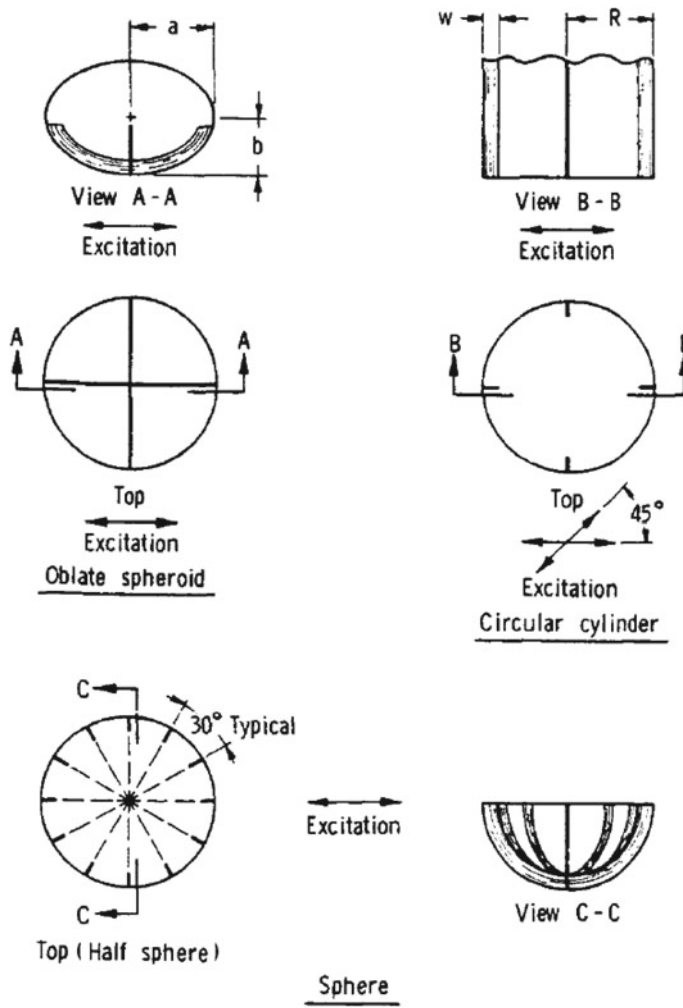
w is the width of the ring baffles, R is the radius of the cross section of the tank, η is the amplitude of oscillation measured at the tank wall from the free surface of the quiescent liquid, and d is the depth of the baffle below the free surface of the quiescent liquid. For circular cylindrical tanks, the damping provided by a series of

ring baffles can be calculated by superposing linearly the contribution of each baffle, when the spacing s between the baffles is greater than the width w of each baffle. For tanks of this shape, ring baffles are usually placed at a distance $s \leq 0.2R$ [10].

Types of baffles studied for circular cylindrical tanks include fixed rings, rings with radial clearance, cruciform baffles, and baffles shaped as conic sections. Baffles have also been studied for spherical tanks and for oblate or prolate spheroidal tanks. Flexible baffles have been compared to rigid baffles, and the former have been found to provide greater damping than the latter under certain conditions [9]. The following figure, due to the courtesy of NASA [6], shows some types of ring baffles used for circular cylindrical tanks.



The following figure, also due to the courtesy of NASA [6], shows some types of cruciform baffles used for tanks of various shapes.



Sloshing loads under low gravity conditions have been found small in comparison with the structural capability of propellant tanks. This topic is dealt with at length in [6, 8].

The lateral sloshing of liquid propellants in their tanks causes a distributed pressure loading on the walls. These loads are important for the structural design of the tanks. In addition, the resultant force and moment due to the distributed pressure are important for the control systems of space vehicles.

The longitudinal sloshing of liquid propellant also causes pressure loads on the tanks. These loads are less important than those due to lateral sloshing. However, the longitudinal pressure modes of a propellant may couple with those of the elastic shell or with those of the feed-line and combustion system. This fact can generate dynamic instability, as is the case with the pogo oscillations.

Loads acting on the top or on the bottom of a circular cylindrical tank can be caused by sudden changes of the net acceleration in the vertical direction. This may occur in such cases as abort just after launch, cut-off of the boost engine, engine start in orbit or in coast flight, et c. These loads are very sensitive to the test conditions and to the shapes of tanks [9].

In case of a circular cylindrical tank subject to lateral sloshing, a simple estimate of the pressure loads can be done by considering the tank pressurisation p_0 , the static pressure $\rho g z$ due to the liquid propellant in the tank, and the pressure due to the lateral sloshing at its lowest natural frequency $f_1 = \omega_1/(2\pi)$, corresponding to the first mode of oscillation. In other words, the maximum pressure p_{\max} (N/m^2) on a tank subject to lateral sloshing occurs in the plane of oscillation and can be expressed by using the following equation of [9]:

$$p_{\max} = p_0 + \rho g z + \rho g \eta \frac{\cosh[1.841(\frac{h-z}{R})]}{\cosh[1.841(\frac{h}{R})]} \sin(\omega_1 t)$$

where ρ (kg/m^3) is the density of the liquid propellant in the operational conditions, g (m/s^2) is the vertical acceleration of the tank, η (m) is the maximum height above the free surface of the quiescent liquid at the wall, R (m) is the radius of the tank, h (m) is the height of the free surface of the quiescent liquid, z (m) is the distance from the free surface of the quiescent liquid to any arbitrary depth (positive downward), and ω_1 (rad/s) is the first natural angular frequency of lateral slosh, whose value has been found above to be

$$\omega_1 = \left[1.841 \frac{g}{R} \tanh\left(1.841 \frac{h}{R}\right) \right]^{\frac{1}{2}}$$

Abramson et al. [9] point out that the total vertical acceleration acting on a particle of the free surface varies between $g - \eta \omega_1^2$ and $g + \eta \omega_1^2$ at the wall of the tank. When the amplitude of the sloshing propellant becomes large enough for the total vertical acceleration to be instantaneously zero, then the sloshing wave breaks up, and turbulent sloshing begins. Taking this condition as an upper limit yields $\eta = g/\omega_1^2$, and therefore the equation expressing the maximum pressure can be re-written as follows

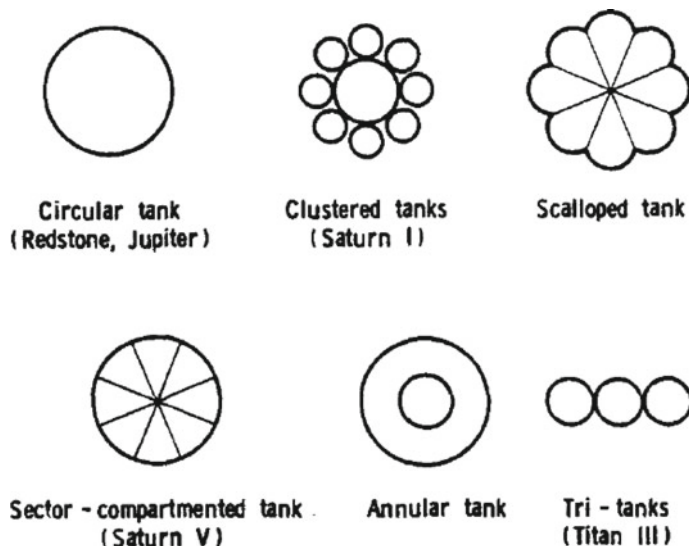
$$p_{\max} = p_0 + \rho g \left\{ z + \frac{R \cosh[1.841(\frac{h-z}{R})]}{1.841 \sinh[1.841(\frac{h}{R})]} \right\}$$

When the height h of the free surface is roughly equal to or greater than the radius R of the tank, the oscillations of the liquid propellant become independent of h , and the equation expressing the maximum pressure can be approximated as follows [9]:

$$p_{\max} = p_0 + \rho g \left[z + \frac{R}{1.841} \exp\left(-1.841 \frac{z}{R}\right) \right]$$

This equation still holds approximately in cases of tanks whose bottom surfaces are not flat. In case of non-cylindrical tanks, the maximum pressure can be expressed by using other formulae, for example, those of [6, 8], or [11].

Generally speaking, one third of the liquid propellant, the part of it which is near the bottom of the tank, is not affected by sloshing, which occurs near the free surface. The equivalent mechanical models consisting of fixed masses and oscillating masses are based on this fact. The sloshing mass and the resultant force decrease considerably in the higher modes of oscillations. For the lower modes, the sloshing mass can be reduced by dividing a tank into radial or concentric compartments. Some typical configurations used for propellant tanks are shown in the following figure, due to the courtesy of NASA [6].



On the effectiveness of dividing a tank into compartments for the purpose of reducing the sloshing mass, Dodge [8] notes that, for a circular cylindrical tank, the division into radial sectors raises the first (or fundamental) slosh frequency and lowers the second, so that the two modes are less separated in frequency. In addition, radial compartments are less effective than ring baffles in reducing the amplitude of forces and moments due to sloshing [8].

When a liquid propellant sloshes in a longitudinal mode, the pressures integrated over the bottom and the walls of the tank have a zero resultant force. An estimate of the pressure p (N/m^2) during sloshing in a circular cylindrical tank at the first longitudinal angular frequency ω_1 (rad/s) can be done by using the following formula of [9]:

$$p = p_0 + \rho g \left\{ z + \eta \frac{J_0(3.83 \frac{r}{R})}{J_0(3.83)} \frac{\cosh[3.83(\frac{h-z}{R})]}{\cosh[3.83 \frac{h}{R}]} \sin(\omega_1 t) \right\}$$

where

$$\omega_1 = \left[3.83 \frac{g}{R} \tanh\left(3.83 \frac{h}{R}\right) \right]^{\frac{1}{2}}$$

Hopfinger and Baumbach [14] is the first of the natural angular frequencies of longitudinal slosh, r (m) is the radial co-ordinate, and $J_0(x)$ is the zero-order Bessel function of the first kind.

When the height h of the free surface is roughly equal to or greater than the radius R of the tank, assuming again $\eta = g/\omega_1^2$, the maximum pressure becomes

$$p_{\max} = p_0 + \rho g \left[z + \frac{R}{3.83} \frac{J_0(3.83 \frac{r}{R})}{J_0(3.83)} \exp\left(-3.83 \frac{z}{R}\right) \right]$$

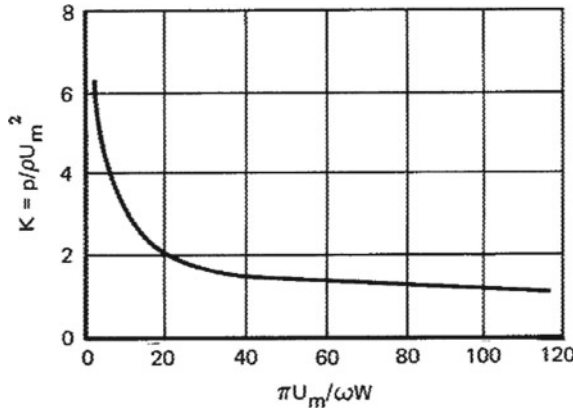
Abramson et al. [9] also point out that the effect of an elastic tank bottom is to lower the natural sloshing frequencies of the free surface slightly below their values in a rigid tank.

Longitudinal accelerations impressed to a partially filled tank can cause a liquid propellant to impinge on the dome of the tank. The problem of dome impact arises when the resultant acceleration acting on the tank reverses its direction. This may occur during engine shutdown of a launch vehicle flying through the atmosphere, or when an engine is ignited while the propellant is located in the upper part of a tank [6]. The impulsive pressure resulting from one of such events must be taken into account when assessing the structural integrity of a tank. This problem is considered at length in [6]. The impact of a liquid propellant on deflector baffles may also produce considerable loads. There being no general methods of analysis for predicting such loads, empirical methods or tests or both are used for this purpose. Ring baffles and other internal devices can reduce fluid impact loads [9].

The maximum pressure p (N/m²) acting on a submerged baffle of width w (m), subject to an oscillating velocity $U = U_m \cos(\omega t)$ (m/s), due a liquid propellant sloshing at an angular frequency ω (rad/s), is given by the following equation of [9]:

$$p = K \rho U_m^2$$

where K is a non-dimensional parameter whose values are given in the following figure of [9, 15]



and ρ (kg/m^3) and U_m (m/s) are respectively the density and the maximum velocity of the liquid propellant in the operating conditions.

The maximum vertical velocity U_m (m/s) of the sloshing liquid at any distance z (m), positive downward, from the free surface of the quiescent liquid to any arbitrary depth in a circular cylindrical tank is given by the following equation of [9]:

$$U_m = \frac{1.841g}{\omega_1 R} \eta \frac{\sinh[1.841(\frac{h-z}{R})]}{\cosh[1.841(\frac{h}{R})]}$$

where g (m/s^2) is the vertical acceleration of the tank, R (m) is the radius of the cross section of the tank, h (m) is the height of the free surface of the quiescent liquid, η (m) is the amplitude of oscillation measured at the tank wall from the free surface of the quiescent liquid, and ω_1 (rad/s) is the first natural angular frequency of lateral slosh, whose value has been found above to be

$$\omega_1 = \left[1.841 \frac{g}{R} \tanh\left(1.841 \frac{h}{R}\right) \right]^{\frac{1}{2}}$$

By using these equation and assuming the height h of the propellant to be equal to or greater than the radius R of the tank, the equation $p = K\rho U_m^2$, which expresses the pressure on the baffle due to the sloshing liquid propellant, can be approximated as follows [9]:

$$p = K\rho\omega_1^2\eta^2 \exp\left(-3.682 \frac{z}{R}\right)$$

After setting again $\eta = g/\omega_1^2$, the maximum pressure on a ring baffle placed at the depth z from the free surface can be expressed as follows

$$p = \frac{K\rho g R}{1.841} \exp\left(-3.682 \frac{z}{R}\right)$$

The pressure acting on a ring baffle can be reduced by perforating the ring baffle with small holes. This is because the oscillating flow through the holes is an additional source of damping. However, this increased damping is partially offset by a decrease in the effective area of a perforated baffle [8].

A ring baffle, which is just above the free surface of a quiescent liquid propellant, is periodically subject to the slapping action of the sloshing wave. In this case, the pressure acting on the baffle is expressed by the following equation of [9]:

$$p = 2\rho U_m^2$$

where U_m is the velocity of the liquid propellant at impact with the baffle.

By setting $U_m = \omega_1 \eta_1$ and substituting in the preceding equation, there results

$$p = 2\rho\omega_1^2\eta_1^2$$

By setting again $\eta_1 = g/\omega_1^2$ and assuming $h \geq R$, the maximum pressure on the baffle is [9]:

$$p_{\max} = \frac{2\rho g R}{1.841}$$

The methods discussed above have shown how to compute sloshing loads on baffles of the ring type.

When baffles of other types, such as anti-vortex baffles and truss-type baffles, are used, then it is still possible to use the preceding equation $p = K\rho U_m^2$, which expresses the maximum pressure on the baffle, but it is also necessary to determine the value of K and the value of U_m which apply to the case of interest. Keulegan and Carpenter [15] gives values of K for oscillatory flow around cylinders and plates.

Such values depend on the baffle shape and on the non-dimensional parameter $U_m T/(2w)$, where T is the natural period of oscillation. This parameter, in turn, requires the evaluation of U_m . For this purpose, in case of a liquid propellant sloshing laterally in a circular cylindrical tank at its first angular frequency ω_1 , the radial component u_r and the tangential component u_θ of the velocity vector \mathbf{u} of the liquid propellant can be computed by using the following equations, due to Bauer [17], taken from [9]:

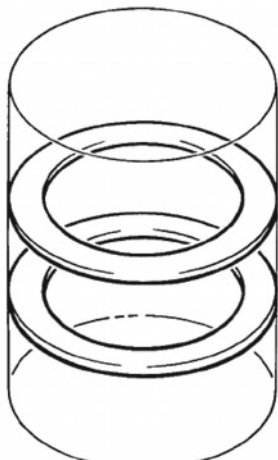
$$u_r = \frac{g\eta}{\omega_1} \left[\frac{1.841 J_0(1.841r/R)}{R J_1(1.841)} - \frac{J_1(1.841r/R)}{r J_1(1.841)} \right] (\cos \theta) \\ \times \frac{\cosh[1.841(h-z)/R]}{\cosh(1.841h/R)} \cos(\omega_1 t)$$

$$u_\theta = -\frac{g\eta}{\omega_1} \frac{J_1(1.841r/R)}{r J_1(1.841)} (\sin \theta) \frac{\cosh[1.841(h-z)/R]}{\cosh(1.841h/R)} \cos(\omega_1 t)$$

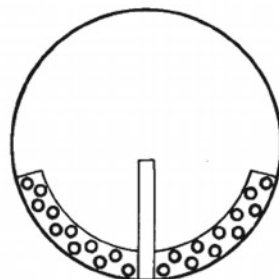
from which the resultant velocity of the liquid propellant can be calculated.

6.6 Slosh-Suppression Devices for Tanks

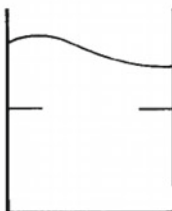
Section 6.5 has shown how to compute structural loads induced by the periodic motion (sloshing) of liquid propellants in their tanks. The present section describes some devices used for slosh damping. Those of them which have been most frequently used for this purpose are shown in the following figure, due to the courtesy of NASA [7].



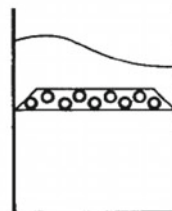
Flat-ring baffles in cylindrical tank



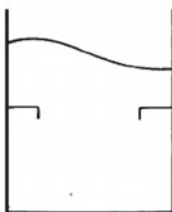
Cruciform baffle (perforated) in spherical tank



Flat ring



Truncated cone (perforated)



Flat ring with lip



Flexible baffle

Such devices are used not only to reduce sloshing loads, but also to protect tank bulkheads from impact loads caused by non-periodic motion of liquid propellants. As has been shown in Sect. 6.5, the sloshing mass m_s of a liquid propellant, that is, the part of the total mass which moves during sloshing, can also be reduced by using tanks of appropriate shapes or divided into compartments. According to [7], slosh-suppression devices include rigid-ring baffles, cruciform baffles, deflectors, flexible flat-ring baffles, floating cans, and positive-expulsion bags or diaphragms. A brief description of them is given below.

The most frequently used manner of providing slosh damping in a tank is to install baffles in the tank. Such baffles are placed in points which are slightly below the level of the free surface of the liquid propellant at the times in which damping is required. The baffles can be installed either for the sole purpose of providing slosh damping in a tank, or also for structural reasons, to be used as wall-stiffener rings. In the latter case, their size is increased to provide the required damping.

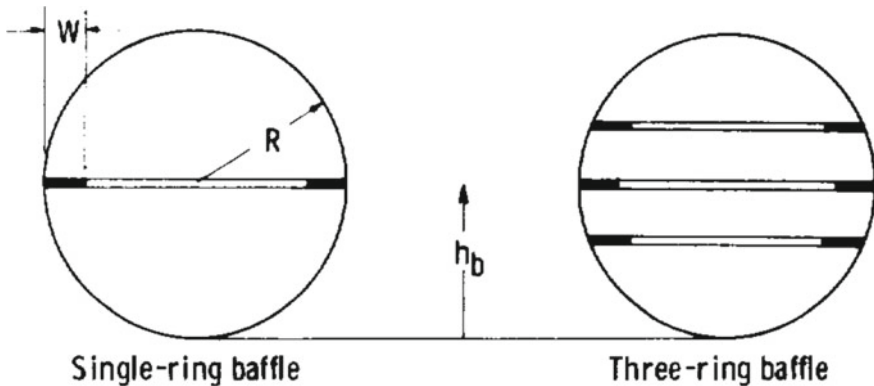
Rigid-ring baffles are widely used as slosh-suppression devices. As has been shown in Sect. 6.5, the damping ratio ζ provided by rigid-ring baffles in circular cylindrical tanks is expressed by the Miles formula [16] as follows

$$\zeta = 2.83 \left[\frac{w}{R} \left(2 - \frac{w}{R} \right) \right]^{\frac{3}{2}} \left(\frac{\eta}{R} \right)^{\frac{1}{2}} \exp \left(-4.6 \frac{d}{R} \right)$$

which holds when the depth h of the liquid propellant is considerably greater than the cross-sectional radius R of the tank ($h/R > 2$). In the preceding formula, w is the width of the rigid-ring baffles, η is the amplitude of oscillation measured at the tank wall from the free surface of the quiescent liquid, and d is the depth of the baffle below the free surface of the quiescent liquid. This formula is based on the assumption that the baffle is completely submerged during a slosh cycle.

A series of flat-ring baffles is the most frequently used slosh-suppression device in circular cylindrical tanks. As has been shown in Sect. 6.5, damping ratios for a series of flat-ring baffles can be calculated by using the principle of linear superposition, when the spacing s between the baffles is greater than the width w of each baffle [10].

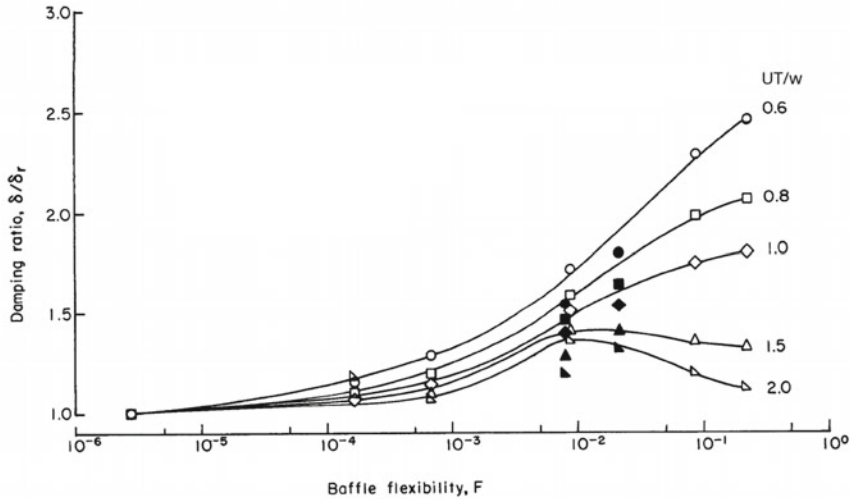
Damping provided by baffles in tanks of other shapes than circular cylinders has also been studied by several authors. An account of such studies is given in [6, 8] for spherical, oblate and prolate spheroidal, and toroidal tanks. An experimental investigation was conducted by Sumner [18] to determine the slosh-suppression effectiveness of rigid and flexible flat-plate annular-ring baffles in spherical tanks subject to oscillations in the horizontal plane. The baffles caused a variation in the fundamental frequency of oscillation, and were found most effective in reducing the slosh forces and increasing the damping when the free surface of the quiescent liquid was slightly above the baffle, so that the latter remained submerged during the oscillatory cycle of the liquid. The optimum baffle width to tank radius ratio was found to be $w/R = 0.125$ for the spherical tanks considered. A side view of the baffles in the spherical tanks is shown in the following figure, due to the courtesy of NASA [18].



Stephens et al. [19] conducted an experimental investigation of the damping of liquid oscillations in an oblate spheroidal tank. The decay of the fundamental mode was studied for a range of liquid depths in tanks with and without baffles. The results indicate that the addition of ring baffles to the tank results in an increase in the available effective damping when the baffle plane is in a region near the equilibrium liquid surface, and that cruciform baffles are effective in the damping of the fundamental mode in the near-empty tank [19].

As has been anticipated in Sect. 6.5, flexible-ring baffles can offer substantial advantages, upon certain conditions, over rigid-ring baffles. Such advantages concern higher damping effectiveness and lower mass. An experimental study conducted by Stephens and Scholl [20] for large-scale cylindrical tanks fitted with both flexible and rigid annular ring baffles has shown that slosh damping comparable to that provided by rigid baffles can be obtained by using smaller and less massive flexible baffles. Stephens and Scholl have shown that the characteristics of the sloshing liquid, the flexibility of the baffles, and the damping can be specified by three non-dimensional parameters. These parameters are: (1) the period parameter P , which describes the velocity of the liquid in the vicinity of the baffle; (2) the flexibility parameter F , which defines the deflection of the baffle per unit loading; and (3) the relative damping parameter δ/δ_r , which is the ratio of the damping factor δ provided by the flexible baffle to the damping factor δ_r provided by a rigid baffle of the same width w and under the same flow conditions as those of the flexible baffle.

The results found by Stephens and Scholl are shown graphically in the following figure, adapted from [20].



The three non-dimensional parameters P , F , and δ/δ_r are defined as follows:

$$P = \frac{UT}{w}$$

where U (m/s) is the maximum velocity of the liquid propellant at the baffle location, T (s) is the natural period of oscillation, and w (m) is the width of the baffle;

$$F = w_1^3 \left(\frac{1 - \nu^2}{E t^3} \right) \frac{\rho w^2}{T^2} f\left(\frac{w_1}{R}\right)$$

where w_1 (m) is the width of the flexible portion of the baffle, w (m) is the width of the baffle, ν is the Poisson ratio of the baffle material, E (N/m²) is the Young modulus of the baffle material, t (m) is the thickness of the baffle, ρ (kg/m³) the density of the liquid propellant, $f(w_1/R)$ is a radius correction factor, whose value is close to unity for most applications, and R (m) is the radius of the cylindrical tank;

$$\frac{\delta_r}{2\pi} = 2.83 \left[\frac{w}{R} \left(2 - \frac{w}{R} \right) \right]^{\frac{3}{2}} \left(\frac{\eta}{R} \right)^{\frac{1}{2}} \exp\left(-4.6 \frac{d}{R}\right)$$

where η (m) is the amplitude of oscillation measured at the tank wall from the free surface of the quiescent liquid, and d (m) is the depth of the baffle below the free surface of the quiescent liquid.

The maximum vertical velocity U of the liquid propellant at the baffle location, due to the lateral oscillation (antisymmetric mode) impressed to the circular cylindrical tank, is given by the following equation of Sect. 6.5:

$$U = \frac{1.841g}{\omega_1 R} \eta \frac{\sinh[1.841(\frac{h-z}{R})]}{\cosh[1.841(\frac{h}{R})]} = \omega_1 \eta \frac{\sinh[1.841(\frac{h-z}{R})]}{\sinh[1.841(\frac{h}{R})]}$$

where h (m) is the height of the free surface of the quiescent liquid propellant, z (m) is the distance from the free surface of the quiescent liquid to any arbitrary depth (positive downward), and ω_1 (rad/s) is the first natural angular frequency of lateral slosh, whose value has been found in Sect. 6.5 to be

$$\omega_1 = \left[1.841 \frac{g}{R} \tanh\left(1.841 \frac{h}{R}\right) \right]^{\frac{1}{2}}$$

By substituting the preceding expression of U into $P = UT/w$ and remembering that $T = 2\pi/\omega_1$, the period parameter P can be expressed as follows

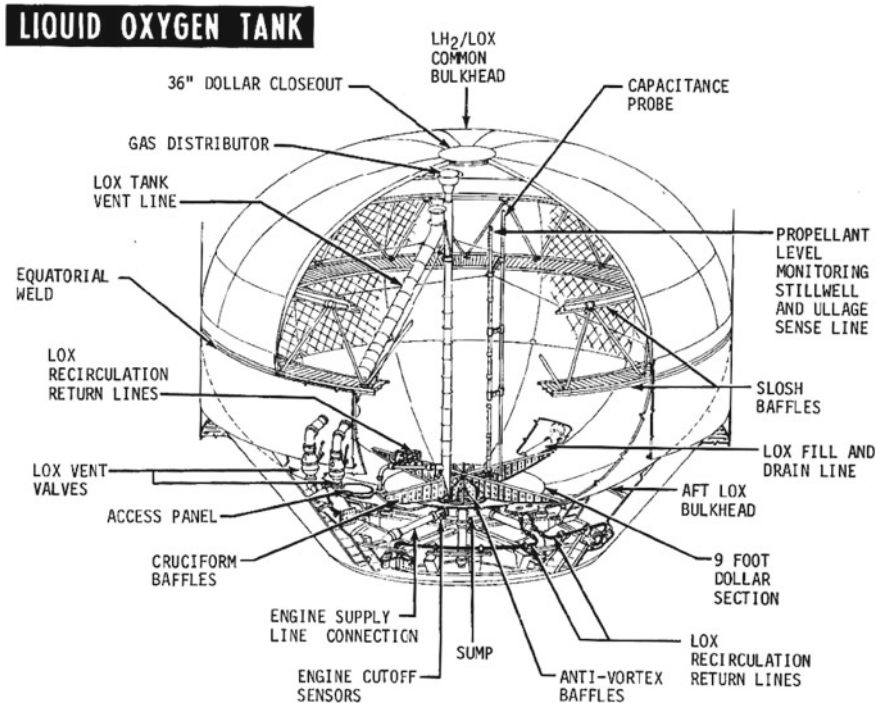
$$P = \frac{2\pi \eta}{w} \frac{\sinh[1.841(\frac{h-z}{R})]}{\sinh[1.841(\frac{h}{R})]}$$

As shown in the preceding figure, Stephens and Scholl [20] considered values of P ranging from 0.6 to 2, the latter value being the highest attainable and having the appearance of a relatively severe slosh.

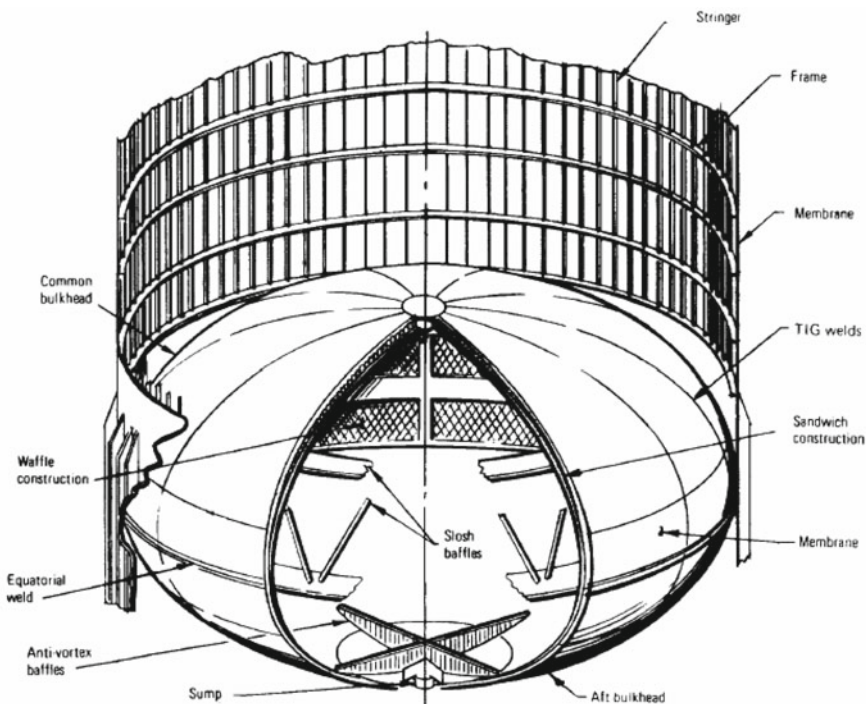
The results found by Stephens and Scholl [20] in their experimental investigation on flexible and rigid baffles can be summarised as follows:

- the damping factor δ provided by a flexible baffle is comparable to or greater than the damping factor δ_r provided by a rigid baffle in the same conditions of oscillatory flow;
- the efficiency of damping per unit of weight of a flexible baffle may greatly exceed that of a rigid baffle;
- as a baffle becomes more flexible (that is, for increasing values of the flexibility parameter F), the relative damping parameter δ/δ_r also increases and reaches a maximum value, which depends on the value of the period parameter P ; and
- as the flexibility parameter increases further, the relative damping parameter δ/δ_r decreases rapidly to the point at which the baffle opposes no resistance to the flow.

Cruciform baffles are located in tanks in the same manner as stringers. This arrangement makes the damping provided by these baffles in cylindrical tanks independent of the liquid height. Their behaviour has also been investigated in spherical or spheroidal tanks, where of course their damping depends on the liquid height. Cruciform baffles provide a smaller amount of damping than is the case with ring baffles, except when a tank is nearly empty, in which case cruciform baffles suppress rotatory motions and formation of vortices near the tank-drain outlet [7]. An example is given in the following figure, due to the courtesy of NASA [21], which illustrates the liquid-oxygen tank of the S-II stage of the Saturn V launch vehicle.



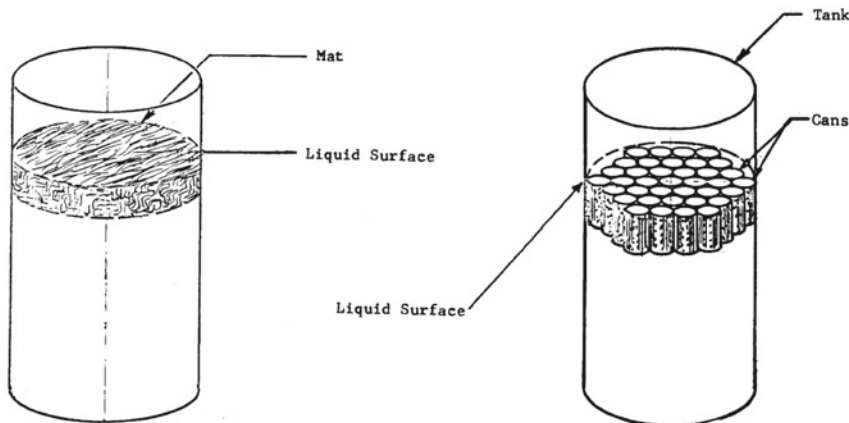
A cutaway view of the same tank is shown in the following figure, due to the courtesy of NASA [22].



The tank illustrated in the two preceding figures has ring baffles attached to the skin stiffeners, which stabilise the tank wall and reduce sloshing. This tank has also a cruciform baffle and anti-vortex baffles (the latter just above the sump) at its base.

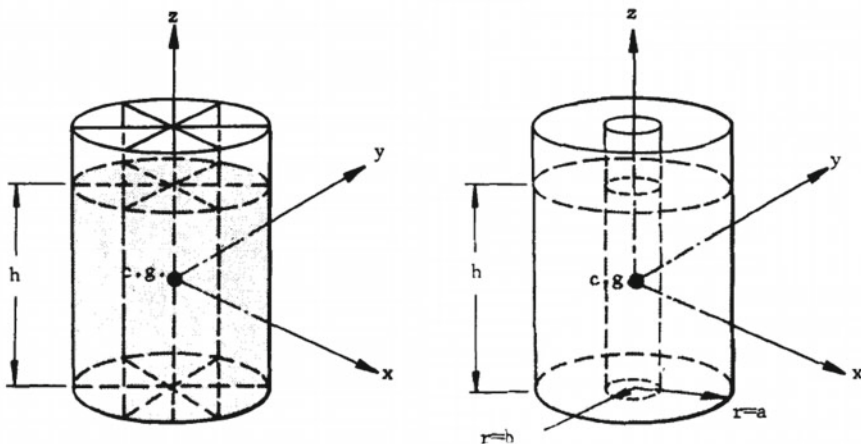
Deflectors have been placed above the surface of a liquid propellant in order to suppress the large-amplitude liquid motions which may be excited by an engine cut-off or by the pulsing of attitude-control engines during orbital coast. Deflectors are shaped as wide, inverted conical-ring baffles. They prevent liquid propellant from reaching the tank vent, and facilitate propellant drainage. They also contribute, when submerged, to damp oscillatory motions [7].

Rigid lids, floating cans or porous mats have also been studied for propellant tanks. Such devices always act at the free surface of a liquid propellant. Rigid lids which cover part of the free surface of a liquid propellant and float up or down as the level changes in the tank have been found effective when they cover 85% or more of the tank diameter [8]. Floating porous mats have also been evaluated for the purpose of increasing viscous effects at the surface. Floating mats (left) and cans (right) are shown in the following figure, due to the courtesy of NASA [23].



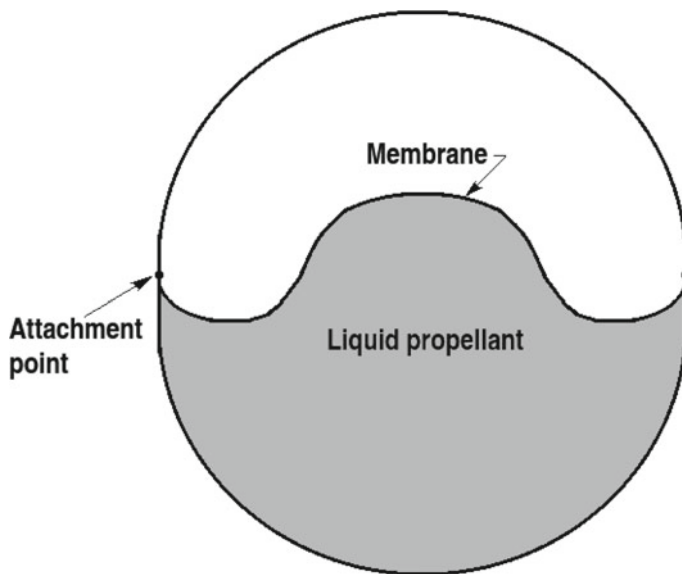
However, lids and covers may “hang up” on internal hardware of a tank, and therefore such devices have not been proved practical for spacecraft [8].

Dividing a tank into radial or concentric compartments has also been used as a means to suppress sloshing motions for the lower frequencies of oscillations. This is shown in the following figure, due to the courtesy of NASA [23].



However, this solution has the drawbacks mentioned in Sect. 6.5.

Positive-expulsion bags and diaphragms of elastomeric materials are used in tanks when it is necessary to transfer liquid propellants in low-gravity conditions or when a large flow rate is desired in rocket engines fed without pumps, as has been shown in Chap. 3, Sect. 3.5. These devices provide an impermeable barrier between the liquid and the gas contained in a tank. For this purpose, a membrane of elastomeric material or a flexible metallic diaphragm is attached around the wall of a tank at some section, as shown in the following figure, re-drawn from [8].



The size of the membrane must be large enough to contain the initial quantity of liquid, and to expel nearly all the liquid which remains near the bottom of the tank.

Stofan and Sumner [24] conducted an experimental investigation to evaluate the slosh-damping effectiveness of positive-expulsion bags and diaphragms in spherical tanks ranging from 0.2413 to 0.8128 m in diameter. The positive-expulsion devices tested were made of butyl rubber and ranged from 0.254 to 1.016 mm in thickness. The excitation was impressed to the tank in the horizontal plane. The maximum slosh forces occurring at the first natural frequency increased with an increase in excitation amplitude and decreased as the thickness of the diaphragm material increased. The damping factor δ was found to be essentially independent of the excitation amplitude and increased with an increase in the thickness of the diaphragm material. The second natural mode force peak and the fluid swirl at the natural mode frequencies, which were observed for the unrestricted liquid sloshing, were completely suppressed [23]. This type of slosh-suppression device has prevalently been used for spherical or oblate spheroidal tanks [8].

6.7 Materials, Processes, and Environmental Conditions of Tanks

The properties of the metallic materials to be considered in the evaluation and selection phases of a given programme have been identified by Wagner and Keller [22] as follows:

- strength/weight efficiency under load/temperature conditions or under other critical failure conditions;
- capability of being fabricated into the desired shapes and sizes without loss of their properties;
- compatibility with all anticipated environments;
- fracture toughness and resistance to subcritical flaw growth;
- availability of shapes and sizes within required schedules; and
- costs of materials and material processing and fabrication.

These properties are discussed below. The principal strength properties to be considered in the design of tanks for rocket vehicles are ultimate tensile strength (F_{tu}), which governs ultimate burst pressure under ductile failure conditions; tensile yield strength (F_{ty}), to comply with the requirement of no yielding at limit load conditions or during proof testing; compressive yield strength (F_{cy}), for compression-critical structures; and the elastic properties (E , G , and ν) of the materials. Further properties are ultimate shear strength (F_{su}), ultimate bearing strength (F_{bru}), and bearing yield strength (F_{bry}), which apply to design details, such as mechanical attachments, and are not usually important factors in the selection of materials. High-frequency, low-stress fatigue data are sometimes required to evaluate the effects of structural vibrations. Low-frequency, high-stress fatigue data are often used to evaluate the effects of multiple pressurisation cycles.

Wagner and Keller [22] have also identified some variable parameters which can affect the mechanical properties of the materials used for tanks. These parameters are temperature, thermal exposure, duration of loading, presence of biaxial and triaxial loads, rate of loading, and unusual environmental conditions such as corrosion and radiation.

The design properties of the materials are to be evaluated for the base metal, for the welds, and sometimes also for the weld zones exposed to heat. It is also necessary to consider the loading direction with respect to the grain orientation of the base metal, and the properties of the materials along and across the direction of the weld. The effects induced on the properties of the materials by processing, forming, and heat treatments are also to be considered.

The metallic materials used for structures of aerospace vehicles form the subject of the military standards MIL-HDBK-5J [25]. The welds form the subject of [26].

A decrease in temperature tends to increase the strength of the material, but often decreases their ductility and toughness. In case of tanks containing cryogenic propellants, an increase in strength at low temperature is desirable, because it results in a mass reduction; however, it is also necessary in this case to ascertain whether the fracture toughness of the material of which the tank is made is adequate to the operational and proof-testing conditions.

Likewise, an increase in temperature tends to reduce the strength of the materials. This fact is to be considered for materials which are particularly sensitive to temperature, as is the case with some titanium alloys. Exposure of such materials to high temperatures for long periods of time can cause a permanent reduction in strength.

Tanks for fluid propellants are required to withstand a high number (sometimes of the order of one hundred) of pressurisation cycles. Such cycles occur in testing and of course in service. Tank failures due to fatigue can occur as a result of these repeated cycles.

Pressurisation stresses in tanks can also cause creep, which is a time-dependent deformation of a material subject to prolonged stresses. Creep usually occurs at high temperatures, but can also occur at moderately high temperatures for some titanium or aluminium alloys.

The multi-axial loading of metals can have significant effects on their mechanical properties. The bi-axial tensile stresses acting in pressurised tanks may in some cases improve, in other cases leave unchanged, and in other cases deteriorate the performance of the materials. Materials which are ductile, homogeneous, and isotropic may show an increase in tensile strength, the amount of this increase depending on the bi-axial stress ratio. The maximum effects usually occurs at a bi-axial tensile-stress ratio of 2:1.

As shown by experience, the magnitude of this effect is often of the order of that predicted by the von Mises criterion [27]. According to this criterion, the effective stress for yielding σ_{eff} in a material element subject to multi-axial loading is

$$\sigma_{eff} = \left[\frac{(\sigma_1 - \sigma_2)^2 + (\sigma_2 - \sigma_3)^2 + (\sigma_3 - \sigma_1)^2}{2} \right]^{\frac{1}{2}}$$

where σ_1 , σ_2 , and σ_3 are the principal stresses, that is, the stresses acting along three mutually orthogonal planes of zero shear stresses ($\tau_{12} = \tau_{23} = \tau_{31} = 0$).

Anisotropic materials do not conform to the von Mises criterion. Such is the case, for example, with titanium processed in such a way as to obtain preferred orientations of the individual crystals or grains. For such materials, other yield criteria can be used, for example, the Hill 1948 criterion [28]. Further information on the Hill 1948 and other criteria for anisotropic materials can be found in [29]. In addition, Wagner and Keller [22] point out that some homogeneous and isotropic alloys do not appear to behave in full accordance with the von Mises criterion.

The strength of some materials may decrease when they are subject to biaxial tension. This effect may occur with low-elongation materials in a biaxial tensile-stress field. This state of stress is typical of spherical tanks, and limits the ductility of the material to the plane which includes its thickness. In other planes, such materials in this state of stress tend to behave in a brittle manner [22].

The capability possessed by a material of being fabricated into the desired shapes and sizes without loss of its properties is one of the principal qualities considered in the design of tanks for aerospace vehicles. This is because not all high-strength materials can also be manufactured economically to form tanks having the desired characteristics. Some essential fabrication requirements, indicated by Wagner and Keller [22], are indicated below:

- availability in suitable forms, sizes, and levels of quality within the necessary schedules;
- capability of being formed, and machined to the required configurations, on the available equipment, and at the appropriate thicknesses and strength level;
- capability of being welded to suit the common methods of assembly; and
- capability of meeting thermal processing requirements.

Some guidelines to be followed by a designer to choose a method of fabrication for a tank have been suggested by Whitfield and Keller [30]. A brief account is given below.

The method of fabrication chosen for a tank of a rocket engine should be reliable, rapid, and cost-effective for the particular case and needs of the programme to which it applies. A fabrication process should be selected so as to afford the best compromise between fabrication schedule and cost, without reducing reliability below a desired level. An engineering study should include trade-off evaluations of fabrication and welding processes, reliability of various processes based on past experience, schedule effects of material processing, and cost connected with fabrication, tools, and facilities.

A comparison of methods of fabrication used for pressure-vessel components is shown in the following table, taken from [22].

Component	Fabrication method	Advantages	Disadvantages
End domes (complete heads)	Drawing: Hydropress (trapped rubber forming)	Moderate production rate Moderate tooling costs Larger sizes than hydroform	Part size and thickness limited Temperature limited Poor control of thickness
	Hydroform (hydraulic fluid forming)	High production rate Better thickness control than hydropress	Limited to small sizes Temperature limited Relatively high tooling costs
	High-Energy-Rate Forming: Explosive	Very large potential sizes (depending on available facility) Good reproducibility Low to moderate tooling costs	Limited to cold forming Low production rate Limited availability of facilities
	Electrical (including spark discharge and magneto-dynamics)	High production rate Good reproducibility	Limited to small sizes Requires specialized equipment and tooling
	Spinning: Shear	Permits integral bosses and skirts Can handle thick material Good thickness control Spinning can be performed hot	Size limited Limited availability of equipment
	Conventional (manual or power)	Moderately large sizes Low tooling costs	Poor thickness control Permits no integral details as formed Temperature limited Thickness limited Low production rate Requires ductile material
	Forging	Not limited to materials with cold- or warm-forming ability Permits complex configurations Permits integral attachments	Size limited High costs Requires considerable machining Low production rate
	Segmenting (formed and welded segments)	Large size capability (starting with smaller individual parts) Reduces difficulty and cost of forming	High total costs – tooling, welding, and inspection Potential for reduced reliability due to increased welding Poor dimensional control Very low production rate
Cylinders	Rolling and Welding	Accommodates large sizes Low cost, simple process	Potential for reduced reliability due to longitudinal weld Permits no integral reinforcements as fabricated
	Shear spinning	Eliminates longitudinal welds Permits integral reinforcements Provides good thickness control Forming can be performed hot	High cost for low production quantity Limited equipment availability Some limitations on size

The size and the shape of a component and the aptitude of its material to be formed and machined are important aspects in choosing a material, a method of fabrication, and a heat treatment. For example, the large size of a component limits the methods of fabrication and the heat treatments which can be chosen.

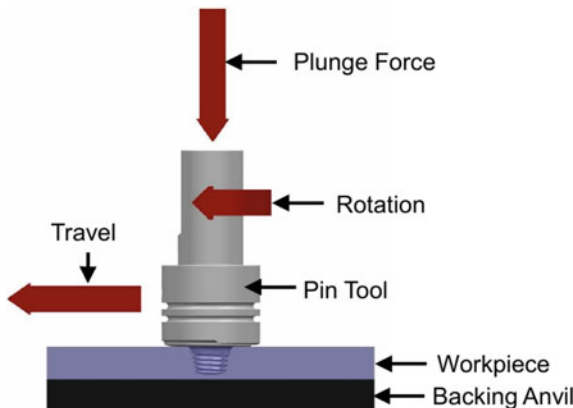
Specific information on the matter can be found in [31] (titanium and its alloys), [32] (stainless steel), and [33] (precipitation-hardening stainless steel).

The welding properties of a metal are of paramount importance in the choice of a metal for a tank. Desirable properties for a weldable metal are its capability of being fused without the formation of unwanted phases or constituents in or near the fusion zone, its ductility in the range from the melting temperature to room temperature (in order to resist cracking), strength, and fracture-resistance.

Generally speaking, according to NASA [34], the welding processes used for space flight hardware are:

- Gas Metal Arc Welding (GMAW also known as MIG Welding), which is used for quickly fusing mild steel, stainless steel, and aluminium of various thicknesses;
- Tungsten Inert Gas (TIG) Welding, which is used for carrying out work of high quality when a high standard of finish is needed without excessive clean-up by sanding or grinding;
- Shielded Metal Arc Welding (SMAW), which is used for manufacturing, construction, and repair, and is well suited for heavy metal size 4 mm and upward;
- Gas or Oxyacetylene Welding, which is commonly used for brazing soft metals such as copper and bronze, and for welding delicate parts of aluminium; and
- Plasma Cutting, which is used to cut steel and other metals of different thicknesses for metal construction and maintenance.

A further process, used specifically for tanks of liquid-propellant rocket engines, is Friction Stir Welding (FSW), whose working principle is shown in the following figure, due to the courtesy of NASA [35].



This welding process uses frictional heating combined with forging pressure to produce high-strength bonds virtually free of defects. Friction Stir Welding transforms the metals from a solid state into a plastic-like state, and then mechanically stirs the materials together under pressure to form a welded joint. This process was invented and patented by The Welding Institute (a British research and technology organisation), and has been applied to aerospace, shipbuilding, aircraft, and automotive industries. In particular, it has been used primarily for square butt welds in aluminium alloys of the 2XXX series.

Carter [35] has given some examples of application of Friction Stir Welding to the aerospace industry. They are

- Space Shuttle external tank;
- United Launch Alliance Delta II, Delta IV, and Atlas V;
- Space X Falcon and Falcon 9;
- Japan—JAXA H-IIB; and

- NASA—Space Launch System core stage.

One of the principal benefits of this technology is that it allows welds to be made on aluminium alloys which cannot be readily welded by fusion arc. An example of such alloys is the Al–Li 2195 alloy, which has been used for the Super Light Weight Tank of the Space Shuttle. A further benefit of Friction Stir Welding is that it has fewer elements than other welding techniques to control. In Friction Stir Welding there are only three process variables to control, namely, rotation speed, travel speed, and pressure, all of which are easily controlled. The increase in joint strength combined with the reduction in process variability resulted in an increased margin of safety and in a high degree of reliability for the external tank of the Space Shuttle.

In Friction Stir Welding, a dowel rotates at an angular velocity between 19 and 31 rad/s [36], depending on the thickness of the material. The pin tip of the dowel is forced into the material under a pressure going from 3.4×10^7 to 6.9×10^7 N/m² [36]. The pin continues to rotate and moves forward at a speed going from 1.48 to 2.12 mm/s [36]. As the pin rotates, friction heats the surrounding material and rapidly produces a softened plasticised area under the pin. Plasticity starts to occur around 700 K for most materials [37]. The temperature due to friction is carefully controlled not to exceed the point of turning the material to a liquid, which occurs at about 922 K in most cases [37]. As the pin travels forward, the material behind the pin is forged under pressure from the dowel and consolidates to form a bond at a molecular level.

Unlike fusion welding, no actual melting occurs in this process, and the weld is left in the same fine-grained condition as the original metal. For the external tank of the Space Shuttle, a through-spindle retractable pin was developed, which can retract or expand its pin tip within the material. This allows for changes of thickness such as on the longitudinal barrel of the tank [36]. The following figure, due to the courtesy of NASA [37], shows retractable pin tools used for the Friction Stir Welding process.



Retractable pin tools were developed by NASA engineers because the original Friction Stir Welding left a opening, known as a keyhole, which was a point of weakness in the weld. The retractable pin tool retracts automatically when the weld

is complete and prevents a keyhole. This improvement makes the weld stronger and eliminates the need to fill the keyhole during manufacturing.

Apart from the choice of a particular welding technique, further processing, such as pre-heat or post-heat or both of them, is generally required for high-carbon, low-alloy steel welds when thickness is higher than 2.5 mm. However, pre-heat and post-heat may be required for welds of thickness equal to or less than 2.5 mm, in order to avoid weld cracking, depending on the material, on the welding process, and on the restraint characteristics of the particular weld. When pre-heat or post-heat is performed by using a torch, then oxidation can reduce the quality of the weld. To avoid this, automatic electric heating is desirable in many cases, because electric heaters controlled by rheostats provide appropriate temperatures and uniform heating. Backup tools made of copper, stainless steel, or refractory-covered metals are used to achieve either high, or low, or negligible heat dissipation, as the case requires, to control the final dimensions and properties of the weld [30]. A reduced strength of a metal in or near the welding zone can be compensated for by increasing its thickness at the joints. Since ductility decreases in the welding zone, then welds are generally located away from high-stress zones. Such zones are those in which a parallel or a meridian of a surface of revolution changes abruptly its radius of curvature.

Residual stresses can still be present in welded zones, unless appropriate steps are taken. For this purpose, such processes as pressure welding and forge welding can reduce residual stresses to minimum values. Residual stresses should be relieved from materials used for tanks to avoid cracking, warping, and reduction of resistance to fatigue and fracture. To this end, such thermal processes as ageing for titanium and heat treatment for steel are applied. For example, the 18%-nickel maraging steel (so called because its strengthening mechanism consists in transforming the alloy to martensite with subsequent age hardening) requires ageing after welding to acquire maximum mechanical properties in welds [22]. Annealing is sometimes required before or during forming of tank components. However, many of the materials commonly used for tanks do not require heat treatments after welding, either to restore mechanical properties or to relieve residual stresses.

The materials which are chosen for tanks of liquid-propellant rocket engines must be compatible with the propellants contained. The following table, due to the courtesy of NASA [22], shows causes and effects of reactions of metals with fluids.

Metal/Fluid reaction	Possible consequences to system	Major sources of metal/fluid reaction			
		A	B	C	D
Metal corrosion (including general corrosion, pitting, intergranular corrosion, and chemical attack)	(1) Metal weakening through loss in cross-sectional area and introduction of stress raisers (2) System contamination with corrosion products	X	X	X	X
Catalytic decomposition of propellants	Loss of efficiency or contamination of system or both			X	
Hydrogen embrittlement of steel	Brittle fracture at low stresses, especially under long-duration loading	X			
Contamination of titanium	Brittle fracture at low stresses	X	X	X	X
Stress corrosion	Metal crack growth or fracture at reduced stress levels	X	X	X	X
Galvanic corrosion	(1) Rapid deterioration of material (2) Stress-corrosion failure	X	X	X	X
Hydrogen-environment embrittlement of metals	Embrittled behavior of metal while exposed to hydrogen gas			X	
Ignition of materials	Catastrophic combustion			X	

Notes:

A = manufacturing fluids and processes

B = proof and system testing

C = service fluid containment

D = atmospheric exposure

The metallic materials used for tanks should be considered alone or in combination with suitable types of protective finish. Such materials should also be resistant to the effects of exposure to all possible types of external environment.

It is also necessary to prevent the deterioration or the contamination of metals used for tanks during their processing, manufacturing, inspection, test, transportation, and storage [22]. For this purpose, they must be protected from all fluids or processes which might have deleterious effects, as shown in the preceding table.

In particular, many high-strength alloys may be attacked or contaminated by fluids and treatments commonly used in the phases of manufacturing and process. This is because some fluids or treatments have given rise to undesirable chemical reactions, and must therefore be carefully checked before being used.

Of the alloys commonly used for rocket tanks, those based on titanium have been found to be the most susceptible to contamination. Examples of contamination of such alloys in the manufacturing phase are

- hydrogen contamination at room temperature or at high temperatures;
- oxygen and nitrogen contamination at high temperatures; and
- halogen contamination, resulting from halide-containing materials, before heat treatment or welding.

Titanium contaminated by hydrogen or oxygen or nitrogen becomes brittle. This undesirable effect, when due to heat treatments in air, can sometimes be removed by machining. However, when a titanium alloy is welded in air, then the entire weld becomes brittle.

Steel can also become brittle when contaminated by hydrogen. This happens typically in electrolytic processes. Steel becomes increasingly susceptible to contamination due to hydrogen as its strength increases.

Other type of alloys used for rocket tanks (such as aluminium alloys and alloys based on nickel and cobalt) may, or may not, become brittle in various degrees when contaminated by hydrogen, depending on temperature [22].

Fluids contained in rocket tanks can cause chemical reactions which results in either corrosion or reduced strength of the materials of which the tanks are made. This holds with both testing fluids and propellants. Fluids commonly used for testing purposes are not dangerous by their nature, but may become dangerous as a result of contamination. Examples are tanks made of titanium alloys pressurised with methanol, or made of steel pressurised with water [22].

Some propellants are corrosive or chemically reactive. The containment of these propellants in tanks made of materials sensitive to chemical reactions is possible only when a film or a layer of stable oxide protects the covered material from further reactions. In order to test the susceptibility of a given material to possible chemical attack due to a given propellant, it is necessary to conduct tests in the same conditions of pressure, temperature, and duration of exposure as those which will be experienced by the material in service.

The decomposition of some propellants may be accelerated by the catalysing action exerted by some metals. Examples of propellants subject to catalytic decomposition are hydrogen peroxide and hydrazine.

A tank whose external surface is exposed to atmospheric agents during part of the life of a space vehicle is subject to moisture, salts, and chemical substances of industrial origin. This part includes the times of manufacturing, storage, testing, transportation, and operation. Some metals used for tanks are resistant to atmospheric corrosion, because of the formation of a thin layer of protective oxide. Such is the case with titanium alloys, stainless steels and super-alloys having high percentages of nickel and chromium, and some aluminium alloys. Other alloys and steels must be provided with a protective finish.

The reactions which occur in conditions of service between the tank materials and the fluids contained can be classified as follows

- stress-corrosion cracking;
- galvanic corrosion;
- loss of ductility due to hydrogen; and
- ignition.

A brief description is given below for each type of reaction.

According to the definition given in [38], stress-corrosion cracking is a cracking process caused by the conjoint action of stress and a corrodent. Stress-corrosion cracking is one of the principal causes of failure of high-stressed tanks. Corrosion can be due to either the fluids contained in the tanks or the environments to which the tanks are exposed. The most common of such environments is atmospheric air, which contains moisture, salts, and other chemical substances due to industrial processes. The effects of stress-corrosion on a given material depend on the stress sustained by the material, the degree of corrosion of the environment, and the time of exposure of the material to the environment.

Means commonly used to avoid stress-corrosion cracking in tanks are

- choice of materials resisting to corrosive environments or protection of susceptible materials from corrosive environments;
- reduction of tensile stresses in materials exposed to corrosive environments; and
- reduction of the times of exposure.

The matter of corrosion and protection of metals from corrosion forms the subject of the military standards MIL-HDBK-729 [39]. In particular, Table XIV on p. 127 of [39] indicates the chemical composition of some titanium alloys used for tanks, and the related corrosive substances, for which stress-corrosion cracking has been observed.

In particular, aluminium alloys of the 2XXX and 7XXX series are susceptible to stress-corrosion cracking in atmospheric environments. Titanium alloys are normally resistant to atmospheric environments, but are susceptible to salt and other sources of chlorine which remain in contact with the metals at temperatures above about 561 K. Some titanium alloys have also been found to be susceptible to sea water at room temperatures [22].

A comparison of the resistance of various alloys to stress-corrosion cracking in atmosphere and in other environments is given in Table VII on pp. 35 and 36 of [22].

Galvanic corrosion, so called after the Italian scientist Luigi Galvani, is an electrochemical phenomenon which occurs either on a macro-scale or on a micro-scale.

On a macro-scale, it is the increased corrosion (deterioration) of the more active metal (anode) of a couple of dissimilar metals in an electrolytic solution or medium and the decreased corrosion of the less active metal (cathode) as compared to the corrosion of the individual metals, when not connected, in the same electrolytic environment. By electrolytic solution, we mean a solution capable of conducting an electric current. An example is common sea water.

The dissimilarity which provides the driving force to galvanic corrosion is the difference in the electrode potential of each of the two metals when they are in electrical contact through the electrolyte. Electrode potential is a measure of the tendency of a metal to become more active than another metal when they are immersed in a given electrolyte.

A galvanic series is a list of metals and alloys based on their order and tendency to corrode independently in a particular electrolytic solution or in other environment.

A galvanic series in sea water, due to the courtesy of NASA [40], is given below. This series is arranged in order of increasing activity.

Galvanic Series In Sea Water

Noble (least active)

Platinum

Gold

Graphite

Silver

18-8-3 Stainless steel, type 316 (passive)

18-8 Stainless steel, type 304 (passive)

Titanium

13 percent chromium stainless steel, type 410 (passive)

7Ni-33Cu alloy

75Ni-16Cr-7Fe alloy (passive)

Nickel (passive)

Silver solder

M-Bronze

G-Bronze

70-30 cupro-nickel

Silicon bronze

Copper

Red brass

Aluminium bronze

Admiralty brass

Yellow brass

76Ni-16Cr-7Fe alloy (active)

Nickel (active)

Naval brass

Manganese bronze

Muntz metal

Tin

Lead

18-8-3 Stainless steel, type 316 (active)

18-8 Stainless steel, type 304 (active)

13 percent chromium stainless steel, type 410 (active)

Cast iron

Mild steel

Aluminium 2024

Cadmium

Alclad

Aluminium 6053

Galvanised steel

Zinc

Magnesium alloys

*Magnesium
Anodic (most active)*

When galvanic corrosion occurs on a macro-scale, the anodic and cathodic areas are easily discerned.

On a micro-scale, galvanic corrosion may occur with one metal having dissimilarities (for example, impurity inclusions, grains of different sizes, difference in composition of grains, differences in mechanical stress), abnormal level of pH, and high temperatures [41]. When galvanic corrosion occurs on a micro-scale, the anodic and cathodic areas can only be discerned by metallographic techniques or deduced by inference or observations of the corroded metal [39].

Galvanic corrosion can occur within a tank containing an electrically conductive fluid, or outside a tank exposed to atmospheric moisture. Generally speaking, in liquid-propellant rocket engines, galvanic corrosion of dissimilar metals is of little or no concern, because most propellants either have little electrical conductivity, or do not develop significant electrode potentials in contact with normal structural metals, or both [22]. However, this problem may arise when new or inadequately tested propellants are used either alone or in the presence of contaminants, or when liquids other than propellants (for example, water) are in contact with dissimilar metals.

Metals can be protected from corrosion by providing them with a coating or a treatment. The coating may be a paint, a sealant, a resin coating, or a metallic coating. Several types of coatings, used to protect specific metals, are described at length in [42]. The treatment may be a surface or bulk treatment, a chemical or mechanical treatment, or a combination of these.

Some metals effectively resist corrosion damages because of their ability to form and maintain, when exposed to an aggressive environment, an adherent and impervious film. These metals are said to have become passivated. However, many of the common or structural metals used for tanks are either scarcely efficient or unable in producing such protective films. Consequently, protective coatings or treatments are applied to many common metals to prevent or reduce corrosion [39].

Metals which are in contact with pure hydrogen should be evaluated for susceptibility to loss of ductility in the presence of hydrogen. This phenomenon, also known as hydrogen-assisted fracture, is due to the easy absorption and subsequent diffusion of hydrogen into metals. On a microscopic scale, hydrogen atoms tend to segregate in certain parts of the crystal lattice of a metal, thereby weakening its chemical bonds. Consequently, the walls of a metallic tank containing hydrogen become brittle, which can lead to failure.

The compatibility of metals with hydrogen has been investigated by several authors. Some of them are Cataldo [43], Caskey [44], San Marchi and Somerday [45], and Chandler [46]. A brief account is given below.

Brittleness of metals due to hydrogen occurs principally in ferrous alloys, such as high-strength and martensitic steels. In most cases, the greater the strength of a metal, the more susceptible it is to brittleness caused by hydrogen. Low-strength metals, such as copper, aluminium, and nickel alloys, have low susceptibility to

hydrogen damage. However, in case of these metals having undergone a strain-hardening process, there would be a greater risk of induced brittleness.

In some cases, steels and alloys of low strength can be used to decrease the risk of loss of ductility. However, of course, the metal chosen must withstand the loads applied to it during operation.

In quantitative terms, the following table, adapted from [43], shows the effects induced by gaseous hydrogen, at a pressure of $6.895 \times 10^7 \text{ N/m}^2$, in various alloys.

**ARRANGEMENT OF MATERIALS IN ORDER OF PERCENT
REDUCTION OF NOTCH STRENGTH IN $6.895 \times 10^7 \text{ N/m}^2$ HYDROGEN**

<u>Alloy</u>	<u>Yield Strength N/m^2</u>	<u>Percent Reduction Notch Strength</u>
18 Ni 250 Maraging	1.710×10^9	88
17-7 PH SS	1.034×10^9	77
H-11	1.682×10^9	76
Rene' 41	1.124×10^9	73
4140	1.234×10^9	60
Inconel 718	1.255×10^9	54
Ti-6Al-4V (STA)	1.076×10^9	45
Nickel 270	0.1568×10^9	30
HY-100	0.6688×10^9	27
Ti-6Al-4V (Annealed)	0.9101×10^9	25
A302	-	22
HY-80	0.5585×10^9	21
304 ELC SS	0.1655×10^9	13
A-517 (T-1)	0.7515×10^9	11
Be-Cu	0.5447×10^9	7
Ti (C.P.)	0.3654×10^9	5
310 SS	-	3
A-286 SS	0.8481×10^9	3
7075-T73	0.3723×10^9	2
6061-T6	0.2275×10^9	0
1100 Al	-	0
OFHC Copper	0.2689×10^9	0
316 SS	0.4413×10^9	0

As has been anticipated above, the reduction in notch strength resulting from the preceding table is inversely related to the ambient strength of the material, but there are exceptions to this rule. For example, the A-286 stainless steel (an age-hardened iron base superalloy) has a high yield strength, but an apparent low susceptibility to hydrogen. The best alloys are aluminium alloys, copper, and stabilised stainless steels [43].

The materials which are used for tanks containing propellants should not be susceptible to ignition or to violent reactions in the presence of the propellants. Consequently, titanium and titanium alloys should not be used for tanks containing oxidisers such as red fuming nitric acid, liquid oxygen, pressurised gaseous oxygen, mixtures of liquid oxygen and liquid fluorine, and other strong oxidisers. It is also necessary to consider the possibility of ignition due to impact, rupture, friction, electricity, heat, or any other source of highly concentrated energy. This holds in particular

with titanium and titanium alloys in contact with oxidisers [22]. For the same reason, copper, lead, zinc, molybdenum, and other alloys which contain free elements should not be used with hydrazine or with other propellants related to hydrazine. As a general rule, it is necessary to ascertain the compatibility of the materials used for tanks with the propellants (in liquid and gaseous phases) to be contained in them, before such materials come in contact with the related propellants.

6.8 Fracture Control of Metals Used for Tanks

Tanks and other pressure vessels containing propellants may have flaws or defects which are either present in the original materials before processing or induced in the materials by processes of fabrication. These defects can reduce the capability of carrying loads and the operational life of the tanks. When such defects are large in comparison with those causing failure, then failure occurs as soon as the tanks are put under pressure for test purposes. When such defects are small, the tanks may withstand several cycles of pressure loading for a considerable number of hours before the size of the defects grows to such an extent as to cause failure.

It is necessary, for reasons of economy, to reduce the possibility of failure of tanks used for a space vehicles during testing. It is mandatory, for reason of both safety of the crew and economy, to reduce the possibility of failure of such tanks during operation.

The present section presents criteria and practices to be used in the design of metallic tanks for propellants, in order to reduce the possibility of failures caused by defects during test, pre-flight, and flight.

For this purpose, it is necessary to consider:

- the initial sizes of the flaws;
- the critical sizes of the flaws (meaning by that, the sizes required to cause fracture at a given level of stress); and
- the subcritical characteristics of the flaws which can cause their growth.

To prevent failures during test, the initial sizes of the flaws must be less than the critical sizes at the level of stress given to the material in test phase. To prevent failures during service, it must be proven that the largest possible size of an initial flaw in a tank cannot grow to the critical size during the required operational life of the tank.

The critical size of a flaw depends on the level of stress, on the toughness of the material to fracture, on the thickness of the wall, and on the location and direction of the flaw. The determination of the initial size of a flaw is limited by the available methods of non-destructive inspection. However, further information may come from the results of a successful proof test. In other words, a proof test in which a tank has not failed provides information on the maximum possible value of the ratio of the initial to critical stress level. This value, in turn, makes it possible to estimate the maximum possible size of the initial flaws.

The growth of subcritical flaws depends on the stress level, the initial size of the flaws, the material, the environment, and the pressure applied as a function of time to a given tank.

Examples of flaws which are rarely detected in metallic tanks or in other pressure vessels are surface flaws and internal flaws. When a tank has an initial flaw whose size exceeds the critical size at the level of stress applied in testing, then the tank fails just in phase of testing. A tank fails in service, when the size of an initial flaw is less than the critical size at the level of stress applied in testing, but this size grows due to the stress applied in service to such an extent as to reach the critical size at the level of stress applied in service. When the size of an initial flaw grows through the thickness of the wall of a tank before reaching the critical size, then leakage occurs.

In the elastic field of stress, the critical sizes of surface and internal flaws depend on the critical value K_{Ic} (Pa m^{1/2}, where 1 Pa = 1 N/m²) of the fracture toughness of the material, and on the level of the stress applied. When the critical sizes of the flaws are small in comparison with the thickness of the wall, then a tank is said to be thick-walled. Otherwise, when the critical sizes of the flaws approach or exceed the thickness of the wall, then a tank is said to be thin-walled.

The critical sizes of surface flaws in uniformly stressed thick-walled tanks can be calculated by using the following equation of [47]:

$$\left(\frac{a}{Q}\right)_{cr} = \frac{1}{1.21\pi} \left(\frac{K_{Ic}}{\sigma}\right)^2$$

The critical sizes of small internal flaws in uniformly stressed thick-walled tanks can be calculated by using the following equation of [47]:

$$\left(\frac{a}{Q}\right)_{cr} = \frac{1}{\pi} \left(\frac{K_{Ic}}{\sigma}\right)^2$$

In the two preceding equations, a (m) is the minor semi-axis of the ellipse of equation

$$\frac{x^2}{c^2} + \frac{y^2}{a^2} = 1$$

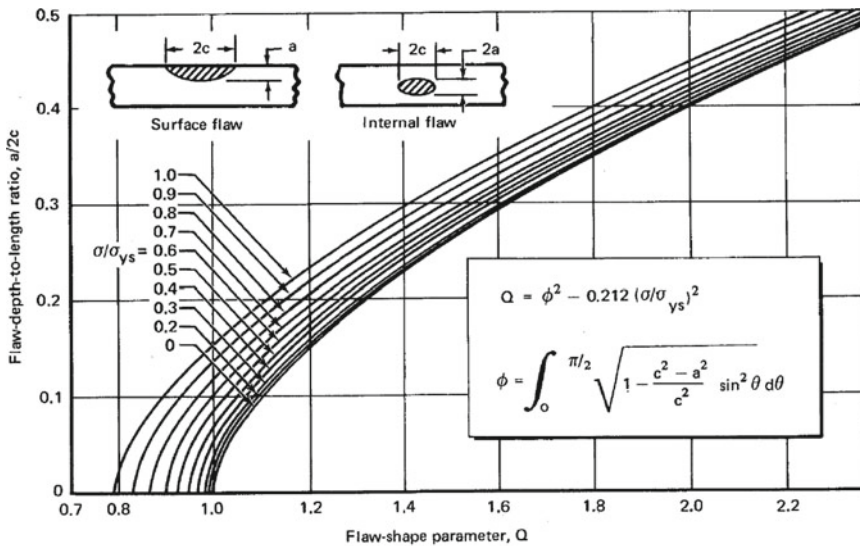
that is, a (m) is the depth of the semi-elliptic surface flaw, $2c$ (m) is the length of the semi-elliptic surface flaw, Q is the flaw-shape parameter defined as follows

$$Q = \phi^2 - 0.212 \left(\frac{\sigma}{\sigma_{ys}}\right)^2$$

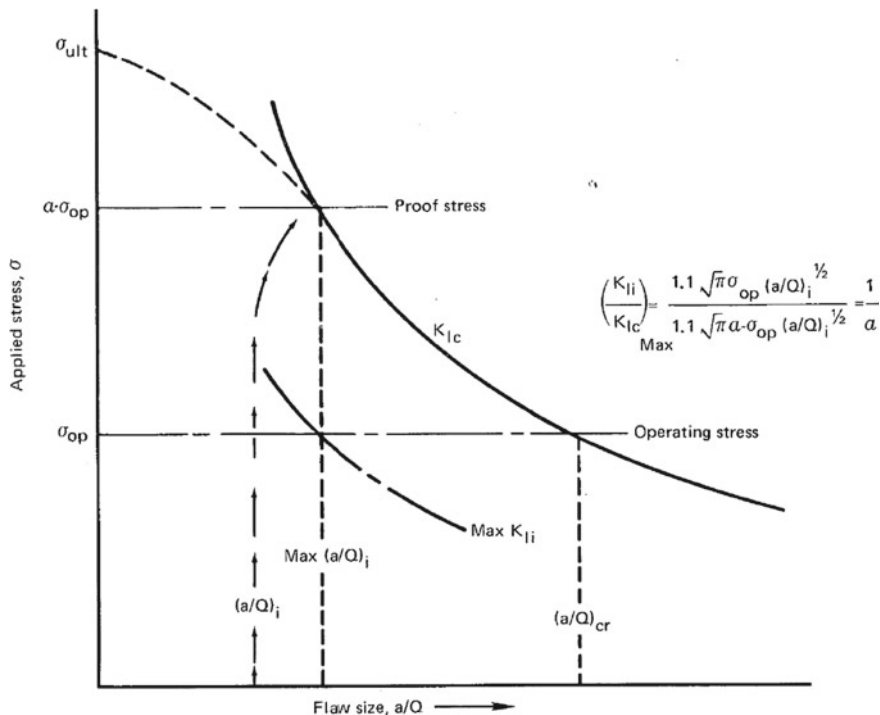
ϕ is the complete elliptic integral of the second kind, of modulus $k = (1 - a^2/c^2)^{1/2}$, defined as follows

$$\phi(k) = \int_0^{\frac{\pi}{2}} (1 - k^2 \sin^2 \theta)^{\frac{1}{2}} d\theta = \int_0^{\frac{\pi}{2}} \left(1 - \frac{c^2 - a^2}{c^2} \sin^2 \theta\right)^{\frac{1}{2}} d\theta$$

θ (rad) is an angular variable of integration, σ (N/m²) is the uniform gross stress applied at infinity in a direction perpendicular to the plane of crack, and σ_{ys} (N/m²) is the uniaxial tensile yield strength of the material. The following figure, due to the courtesy of NASA [47], shows the relationship between the flaw-shape parameter Q and the flaw depth-to-length ratio $a/(2c)$.



The following figure, also due to the courtesy of NASA [47], is a graphical representation of the preceding equation $(a/Q)_{cr} = (K_Ic/\sigma)^2/(1.21 \pi)$.



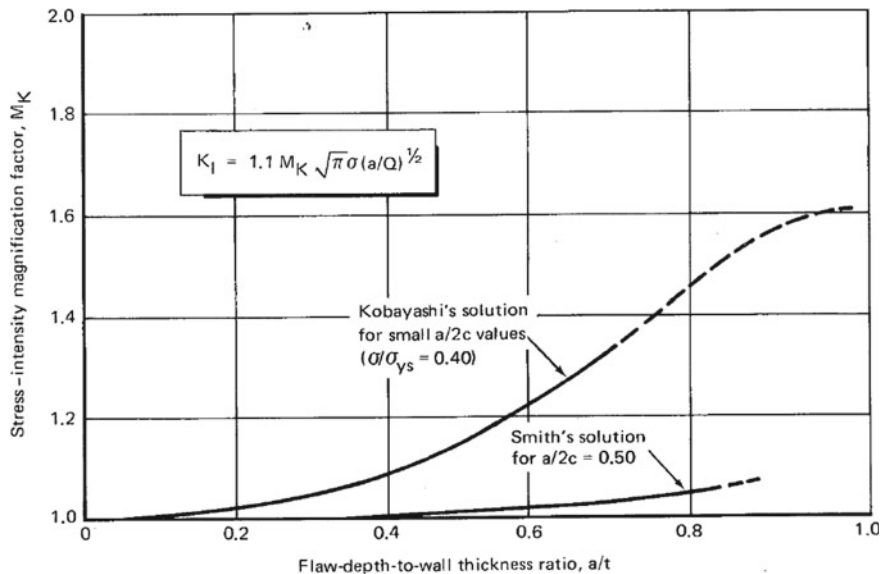
By the way, the complete elliptic integral of the second kind can be evaluated numerically by using the following expansion [48]:

$$\phi(k) = \frac{\pi}{2} \left[1 - \left(\frac{1}{2} \right)^2 k^2 - \left(\frac{1 \cdot 3}{2 \cdot 4} \right)^2 \frac{k^2}{3} - \left(\frac{1 \cdot 3 \cdot 5}{2 \cdot 4 \cdot 6} \right)^2 \frac{k^2}{5} - \dots \right]$$

where $|k| < 1$.

In order to predict critical flaw sizes, failure modes, and operational life of thin-walled tanks or pressure vessels, it is necessary to know the stress intensity for flaws which become very deep with respect to the wall thickness. The solution given by the preceding equation $(a/Q)_{cr} = (K_{Ic}/\sigma)^2/(1.21\pi)$ for a semi-elliptic surface flaw has been found to be sufficiently accurate for flaw depths up to about 50% of the thickness of the material [47]. For flaws of greater depths, the intensity of the stress applied is magnified by the effect of the free surface near the flaw tip. In other words, in thin-walled tanks, the flaw-tip stress intensity can reach the critical value K_{Ic} at a flaw size smaller than that which results from the preceding equation $(a/Q)_{cr} = (K_{Ic}/\sigma)^2/(1.21\pi)$.

The effect of the magnification factor M_K on the critical value K_{Ic} of the fracture toughness of a material is shown in the following figure, due to the courtesy of NASA [47].



The magnification factor M_K is applied to the equation $(a/Q)_{cr} = (K_{Ic}/\sigma)^2/(1.21\pi)$ as follows

$$K_{Ic} = 1.1 M_K \pi^{1/2} \sigma \left(\frac{a}{Q} \right)_{cr}^{1/2}$$

This application determines the critical value of the fracture toughness in case of deep surface flaws (such that the value of $a/(2c)$ is small).

As shown in the preceding figure, the value of M_K has been found to vary from less than 1.1 for semi-circular flaws ($a = c$, and therefore $a/(2c) = 0.50$) to 1.6 for flaws having smaller values of $a/(2c)$.

In case of tanks having flaws which are long with respect to their depth ($Q \approx 1$), the following equation can be used for a thin-walled tank

$$K_{Ic} = 1.1 M_K \pi^{1/2} \sigma a^{1/2}$$

and the following equation can be used for a thick-walled tank

$$K_{Ic} = 1.1 \pi^{1/2} \sigma a^{1/2}$$

In order to predict the critical sizes for surface and internal flaws by using the preceding equation $(a/Q)_{cr} = (K_{Ic}/\sigma)^2/(1.21\pi)$, it is necessary to know the values of K_{Ic} for the original material and for the welds of a tank. These values can be obtained from laboratory tests.

In order to prevent failure in a tank, either the actual initial flaw sizes or the maximum possible initial flaw sizes must be known. Non-destructive inspection is the only means of determining the actual initial flaw sizes. A successful proof test provides a measure of the maximum possible initial-to-critical stress intensity ratio, and this in turn makes it possible to estimate the maximum possible initial flaw sizes.

Non-destructive inspection techniques commonly used for rocket tanks are radiographic testing, ultrasonic testing, liquid penetrant testing, and magnetic particle testing. Other techniques are eddy current testing and infrared testing [47].

When multiple inspection techniques (for example, radiographic testing, ultrasonic testing, and liquid penetrant testing) are used, then most surface and internal flaws are detected. However, it is not safe to assume that all existing flaws can be detected at any time, because some of them (for example, tight cracks) are particularly difficult to detect. The largest initial flaw sizes which cannot escape detection cannot be established with confidence. The inspection techniques commonly used do not measure precisely the lengths and the depths of the initial flaws to be used in a fracture mechanics analysis. However, it is necessary to rely on non-destructive inspection to prevent proof-test failures of most high-strength tanks [47].

Proof-pressure testing is probably the most reliable non-destructive inspection technique available to ensure the absence of initial flaws of sufficient sizes to cause failure of a tank in operating conditions. Let K_{Ii} ($\text{Pa m}^{1/2}$) and K_{Ic} ($\text{Pa m}^{1/2}$) be respectively the plane-strain stress-intensity factor at the initial conditions and the fracture toughness of a given material. A successful proof test conducted at a pressure of α times the maximum pressure in operating conditions indicates that the maximum possible value of the ratio K_{Ii}/K_{Ic} is equal to $1/\alpha$. This value can be used with subcritical flaw-growth data to estimate the minimum life of a tank.

From the point of view of the initial design, the minimum required proof-test factor α for a tank is

$$\alpha = \frac{1}{\text{allowable value of the ratio } K_{Ii}/K_{Ic}}$$

The allowable value of the ratio K_{Ii}/K_{Ic} depends on the required service life of the tank and on the subcritical flaw-growth properties of the material [47].

In order to prevent yielding in proof testing, the membrane stresses applied to a tank are limited to a value equal to or less than the yield strength of the material.

In practice, the local level of stress may exceed the yield strength of the material, because there may be discontinuities due to design or manufacturing, and also because of the presence of residual stresses. When the applied stress approaches and exceeds the yield strength of the material, the critical flaw-size curve deviates from the theoretical curve based on a constant value of K_{Ic} , and therefore the critical flaw sizes are smaller than those predicted by the linear-elastic theory of fracture mechanics.

When the stress applied to a tank at proof pressure exceeds the yield strength of the material and the tank also passes the proof test, then the maximum possible value of the ratio K_{Ii}/K_{Ic} resulting from the test is smaller than $1/\alpha$. In this case,

the minimum operational life of the tank should exceed the required life, which has previously been used to determine α .

It is to be observed that the equation $\alpha = 1/(\text{allowable value of the ratio } K_{ii}/K_{ic})$, which expresses the required minimum proof-test factor α for a tank, does not take account of the thickness of the tank. However, the value of the proof test in providing assurance against failure in service changes with decreasing wall thickness or with increasing fracture toughness K_{Ic} of the material [47].

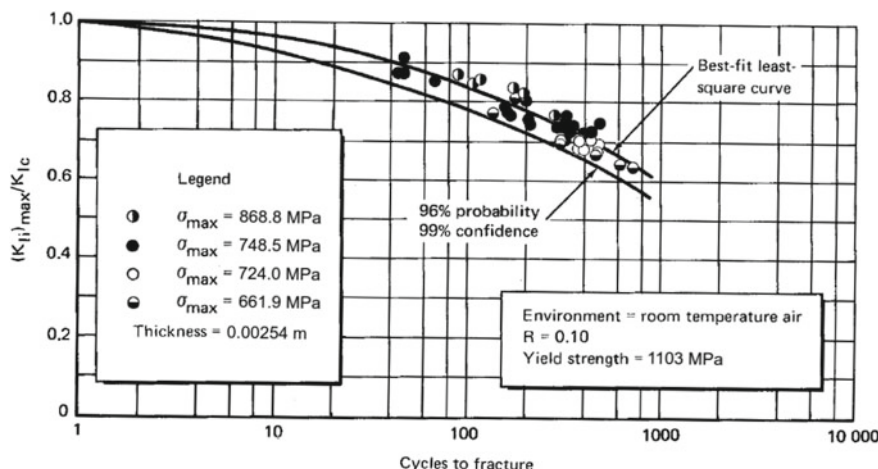
When a proof test is performed at a temperature which differs from the temperature in operating conditions, then the required minimum value of the proof-test factor is expressed by the following equation of [47]:

$$\alpha = \frac{1}{\text{allowable } K_{ii}/K_{Ic} \text{ at operating temperature}} \times \frac{K_{Ic} \text{ at proof - test temperature}}{K_{Ic} \text{ at operating temperature}}$$

The choice of the proper fluid to be used in a proof test is an important consideration for all alloys. Water may have a detrimental effect in high-strength alloys, because it promotes slow growth of flaws due to the effect of hydrogen cracking. This problem has been solved by using either other fluids, such as oil, or water with corrosion inhibitors, such as sodium bichromate ($\text{Cr}_2\text{Na}_2\text{O}_7$), or distilled water.

Subcritical flaw growth can occur after cyclic loading, sustained-stress loading, and combined cyclic and sustained-stress loading. Data from fracture specimen tests can be used in a fracture mechanics analysis to predict the number of cycles or the time needed for an initial flaw in a tank under sustained pressure to grow to critical size. The time or the number of cycles needed to cause failure has been found to depend primarily on the ratio K_{II}/K_{Ic} .

The following figure, adapted from [47], shows the ratio K_{II}/K_{Ic} versus cycles to fracture for a heat-treated Ti-6Al-4V alloy in air at room temperature. The quantity R is the ratio of the minimum stress to the maximum stress during a cycle. Both the best-fit, least-square curve and the 96% probability, 99% confidence are shown in the plot.



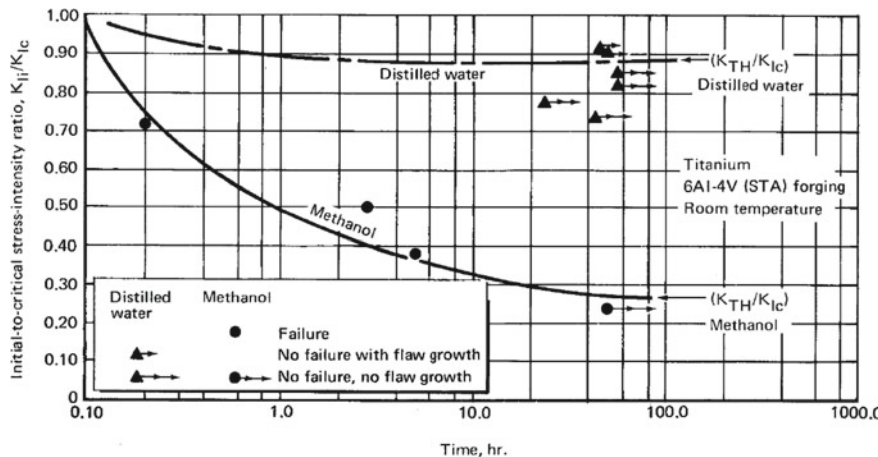
An important property observed in all sustained-stress experiments of flaw growth is the existence of a threshold level of stress intensity for a given material in a given environment.

In other words, below a given value of stress intensity (or of K_I/K_{Ic} ratio), flaw growth has not been detected. Above this value, flaw growth occurs and can result in fracture. This stress intensity has been designated as K_{TH} .

The discovery of a unique value of K_{TH} for a given material in a given environment makes it possible to design a safe tank subject to a sustained load.

K_{TH} may be 80% of K_{Ic} or higher in an inert environment, but may also be less than 50% of K_{Ic} in a hostile environment.

The threshold value K_{TH} for a Ti-6Al-4V alloy subject to sustained load in two different liquids (distilled water and methanol) is shown in the following figure, due to the courtesy of NASA [47].



The value of K_{TH} has been found to decrease with increasing yield strength in steel alloys. The flaw growth for sustained load has the highest values in conditions of plane strain. The values of K_{TH} , determined from tests of specimens cracked through the thickness, increase with decrease in specimen thickness.

In chemically inert environments, the crack growth rate initially decreases with increasing stress intensity. When the initial stress intensity is sufficiently low, the crack may halt. At higher stress intensities, the crack growth rate passes through a minimum value and then increases steadily until the crack becomes unstable. This behaviour has been observed for AM 350® steel (a heat-treatable austenitic or martensitic alloy, depending on heat treatment) in a purified argon environment.

For some alloys, such as Ti-5Al-2.5Sn (ELI) and 2219-T87, two thresholds have been observed in environments of room air, liquid nitrogen, and liquid hydrogen. One of these threshold stress intensities was defined as the value of stress above which flaw growth to failure can be expected. The other of them was defined as the value of stress below which there is no flaw growth. In the interval between these

two threshold intensities, small amounts of flaw growth can occur, but the growth apparently arrests after a short time at load [47].

Some examples of ratios K_{TH}/K_{Ic} , determined experimentally, are shown in the following table, adapted from [47].

Material	Temp., K	σ_{ys} , MPa	Fluid environment	$\frac{K_{TH}}{K_{Ic}}$
6Al-4V (STA) titanium forging	RT ^a	1100	Methanol	0.24
	RT	1100	Freon M.F.	0.58
	RT	1100	N_2O_4 (.30 % NO)	0.74
	RT	1100	N_2O_4 (.60 % NO)	0.83
	RT	1100	H_2O + sodium chromate	0.82
	RT	1100	H_2O	0.86
	RT	1100	Helium, air, or GOX	0.90
	RT	1100	Aerozine 50	0.82
	305	1100	N_2O_4 (.30 % NO)	0.71
	305	1100	N_2O_4 (.60 % NO)	0.75
6Al-4V titanium weldments (heat-affected zones)	314	1100	Monomethyl-hydrazine	0.75
	316	1100	Aerozine 50	0.75
5Al 2.5 Sn (ELI) titanium plate	RT	869	Methanol	0.28
	RT	869	Freon M.F.	0.40
	RT	869	H_2O	0.83
	RT	869	H_2O + sodium chromate	0.82
2219-T87 aluminum plate	77.6	1240	LN_2 ($\sigma <$ proportional limit)	>0.90
	77.6	1240	LN_2 ($\sigma >$ proportional limit)	0.82
	20.4	1450	LH_2	>0.90
4330 steel 4340 steel	RT	400	Air	0.90 ^b
	77.6	455	LN_2	0.82 ^b
	20.4	496	LH_2	>0.85 ^b
GTA welds: 18Ni (200) steel 18Ni (250) steel 12Ni-5Cr- 3 Mo steel 9Ni-4Co- 2.5C steel Inconel 718	RT	1410	Water	0.24
	RT	> 1380	Salt water	<0.20
	RT	1380	Salt water spray	>0.70
	RT	1620	Salt water spray	>0.70
	RT	1170	Salt water spray	>0.70
	RT	1170	Salt water spray	>0.70
	RT	1140	Gaseous hydrogen at 34.58 MPa (absolute)	<0.25

^a Room temperature.

^b No failure K_{TH} , some growth observed at lower values.

Some criteria to be observed in the design of metallic tanks for rocket engines have been identified by Tiffany [47]. They may be summarised as follows. All tanks must be designed to avoid failure in service caused by flaws and to ensure a very low probability of catastrophic failure caused by flaws during proof tests. For this purpose, it is necessary to consider not only the internal pressure to which a tank is subject, but also the pressures, temperatures, environments, and stresses to which the tank is exposed.

The materials used for tanks must have appropriate characteristics of fracture-growth and flaw-growth. These characteristics must come from reliable sources of data, for example, from the military standards MIL-HDBK-5 J [25], and must also be confirmed by tests.

The critical flaw sizes must be determined for the stress levels of interest by either analysis or tests, as appropriate. If possible, the maximum size of initial flaws allowable in tanks should be so great as to be detected by non-destructive inspection, but not so great as to grow to critical size during life in service.

The allowable initial size of flaws must be less than the critical size at the level of stress of proof pressure. The initial stress intensity ratio allowable in a tank must be chosen to ensure that the critical intensity ratio is not attained during the design life of the tank.

Each tank must be proof tested. The level of proof pressure must be chosen to demonstrate that the tank is free of flaws larger than the allowable initial size, or that the actual initial stress-intensity ratio is less than the allowable initial stress-intensity ratio. Account must be taken of the differences between the proof test temperature and the service temperature, and of the time required to apply or remove pressure during the proof test.

In order to prevent failures in proof tests, low levels of stress and materials having high values of fracture toughness must be used during such tests. By so doing, the critical sizes of flaws are large and greater than the thickness of the tank walls. Consequently, the worst case which can occur during proof testing is leakage. In order to obtain maximum assurance of safe performance in service, it is desirable to use large proof-test factors, low levels of operational stresses, and materials having low rates of flaw growth under cyclic loads and high values of K_{TH} in the expected environment of service.

On the other hand, the use of large proof-test factors, low levels of operational stresses, and materials having high values of fracture toughness leads often to high masses of tanks. Therefore, trade-offs can and should be made to arrive to an optimum compromise for a given tank.

6.9 Structural Elements of Tanks

The structural elements considered in the present section are tank shells, weld joints, access openings, support fittings, and accessory attachment provisions.

Not only the tank shells but also the other elements are required to withstand internal and external pressures, the latter acting during propellant servicing or during decontamination. Vacuum is frequently used to remove gas from the liquid side of expulsion devices (described in Sect. 6.6), and also to remove residual propellants from tanks. The tank shells and the other elements are required to withstand an external pressure of one atmosphere (101325 N/m^2).

One of the principal requirements of tanks for rocket engines is low mass. Other requirements are cost, schedule times, easiness of manufacturing, reliability and availability of the materials used for them, technical skills of the personnel, tools, and testing facilities.

In the phase of structural design, the detailed design of a tank includes sidewall, fore and aft bulkheads, access openings, and accessory mounting provisions. The design of these elements depends on the material chosen for the tank. The detailed design of a tank also includes the primary structural junctures.

The design of a tank is based on the relation between the loads imposed and the capability of the tank to withstand such loads. Wagner and Keller [22] have identified the following factors to be taken into account in the analysis of the loads imposed on a tank:

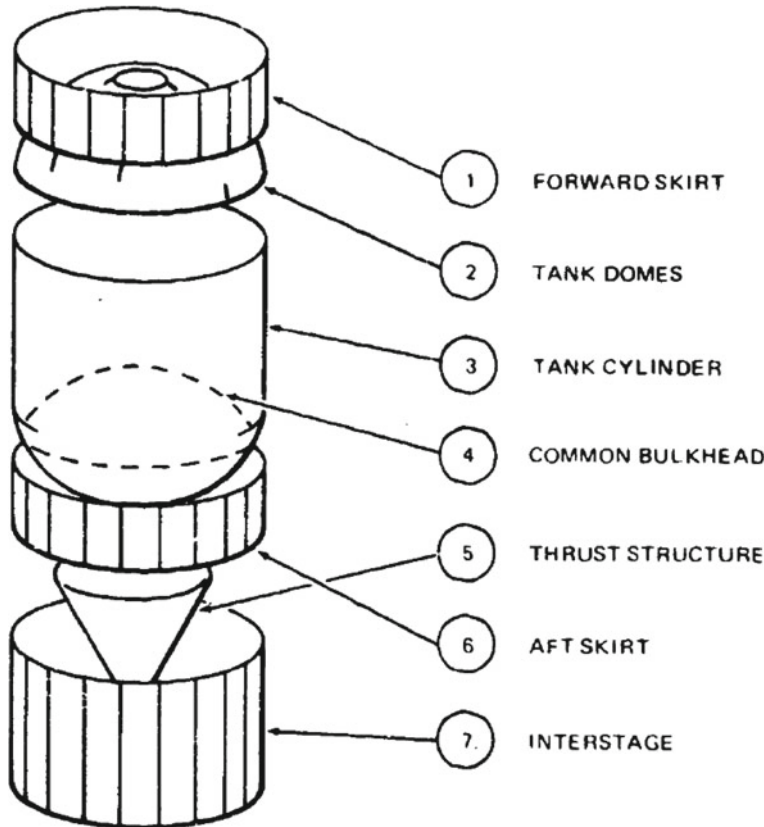
- limit load or stress, which is the maximum stress or pressure which the tank structure is expected to bear, in the specified operating conditions and with allowance for possible variations;
- design safety factor, which is a multiplier, whose value (greater than unity) is chosen by the designer to take account of small variations of the properties of the material, of the quality of manufacturing, and of the magnitude and distribution of the load in the structure;
- design load or stress, which is the limit load multiplied by the design safety factor;
- allowable load or stress, which is the load not to be exceeded to avoid failure, the latter being due to either buckling, or yield, or ultimate loading; and
- margin of safety (m_s), which is the fraction by which the allowable load exceeds the design load, as follows

$$m_s = \frac{\text{allowable load or stress}}{(\text{limit load or stress}) \times (\text{design safety factor})} - 1$$

The magnitude of the design safety factor depends on the degree of confidence in the properties of the materials, on the processes of production, and on the validity of the predicted conditions of use. In practice, a uniform design safety factor is chosen by the designer for the entire structure of a rocket vehicle on the basis of experience and judgement. Values in use for the design safety factor range from 1.0 to 1.1 for yield stress and from 1.25 to 1.5 for ultimate stress, the higher values being used for manned flight vehicles.

The structure of a rocket tank is required to withstand the stresses due to vibration, thermal shock, propellant slosh, and internal pressure. This structure is also required

to provide the load path for the loads acting on the body of the rocket vehicle. The structural elements of a rocket tank are subject to different types of stresses, which are briefly described below for each element. The following figure, due to the courtesy of NASA [49], shows schematically the structural elements of the S-IVB (the third stage of the Saturn IV launch vehicle), which has one J-2 engine.



The tank sidewall of a tank is subject to pressure, inertial forces due to the propellant, axial loads, and bending moments. The circumferential stresses are determined by combining the ullage pressure, the load pressure, and the inertial force due to the propellant. The meridian stresses are determined by combining the ullage pressure, the axial loads, and the bending moments.

The stresses acting on the end closures of a tank result from the ullage pressure and the acceleration impressed on the propellant. During the boost time, the aft bulkheads of tanks have a maximum pressure at the apex, and the forward bulkheads have a minimum pressure at the apex. In order to evaluate the stress at a specific location on the end closures, the pressure and the shape of the closure must be considered.

When there are separate bulkheads on two contiguous tanks, the load acting on each of them is to be determined as indicated above for end closures of tanks.

A single common bulkhead is subject to either burst or collapse loads and to temperature gradients through its thickness. The pressure loads acting at any given point of a common bulkhead are determined as described above for end closures of tanks, but a common bulkhead is subject only to the difference between the forward pressure and the aft pressure acting at any given point. The stability under collapsing pressure loads is obtained by designing a bulkhead of large bending stiffness in comparison with its membrane stiffness. A stiffened skin for a tank requires a more complex analysis of internal loads. In this case, a multi-layer shell of revolution is frequently used.

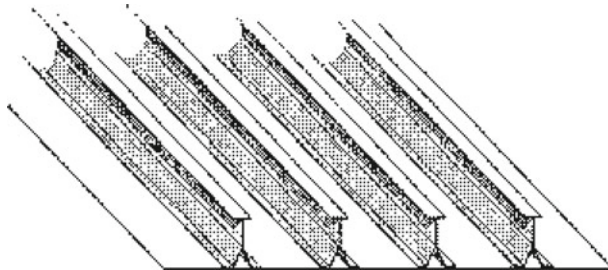
A tank is also subject to local loads at any point in which it is mated to other components of a rocket vehicle. The magnitudes and the directions of these loads depend on the weight of each component multiplied by an amplification factor due to acceleration and vibration. The magnitude of these loads is felt to its full extent by the attachment bolts and by the immediate structural elements. It is felt to a lesser extent by the contiguous structural elements. This lower magnitude is evaluated according to criteria suggested by experience and judgement, taking account of the damping which occurs away from the point of excitation.

In most cases, tanks for liquid-propellant rocket engines are thin-walled surfaces of revolution, meaning by that, structures whose thickness t is assumed constant and much smaller than the radii R of curvature of its middle surface [2]. In practice, the value of R/t is assumed greater than 10. As has been shown in the first four sections of the present chapter, this assumption permits the use of simple formulas for stress and strain, such as those which are given in [3].

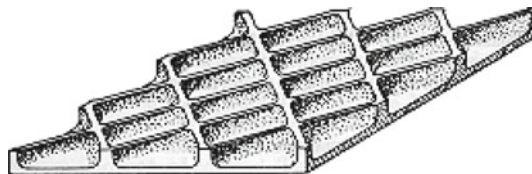
The choice of the materials and the evaluation of the corresponding thicknesses and stresses can be done by using only data on mechanical properties with safety factors selected by the designer. Of course, practical considerations concerning manufacturing, handling, and stiffness are also taken into account in this preliminary choice. Before this choice can take place, the level of stress in working condition, the thickness of the skin, and the fracture strength of the materials must be evaluated. The proposed material must possess appropriate values of toughness and resistance to the growth of subcritical flaws, in order to comply with the requirements of life service for a given tank.

After a material has been chosen, the proof-test stress, the operational stress, and the non-destructive inspection requirements are defined according to the desired mission performance. The skin thickness is determined by taking account of the most restrictive conditions, such as safety factor, criteria of fracture control, manufacturing, and handling. The skin thickness for the sidewall of a tank depends on the product of the circumferential tension load under the predicted maximum pressure times the factor of safety [22]. In order to reduce mass, the skin thickness should be as low as possible. There are several methods for constructing thin-walled tanks. Sometimes, a tank can be put under internal pressure to keep its walls from buckling. This is because the net tensional force due to internal pressure is made greater than the compressional force due to the flight loads. Consequently, the tank is only subject to tension, and buckling is avoided. Such was the case with the Atlas and Centaur launch vehicles, in which additional membrane rigidity was obtained through the internal

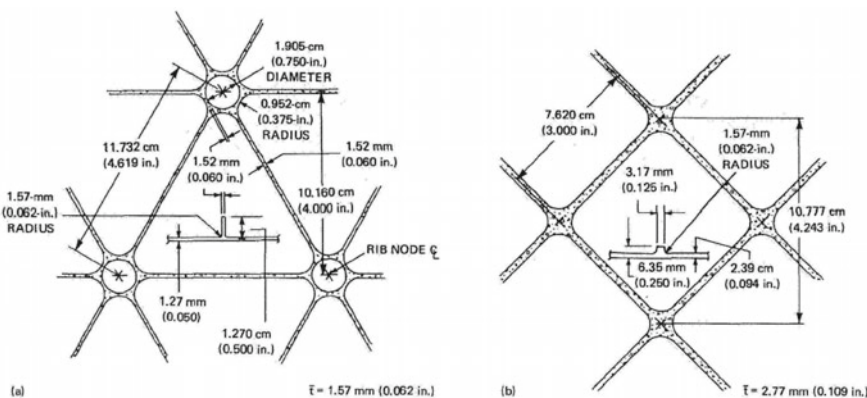
working pressure within the tank [22]. Another method of stabilising thin metallic sheets is used in the construction of conventional aircraft. In this method, stiffening members (stringers) are fastened to the skin in the direction of the compressive loads, as shown in the following figure, due to the courtesy of NASA [50].



The same result can also be obtained in a single piece of metal by chemically milling or machining a solid sheet to remove all metal except ribs or waffles which act as stringers, as shown in the following figure, due to the courtesy of NASA [50], which illustrates a rectangular waffle structure.



Still another method (developed by McDonnell Douglas) of stiffening a skin is the use of an isogrid structure, in which the ribs are arranged in a repetitive equilateral triangular pattern, as shown in the following figure, due to the courtesy of NASA [51], where an isogrid structure (left) and a square waffle structure (right) are illustrated.



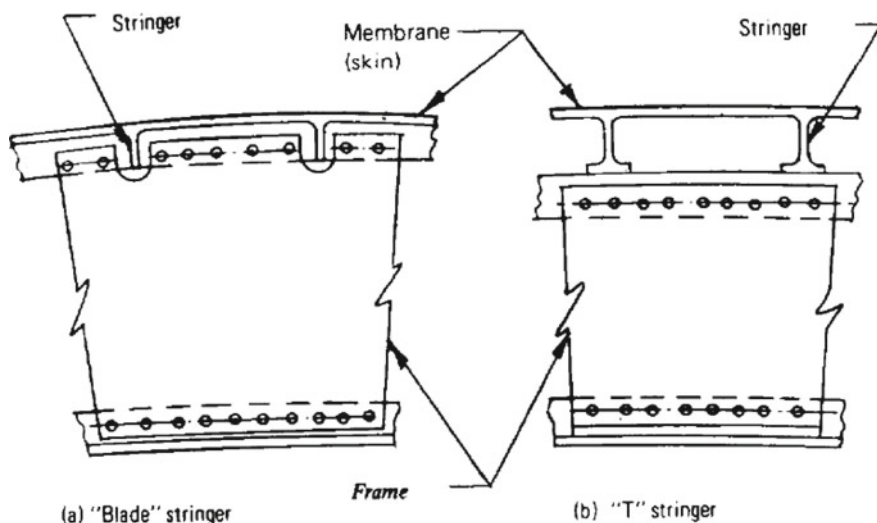
An isogrid structure results in a surface whose stiffness is orthogonally isotropic. Details and methods of calculation for isogrid structures are given in [49]. This method was used for the external skin structure of the Delta launch vehicle [51].

Summarising, the sidewall skin is usually stiffened against buckling by using stringers, frames, or ribs spaced in a grid pattern (either isogrid or rectangular waffle). The sidewall design is particularly important for tanks of large space vehicles. This is because the sidewall in such vehicles not only contains the propellant but also transmits the body loads. The principal types of sidewall designs for tanks under pressure are skin-stringer-frame, grid, and monocoque.

The choice of one or another type of design for a tank depends on the magnitude of the body loads applied externally and on the type of propellant to be contained in the tank. A highly loaded sidewall is usually designed with the skin-stringer-frame structure, whereas a lightly loaded sidewall is designed with the waffle or isogrid structure. A very lightly loaded sidewall can be designed with the monocoque structure, but pressurising is often required for stability.

Integral stiffening is the type of skin-stringer design which is best suited to propellant tanks [22]. This type of design eliminates the many sources of possible leakage associated with the points of mechanical attachment involving the skin, the stringers, and the frames constructed in the conventional manner.

The following figure, due to the courtesy of NASA [22], shows two types of skin-stringer designs. They are: (a) "Blade" stringer; and (b) "T" stringer.



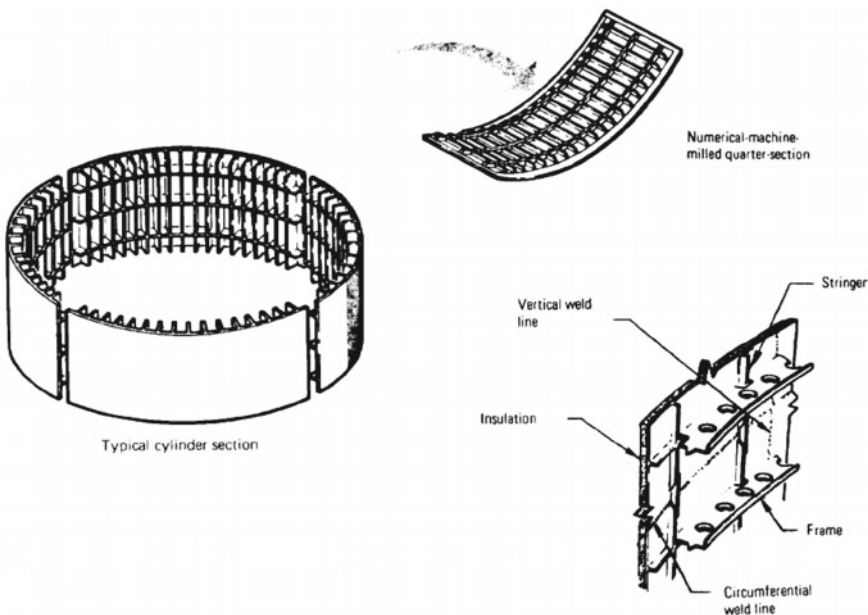
The type (a), shown on the left-hand side of the preceding figure, consists of panels in which the skin, the "blade" stingers, and the horizontal ribs are machined as an integral unit, where the frames are attached mechanically to the horizontal ribs after the panels are formed.

The type (b), shown on the right-hand side of the preceding figure, consists of panels in which only the skin and the "T" stringers are machined, and the frames are added after forming by mechanical attachment to the inboard flanges of the "T" stringers [22].

The thickness of the skin depends on the circumferential tensional loads under maximum internal pressure. The stringer spacing depends on the local requirements of stability. The stringer configuration and the frame spacing for tanks of minimum mass depend on general requirements of stability under axial compressive loads combined with internal pressures.

The material used for a sidewall of skin-stringer-frame design must be readily machinable and must also have good forming and welding properties. Compensation should be made by increasing the thickness at the weld joints, because the design strength of a weld is generally taken lower than the strength of the original material. The stringer spacing should be designed so as to keep the skin from buckling at limit load, account being taken of the buckling data of the curved panel and also of the stabilising effect of the internal pressure.

The following figure, due to the courtesy of NASA [22], shows a typical sidewall design used successfully for the liquid-hydrogen tank of the Saturn S-II stage.

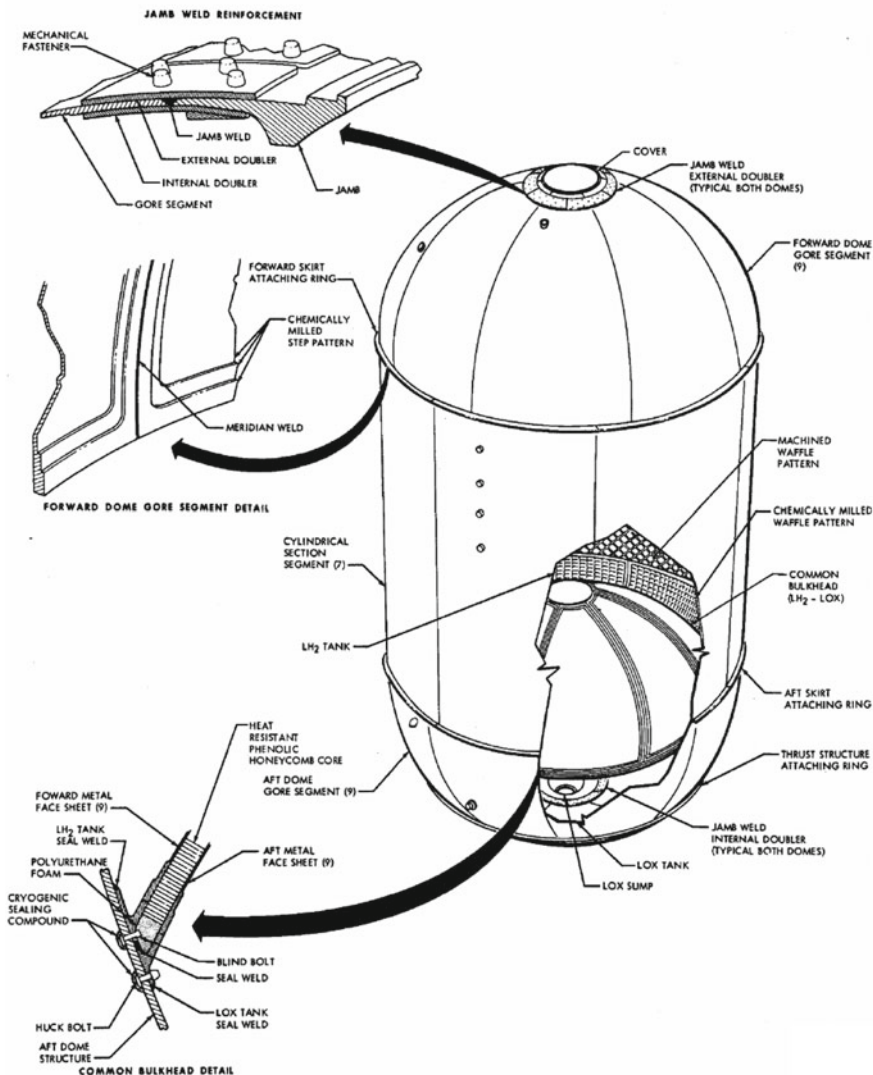


As has been shown above, the skin of a tank can also be stiffened by using integral ribs spaced in a grid pattern (either isogrid or rectangular waffle).

The integral rib stiffeners are usually formed by mechanical or chemical milling of the waffle pattern in a thick plate. Mechanical milling is more efficient than the other method [22]. The waffle structure is usually designed according to criteria of shell stability. Aluminium alloys are frequently used for the waffle plate material.

A waffle design was used for the propellant tank structure of the Saturn S-IVB stage. The waffle pattern of the S-IVB consisted of pockets 241.3 mm on centre, which were oriented $\pm\pi/4$ rad with respect to the longitudinal axis of the vehicle. These pockets were surrounded by ribs which were 15.93 mm high and 3.658 mm wide. The skin or web thickness at the bottom of the pocket was 3.124 mm, and the weld land areas at the edges of these segments were 6.4 mm thick. The following figure, due to the courtesy of NASA [52], shows the propellant tank structure of the Saturn S-IVB stage and, in particular, the machined waffle pattern.

S-IVB PROPELLANT TANK STRUCTURE



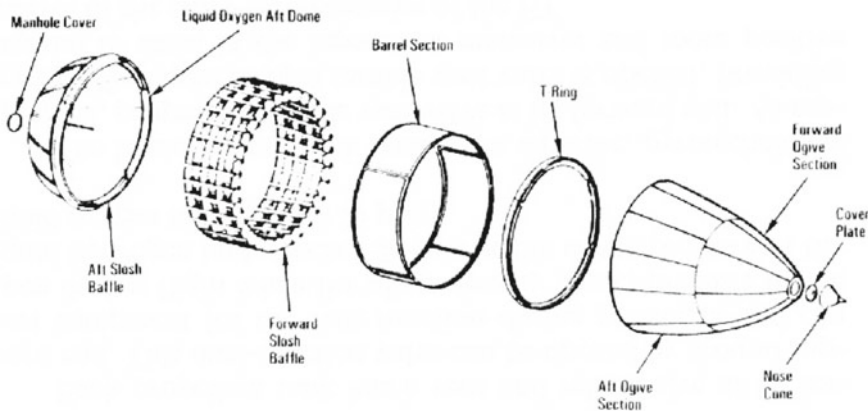
The isogrid pattern has the following advantages over the rectangular or square pattern:

- high twisting rigidity of the structure, which distributes the loading over a wide region;
- isotropic behaviour of the material, which has the same strength in all directions; and

- uncoupling of the bending and the in-plane resultants.

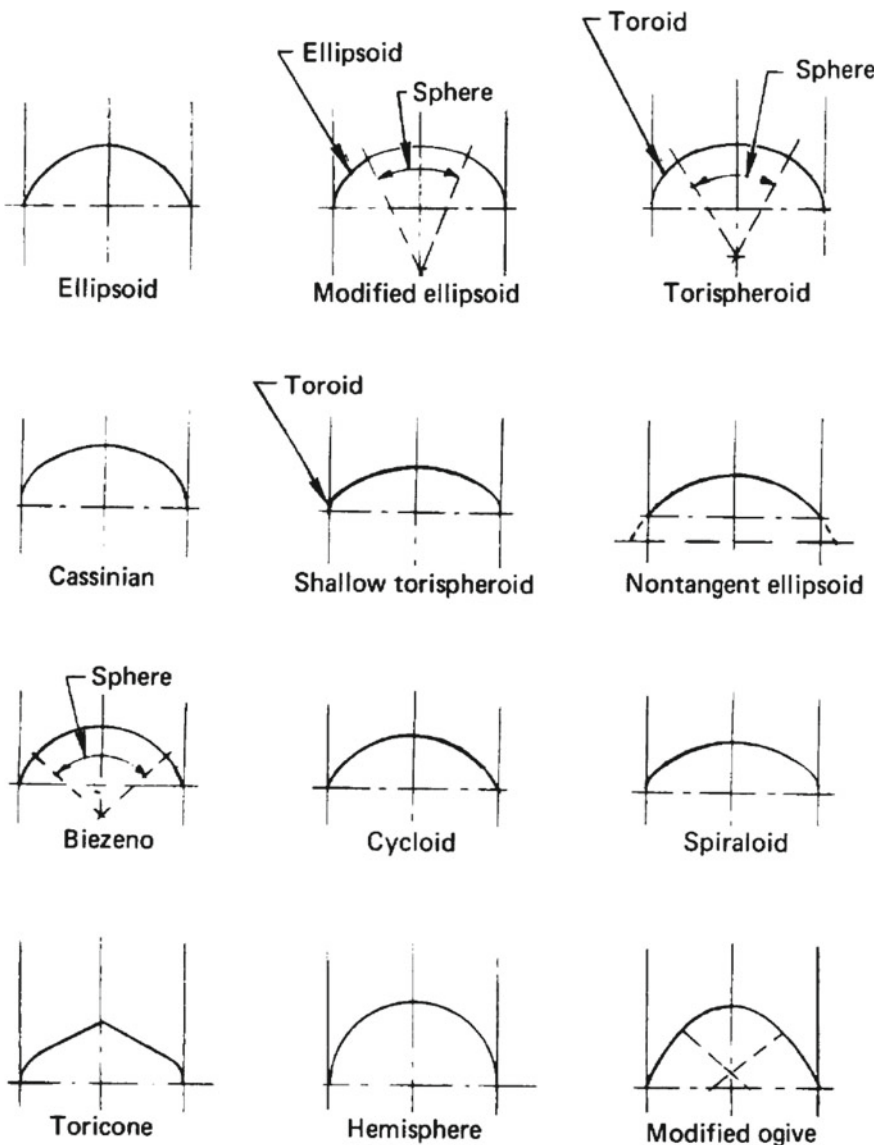
Therefore, the isogrid pattern makes it possible to apply the many available solutions of the classical theory of plates. In other words, a structure stiffened by an isogrid pattern can be analysed as a solid continuous sheet of material having appropriate thickness and elastic modulus [49].

A monocoque structure stabilised by internal pressure has the lowest structural mass. This type of structure requires a material having a high tensile stress. Extreme care must be taken during manufacturing and transportation to avoid handling damage. In order to prevent buckling in a monocoque pressure-stabilised structure, the meridian tensile stress due to internal pressure must be greater than the meridian compressive stress due to external loads. This type of structure has been used for the Atlas and Centaur launch vehicles. It has also been used for the liquid-oxygen tank of the Space Shuttle, which is shown in the following figure, due to the courtesy of NASA [53].



Liquid Oxygen Tank Structure

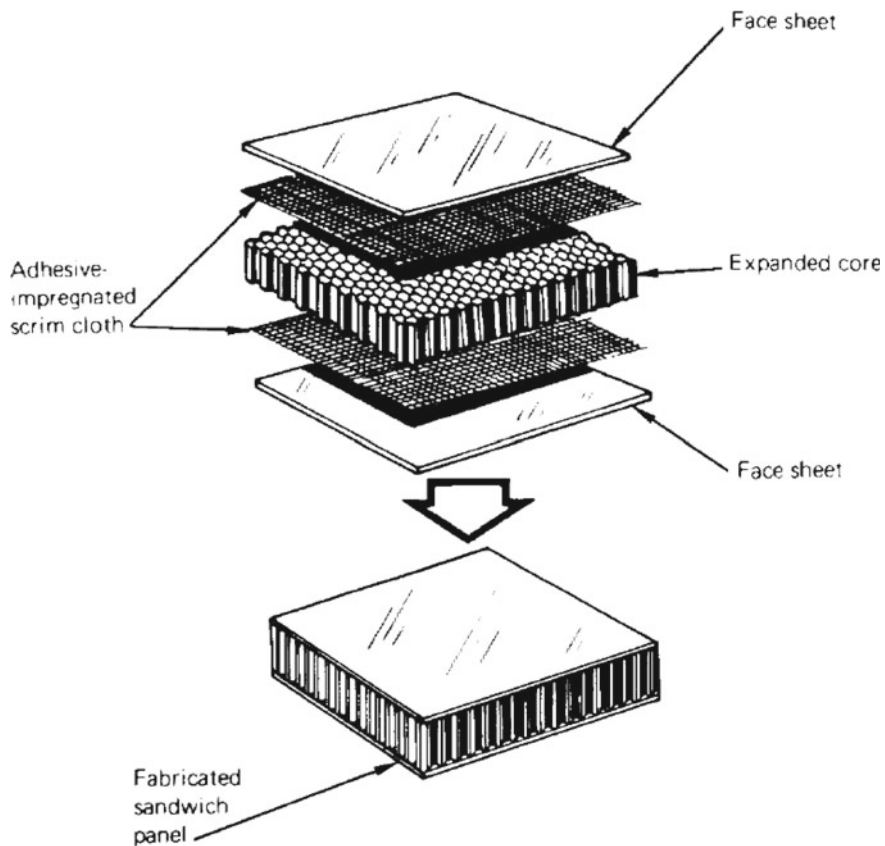
The shape of the end closures of tanks affects their lengths and also the means used for structural stiffening, to an extent which depends on the materials chosen. A choice should also be made on whether using two separate closures or a common closure for two tanks stacked onto each other. Some surfaces of revolution, which have been analysed by computer subroutines for end closures, are shown in the following figure, due to the courtesy of NASA [22].



In practice, end closures of hemispherical shape were chosen for the tanks of the Titan and for those of the Saturn S-IV. Oblate spheroids were chosen for the Saturn S-II, and ellipsoids were chosen for the Atlas, the Saturn I-C, and the Centaur [22].

A sandwich structure is used to resist buckling in the presence of compressive loads. Where only tensional loads exist, monocoque structures can be used.

An example of honeycomb sandwich structure is shown in the following figure, due to the courtesy of NASA [22].



Further information on sandwich structures is given in several textbooks. A short course on the matter can be found in [54].

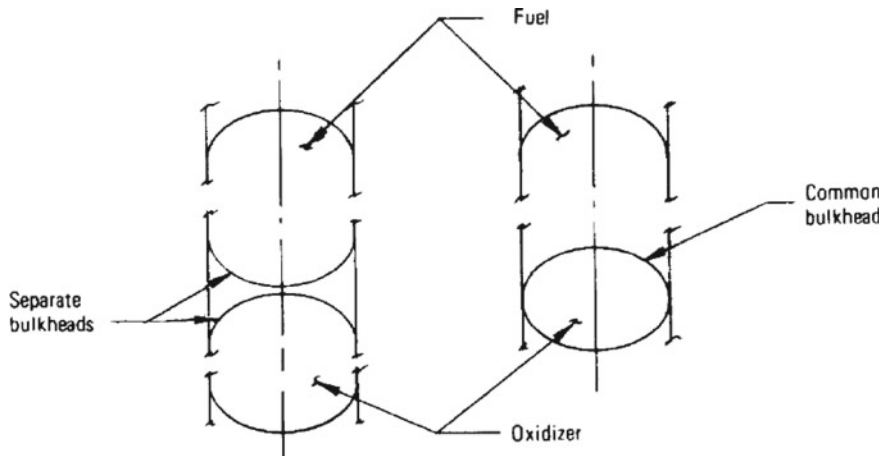
The forward bulkhead of a tank is usually a surface of revolution, convex on its external side, which is loaded principally by internal pressure. A thin skin subject to membrane stresses is the structural scheme generally used. Compressive stresses should be carefully determined, especially where the radius of curvature of the surface of revolution changes, in order to avoid circumferential buckling, and the results found analytically should be confirmed by tests.

To reduce mass, it is desirable to vary the thickness of the shell so that the bulkhead is subject to the maximum allowable stress along its meridians. On the other end, to reduce cost, it is desirable a shell of constant thickness.

As has been shown in the preceding figures of this section, a bulkhead is generally manufactured by welding together an apical tank skin (also known as the dollar hatch) to a welded sub-assembly consisting of some triangular segments or gores. This method avoids the juncture of the multiple welds where the gore segments meet at a common point.

The aft bulkhead of a tank differs from the forward bulkhead only because some forces can act on it under certain conditions. For example, such forces act during the filling of a tank with a liquid propellant and during the propelled flight. Aft bulkheads are constructed by using sandwich or waffle structures. Engine feed-lines are usually located in the central part of a bulkhead, in case of a single engine.

The fuel and the oxidiser of a bi-propellant rocket engine are separated by either two distinct bulkheads or one common bulkhead, according to the scheme shown in the following figure, due to the courtesy of NASA [22].



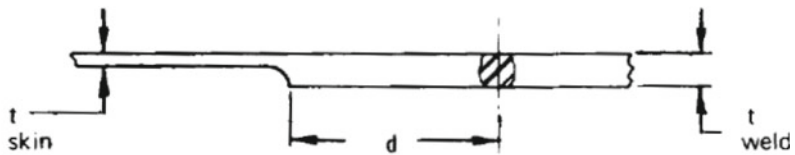
A common bulkhead, if present, may be either self-supporting or pressure-stabilised. A common bulkhead of the self-supporting type must be designed for both bursting and collapsing pressures. Sandwich or waffle structures are generally used for this purpose. The forward surface of a common bulkhead is usually convex, as shown in the preceding figure.

The attachment junctures used in a tank for propellants include:

- weld joints;
- bulkhead/sidewall juncture; and
- bosses and support provisions.

A brief description is given below for each of these elements.

The principal welding processes used in space flight hardware have been described in Sect. 6.7. We describe here the weld joints used specifically in tanks for propellants. Since the strength of the material in the weld area is less than the strength of the original material, then an increase in thickness is necessary at the weld joints. The thicker weld land ($t_{weld} > t_{skin}$) is usually asymmetrical on the two sides (external and internal) of the skin at a weld joint, as shown in the following figure, due to the courtesy of NASA [22].



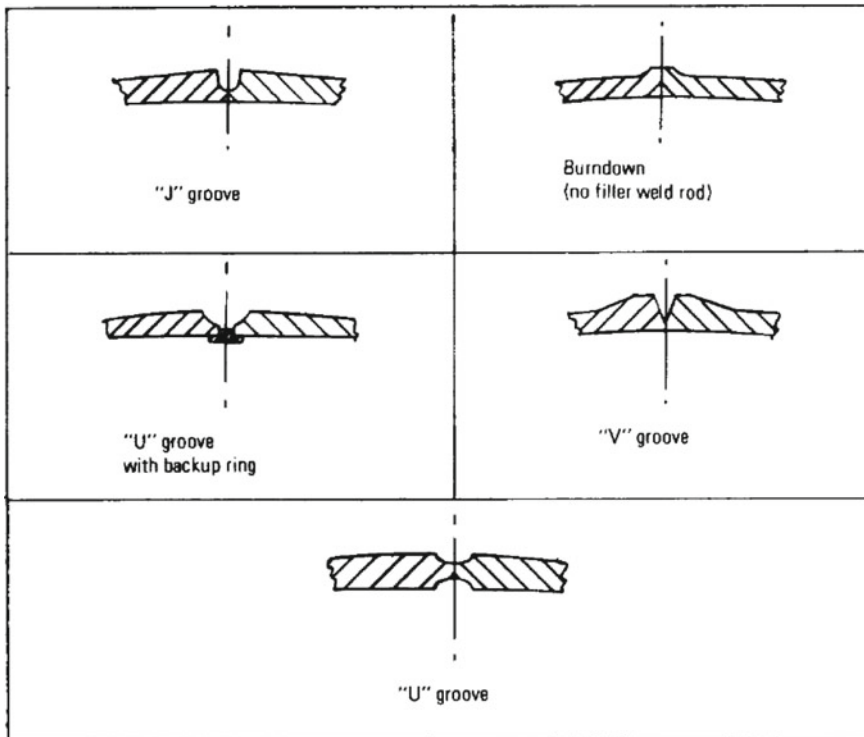
(a) Abrupt termination of weld land



(b) Stepped or tapered termination of weld land

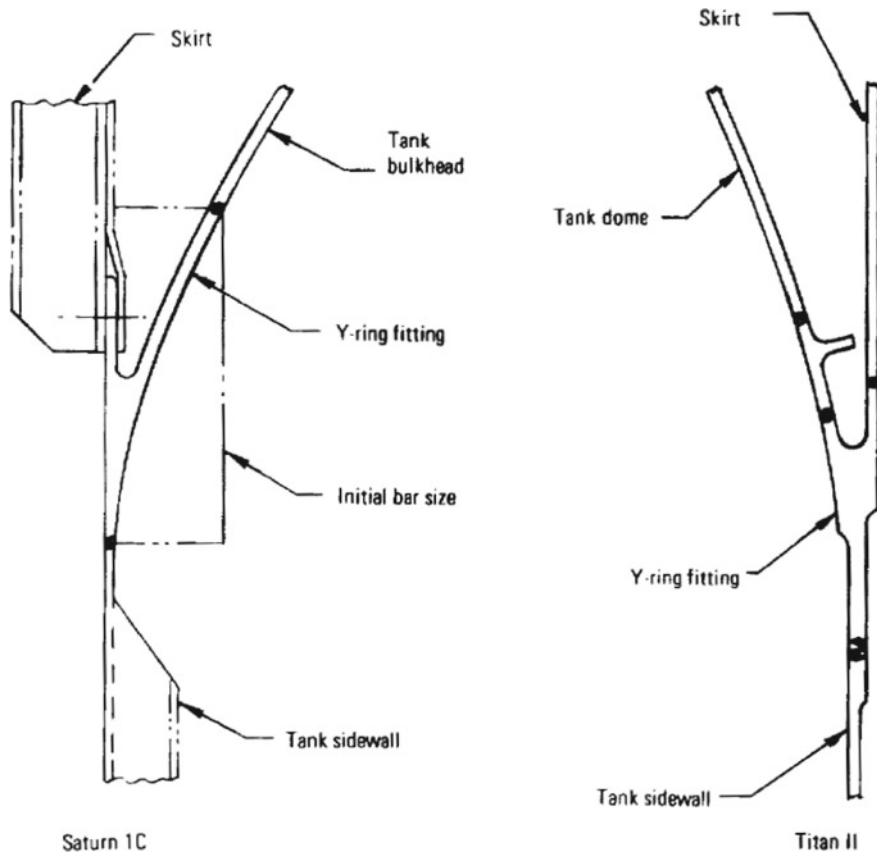
This is because it is desirable to maintain a smooth external surface for aerodynamic reasons, and also because milling on the two sides of a weld land is more expensive than milling on one side only. The preceding figure illustrates two types, (a) and (b), of weld land for aluminium alloys 2014-T6 and 2219-T87, which are materials commonly used for propellant tanks. The thickness t_{weld} of a weld land is greater, by a factor ranging from 2 to 2.25, than the thickness t_{skin} of the skin. The width d of a weld land ranges from 32 to 51 mm. The stepped or tapered termination (type b) of a weld land has the advantage, over the abrupt termination (type a), of avoiding bending stresses and strength reduction where the skin meets the weld land [22].

The following figure, due to the courtesy of NASA [22], shows some pre-weld joint preparations which have proven satisfactory for tank design.

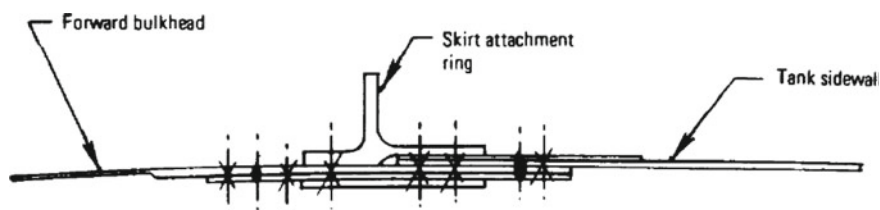


When possible, cylindrical sections of tanks are manufactured by spin forging, in order to eliminate longitudinal welds. Post-weld processing of tanks is limited to ageing, to relieve internal stresses caused by welding. This is because heat treatments after welding could induce distortion and oxidation, and also because complex equipment would be needed for that effect.

Junctures are also needed in a tank between bulkhead and sidewall and between skirt and sidewall. These junctures are usually made at a common location with an appropriate fitting. A fitting commonly used is a Y-ring, so called due to its shape, which has been used for the Saturn I-C and for the Titan II. A Y-ring fitting is shown in the following figure, due to the courtesy of NASA [22].



A different type of fitting for the bulkhead/sidewall juncture is shown in the following figure, due to the courtesy of NASA [22]. It was used for the Centaur rocket stage.



A Y-ring fitting provides a structural path for the loads from the bulkhead to the tank and from the skirt to the tank. It also makes the tank leak-proof at the bulkhead/sidewall juncture.

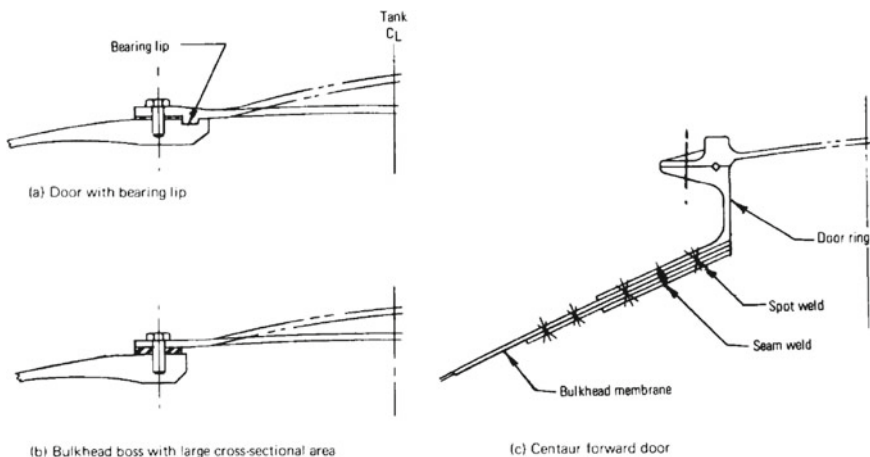
The system components and the tank mounting structure are usually attached by means of bosses. Such bosses are made deep enough to accommodate mechanical

fasteners, in order to avoid tank penetration. When the basic structure is of sufficient thickness, then the bosses are integrally milled with the basic structure. When the basic structure is a thin shell, then the use of integral bosses requires a material of larger initial thickness and a more extensive milling.

Bosses can also be fabricated by welding a circular machined ring, containing the bosses, to the bulkhead. However, this method induces residual stresses in the material as a result of the welding process.

Non-integral support provisions are machined fittings, such as ports, flanges, and support pads, which are welded to the tank skin. For this purpose, it is necessary to provide a material whose thickness is greater than the thickness of the tank skin, in order compensate for the loss of strength due to welding. Otherwise, for the same reason, it is necessary to lower the permissible operating pressure of the tank. In tanks for liquid propellants, a single access opening is frequently used. This is obtained by using a close-out cover which contains the lines for input and output. When multiple tanks are connected in series, the inlet lines are connected to standpipes within the tanks, in order to preclude reverse flow of propellant and to ensure feed-out in series.

Openings and access doors are ports and access points in the skin of a tank. Three examples are shown in the following figure, due to the courtesy of NASA [22].



Openings and access doors are usually located in or near the apex of a bulkhead. The primary requirements for these access points is the prevention of leakage during the entire service life of a rocket vehicle. The method marked with (a) in the preceding figure uses a door with a bearing lip and oversized holes, in order to reduce rotation at the joint because of eccentric bolt shear loading. The method marked with (b) uses a bulkhead boss of large cross-sectional area, in order to force most of the load to remain in the bolting ring instead of going through the door. The method marked with (c) uses a door ring placed above the apex of the bulkhead, and has been chosen for the forward door of the Centaur rocket stage.

References

1. Anonymous, Space Shuttle, NASA SP-407. <https://history.nasa.gov/SP-407/p38.htm>
2. Flügge W, Sobel LH (1965) Stability of shells of revolution: general theory and application to the torus. Ph.D. Dissertation, Mar 1965, 138 pp. <https://apps.dtic.mil/dtic/tr/fulltext/u2/617197.pdf>
3. Young WC, Budynas RG (2002) Roark's formulas for stress and strain, 7th edn. McGraw-Hill, New York. ISBN 0-07-072542-X
4. Flügge W (1960) Stresses in shells. Springer, Berlin
5. The Engineering Toolbox, Young's modulus—tensile and yield strength for common materials. https://www.engineeringtoolbox.com/young-modulus-d_417.html
6. Abramson HN (ed) (1966) The dynamic behaviour of liquids in moving containers with application to space vehicle technology, Southwest Research Institute, NASA SP-106, 464 pp, Jan 1966. <https://ntrs.nasa.gov/archive/nasa/casi.ntrs.nasa.gov/19670006555.pdf>
7. Abramson HN (1969) Slosh suppression, NASA SP-8031, 36 pp, May 1969. http://everyspec.com/NASA/NASA-SP-PUBS/NASA-SP-8031_20669/
8. Dodge FT (2000) The new "Dynamic behaviour of liquids in moving containers". Southwest Research Institute, 202 pp. ftp://apollo.ssl.berkeley.edu/pub/ME_Archives/Government%20and%20Industry%20Standards/NASA%20Documents/SwRI_Fuel_Slosh_Update.pdf
9. Abramson HN, Bhuta PG, Hutton RE, Stephens DG (1968) Propellant slosh loads, NASA SP-8009, 32 pp, Aug 1968. <https://ntrs.nasa.gov/archive/nasa/casi.ntrs.nasa.gov/19690005221.pdf>
10. Pérez JG, Parks RA, Lazor DR (2012) Validation of slosh model parameters and anti-slosh baffle designs of propellant tanks by using slosh testing, NASA, 27th Aerospace testing seminar, Oct 2012. <https://ntrs.nasa.gov/archive/nasa/casi.ntrs.nasa.gov/20130000590.pdf>
11. Lomen DO (1965) Liquid propellant sloshing in mobile tanks of arbitrary shape, NASA CR-222, NASA Langley Research Centre, 72 pp, Apr 1965. <https://ntrs.nasa.gov/archive/nasa/casi.ntrs.nasa.gov/19650012759.pdf>
12. Fries N, Behruzi P, Arndt T, Winter M, Netter G, Renner U (2012) Modelling of fluid motion in spacecraft propellant tanks—sloshing. In: Space propulsion 2012 conference, 7th–10th May 2012, Bordeaux, France, 11 pp. https://www.flow3d.de/fileadmin/download_publikationen/modelling-fluid-motion-in-spacecraft-propellant-tanks-sloshing-2012.pdf
13. Stephens DG, Leonard HW, Perry TW Jr (1962) Investigation of the damping of liquids in right-circular cylindrical tanks, including the effects of a time-variant liquid depth, NASA TN D-1367, July 1962, 32 pp. <https://ntrs.nasa.gov/archive/nasa/casi.ntrs.nasa.gov/19620004069.pdf>
14. Hopfinger EJ, Baumbach V (2009) Liquid sloshing in cylindrical fuel tanks. Progr Propul Phys 1:279–292. <https://www.eucass-proceedings.eu/articles/eucass/pdf/2009/01/eucass1p279.pdf>
15. Keulegan GH, Carpenter LH (1958) Forces on cylinders and plates in an oscillating fluid. J Res Natl Bur Stan 60(5):423–440, Research Paper 2857. https://nvlpubs.nist.gov/nistpubs/jres/60/jres60n5p423_A1b.pdf
16. Miles JW (1958) Ring damping of free surface oscillations in a circular tank. J Appl Mech 25(2):274–276
17. Bauer HF (1960) Theory of the fluid oscillations in a circular cylindrical ring tank partially filled with liquid, NASA TN D-557, 124 pp
18. Sumner IE (1964) Experimental investigation of slosh-suppression effectiveness of annular-ring baffles in spherical tanks, NASA TN D-2519, 22 pp, Nov 1964. <https://ntrs.nasa.gov/archive/nasa/casi.ntrs.nasa.gov/19650001203.pdf>
19. Stephens DG, Leonard HW, Silveira MA (1961) An experimental investigation of the damping of liquid oscillations in an oblate spheroidal tank with and without baffles, NASA TN D-808, 28 pp, June 1961. <https://ntrs.nasa.gov/archive/nasa/casi.ntrs.nasa.gov/19990017908.pdf>
20. Stephens DG, Scholl HF (1967) Effectiveness of flexible and rigid ring baffles for damping liquid oscillations in large-scale cylindrical tanks, NASA TN D-3878, Mar 1967, 34 pp. <https://ntrs.nasa.gov/archive/nasa/casi.ntrs.nasa.gov/19670010559.pdf>

21. Anonymous, Saturn V Flight Manual SA-503, NASA-TM-X-72151, MSFC-MAN-503, Nov 1968, 243 pp. <https://ntrs.nasa.gov/archive/nasa/casi.ntrs.nasa.gov/19750063889.pdf>
22. Wagner WA, Keller RB Jr (ed) (1974) Liquid rocket metal tanks and tank components, NASA SP-8088, 165 pp, May 1974. <https://ntrs.nasa.gov/archive/nasa/casi.ntrs.nasa.gov/1975004950.pdf>
23. Roberts JR, Basurto ER, Chen PY (1966) Slosh design handbook I, NASA CR-406, 328 pp, May 1966. <https://ntrs.nasa.gov/archive/nasa/casi.ntrs.nasa.gov/19660014177.pdf>
24. Stofan AJ, Sumner IE (1963) Experimental investigation on the slosh damping effectiveness of positive-expulsion bags and diaphragms in spherical tanks, NASA TN D-1712, 22 pp, June 1963. <https://ntrs.nasa.gov/archive/nasa/casi.ntrs.nasa.gov/19630006725.pdf>
25. MIL-HDBK-5J: Metallic materials and elements for aerospace vehicle structures, 31 Jan 2003. http://everspec.com/MIL-HDBK/MIL-HDBK-0001-0099/MIL_HDBK_5J_139/
26. Hood DW, Eichenberger TW, Lovell DT (1968) An investigation of the generation and utilisation of engineering data on weldments, The Boeing Company, Technical Report AFML-TR-68-268, Oct 1968. <https://apps.dtic.mil/dtic/tr/fulltext/u2/851938.pdf>
27. von Mises R (1913) Mechanik der festen Körper im plastisch- deformablen Zustand, Nachrichten von der Gesellschaft der Wissenschaften zu Göttingen, Mathematisch-Physikalische Klasse, vol 1913, pp 582–592. <http://eudml.org/doc/58894>
28. Hill R (1948) A theory of the yielding and plastic flow of anisotropic metals. Proc R Soc A 193(1033):281–297. <https://royalsocietypublishing.org/doi/pdf/10.1098/rspa.1948.0045>
29. Meuwissen MHH (1995) Yield criteria for anisotropic elasto-plastic materials. Eindhoven University of Technology, 24 pp. <https://pure.tue.nl/ws/portalfiles/portal/4299264/653055.pdf>
30. Whitfield HK, Keller RB Jr (eds) (1970) Solid rocket motor metal cases, NASA SP-8025, Apr 1970, 110 pp. <https://ntrs.nasa.gov/archive/nasa/casi.ntrs.nasa.gov/19700020430.pdf>
31. Gerds AF, Strohecker DE, Byrer TG, Boulger FW (1966) Deformation processing of titanium and its alloys, NASA TM X-53438, Apr 1966. https://ia601209.us.archive.org/13/items/NASA_NTRS_Archive_19660016988/NASA_NTRS_Archive_19660016988.pdf
32. Strohecker DE, Gerds AF, Henning AF, Boulger FW (1966) Deformation processing of stainless steel, NASA TM X-53569. https://ia800308.us.archive.org/22/items/nasa_techdoc_19670022702/19670022702.pdf
33. Slunder CJ, Hoenie AF, Hall AM (1967) Thermal and mechanical treatment for precipitation-hardening stainless steel, NASA SP-5089, Jan 1967, 207 pp. <https://ntrs.nasa.gov/archive/nasa/casi.ntrs.nasa.gov/19680010964.pdf>
34. Corbett J (2017) Welding, NASA, 7 Aug 2017. https://www.nasa.gov/centers/wstf/supporting_capabilities/machining_and_fabrication/welding.html
35. Carter B (2013) Introduction to friction stir welding (FSW), NASA, Glenn Research Centre, Advanced Metallics Branch, 8 May 2013, 25 pp. <https://ntrs.nasa.gov/archive/nasa/casi.ntrs.nasa.gov/20150009520.pdf>
36. Anonymous, Space Shuttle Technology Summary, Friction Stir Welding, NASA Marshall Space Flight Centre, FS-2001-03-60-MSFC. https://www.nasa.gov/centers_marshall/pdf/104835main_friction.pdf
37. Anonymous, A Bonding Experience: NASA Strengthens Welds, NASA. https://www.nasa.gov/topics/nasalife/friction_stir.html
38. Brown BF (1970) Stress-corrosion cracking: a perspective review of the problem, NRL Report 7130, Naval Research Laboratory, Washington, D.C., 24 pp, 16 June 1970. <https://apps.dtic.mil/dtic/tr/fulltext/u2/711589.pdf>
39. MIL-HDBK-729: Corrosion and corrosion prevention metals, 21 Nov 1983, 251 pp. http://everspec.com/MIL-HDBK/MIL-HDBK-0700-0799/MIL_HDBK_729_1946/
40. McDaniels S (2018) Forms of corrosion, galvanic corrosion, NASA, Corrosion Engineering Laboratory, J. F. Kennedy Space Centre, 7 Nov 2018. <https://corrosion.ksc.nasa.gov/Corrosion/FormsOf#Galvanic%20Corrosion>
41. DOE-HDBK-1015/1-93, DOE Fundamentals handbook—chemistry, vol 1 of 2, FSC-6910, U.S. Department of Energy, Jan 1993. <https://www.isibang.ac.in/~library/onlinenz/resources/chem-v1.pdf>

42. MIL-STD-889C (2016) Dissimilar metals, 22 Aug 2016. http://everyspec.com/MIL-STD/MIL-STD-0800-0899/MIL-STD-889C_55344/
43. Cataldo CE (1968) Compatibility of metals with hydrogen, NASA TM X-53807, 26 Dec 1968, 26 pp. <https://ntrs.nasa.gov/archive/nasa/casi.ntrs.nasa.gov/19690009664.pdf>
44. Caskey GR Jr (1983) Hydrogen compatibility handbook for stainless steels, U.S. Department of Energy, Office of Scientific and Technical Information, June 1983. <https://www.osti.gov/servlets/purl/5906050>
45. San Marchi C, Somerday BP (2012) Technical reference for hydrogen compatibility of materials, Sandia Report SAND2012-7321, Sept 2012. https://www.sandia.gov/matlsTechRef/chapters/SAND2012_7321.pdf
46. Chandler DL (2019) Observing hydrogen effects in metal, MIT News, Massachusetts Institute of Technology, 4 Feb 2019. <http://news.mit.edu/2019/observing-hydrogens-effects-metal-0205>
47. Tiffany CF (1970) Fracture control of metallic pressure vessels, Technical Report NASA SP-8040, 65 pp, May 1970. <https://ntrs.nasa.gov/archive/nasa/casi.ntrs.nasa.gov/19710004655.pdf>
48. Abramowitz M, Stegun IA (eds) (1972) Handbook of mathematical functions with formulas, graphs, and mathematical tables, National Bureau of Standards, United States Department of Commerce, Dec 1972. http://people.math.sfu.ca/~cbm/aands/abramowitz_and_stegun.pdf
49. McDonnell Douglas, Isogrid design handbook, NASA-CR-124075, Feb 1973, 222 pp. https://femci.gsfc.nasa.gov/isogrid/NASA-CR-124075_Isogrid_Design.pdf
50. Garber S (1959) Structures and materials. In: Space handbook: Astronautics and its applications, , Staff report of the select committee on astronautics and space exploration, United States, Government printing office, Washington. <https://www.history.nasa.gov/conghand/structur.htm>
51. Knighton DJ (1972) Delta launch vehicle isogrid structure NASTRAN analysis, NASA, Conference paper, Sept 1972, 23 pp. <https://ntrs.nasa.gov/archive/nasa/casi.ntrs.nasa.gov/19720025227.pdf>
52. Anonymous, Skylab Saturn IB flight manual, NASA TM-X 70137, NASA, George C. Marshall Space Flight Centre, 30 Sept 1972, 273 pp. <https://ntrs.nasa.gov/archive/nasa/casi.ntrs.nasa.gov/19740021163.pdf>
53. NASA. https://science.ksc.nasa.gov/shuttle/technology/images/et-lox_1.jpg
54. Joyce P, Sandwich structures, United States Naval Academy. https://www.usna.edu/Users/mecheng/pjoyce/composites/Short_Course_2003/13_PAX_Short_Course_Sandwich-Constructions.pdf

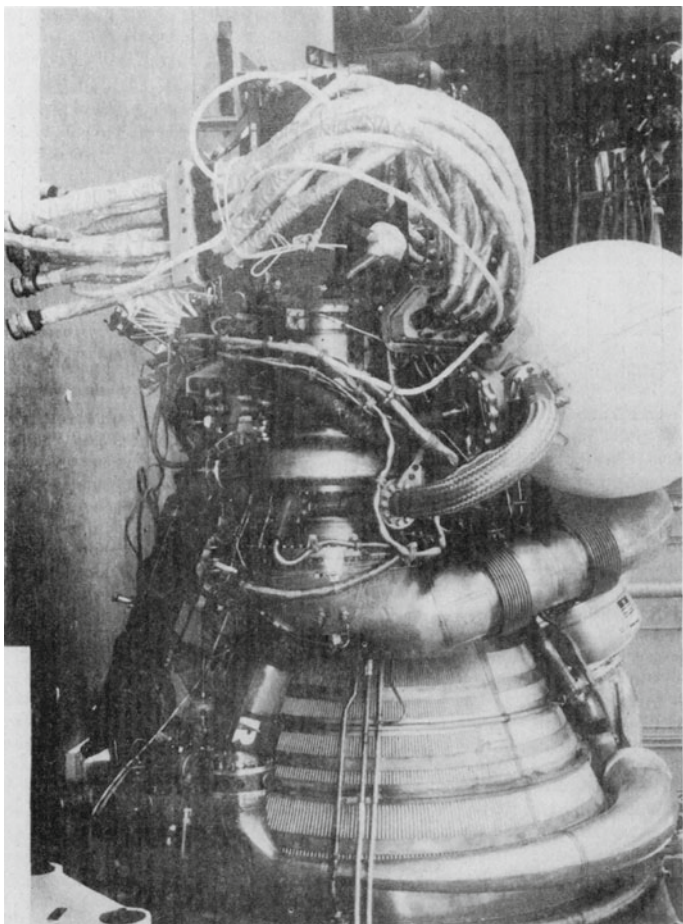
Chapter 7

Interconnecting Components and Structures



7.1 Fundamental Concepts

The present chapter describes interconnecting structures and fluid-carrying ducts which incorporate elements such as bellows, flexible joints, flexible hoses, and flanges. An example is provided by the propellant-supply ducts which convey the fuel and the oxidiser from their tanks in a rocket stage to the respective turbo-pumps. These ducts employ flexible components (hoses, bellows, and joints) to permit freedom of movement during engine gimballing. Some typical assemblies for lines, bellows, and hoses are shown in the following figure, due to the courtesy of NASA [1], which illustrates the J-2 engine, used for the Saturn IB and Saturn V launch vehicles.



The ducts of a liquid-propellant rocket engine have often filters, which maintain the fluids at a desired level of cleanliness, by removing contaminant particles which such fluids may contain. A definition of the principal terms used in this chapter is given below. A line or duct is an enclosed leak-proof passageway through which a fluid is conveyed from one component of a rocket engine to another. A bellows is a cylinder, corrugated along its sidewall, which may be enclosed in a line to permit movement by deflection of its corrugations. A bellows joint may be either a bellows with a restraint linkage or a free bellows alone. A flexible hose is a bendable duct used to carry or transfer a fluid from one point to another. A flange is a rib or rim placed at one end of a duct for attachment to another piece or duct. A flange joint is an attachment of ducts, where the connecting pieces have flanges by which the parts are bolted together. A filter is a device which removes a contaminant from a fluid by

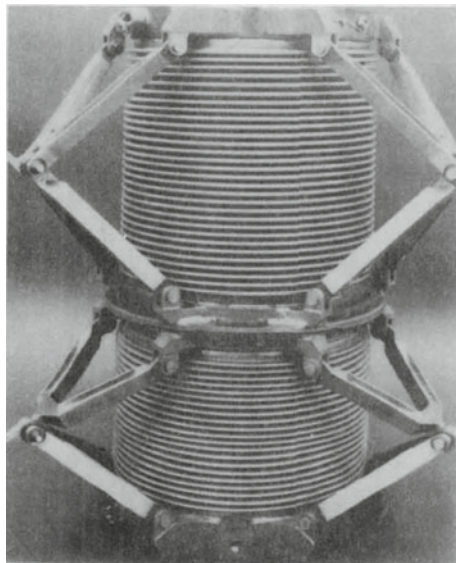
trapping particles of the contaminant within or on the surface of a porous material. According to Howell and Weathers [2], flexible ducts are considered for use instead of rigid ducts under any of the following conditions:

- existence of angular or lateral misalignment of the points to be connected;
- necessity of removing ducts for repair or replacement;
- occurrence of relative motion caused by thermal expansion, duct movement, or structural bending; and
- presence of severe vibration.

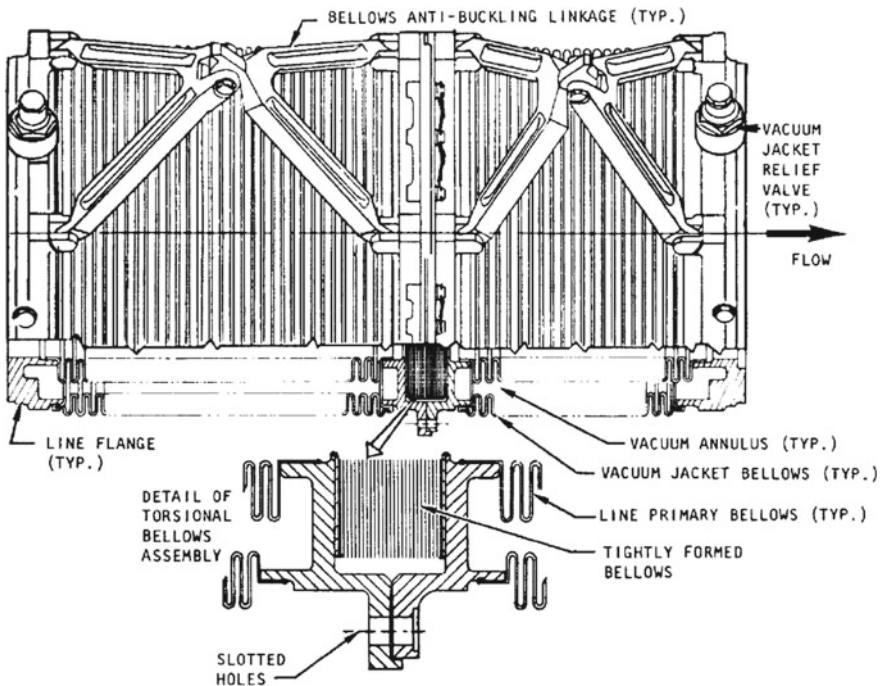
The principal interconnecting ducts and structures in a rocket engine are described in Sect. 7.2. The following sections describe materials, construction, design criteria, and methods of calculation.

7.2 Interconnecting Ducts and Structures in a Rocket Engine

Propellant-supply ducts convey the fuel and the oxidiser from their tanks to the respective turbo-pumps. These ducts, due to their location at the centre of an engine gimbal, are subject to bending and torsional loads. They are also subject to internal pressure, due to the fluids carried by them. The principal requirement for propellant-supply ducts is to keep the pressure losses between the tank outlets and the pump inlets to the minimum possible value. As a result of the many forces acting upon these ducts, restrainers against buckling are frequently required. Such restrainers, if located inside the ducts, contribute to undesired pressure losses. On the other hand, the external location of the restrainers increases the duct size and may create problems of interference of the ducts with other components of the engine. The following figure, due to the courtesy of NASA [1], shows a bellows of the compressed type, externally restrained against buckling.



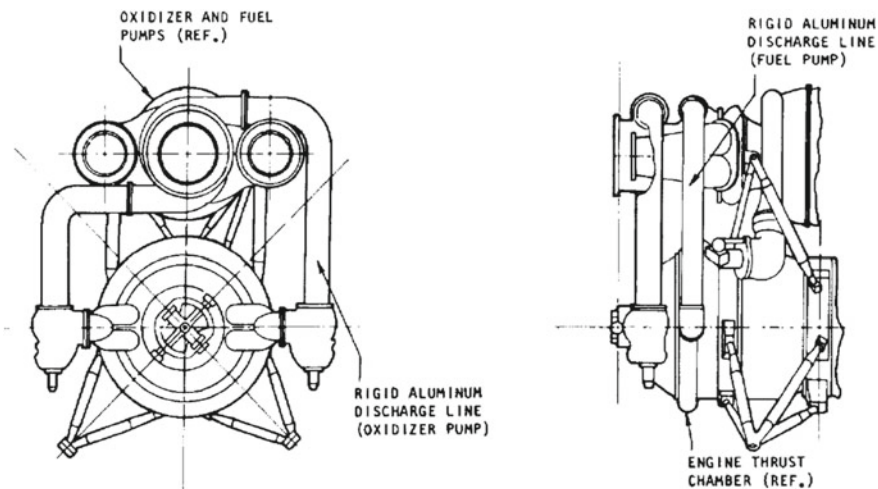
The following figure, also due to the courtesy of NASA [1], shows an anti-buckling device designed to absorb torsional deflection in a pump inlet duct.



The device shown above is a tightly formed bellows assembly, which was incorporated into the pump inlet ducts of the J-2 engine, when the torsional moment of the ducts was found to be too high for the resistance of the pump casing. The bellows is thin-walled (0.254 mm) and over 2540 mm long. It has 40 deep corrugations stacked in a 31.75 mm height. Flanges encompass the bellows and permit the application of only torsional deflections. The joint is substantially a torsion spring of low elastic constant, which can absorb torsional rotations up to $\pi/60$ rad or 3° [1].

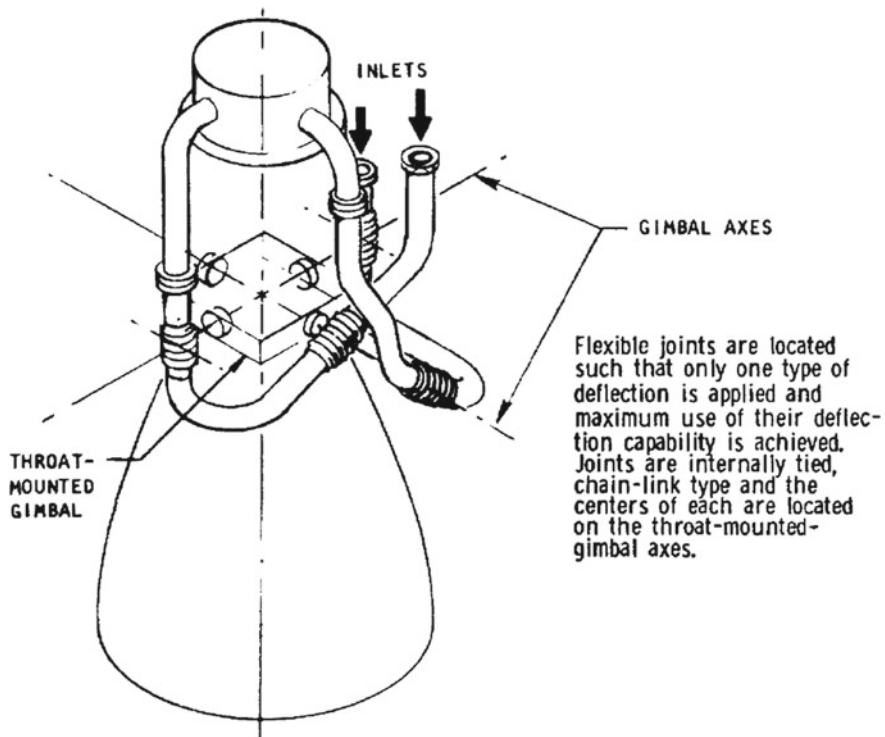
The manufacturer of a rocket vehicle must know the sizes of the connecting flanges, the types of gasket used, and the forces transmitted by the engine ducts to the vehicle when the engine is gimballed. This information is provided by the engine designer. In pump-feed rocket engines, the working relative pressure of propellant-supply ducts ranges from 0.3447×10^6 N/m² to 0.6895×10^6 N/m² and over. In pressure-fed rocket engines, the working absolute pressure of the propellant ducts is less than 3.447×10^6 N/m² [3].

In rocket engines fed by turbo-pumps, the high-pressure propellant ducts for pump discharge connect the outlet sections of the pumps (for respectively the oxidiser and the fuel) to the main fuel valves attached to the thrust chamber. These ducts also contain bellows components. However, some engines have also had rigid (instead of flexible) components, as shown in following figure, due to the courtesy of NASA [1].



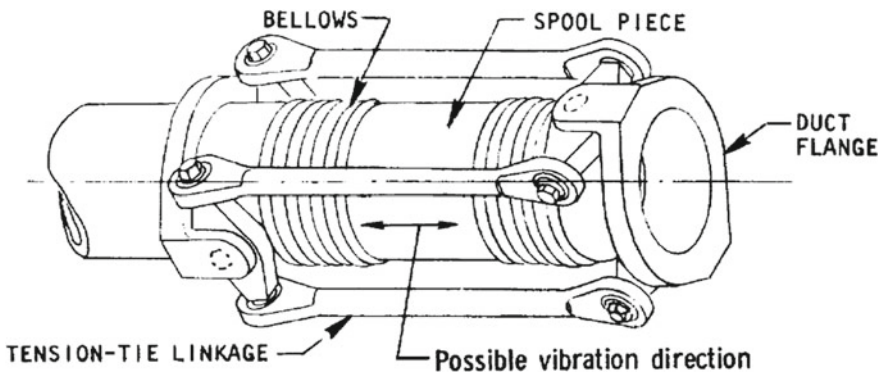
The early F-1 engines incorporated bellows joints in the pump discharge ducts, but these joints were later replaced by hard lines of aluminium with large bends for flexibility. The low modulus of elasticity of aluminium permitted lower end reactions for a given deflection than did a comparable duct of steel or nickel-base alloy. This change was possible because the ducts were not gimballed and were required to absorb only misalignments and thermal effects.

In case of gimbaling engines, a classic configuration for pump discharge ducts is the wraparound duct arrangement, which is shown in following figure, due to the courtesy of NASA [1].



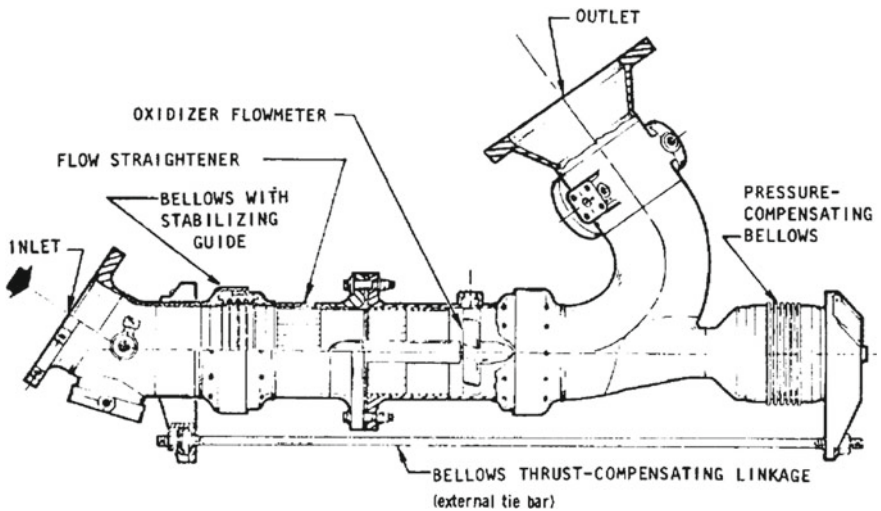
The term wraparound indicates a flexible duct or hose which, as it were, wraps around the thrust-vector-control gimbal of a rocket engine in the plane of the gimbal. This configuration was used for the Navaho, Atlas, Thor, and Jupiter engine pump discharge ducts, for the pump inlet ducts of the H-1 engine, for the gimbaling feed lines of the Apollo Service Module engine, and for the descent engine of the Apollo Lunar Module. This configuration was also used for all of the vehicle-to-engine interface lines of the F-1 engine on the S-IC, except the main propellant lines. In addition, the wraparound concept was used extensively for each of the three main engines of the Space Shuttle. Details on the matter can be found in [1, 4].

The following figure, due to the courtesy of NASA [1], shows a typical pump-discharge high-pressure propellant duct with restraining linkage.



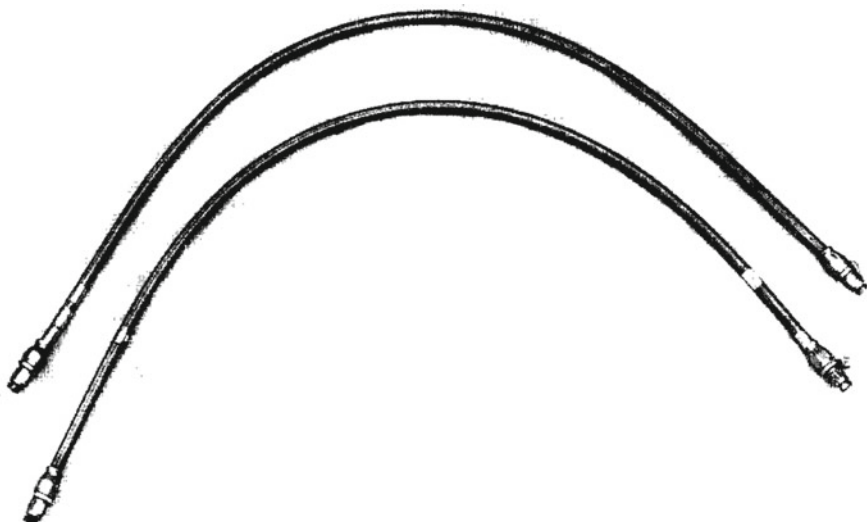
The duct shown above has two bellows separated by a spool piece. This type of duct is subject to vibration of the long unsupported mass.

The following figure, also due to the courtesy of NASA [1], shows a bellows thrust-compensating linkage with external tie bar installed in the oxidiser high-pressure duct of the J-2 rocket engine.



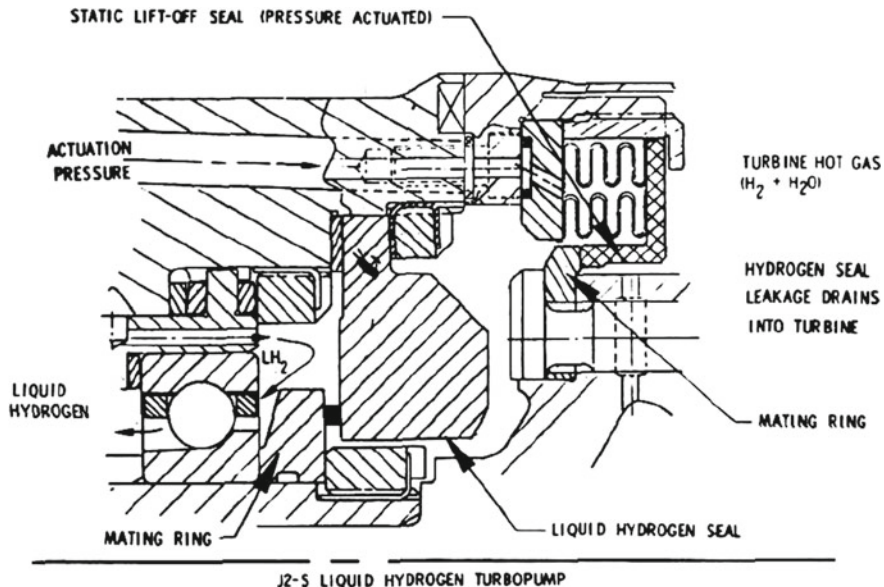
This duct has an external tie bar which acts as a thrust compensator, and two bellows held together by the external tie bar, which limits the movements of the two bellows. One bellows opposes the other in balancing the pressure exerted by the propellant flowing in the duct.

Pressurisation lines for the propellant tanks are used to connect the propellant tanks to sources of pressures, such as gases stored under pressure, gas generators, and heat exchangers for cryogenic propellants. For this purpose, high-pressure hoses and tubing are used. The following figure, due to the courtesy of NASA [5]. shows two 6.35 mm, 34.6 MPa (relative pressure) flexible hoses, which were used for the Saturn I-B rocket stage.



Seal drain lines are often used in case of dynamic seals applied to the shafts or to other moving components of turbo-pumps. Since perfect sealing is difficult to obtain, then drain lines are used between two dynamic seals placed in series. The seal drain lines, which include flexible hoses and tubing, are routed away and overboard. In case of a combination of liquid oxygen with RP-1, the seal drain lines can be routed along the wall of the thrust chamber up to the exit plane of the nozzle. In case of combinations of propellants which can form highly explosive mixtures, these lines are routed to vent ports at the periphery of space vehicles. The seal drain lines are usually routed to the periphery of the vehicles during boost flight, and to the exit of the thrust chamber during stage operation [3].

Seal drains for liquid hydrogen are routed to a safe disposal area, because of the hazard of mixing liquid hydrogen with atmospheric air. Therefore, leaking hydrogen is not allowed to accumulate inside a rocket vehicle. For liquid-hydrogen turbo-pumps, the external drains are usually eliminated, and the seal leakage is allowed to vent into the turbine area, as shown in the following figure, due to the courtesy of NASA [6], which illustrates a particular of the liquid-hydrogen turbo-pump used for the J2-S engine.



Pneumatic supply lines are used in rocket engines to provide pneumatic pressure required for several purposes. For example, as described at length in [4], the pneumatic control assembly of the Space Shuttle provide central control of all pneumatic functions, such as:

- engine preparation and shutdown purges;
- bleed valve operation; and
- engine pneumatic shutdown, including pogo post-charge.

The pneumatic pressure is provided by gases stored in vessels, which are charged before flight through high-pressure flexible lines. The design of such lines depends on the mating connexions on the vehicle side, on the type of gas used, and on its temperature and pressure.

Cryogenic-propellant bleed lines are used in cryogenic-propellant engines feed by turbo-pumps. This is because adverse conditions for such engines may occur during start, when the metallic walls containing cryogenic fluids are at insufficiently low temperatures, and also when the cryogenic fluids downstream of the tank outlet are superheated. In addition, the pressure which opens the main valves and starts the turbo-pumps reduces further the static pressure at the inlet of the turbo-pumps, and this accelerates the production of gas. This, in turn, may lead to cavitation in the pumps and to malfunction of the gas generator.

In order to avoid such undesirable events, a continuous bleed from a point farthest downstream of the pump inlet is applied before engine start. By so doing, fresh liquid at the bulk temperature of the tank replaces continuously the warming fluid and cools the metallic walls of the containers. The bleeds are ducted away from the launch site, because they can form combustible or even explosive mixtures. This

requires a line to duct away the bleeds. Wire-braided flexible hoses and tubing are generally used for such lines. In case of cryogenic-propellant engines used for upper stages of rockets, a re-circulation system is used, which re-directs the propellants to their tanks instead of dumping them overboard. Flexible lines between the engine and the rocket vehicle are required for this purpose. In order to reduce bleeds and re-circulating flows, it is possible to provide the rocket vehicle with means (such as cooling, thermal insulation, etc.) apt to keep the bulk temperatures of the propellants sufficiently below their boiling temperatures at the operating pressures in the tanks.

Purge lines are required for rocket engines. This is due to the necessity of performing purges during the start and shutdown sequence, and also before and after servicing, to keep the engines dry. These purges are executed by using non-reactive gases, such as nitrogen at ambient temperature, in order to prevent the formation of combustible mixtures, and to expel residual propellants.

As an example, for the F-1 engine, a gaseous nitrogen purge is applied for thermal conditioning and for elimination of explosive mixtures under the engine envelope. Since low temperatures may exist in the space between the engine and its envelope for thermal insulation, then heated nitrogen is applied to this space. This purge is manually operated, whenever there is a prolonged hold of the countdown with liquid oxygen onboard and with an ambient temperature below approximately 286 K. This purge is turned off five minutes prior to ignition command and is continued during the time of umbilical connexion.

A continuous nitrogen purge is also required to expel propellant leakage from the seal housing of the liquid-oxygen turbo-pump and from the liquid-oxygen injector of the gas generator. The pressure of the purging gas improves the properties of the liquid-oxygen seal. This purge is required from the time at which the propellants are loaded and is continuous throughout flight.

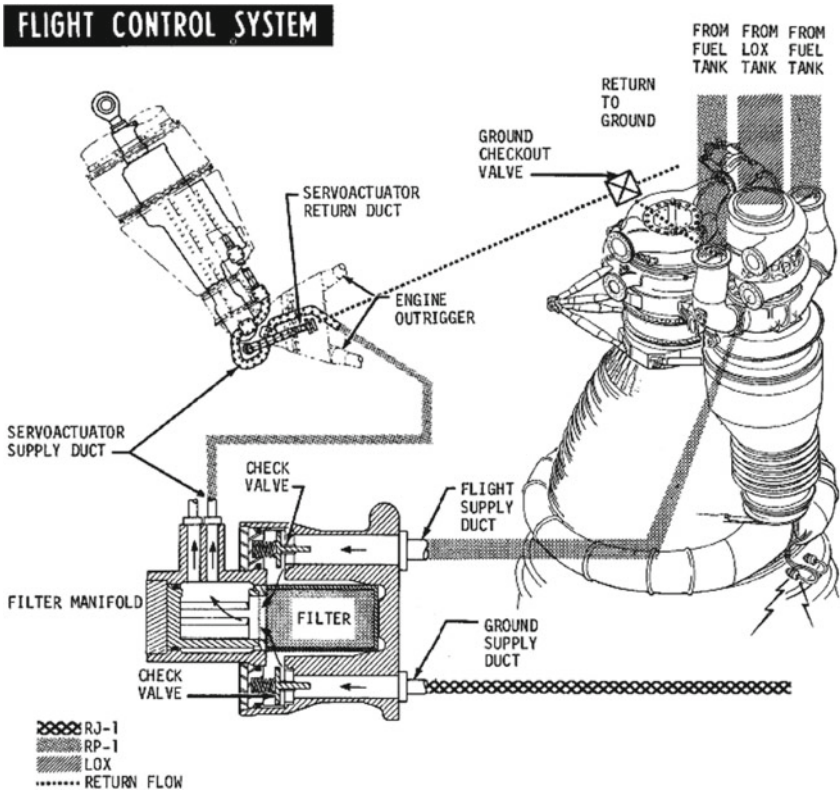
A nitrogen purge prevents contaminants from accumulating on the viewing surfaces of the radiation calorimeter. This purge is started 52 s before scheduled lift-off time and is continued during flight.

A gaseous nitrogen purge is required to prevent contaminants from entering the liquid-oxygen system through the liquid-oxygen injector of the main engine or the liquid-oxygen injector of the gas generator. This purge is started prior to engine operation and is continued during the time of umbilical connexion.

At approximately 13 h before scheduled lift-off time, an ethylene glycol solution fills the thrust tubes and the manifolds of the engine. This inert solution serves to smooth out the combustion sequence at engine start. Flow is terminated by a signal from an observer at the engine.

At approximately 5 min before scheduled lift-off time, 186.3 l (0.1893 m³) are supplied to top off the system to compensate for liquid loss which occurred during engine gimballing [7].

Hydraulic ducts for high-pressure liquids are used in liquid-propellant rocket engines, as shown in the following figure, due to the courtesy of NASA [7], which illustrates the outboard engine fluid system used for the five F-1 engines of the S-IC first stage of the Saturn V rocket.



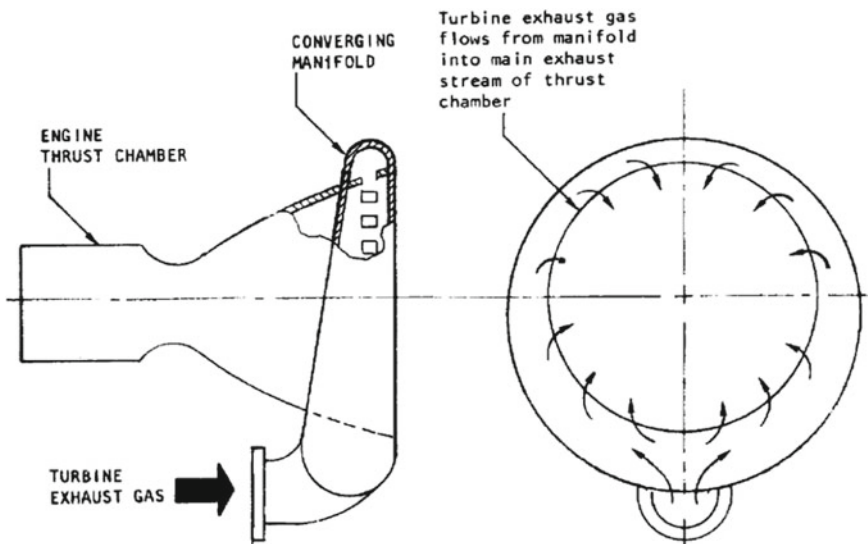
The flight control system of the S-IC gimbals the four outboard engines to provide attitude control during the burn phase of the S-IC. For this purpose, the hydraulic pressure is supplied from a Ground Support Equipment (GSE) pressure source during test, pre-launch checkout, and engine start. When the engine starts, hydraulic pressure is generated by the turbo-pump of the engine.

Pressure from either source is made available to the engine valves, such as the main fuel and liquid-oxygen valves and the igniter fuel valve. These valves are sequenced and controlled by the terminal countdown sequencer, stage switch selector and by mechanical and fluid pressure means. Fluid under pressure also flows through a filter, shown in the preceding figure, and to the two flight control servo-actuators on each outboard engine. The fluid power system illustrated above uses both RJ-1 ramjet fuel and RP-1 rocket propellant as hydraulic fluid.

The RJ-1 is used by the Hydraulic Supply and Checkout Unit (GSE pressure source). RP-1 is the fuel used in the S-IC stage. It is pressurised by the engine turbo-pump. The two pressure sources are separated by check valves while return flow is directed to GSE or stage by the ground checkout valve. Drilled passages in the hydraulic components (valves and servo-actuators) permit a flow of fluid to thermally condition the units and to bleed gases from the fluid power system [7].

In most rocket engines feed by turbo-pumps, the gas generator is connected directly to the turbine inlet, and consequently no special ducts are necessary. In other rocket engines, high-pressure hot-gas ducts are required to connect the gas generator to the turbines. Such is the case with engines having two individual turbo-pumps. Still in other rocket engines, high-pressure hot-gas ducts are required to connect the tap-off ports of the thrust chamber with the turbine. Such is the case with engines (the J-2S, for one) based on the thrust chamber tap-off cycle, which has been described in Chap. 2, Sect. 2.7. High-pressure hot-gas ducts have rigid portions and also flexible portions, which are made of stainless steels and nickel-based alloys apt to resist temperatures up to about 1200 K. These ducts must be capable of absorbing deflections due to thermal expansion and also deflections due to misalignments and dynamic loads [3].

Liquid-propellant rocket engines have ducts for the hot gases exhausted by the turbines. These gases may be ducted either to a region near the exit plane of the nozzle or to a manifold of the thrust chamber. By the way, a manifold is a duct having one or more branches off the main flow stream. Common types are T-shaped and Y-shaped manifolds. The main function of a manifold is to distribute flow from one or more inlet passages to one or more outlet passages. A typical manifold for turbine exhaust gas used in a liquid-propellant rocket engine is shown in the following figure, due to the courtesy of NASA [1].

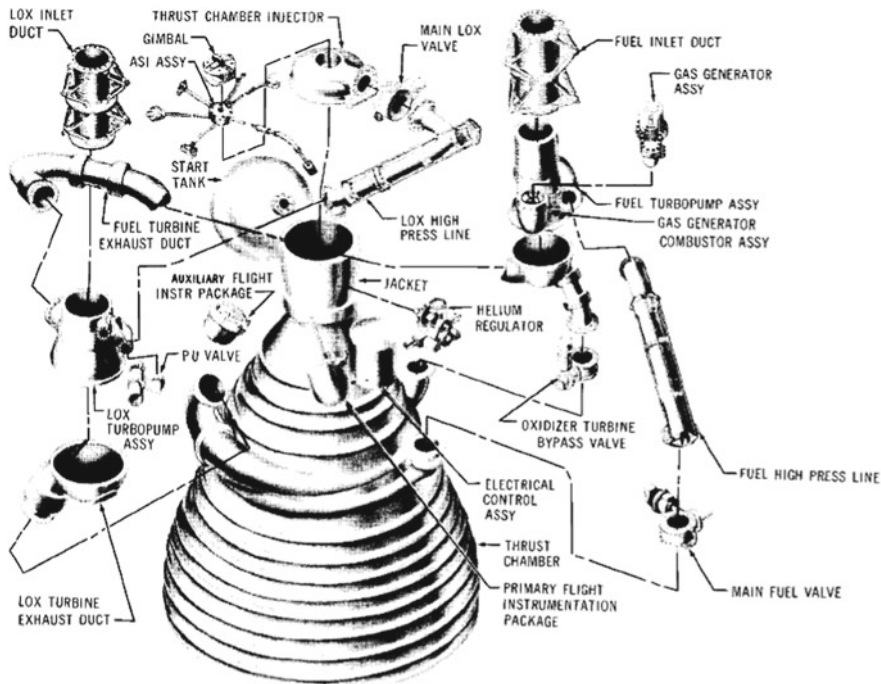


The manifold illustrated in the preceding figure is designed for equal distribution of flow. In other words, the flow areas inside the manifold are designed so as to split equally the flow among the branches. The gas exhausted by the turbine is dumped into the mainstream exhaust of the thrust chamber through an annular manifold. The cross-sectional area of the manifold decreases as it wraps around the thrust chamber,

in order for the gas to maintain a constant velocity as it is bled off through openings in the wall of the thrust chamber [1].

In the particular case of the J-2 engine, the turbines of the oxidiser (liquid oxygen) and fuel (liquid hydrogen) turbo-pumps are connected in series by exhaust ducting which directs the discharged exhaust gas from the fuel turbo-pump turbine to the inlet of the oxidiser turbo-pump turbine manifold. One static and two dynamic seals in series prevent the turbo-pump oxidiser fluid and the turbine gas from mixing. Both turbo-pumps are powered in series by a single gas generator, which uses the same propellants as the thrust chamber. During burn periods, the liquid-oxygen tank is pressurised by liquid oxygen flowing through the heat exchanger in the oxidiser turbine exhaust duct. The heat exchanger heats the liquid oxygen, causing it to expand. The liquid-hydrogen tank is pressurised during burn periods by gaseous hydrogen from the thrust chamber fuel manifold [7].

The following figure, due to the courtesy of NASA [8] is an exploded view of the principal interconnecting components of the J-2 engine.

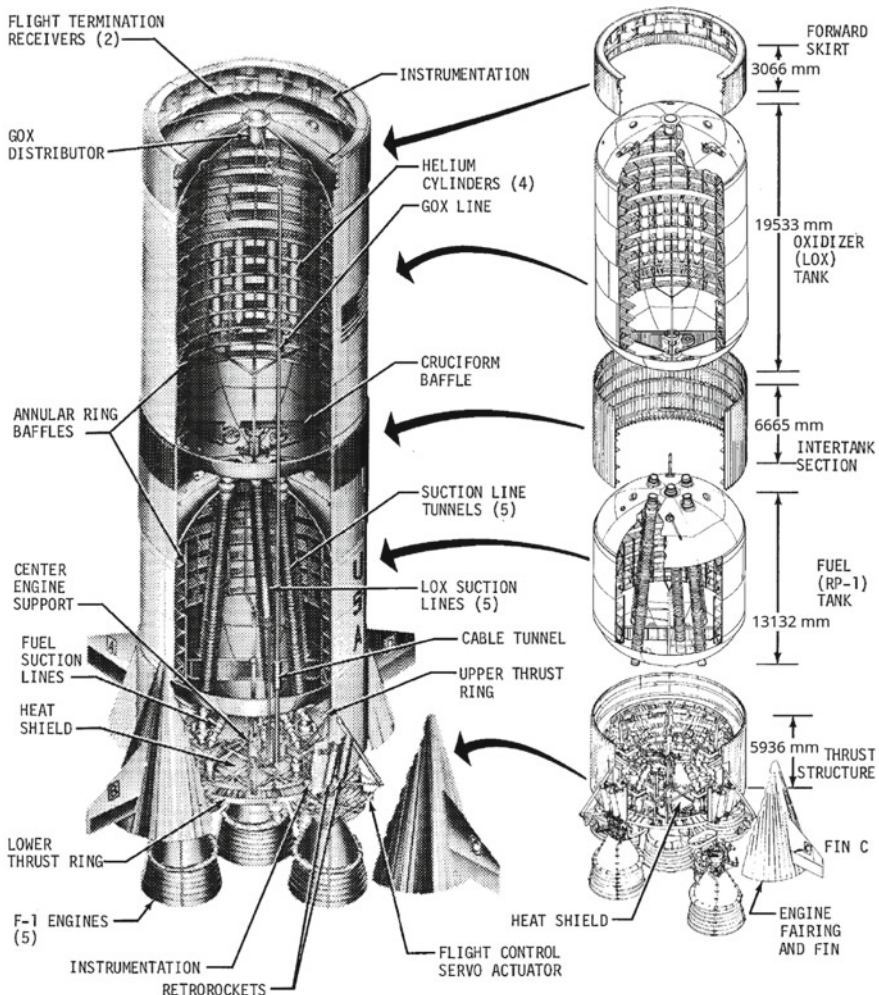


Each stage of a rocket vehicle has a thrust structure assembly, whose principal function is to redistribute the loads applied locally by the engines into a uniform loading about the periphery of a tank (usually, the fuel tank). It also provides support for the engines, engine accessories, base heat shield, engine fairings and fins, propellant lines, retrorockets, and environmental control ducts.

The following figure, adapted from [7], shows the S-IC stage of the Saturn V launch vehicle. This stage is propelled by five F-1 engines.

The lower thrust ring shown in the following figure has four hold-down points, which support the fully loaded Saturn/Apollo (approximately 2.722×10^6 kg) and also, as necessary, restrain the vehicle from lifting off at the full thrust of the F-1 engines. The skin segments are made of 7075-T6 aluminium alloy.

S-IC STAGE



In most liquid-propellant rocket engines fed by turbo-pumps, the complete engine assembly is gimballed by using a gimbal mechanism having a spherical joint, as has been shown in Chap. 5, Sect. 5.6. This joint connects the thrust chamber to the thrust structure (described above) of the rocket vehicle.

A turbo-pump structure is used to fasten the turbo-pumps to either the thrust chamber or other structural elements, such as the thrust structure. The turbo-pump mounts are the connexions between the turbo-pump assembly and the engine. These mounts support the loads due to the weight of the turbo-pump assembly and also react to the loads due to engine inertia, propellant inertia, engine gimballing, differences of pressure in fluids, forces on the flanges, and gyroscopic forces. In addition, the turbo-pump mounts adapt to the differential thermal expansion or contraction of the turbo-pump assembly and of the thrust chamber assembly [9].

The most common types of turbo-pump mounts use struts having at least one ball-joint end connexion to accommodate dimensional tolerances and differential thermal expansion or contraction. Ball-ended struts can be arranged triangularly, to yield the lightest structure by loading its members in pure compression or tension. Another arrangement consists of close-coupled, rigid pads at one end of the turbo-pump, and one or two ball-ended struts at the other end to accommodate the dimensional variations [9].

7.3 Materials Used for Tubing in Rocket Engines

The 18–8 (18% chromium and 8% nickel) corrosion-resistant steels are the most frequently used materials for lines and bellows in rocket engines. Nickel-base alloys, such as those of the Inconel® and Hastelloy® families, are also used for ducts and bellows, because of their higher strengths, greater fatigue lives, and better corrosion resistances. Aluminium alloys are used in some non-critical or low-stress applications. Due to forming requirements, only high-ductility alloys in the annealing condition are used for corrugated sections [1].

Bellows-joint restraining brackets for cryogenic propellants are made of metals having face-centred cubic structure, which have high toughness at low temperatures. Restraining brackets for storable propellants are made of high-strength steels having body-centred cubic or face-centred cubic structure.

Flexible hoses, including wire braid, are made of 321 CRES, which is a stabilised austenitic stainless steel with addition of titanium.

Other alloys, such as Hastelloy® C and Inconel® 718, are used for applications in special environments.

Materials used for tubing in rocket engines are chosen according to criteria of chemical compatibility with fluids, physical and mechanical properties, formability, weldability, and costs. These criteria have been considered at length in Chap. 6, Sect. 6.7 for propellant tanks. A brief account is given here for what concerns specifically fluid-carrying ducts and their flexible components.

As to chemical compatibility of fluids with tubing materials, gaseous hydrogen at high pressure causes a loss of ductility in many metallic alloys. This effect depends on the temperature, pressure, and purity of the gas, and also on the exposure time and level of stress.

Ferritic, martensitic, and bainitic steels, nickel-base alloys, and titanium alloys become brittle when exposed to pure hydrogen at room temperature, this effect being higher at increasing pressure. High-strength alloys are often more susceptible than low-strength alloys to loss of ductility.

Austenitic stainless steels such as 310 and 316, some aluminium alloys such as 6061-T6, 2219-T6, and 7075-T73, pure copper and beryllium copper, and the precipitation-hardened stainless steel A-286 are slightly affected. Inconel® 718, Inconel® X-750, Waspaloy®, and René® 41 are highly susceptible to loss of ductility when exposed to gaseous hydrogen at high pressure [1].

The loss of ductility due to hydrogen is associated with a loss of fracture toughness. The presence of hydrogen, water vapour, and other gases increases the effects of crack initiation and crack growth rate.

In addition to hydrogen, substances which can have undesirable effects on metallic tubing are:

- propellants susceptible to catalytic decomposition, such as anhydrous hydrazine, mono-methyl-hydrazine, and Aerozine 50, which generate hot gas in the presence of molybdenum, iron, copper, or silver;
- nitric acid resulting from absorption of water in nitrogen tetroxide, which attacks aluminium alloys;
- chlorides from cleaning fluids, which can induce stress-corrosion cracking in stainless steel 321 CRES; and
- uninhibited (brown) nitrogen tetroxide, which can induce corrosion cracking in titanium alloys.

It is also necessary to take account of the environment to which metals used for tubing are exposed. For example, titanium exposed to oxygen can ignite and oxidise explosively as a result of an impact.

The principal physical and mechanical properties of metals used for tubing are strength, elongation, and density.

Minimum bend radius and fatigue resistance are desirable properties in materials to be used for corrugated walls of bellows. Cryogenic temperatures reduce the toughness of most materials having body-centred cubic structure. Data of some metals and non-metals exposed to low temperatures (from 20.37 to 533.15 K) are given in [10].

Some materials used for flexible lines are aluminium alloy 6061-T6, stainless steel 321 CRES, Hastelloy® C, Inconel® 625, titanium alloy Ti-6Al-4 V annealed, and Inconel® 718 age-hardened. The principal physical and mechanical properties of these materials are given in Table 3, page 45, of [1].

The materials to be used for flexible parts of interconnecting ducts must be chosen with more demanding requirements than the materials for the remaining parts. Among these requirements, the most important are those of formability, and resistance to corrosion and fatigue. In particular, the materials chosen for bellows corrugations or

inner cores of flexible hoses must be ductile. Corrosion resistance is also required for these materials in order to avoid holes and cracks which can give rise to leakage. Fatigue resistance is required in order for a bellows to bear the desired number of flexural cycles. Materials which have shown good properties of strength-to-weight ratio, weldability, and elongation are Inconel® 718, Nitronic® 40 (a high-manganese stainless steel with high strength and excellent resistance to corrosion at high temperatures), and 321 and 347 CRES. In particular, the Nitronic® 40 alloy is scarcely affected by loss of ductility due to hydrogen.

Bolts and nuts for aerospace applications are usually made of corrosion-resistant metals, such as Inconel® 718, Inconel® X-750, Monel® K-500, and René® 41.

The materials indicated above for fluid-carrying ducts have generally good properties of ductility, and therefore deform plastically under stress around the tips of cracks. However, particular conditions of either load or temperature can cause a loss of ductility, in which case a material may fail. Therefore, the choice of a possible material should take account of its fracture toughness and resistance to subcritical flaw growth, as has been shown in Chap. 6, Sect. 6.8.

The formability of a given material depends on its ductility, that is, on its aptitude to form rolls, bends, fittings, and corrugations for bellows. Under this aspect, corrosion-resistant steels and nickel-base alloys have proven to be the best materials for all formed elements of fluid-carrying ducts.

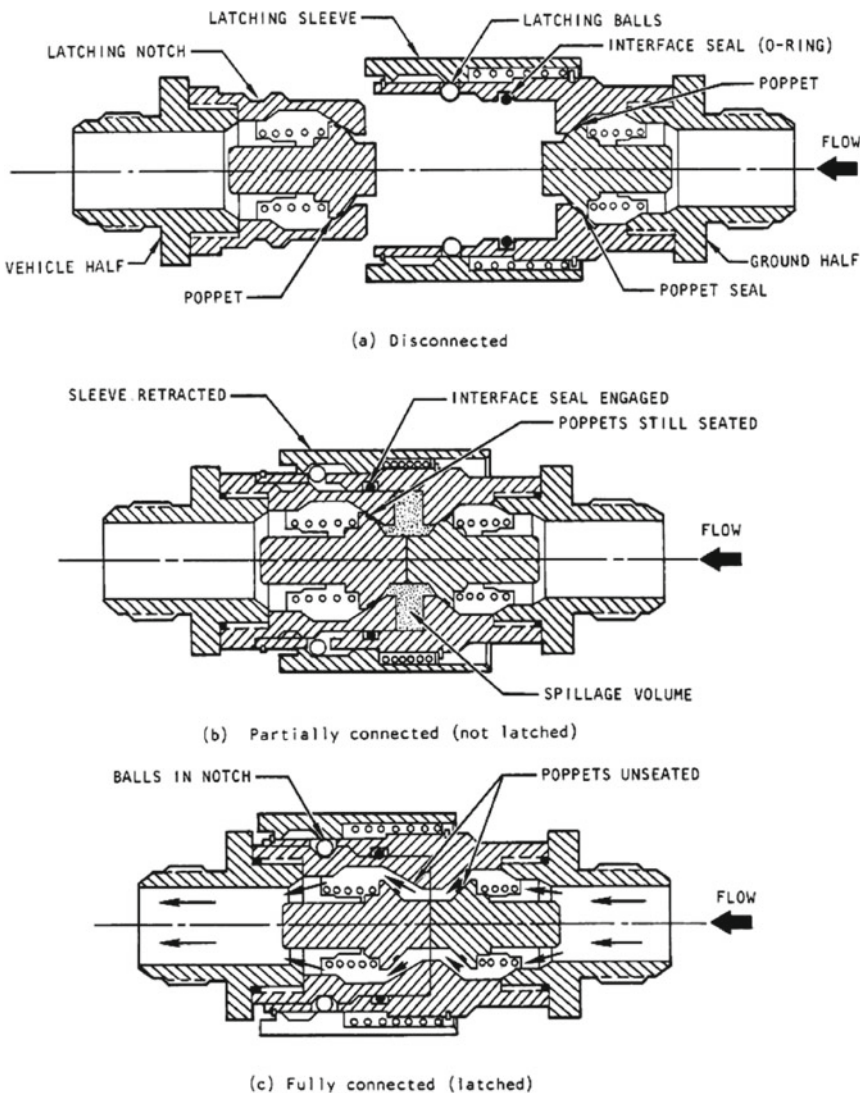
The weldability of a material is important, because welding is the most used method of joining permanently various elements of a line. In case of flexible hoses, brazing is the most common method of connecting permanently the braid of a hose to each of the connecting points. Methods of welding elements of lines include tungsten-inert-gas (TIG) and electron beam, as has been shown in Chap. 6, Sect. 6.7.

Lubricants are sometimes used on the surfaces of bellows or other elements of lines. For this purpose, a corrosion-inhibiting type of molybdenum disulfide (MoS_2) coating can be used for corrosion-resistant steels. Nickel-base alloys resist better than steels to chemical attack. Plating or lubricants are also used on bolts and nuts to prevent thread galling. A thread lubricant used for the Saturn engine systems was a phosphoric-acid-bonded dry-film lubricant. Platings are used at temperatures higher than 422 K [1].

7.4 Coupling Components for Tubing

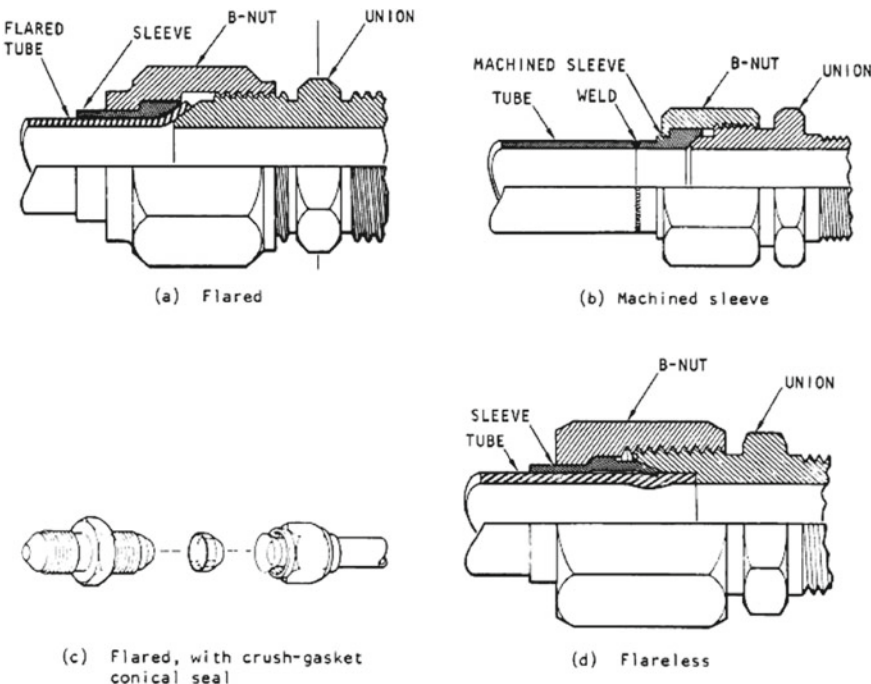
The components described here are devices which contain and control the flow of fluids in ducts. These devices can be classified into the following categories: disconnects, couplings, fittings, fixed joints, and seals. A brief description is given below for each category.

A disconnect is a type of separable connector consisting of two separable halves, an interface seal, and usually a latch-release locking mechanism. The following figure, due to the courtesy of NASA [11], shows three stages of operation of a typical manually-operated disconnect.



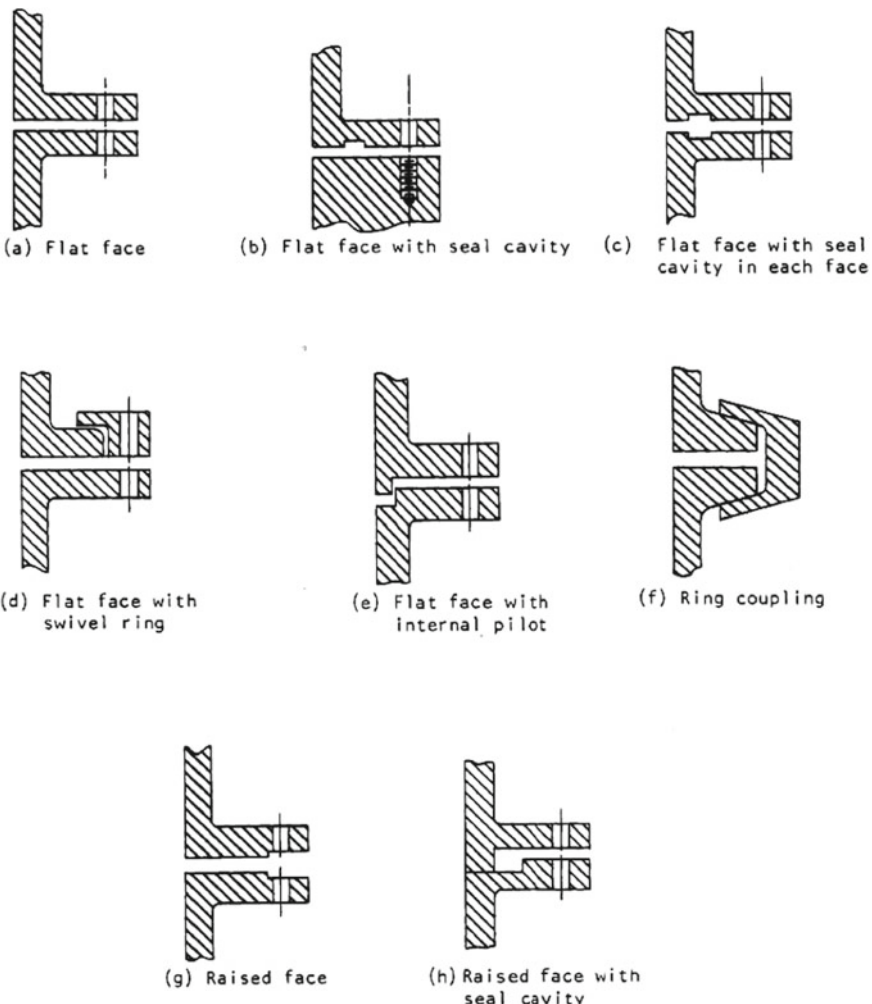
Disconnects are used as interfaces between rocket vehicles and ground systems, or between stages of a rocket vehicle.

A coupling is a mechanically-actuated, separable connector which requires more than a few seconds for engagement or disengagement. Examples of couplings are threaded connectors, bolted flanges, and dynamic swivel couplings. A threaded connector is a line fitting which provides a separable mechanical joint secured by a single threaded nut, whereas a bolted flange connector uses several bolts, a clamp, or a combination of these to secure the joint [2]. The following figure, due to the courtesy of NASA [11], shows four types of threaded connectors.



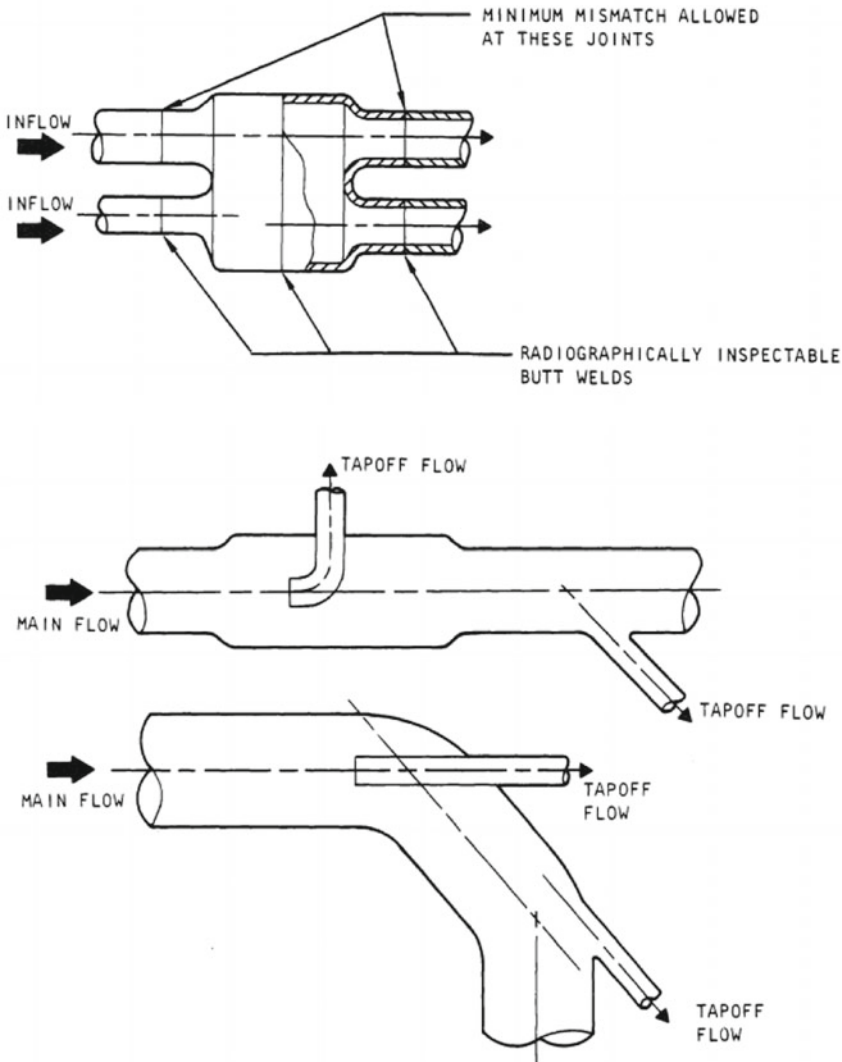
The choice between threaded and flanged connectors is determined by the size of the line and by the amount of preloading required to establish a satisfactory seal over the entire range of loads [2]. Flanged connectors are used where loads require the type of restraining force provided by bolts or clamps, or where coupling reliability dictates the use of more than one threaded clamping fastener [11].

The following figure, due to the courtesy of NASA [11], shows eight types of flanged connectors.



A dynamic swivel coupling is a joint designed such that the swivelling or rotary tubular shaft is pressure-balanced, so as to eliminate high sealing and bearing friction forces caused by axial pressure thrust [2]. On the Saturn engines, swivel couplings were used successfully between moving members of mechanical components (for example, valve stems, actuator shafts, and pistons). However, provisions were made to dispose of leakage, which is inherent in this type of coupling [11].

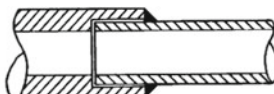
Fittings are devices used to change flow area or direction while connecting two or more straight elements in a tubing, line, or ducting assembly. Such devices are the L-shaped, T-shaped, Y-shaped, et c. tubes used to route fluids to required areas. The following figure, due to the courtesy of NASA [11], shows (above) a low-pressure-loss fitting for joining tubes of different sizes, and (below) two types of tap-off fittings.



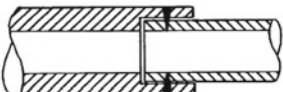
Fixed joints are permanent (that is, non-separable) connexions of fluid-carrying ducts. They are used when low weight and high reliability are more important than ease of separation [2]. The joining methods used for fixed joints are welding, brazing, diffusion bonding, soldering, and interference fit. The following figure, due to the courtesy of NASA [11], shows six types of welded joints used in tubing.



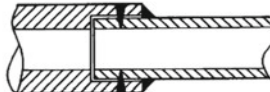
(a) Butt weld



(b) Fillet weld



(c) Sleeve weld



(d) Combination fillet/sleeve



(e) Sleeve weld with separate sleeve

(f) Combination fillet/sleeve with separate sleeve
(eliminates both internal and external crevices)

With reference to the preceding figure, the butt (a), fillet (b), and sleeve (c) types of welded joints are very common. These three types are sometimes used in combinations, the most common of them being fillet and sleeve (f).

When possible, weld joints are located in areas free from vibrations. In particular, locations in which vibrations are perpendicular to the tube axis are avoided. Tungsten Inert Gas (TIG) Welding is the most widely used of the joining methods for fixed joints. Gas Metal Arc (GMA) Welding is also used to join heavy sections, when it is desirable to reduce the number of weld passes needed to complete a joint. These methods have been described in Chap. 6, Sect. 6.7. Electron Beam (EB) Welding (a vacuum-based process in which a beam of high-velocity electrons is applied to the two metals to be joined) is applied in particular cases, for example, to join metals where a narrow weld bead or minimum heat input to the parts is necessary, or to join parts made of titanium alloys, which must be protected from oxygen.

According to Howell and Weathers [2], brazing is a metal-joining operation performed at temperatures ranging between those of welding and soft soldering, where soft soldering temperatures are considered to be below 723 K. Brazing differs from welding, because in the former: (1) bonding results from wetting rather than melting the base alloy; (2) the brazing filler metal (brazing alloy) is made to flow into the joint by capillary action to create the bond; and (3) the brazing filler metal is an alloy having a composition different from that of the metals to be joined. Brazing filler metals used are often alloys of silver, aluminium, gold, copper, cobalt, or nickel.

According to Kazakov [12], diffusion bonding is a process by which a joint can be made between similar and dissimilar metals, alloys, and non-metals, through

the action of diffusion of atoms across the interface, brought about by the bonding pressure and heat applied for a specific length of time.

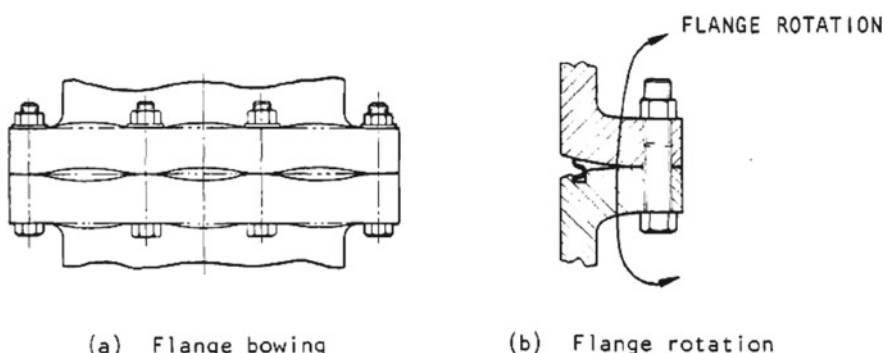
Diffusion bonding has been used for a titanium-to-stainless-steel tubular transition section. These transition joints were developed to provide a fixed joint between titanium propellant tanks and stainless steel lines. Materials commonly diffusion bonded are Ti-5Al-2.5Sn or Ti-6Al-4 V alloys with 304L, 321, and 347 stainless steel. All titanium alloy-to-stainless-steel combinations have been used successfully [11].

Soldering is a metal-joining operation similar to brazing, but takes place with fillers (also known as solders) which melt at a temperature below 723 K.

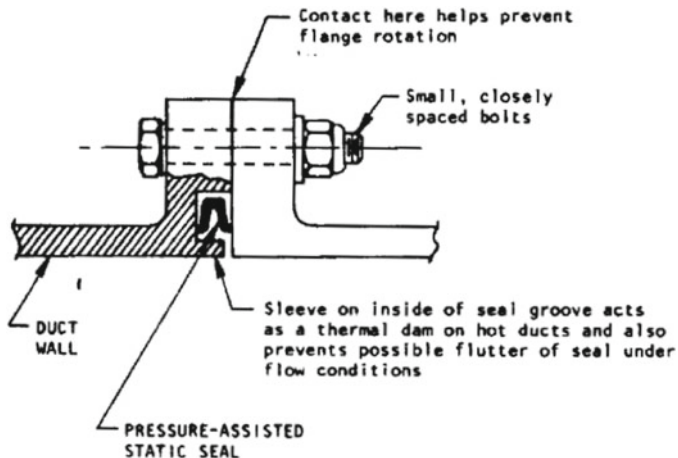
Soldered joints have been successful in low-pressure applications. They are light, require simple heating tools, can be assembled in a minimum envelope, do not need inert-gas shielding, and are readily made on in-place hardware [11].

An interference fit joint, also known as tight fit connector, is a fastening between two parts which uses the pressure exerted by one of the parts against the other to obtain the desired result. For this purpose, the inner diameter of enveloping part (also known as the hole or the hub) is smaller than the outer diameter of enveloped part (also known as the shaft). Therefore, in order to fasten the two parts, it is necessary to apply force during assembly. After the parts are joined, the enveloped part exerts a pressure against the enveloping part along the mating surface, with consequent elastic deformation of the whole assembly. Interference fit joints without the use of some other joining method are not used in ducts for propellants, but are used sometimes in ducts for pneumatic or hydraulic fluids [11]. The definitions of the joining methods indicated above (welding, brazing, diffusion bonding, etc.) are rather intuitive than rigorous, for the sake of clarity. Formal definitions of such methods can be found, for example, in [13].

Connecting flanges or glands for tubing used in aerospace vehicles should be rigid enough to maintain the integrity of static seals. Flanges should have the surface finish, the radial clearances, and the rigidity required by the specific seal used. Flanges having insufficient rigidity or inadequately bolted are susceptible to rotation under operational loads. Two types (bowing and rotation) of flange deflection due to lack of rigidity are shown in the following figure, due to the courtesy of NASA [11].



As a general rule, it is desirable to keep the bolt circumference of a flanged joint as close as possible to the seal, and to use rather many bolts of small diameter than a few bolts of large diameter. NASA [1] recommends the following design for a flanged joint.

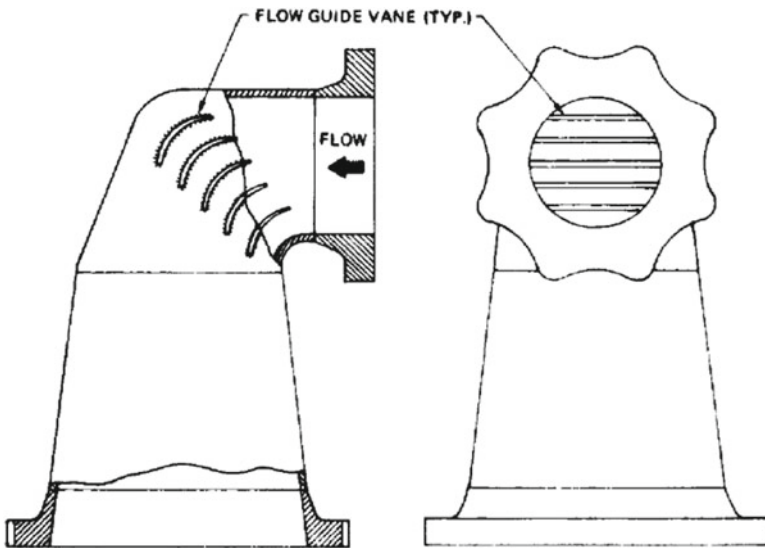


7.5 Control of Pressure Loss in Tubing

Causes of pressure loss in tubing are changes of flow direction, changes of flow area, changes of flow distribution, and friction between a flowing fluid and the walls of a duct.

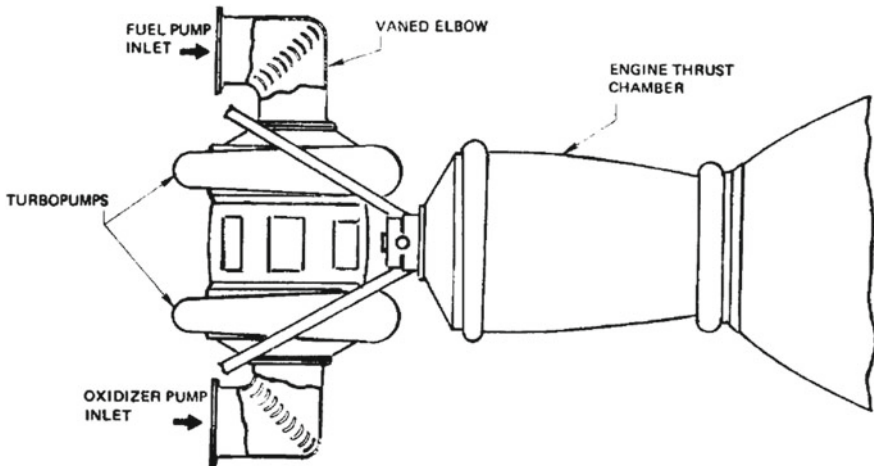
As to the first cause, when the interfaces between the tanks and the pumps or between the pumps and the combustion chamber of a rocket engine do not permit rectilinear ducts, then elbow-shaped parts of tubing must be used. For a given Reynolds number, the pressure loss coefficient for an elbow decreases, reaches a minimum value, and then increases as the ratio R/D of the bend radius to the inside diameter of the elbow increases.

When the routing of a line requires elbows of small bend radii, the consequent pressure losses can be reduced by either choosing the optimum value of the R/D ratio for each elbow, or adding flow guide vanes to the elbows, as shown in the following figure, due to the courtesy of NASA [1].



Flow guide lines have been used in sharp elbows at the pump inlet ducts of the engines of the Centaur, Thor, Atlas, and Saturn S-IC. Such vanes have also been used in the pump discharge ducts of the Thor and Jupiter. The reduction of pressure losses improves the performance of a rocket engine. Since oscillations of the fluid can excite the flow guide vanes, then their natural frequencies must be calculated, in order to avoid resonance phenomena.

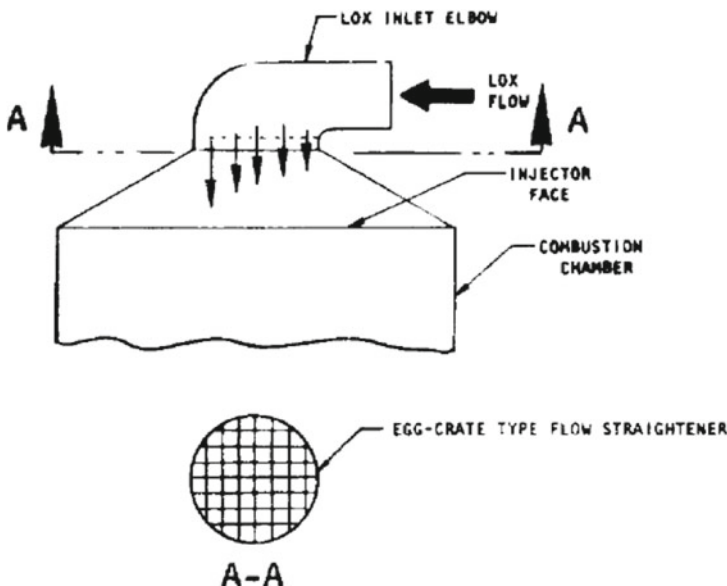
The following figure, due to the courtesy of NASA [1], shows flow guide vanes used in elbows at the inlet ducts of centrifugal turbo-pumps.



In bellows, flow liners are frequently used to reduce the high losses due to friction at the corrugations.

A change in flow area occurs frequently at the two ends of a duct. The shape of the transition portion near each end is to be determined in such a way as to prevent excessive pressure losses, which would take place in case of an abrupt change in flow area. For the same purpose, the edges of a duct at each end should be rounded instead of sharp. In case of expanding conical ducts, the included angle of the cone frustum should be less than or equal to $\pi/18$ rad (10°). For ducts of small diameter having threaded fittings, it is necessary to determine the pressure losses by taking account that the inner diameter of the fitting is usually smaller than the inner diameter of the duct.

The flow distribution at the exit of a duct (for example, at the exit of a feed duct for a rocket engine) is to be determined carefully because of its implications on the performance of the components. For example, when the pumps of a rocket engine have discharge ports placed oppositely, care must be taken in order to have equal pressure losses at the two ports. A flow distribution can be improved by using either flow guide vanes at the elbows, as shown in the preceding figure, or flow straighteners of the egg-crate type placed downstream of the elbows, as shown in the following figure, due to the courtesy of NASA [1].



Another method of achieving a balanced distribution of pressure loss at the terminal ends of two ducts is based on a flow splitter. This method was used in the propellant feed lines of the descent engine of the Apollo Lunar Module.

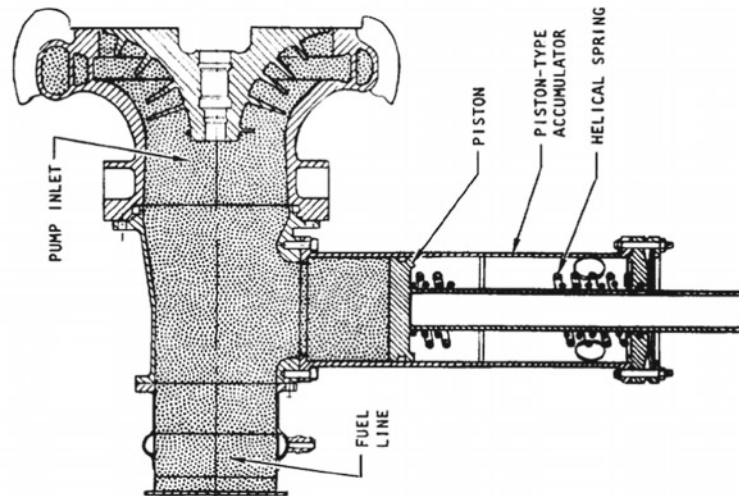
Friction between the walls of a duct and the fluid flowing into it can cause large losses of pressure, in case of ducts having rough walls. To reduce friction, it necessary to use ducts with smooth walls and to avoid protrusions into the flow stream, such as those which are sometimes caused by welds.

7.6 Control of Vibrations at the Inlet of Pumps

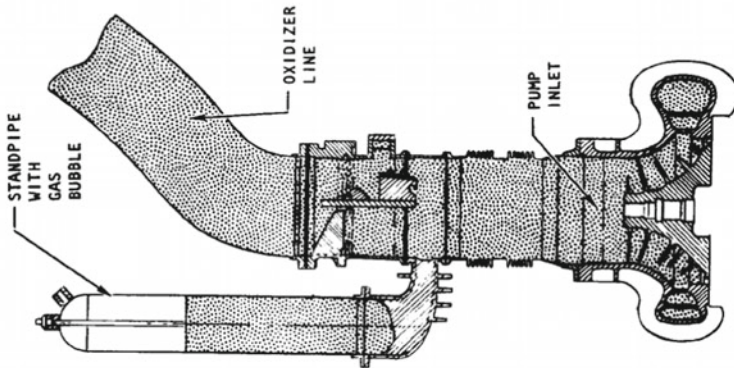
The fundamental concepts on the longitudinal vibrations, called pogo vibrations, of a rocket vehicle have been discussed in Chap. 2, Sect. 2.9. The present paragraph is meant to show in further detail how such vibrations can be suppressed by using devices installed in the feed lines of rocket engines.

The pogo vibrations are due to a feedback interaction between the propulsion system and the structure of a rocket stage. These vibrations are generated by pulsations in the thrust force, which cause a response in the structure. The structural response applies accelerations to the suction part of a propellant feed system. The two feed lines (for respectively the fuel and the oxidiser) respond separately to these accelerations, and cause pressure pulses at the inlet of the two pumps. As a result of these pressure pulses, the pumps and the discharge lines transmit a varying rate of propellant flow to the combustion chamber. The combustion chamber, in turn, generates a pulsating pressure and a pulsating thrust. Instability occurs when the pulsating thrust is fed back to the structure, so as to reinforce the initial perturbation.

The following figure, due to the courtesy of NASA [1], illustrates the vibration suppressing method used for the two pumps of the Titan II.



Spring-loaded accumulator for Pogo suppression,
Titan II fuel pump inlet line.

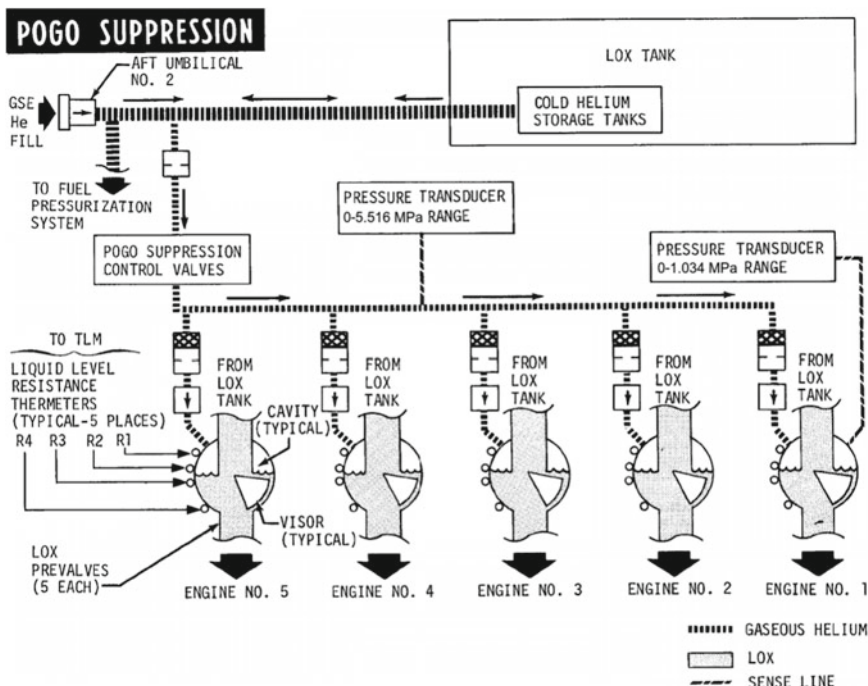


Standpipe with bubble for Pogo suppression,
Titan II oxidizer pump inlet line.

In the Titan II, a bubble of gas was enclosed in a standpipe connected to the oxidiser feed-line. This bubble provided a cushion or a soft spring, which acted on the mass of the oxidiser in the standpipe. In this manner, the energy due to the pressure oscillations in the oxidiser feed-line was transferred to this spring-and-mass system, by choosing judiciously the volume or the height of the bubble enclosed in the standpipe. The fuel feed-lines had accumulators of the piston type, which used a mechanical arrangement comprising an helical spring and a piston to provide the desired soft-spring action. The fixed mass of this mechanical arrangement and the mass of fuel in the accumulator provided the equivalent mass required for a resonant mechanical system. The oscillation suppression devices described above were designed and tuned so that their frequency responses, coupled with the feed-line

properties, would provide the maximum possible attenuation of pressure oscillations in the suction ducts of the pumps, as a result of the tank-structure oscillations.

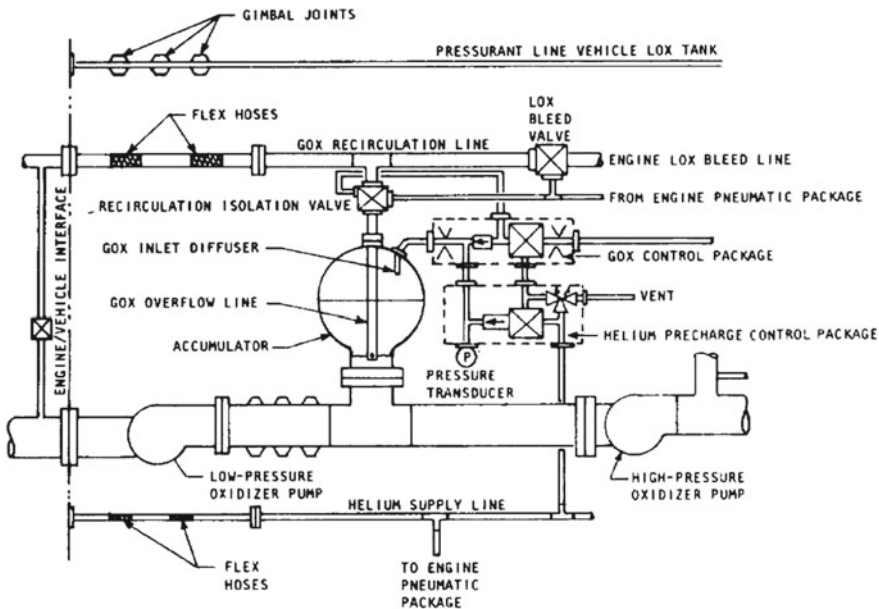
The pogo suppression system used for the S-IC stage of the Saturn V launch vehicle is shown in the following figure, adapted from [7].



This system shown above uses the liquid oxygen pre-valve cavities as surge chambers to suppress the pogo vibrations. The liquid oxygen pre-valve cavities are pressurised with gaseous helium 11 min before scheduled lift-off time from ground supply by opening the pogo suppression valves. During the initial fill period (from 11 to 9 min before scheduled lift-off time), the filling of the valves is closely monitored by using measurements supplied by the liquid level resistance thermometers R₃ (primary) and R₂ (backup). The gaseous helium ground fill continues to maintain the cavity pressure until umbilical disconnect. After umbilical disconnect, the cavity pressure is maintained by the cold helium spheres located in the liquid oxygen tank. The status on the system operation is monitored through two pressure transducers and four liquid level resistance thermometers. One pressure transducer (0–5.516 MPa absolute pressure) monitors the system input pressure. A second pressure transducer (0–1.034 MPa absolute pressure) monitors the pressure inside the No. 1 engine liquid oxygen pre-valve cavity. The pressure readings are transmitted via telemetry to ground monitors. The liquid level within the pre-valves is monitored by four liquid level resistance thermometers in each pre-valve. These thermometers transmit

a “wet” (colder than 108 K) and a “dry” (warmer than 108 K) reading to ground monitors [7].

The following figure, also due to the courtesy of NASA [1], is a scheme of the pogo suppression system used in the liquid oxygen feed-lines on the main engines of the Space Shuttle.



The pogo suppression system shown in the preceding figure is incorporated in the feed system of liquid oxygen at the inlet of the high-pressure oxygen turbo-pump. This system uses an accumulator filled with gas to suppress flow oscillations induced by the vehicle. Gaseous oxygen is tapped off the heat exchanger in the oxidiser-tank pressurisation system. This gas is used as the compliant medium after an initial helium precharge. The system controls the level of liquid oxygen in the accumulator by means of an overflow line, which routes overflowing fluids to the inlet of the low-pressure oxygen turbo-pump.

The accumulator, which is shown in detail in Chap. 2, Sect. 2.9, serves as an attenuator in the flow of liquid oxygen in the circuit, and prevents the transmission of the flow oscillations (at frequencies ranging from 20 to 30 Hz) into the high-pressure oxygen turbo-pump. This system is designed to provide sufficient overflow at the maximum decreasing pressure transient in the discharge duct of the low-pressure oxygen turbo-pump. The engine controller (shown in detail in Chap. 5, Sect. 5.2) provides signals for valve actuation, and monitors the system operation [1].

7.7 Bellows Joints

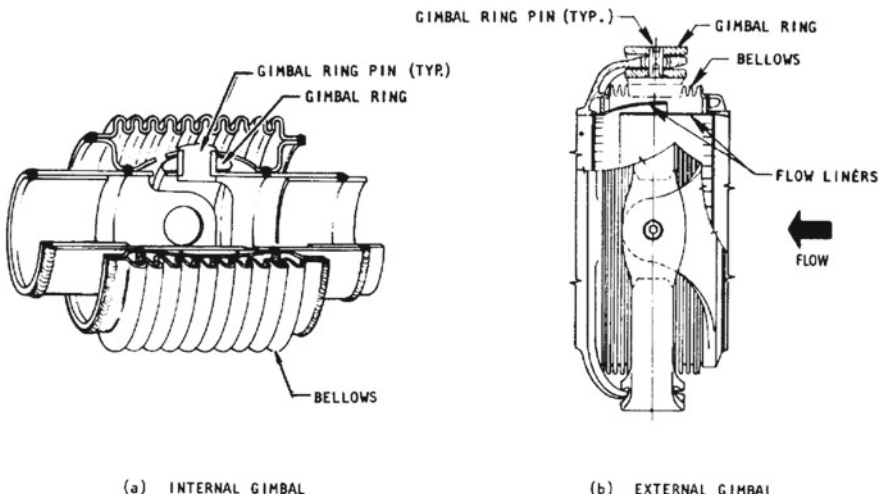
According to the definition given by Howell and Weathers [2], a bellows joint is an elastic, corrugated, tubular connector used for conducting a fluid between points of relative angular, transverse, lateral, or combined motion.

Bellows joints are used where axial, lateral, angular, or combined deflections exist between interconnected components of lines. A bellows joint in a line consists of the following parts:

- a bellows, which is the flexible corrugated tube carrying the pressure exerted by the fluid conducted in the line;
- restraints on the bellows, which prevent movements caused by internal pressure;
- means of attaching the bellows to the line; and
- a flow liner for the bellows.

A bellows joint in a duct can absorb deflections with much smaller reaction loads than the loads in a hard line. A free bellows can absorb four types of motion applied to its ends: (a) axial motion due to tension or compression forces; (b) offset motion with end planes parallel; (c) angular motion about its centre; and (d) torsional motion about its axis.

Various restraints or linkages can be used in order for a bellows to absorb only certain types of motion. For example, a gimbal ring linkage allows a bellows to absorb only angular motion. An internal (left) and an external (right) mounting of gimbal rings for a bellows joint are shown in the following figure, due to the courtesy of NASA [1]. Other drawings showing bellows joints mounted on gimbals or hinges can be found in [14].



A bellows joint must also absorb vibrations, which are due to motions of either the fluid conducted in the line or mechanical parts of the engine. The frequencies of

these vibrations are of the order of magnitude of several thousand hertz. When the stresses resulting from such vibrations exceed the fatigue limits of the material of which a bellows is made, then failure occurs.

Bellows are used for ducts of rocket engines in various sizes and operating conditions. A bellows operates usually in the plastic range of the material of which it is made. This is because the necessity of reducing weight implies small values of thickness for the bellows walls, provided that the magnitudes of the reactions at the bellows ends are acceptable. A formed bellows with straight corrugated sidewall is the type most frequently used for rocket engines.

The types of pressures to be carried by a bellows in operating conditions are:

- normal operating pressure;
- surge pressure;
- proof pressure; and
- burst pressure.

By surge pressure we mean the variation of pressure which occurs in a line conducting fluid as a result of a change in the flow velocity. This variation of pressure may occur in a line, for example, when a pump starts or stops, or a valve is opened or closed rapidly, or the diameter of the line changes abruptly. When a valve is closed rapidly, the velocity head of the fluid moving forward in a line decreases whereas its pressure head increases suddenly, due to the compression which occurs upstream of the valve. By proof pressure we mean:

$$\text{proof pressure} = (\text{normal operating pressure} + \text{surge pressure}) \times \text{safety factor}$$

As has been shown in Chap. 6, Sect. 6.9, the safety factor is a multiplier, whose value (greater than unity) is chosen by the designer to take account of small variations of the properties of the material, of the quality of manufacturing, and of the magnitude and distribution of the load. Finally, by burst pressure we mean:

$$\text{burst pressure} = \text{proof pressure} \times \text{safety factor}$$

These pressures generate hoop (circumferential) stresses and bulging (meridian) stresses, which must be carried by the corrugated sidewall. A bellows must resist column buckling under application of proof pressure. Under application of burst pressure, a bellows is permitted to deform and take permanent set, but not to leak. The limiting bulging stresses and allowable motion stresses (bending stresses) of materials frequently used for bellows are given in the following table, adapted from [1].

Material	Material condition	Limiting bulging stress ^a , MPa		Allowable motion stress, MPa	
		$t \leq 0.3048$ mm	$t > 0.3048$ mm	1000 cycle life	10000 cycle life
321, 347 CRES	Cold worked as formed R_c 10–40	965.3	827.4	827.4	510.2
A-286	Heat treated; R_c 29–40	1379	1103	1379	827.4
Inconel 718	Heat treated, R_c 38–45	1379	1103	1448	930.8
Inconel X-750	Heat treated. R_c 30–37	1379	1103	1138	724.0
Hastelloy C	Cold worked as formed R_c 10–40	1034	896.4	1276	724.0

^aReduction in material properties for thicker sheet is due to poorer surface finish and greater variation in thickness than in thinner sheets

R_c —hardness on Rockwell C scale

The principal causes of problems affecting bellows joints used in ducts for liquid-propellant rocket engines are:

- fatigue;
- buckling;
- corrosion;
- manufacturing difficulties; and
- handling damage.

These causes are briefly considered below.

As to fatigue, bellows are subject to large deflections at their ends, due to the offset motion cited above. Bellows have usually thin walls, in order to reduce weight. Consequently, the materials of which bellows are made operate under stresses near or in the plastic range, with resulting low fatigue lives.

Bellows are also subject to vibrations, caused by the fluids or by mechanical parts. They must be designed so that no reduction in fatigue life is caused by vibration. In order to predict vibratory stresses, it is possible to use known vibration inputs relating to other engines in the same conditions, and compare such inputs with the frequencies of resonance of the given ducts, which can be calculated. Otherwise, it is possible to construct a prototype and test it on various engines, while the vibration environment is measured. When a bellows operates at excitation frequencies matching any of its natural frequencies of vibration, then its fatigue life can be exceeded in a short interval of time.

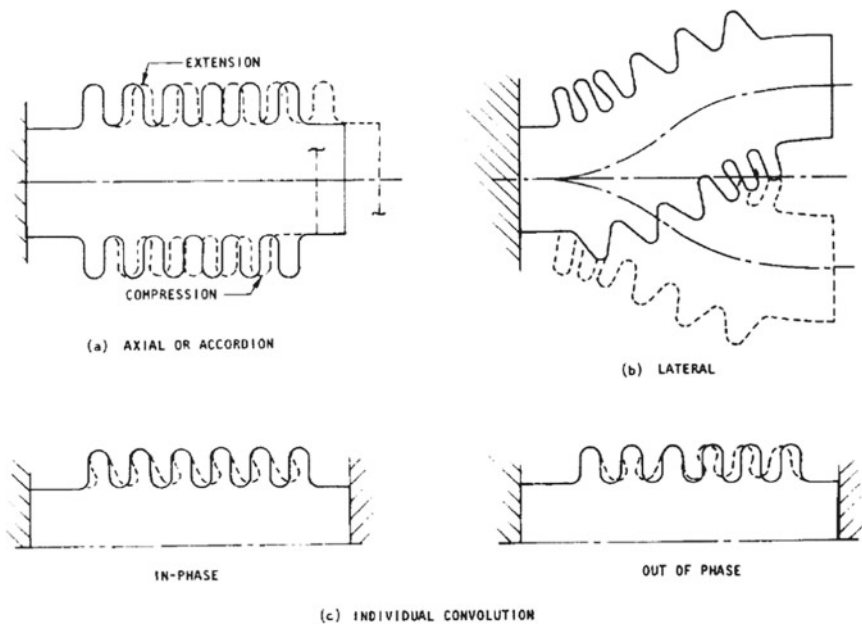
The most frequent failure mode for a bellows is a fatigue crack, which gives rise to leakage through the corrugated wall. The cracks develop circumferentially in areas of maximum bending stress, which are the crowns and the roots of the corrugations.

The primary modes of vibration for a bellows are:

- the axial or accordion mode;
- the lateral mode; and
- the individual convolution mode, in which the individual corrugations rotate back and forth at the inner diameter, and pivot about the outer diameter.

In particular, the individual convolution mode occurs often in vibrations of braided hoses caused by flow oscillations, where the outer diameter of the corrugations is restrained by the braid friction, and consequently the outer point of each corrugation is a fixed pivot point for the corrugation excited by flow forces. The individual convolution mode may be in phase or out of phase, depending on how each corrugation moves with respect to the others.

The primary modes of vibration (a), (b) and (c) described above are shown in the following figure, due to the courtesy of NASA [1].



Bellows incorporated in flexible flow lines are frequently subject to vibrations induced by fluids moving at high velocity, with consequent failure due to fatigue stresses. This type of failure is avoided by using internal flow liners, which prevent the flow stream from impinging on the corrugations. However, care must be taken, because internal flow liners, too, may be subject to flow-induced vibrations.

Bellows are also subject to vibrations induced by mechanical parts of engines. When the frequencies of the exciting vibrations are known, for example, through measurements, then bellows can be designed so that their natural frequencies should not match the excitation frequencies.

Bellows may be subject to buckling due to excessive internal or external pressure. Buckling due to high internal pressure results in column instability, whereas buckling due to high external pressure results in crushed corrugations. Buckling can occur only when the pressures in actual operating conditions are beyond the pressures predicted in the original requirements.

A bellows may be subject to corrosion, depending on the material of which it is made. A material commonly used for bellows is stainless steel 321 CRES, which is resistant but still susceptible to corrosion, because of its high percentage of iron. This and other materials have been discussed in paragraph 3.

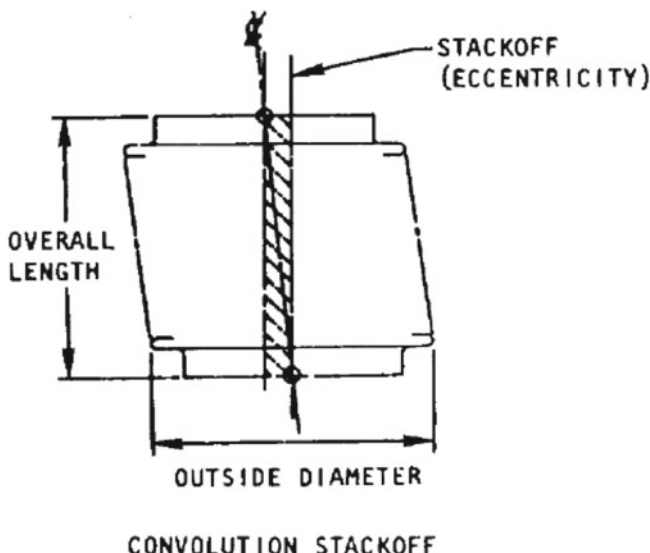
The principal difficulties in the manufacturing of bellows are material thinning, heat-treatment control, welding, and convolution stack-off.

Bellows are thinned at the corrugation crowns, about 5% or 10% below the nominal thickness of the wall. As a result of this thinning, higher deflection takes place in the thinned section, because its stiffness is reduced, and consequently higher stresses and lower resistance to fatigue can occur.

Heat treatment of bellows is controlled in order to avoid degraded performance caused by improper treatment. In particular, this control requires the maintenance of the proper gaseous environment during heat treatment, to avoid oxidation and consequent strength reduction.

Welding problems are due to insufficient quality control. Such problems can be avoided by inspecting radiographically all welds.

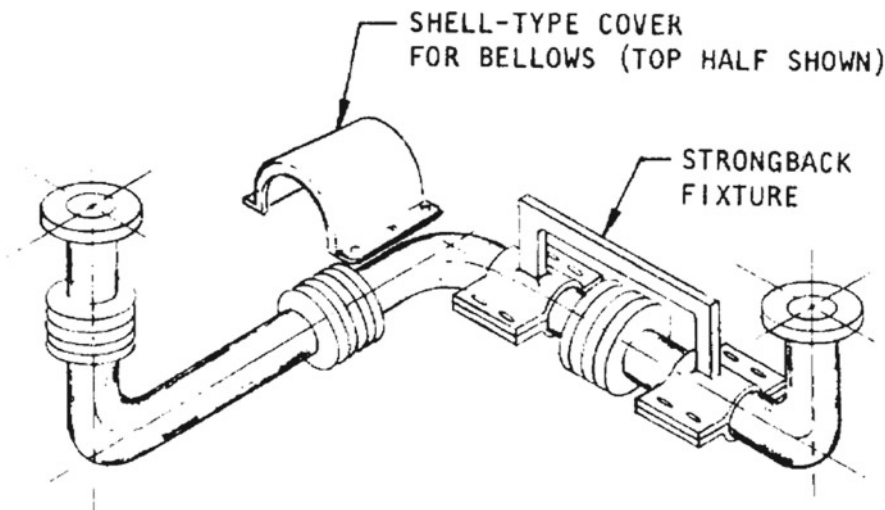
Convolution stack-off is the eccentricity of convolutions or corrugations of the bellows with respect to each other. Since this eccentricity depends on the tools used in the process of fabrication, then all of the eccentricity is accumulated in the same direction, as shown in the following figure, due to the courtesy of NASA [1].



Convolution stack-off makes it difficult to align the bellows for welding into its next assembly. This accumulation can be controlled by rotating the bellows after the forming of each convolution.

It is necessary to use handling-protection devices in the duct assembly and during processing, shipping, and installation of bellows. This is particularly important in case of bellows having thin walls (less than or equal to 0.762 mm).

In order to protect the bellows joints incorporated in a duct from over-deflection, it is necessary to use strong-back fixtures which attach to the duct on either side of each bellows joint and form a protective bridge around it. The following figure, due to the courtesy of NASA [1], shows (right) a strong-back fixture and (left) a shell-type cover for protection of bellows.



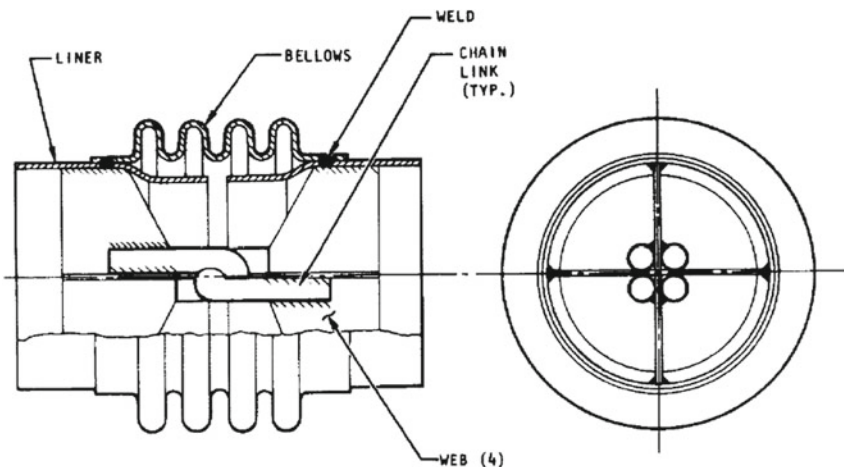
As has been shown above, the most common type of restraint used for bellows joints is the one mounted on gimbal rings. Other types of restraint are the hinged joint, the ball joint, and the braided wire sheath.

The gimbal-ring joint can be designed to withstand high pressures and temperatures. It can also withstand torsional loads and absorb angular deflections in all planes. Excessive angular motion of the bellows can be prevented by means of stops, and the pivot pins which carry the loads can be designed for either single-shear or double-shear support. The same considerations apply to the hinged joint, which allows angular motion in only one plane.

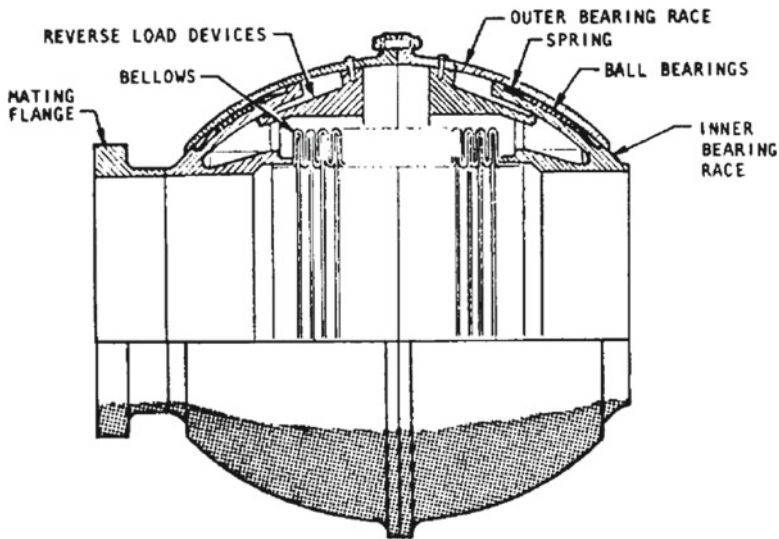
Another type of external, tension-tie restraint is a braided wire sheath, as is the case with a flexible hose. A joint of this type can absorb both angular and shear deflections. It also acts as a vibration damper for the bellows. Friction between the braid and the bellows can be reduced by using an adapter, which provides clearance at the end of the corrugations, and by applying a solid dry-film lubricant on the outer surface of the bellows and on the inner surface of the braid.

The lubricants used for this purpose must be compatible with liquid oxygen, when this is the fluid conducted through the given line.

A link joint with internal tie restraint can be used instead of a gimbal joint when a duct is subject to small or medium pressures. It is used frequently in low-pressure ducts of gas turbines. It has de disadvantage of high friction losses, due to the restriction to flow in the frontal section. In particular, a chain-link joint is a link joint in which the pivot point of the linkage is not fixed, but depends on the plane in which the joint lies. A chain-link joint with internal tie restraint is shown in the following figure die to the courtesy of NASA [1].

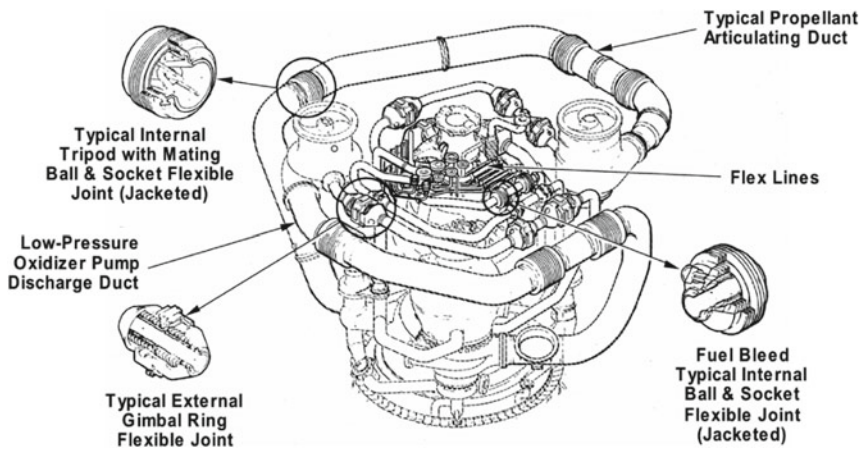


A ball-bearing ball-joint restraint is shown in the following figure due to the courtesy of NASA [1]. This type of joint was used for test in the inlet line to the liquid-oxygen pump of the F-1 engine.



The bellows joint using the restraint illustrated in the preceding figure was located immediately upstream of the pump inlet flange, due to the large pressure separating load. This joint could provide a restraint and a motion of the gimbal type while applying a uniform circumferential load to the pump flange.

The flexible joints used for the RS-25 engine (burning liquid oxygen and liquid hydrogen) are shown in the following figure, due to the courtesy of Boeing-Rocketdyne [4].



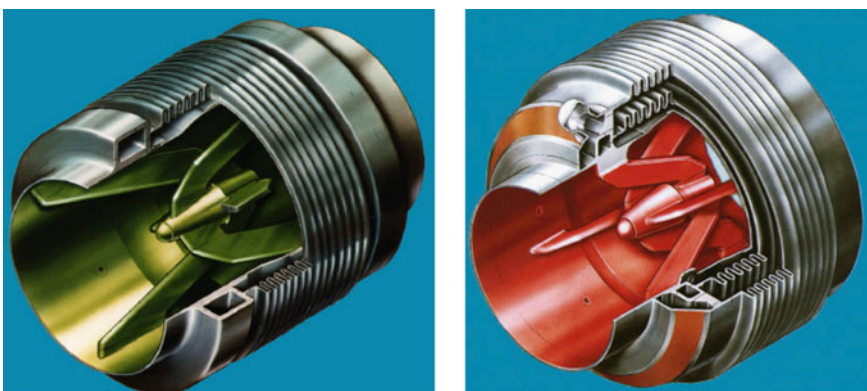
The flexible joints in the lines of the RS-25 engine allow movement for vehicle steering, while maintaining the internal pressure and temperature in the lines. These joints must be flexible, because the lines connect either the gimballed engine with the vehicle or the gimballed engine with non-gimballing components.

A flexible metallic bellows is used as the pressure vessel. This bellows has each of its ends welded into a section of fluid ducting, in order to provide a continuous, leak-proof pathway. The bellows have several thin plies in a sandwich configuration, instead of a single thick sheet of metal. This arrangement makes the bellows more flexible and maintains integrity against pressure.

The ducts which contain flexible joints internally tied have an internal diameter large enough to allow an internal support mounted on gimbals. This internal support arrangement saves weight in comparison with an external support. Were it not for the gimbal joint, which holds both ends of the flexible joint together, the internal operating pressure of the duct would expand the flexible bellows longitudinally like an accordion. The joint of the internal gimballed support is of the ball-and-socket type. Ducts with small internal diameters use an internal gimbal ring to restrain the bellows. The ends of the flexible joint are attached to the gimbal ring (which is centred over the bellows) at two points, so as to form a universal-type joint.

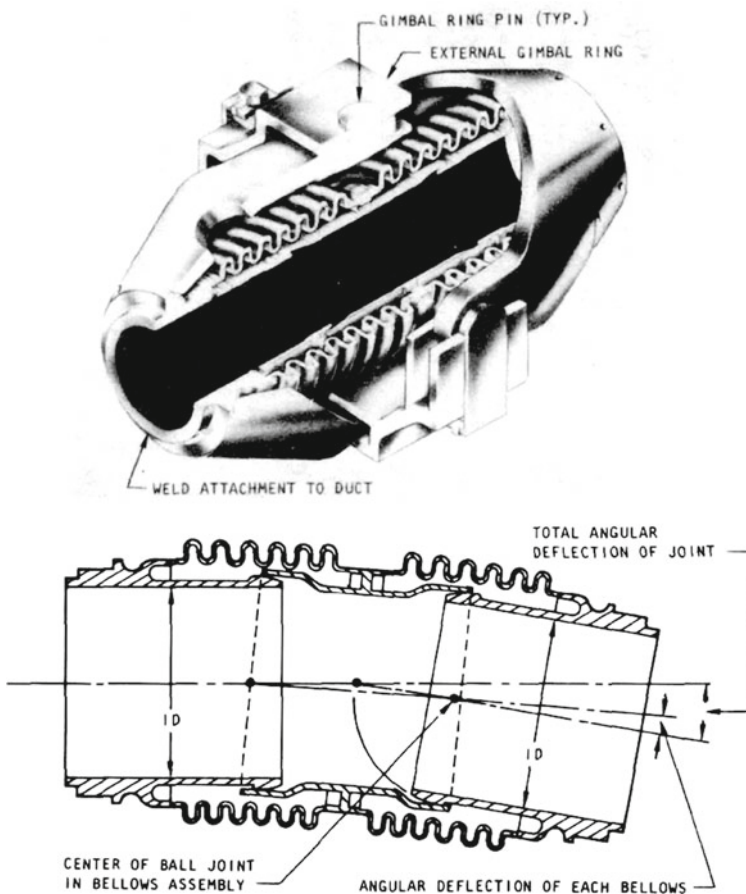
The flexible joints contain an integral flow liner. This liner prevents the propellant flowing through the duct from impinging on the corrugations of the bellows, which could cause turbulence in the flow and vibrations in the materials. The liner is made up of two or three overlapping pieces. The outside ends of the end pieces are welded into the flexible joint, so as to form a continuous, smooth internal diameter when the flexible joint is welded into a duct. The overlapping portions of the liner are shaped as a truncated ball and socket, to allow movement of the flexible joint. The liner allows propellant to fill the space between it and the bellows. Screened ports at the upstream ends of the flow liner provide a path for propellant to exit the space behind the liner after engine shutdown [4].

The flexible joints used in the RS-25 engine are the internal tripod and the external-gimbal ring joints. The internal tripod joint is used for the low-pressure discharge ducts, where the pressure loss can be tolerated and the overall joint envelope must be kept as small as possible. The following figure, due to the courtesy of Boeing-Rocketdyne [4], shows the internal tripod joint non-jacketed (left) and jacketed (right).



According to the data given in [4], these joints are made of Inconel® 718 and ARMCO 21-6-9 stainless steel, and their design life is 200 operational, 1400 non-operational full deflection cycles. The non-jacketed joint is used for the low-pressure discharge duct of the oxidiser. It works at an operating pressure of 2.916 MPa and at an operating temperature of 92.04 K. Its inside diameter is 160 mm, and its angular displacement is ± 0.2269 rad ($\pm 13^\circ$). The jacketed joint is used for the low-pressure discharge duct of the fuel. It works at an operating pressure of 1.924 MPa and at an operating temperature of 22.04 K. Its inside diameter is 132 mm, and its angular displacement is ± 0.2007 rad ($\pm 11^\circ 30'$).

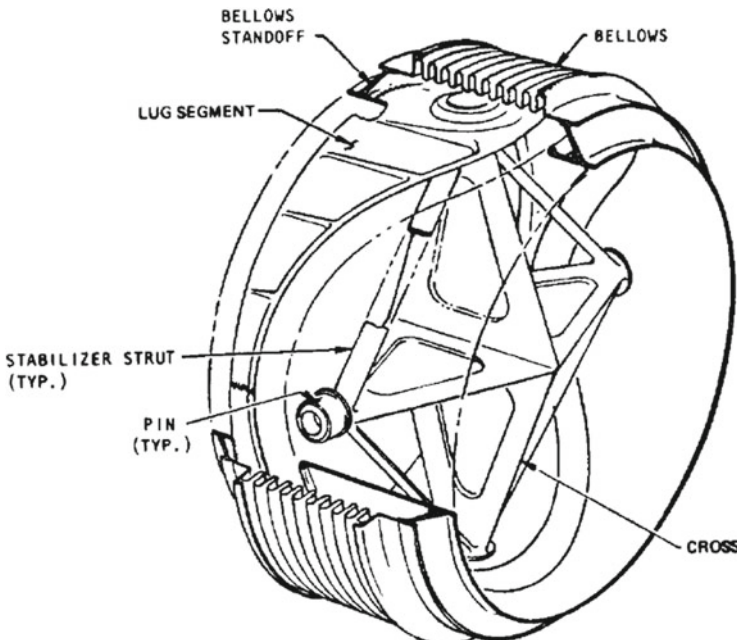
The externally-tied gimbal ring joint used in the RS-25 engine is shown in the following figure, due to the courtesy of NASA [1].



This joint is used in the RS-25 engine on small-diameter (50.80–68.58 mm) high-pressure ducts, where the pressure losses associated with internal ties are not acceptable. The high pressures and gimbal angles of the externally-tied joints make it necessary to use long bellows, which are unstable in column buckling.

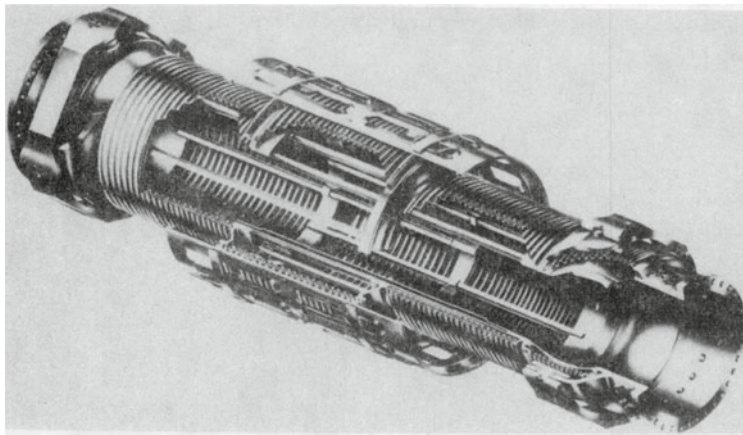
This joint is stabilised by a linkage, shown in the preceding figure, which provides lateral support at the mid-span of the bellows live length. By so doing, the angular deflection of the joint assembly is equally distributed between the two bellows.

A flexible joint with linkage restraint known as “Gimbar” (gimbal ring with crossed bars for structural strength) is used in the fuel and oxidiser drain ducts of the Shuttle Orbiter. This joint is shown in the following figure, due to the courtesy of NASA [1].



This joint is lighter than a gimbal ring joint having internal or external ties, and can be used in ducts of large diameters carrying fluids moving at low velocities, in which the pressure loss due to the structure across the flow stream can be tolerated. This joint is also capable of carrying torsional loads, by means of its linkage.

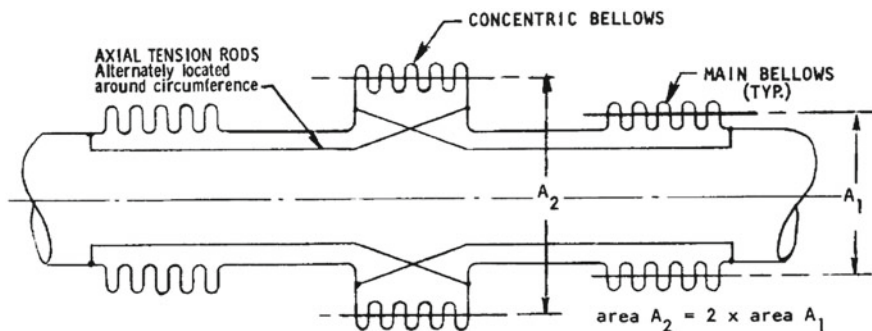
Thrust-compensating bellows are sometimes necessary to offset the thrust of primary bellows. An example of thrust-compensating bellows is shown in the following figure, due to the courtesy of NASA [1].



In a thrust-compensating bellows, the axial thrust due to the pressure separating force is balanced by the compensating bellows. Of course, in order to compensate for thrust, the volume of the bellows must also be compensated.

Thrust-compensating bellows also eliminate volumetric changes which occur in straight-run gimbaling ducts. Such changes cause pressure perturbations which are detrimental to engine operation.

In the duct at the inlet of the pump of the F-1 engine, a bellows (which is external to and concentric with the main bellows) offsets the separating force of the main bellows, as shown in the following figure, due to the courtesy of NASA [1].

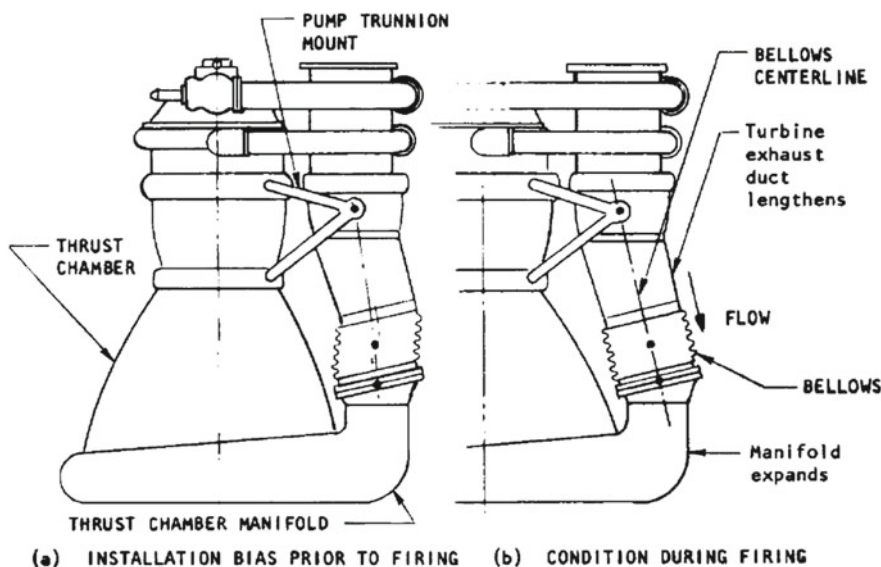


The annular chamber is vented to internal duct pressure. Axial-tension rods tie across the bellows alternately along the circumference. Telescopic flow sleeves can also be provided [1].

Bellows joints are also used in compression systems. A compression system consists of one or more bellows having no tension ties, which are used to absorb the deflections of a duct in operating conditions. In a compression system, the mating structure of the engine reacts to the pressure separating forces and to the elastic forces due to the fluid moving in the duct. The reaction exerted by the mating structure places the duct in compression.

In engines having ducts with compression-restrained bellows (for example, low-pressure ducts, such as those at the outlet of turbines), the support structure of the engine can be overloaded with moments caused by eccentric pressure separating forces acting on the bellows. These moments cause shear stresses in the bellows.

When the deflections induced in a bellows in operational conditions are known, then that bellows can be installed in an engine with a bias which gives rise to opposite deflections. By so doing, the bellows move, when placed in operational conditions, toward a nearly neutral position, corresponding to little or no stress. An installation of a compressed-restrained bellows made according to this criterion is shown in the following figure, due to the courtesy of NASA [1].



As has been shown above, bellows are made of thin, sometimes laminated, and often dissimilar materials. Consequently, junctions between bellows and adjacent parts of higher thickness require the use of careful manufacturing techniques. Electron-beam welding and diffusion bonding (discussed in paragraph 4) offer advantages over other techniques when parts made of dissimilar metals and having different thicknesses are to be joined.

Bellows made of heat-treatable alloys can be welded to ducts made of non-heat-treatable alloys without disturbing the heat treatments in the bellows materials. For this purpose, a transition portion of the duct is welded to the bellows before heat treating the bellows material, so that the final weld to the duct involves identical alloys.

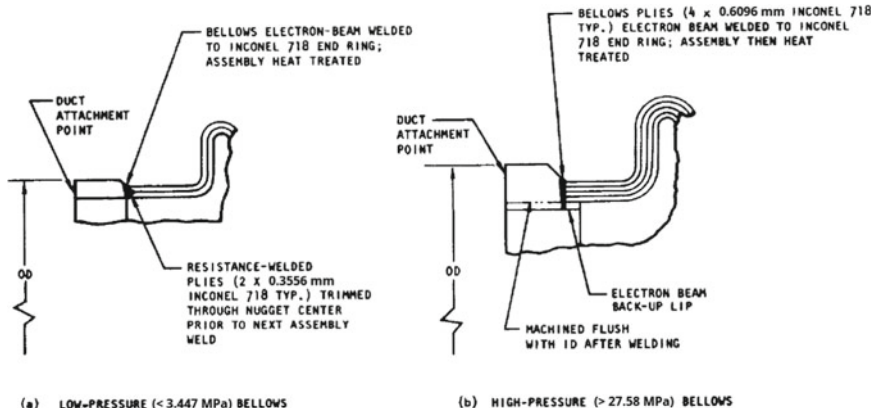
In the RS-25 engine, the welds of the bellows to the ducts are of two principal types:

- (a) welds for thin-wall bellows subject to low pressures; and

(b) welds for thick-wall bellows subject to high pressures.

The necks of the thin-wall bellows are resistance-welded together, then trimmed around the circumference through the centre of the nugget. The bellows is then electron-beam welded to end rings, and the resultant assembly is heat treated.

The two types of welds indicated above are shown in the following figure, adapted from [1].



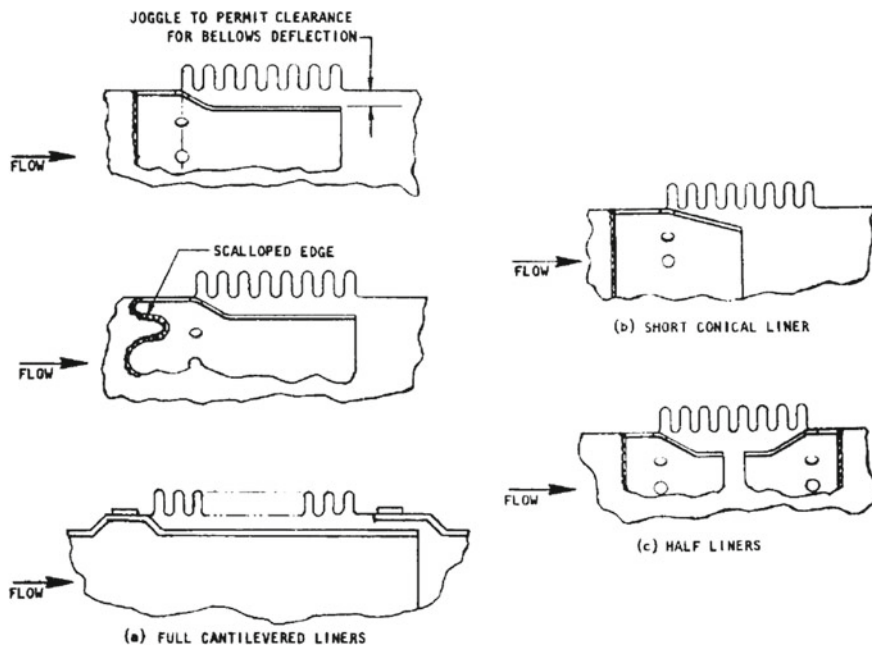
Internal flow liners or sleeves for bellows are used to solve the problem of fatigue failures of bellows. Such failures are due to vibrations induced by the fluid stream. Flow liners are also used to reduce the pressure losses which occur at the joints. Flow liners have been used as structural members supporting tube coils in heat exchangers mounted on the J-2 and J-2S engines.

Flow liners must be designed so that they should not bottom out or bind on either the bellows or the ducts, when the bellows are at the maximum limits of excursion. They must also be designed with drain holes placed as near as possible to the weld attachment, in order to make it possible to remove cleaning fluids and contaminants.

Fatigue failures of flow liners have occurred, in which cracks have appeared in the trailing edge and in the weld joint. These failures have been attributed to vibrations of the cantilevered end of the sleeve. This problem has been solved by an increase in the thickness of the wall, with a consequent increase in the rigidity of the liner [1].

Collapse of liners has also occurred as a result of pressure on the outer diameter of the liner exceeding that of the inner diameter. This has been attributed to sudden changes in flow rates, which cause a different static pressure across the wall of the liner. Vent holes in the liner can reduce some of this difference of pressure. Otherwise, the liner can be strengthened to withstand the applied load.

Some typical configurations for flow liners are shown in the following figure, due to the courtesy of NASA [1].



7.8 Flexible Hoses

A flexible hose consists of a flexible inner liner which conducts a fluid, a reinforcement which braces the inner liner, and two end fittings, which connect the hose ends to other portions of a duct.

Flexible hoses are used more often in large liquid-propellant rocket engines (meant for boosters and upper stages) than in small engines (meant for attitude control or reaction control). This is because little flexibility is required in lines of small engines, which are not mounted on gimbals and use storable propellants.

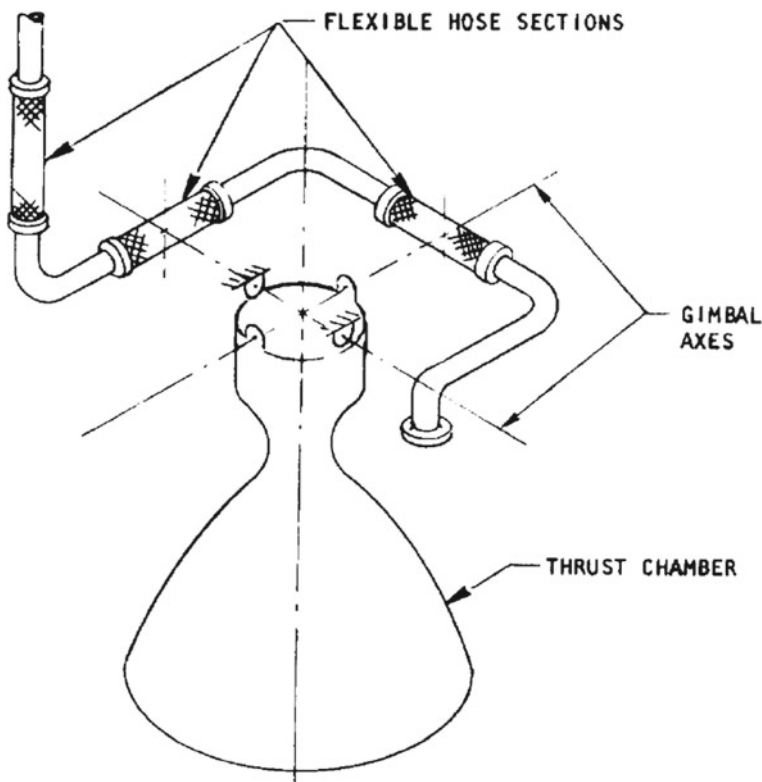
The J-2 and F-1 engines (both of which have been used in the Saturn V launch vehicle) have many fluid-carrying lines between the engine and the vehicle. These lines are flexible, in order for the engine to be moved on gimbals.

On the J-2 engine, all the lines are flexible hoses and are clamped together to assist in maintaining their relative positions.

On the F-1 engine, the flexible hoses cross the gimbal plane and are attached to non-gimballing flexible hoses on the engine [1].

Coiled tubing is sometimes used in heat exchangers for tank pressurisation. This is done in order to provide the maximum area possible for heat transfer in the minimum space. In the Centaur stage, a coiled tube is used for the pneumatic lines to the main engines, and flexible bends in lines for propellant recirculation and in lines for tank pressurisation, all of which are less than or equal to 25.4 mm in diameter [1].

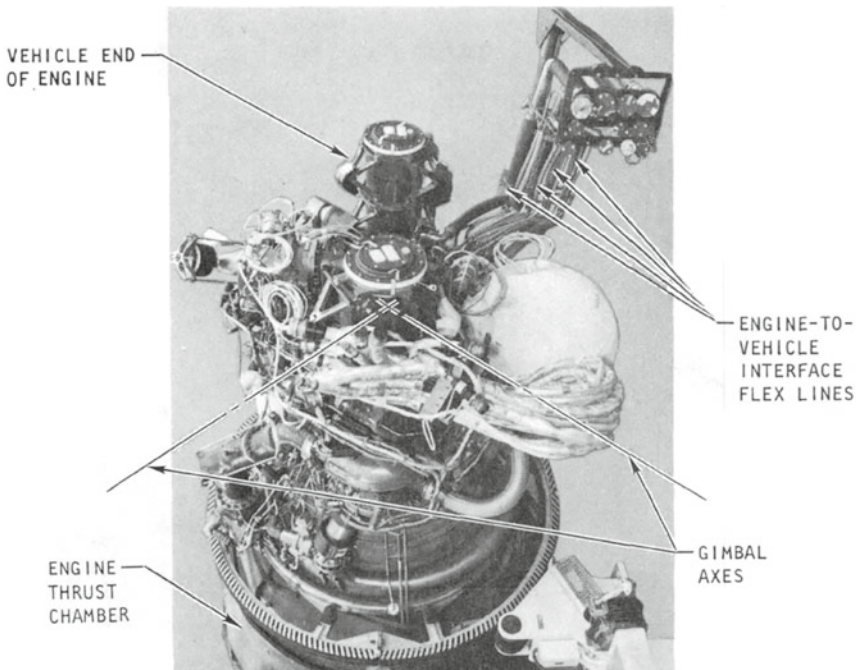
A typical assembly of flexible hoses is shown in the following figure, due to the courtesy of NASA [1].



The flexible hose sections shown in the preceding figure are located so as to achieve the maximum motion possible of the line with the minimum motion of the flexible hose sections. In addition, the entire wraparound lies in the gimbal plane rather than passing through it. The preceding figure illustrates a gimbal system mounted on the head of the thrust chamber for thrust vector control. The longitudinal axes of two of the three flexible hose sections are located in the gimbal plane. The midpoint of each of these two flexible hose sections is located on each of the two gimbaling axes. The third flexible hose section is located in the vertical direction, to provide universal motion of one end of the line with respect to the other. This method of locating the flexible hose sections limits their motions to the gimbal angles only, in order to reduce bending stresses and consequent fatigue. When the hoses are not stiff enough to resist motions caused by either mechanical vibrations or accelerations load, then clamps and support brackets are used [1].

Other arrangements for flexible hoses than the wraparound arrangement described above have been used, when lack of available space made it necessary to do so. For example, the flexible lines of the J-2 engine at the interface between the engine and

the vehicle have been arranged in a U-shaped routing configuration, with a section of braided flexible hose in each leg of the U, as shown in the following figure, due to the courtesy of NASA [1].



Flexible hoses are sized so that the velocities of gases are kept below the value 0.3 of the Mach number. This avoids pressure losses and vibrations induced by the flow.

The inner core of a flexible hose is subject to vibrations caused by the flow and by mechanical parts, as is the case with a bellows (see paragraph 7), the only difference being that the braid of a flexible hose restrains the corrugations to vibrate individually. Other considerations concerning pressure carried, resistance to corrosion, manufacturing methods, and handling protection for flexible hoses are similar to those which have been discussed in paragraph 7 for bellows.

As a general rule, only metallic materials are used for inner cores of flexible hoses installed in rocket engines, due to the very high or very low temperatures reached in such engines. Some exceptions to this rule are cited below.

The type most frequently used is the metallic, annularly convoluted inner core. The metallic, helically convoluted inner core type is not used in aerospace applications. Rolled and welded tubes or seamless tubes are used, but those of the seamless type are much more expensive. The welds of those of the rolled and welded type require X-ray and leakage verifications before use.

The engines of the Titan III have used successfully inner cores of both normal and carbon-impregnated Teflon® (poly-tetrafluoroethylene) in sizes ranging from 9.525

to 25.4 mm in diameter. On the S-IC stage of the Saturn V launch vehicle, inner cores of Teflon® have been used successfully with RP-1 at a working pressure of 15.17 MPa. Inner cores made of Teflon® have also been used successfully for the airborne hydraulic system on the Centaur. Rubber has been used only for applications involving non-cryogenic or non-high temperatures. In addition, the quality of rubber is subject to deterioration with time.

Bending moments to flexible hoses are to be considered, because the components adjacent to a hose are loaded. Low values of bending moments are desirable, because low bending moments applied to flexible hoses which cross the gimbal plane result in low loads applied to the actuators which gimbal the engines. Bending moments can be reduced by using lubricants applied to braid wires and to the other surfaces of the inner core. An inner core may be compressed axially before installing the braid. This results in a higher number of convolutions per unit length and in a lower bending stiffness, but also in greater weight and cost of the materials. A compressed inner core also improves the ability of a flexible hose to withstand pressure impulses.

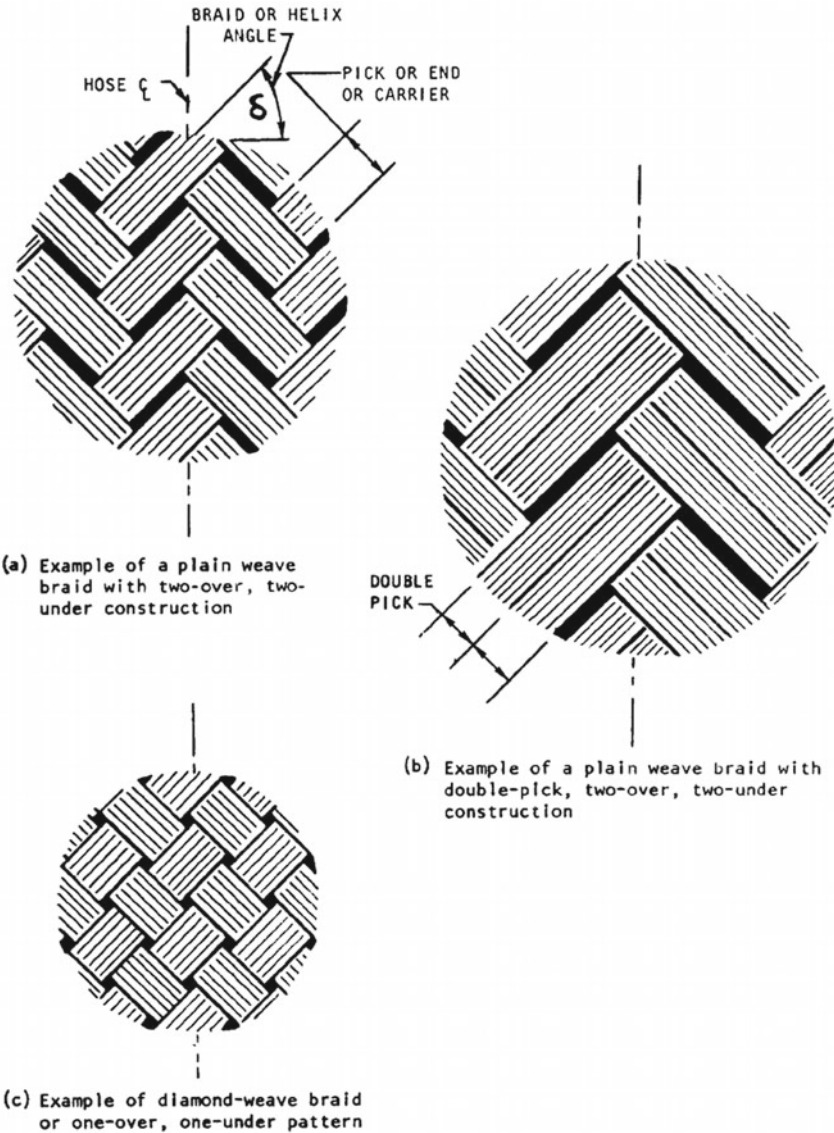
Buckling stability is not a concern in the design of flexible hoses. This is because the support provided by the braid for the inner core prevents buckling.

The braid of a flexible hose is a woven tubular cover, which restrains the inner core against elongation and gives it lateral support and protection. The braid absorbs the entire separating load of a flexible hose. In rocket engines, the braid is woven of wire made of stainless steel.

Tubular braid may be woven directly on the inner core of flexible hoses. Sections of braid are cut at a length slightly greater than the length of the convoluted inner core. A tensile load is applied to the ends of the braid section, and the section is attached to end fittings by brazing or welding [1].

The pattern of a braid weave must be such as to prevent the wires from binding or bottoming out, within the design limits of angular deflection for a particular section of flexible hose.

Typical configurations of braids used for flexible hoses are shown in the following figure, due to the courtesy of NASA [1].



The braid angle or helix angle δ shown in the preceding figure is the angle whose tangent is the pitch divided by the circumferential length of the braid per pitch. The pitch is the axial distance taken by any given wire to make one complete turn. An angle δ of about $\pi/4$ (45°) is presumed to give the maximum flexibility together with good end strength and resistance to pressure for flexible hoses with metallic inner core [1].

Multiple layers of braid may be used to achieve greater strength. The second layer is assumed to have an efficiency (see below) of about 80%, due to the difficulty of obtaining a perfect distribution of load between two layers.

Tubular braid is available in various metals and sizes up to 457.2 mm in diameter. The ultimate tensile strength of a braid wire made of stainless steel is about 827.4 MPa, but braid wires of higher strength can also be found [1].

The end strength F_B (N) of a braid can be calculated by using the following formula of [1]:

$$F_B = n F_w B_e \sin \delta$$

where n is the total number of wires in a braid, F_w (N) is the strength of a single wire in a braid, B_e is the braid efficiency factor (whose values are 0.93 for an annealed wire, 0.85 for a hard-drawn wire, and 0.80 for a second layer), and δ is the braid angle defined above.

The burst pressure is the maximum pressure which a hose can retain without losing pressure or fluid. The burst pressure p_b (N/m^2) of a bellows-type metallic braided hose can be calculated by using the following formula of [1]:

$$p_b = \frac{F_B}{A_{\text{eff}}}$$

where F_B (N) is the end strength of a braid defined above, and A_{eff} (m^2) is the effective area of the bellows, which results from

$$A_{\text{eff}} = \frac{\pi D_m^2}{4}$$

and D_m (m) is the mean diameter of the bellows, such that $D_m = (D_o + D_i)/2$, where D_o (m) and D_i (m) are respectively the outside diameter and the inside diameter of the bellows.

The elongation ξ (m) of the braid, when a flexible hose is under pressure, can be calculated approximately by using the following formula of [1]:

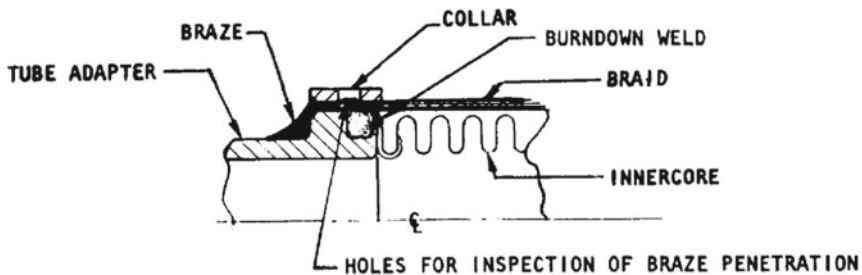
$$\xi = \frac{p_i \ell A_{\text{eff}}}{n E A_w}$$

where p_i (N/m^2) is the internal pressure, ℓ (m) is the total length of one braid wire between its end connexions, E (N/m^2) is the Young modulus of a braid wire, and A_w (m^2) is the cross-sectional area of each wire. The preceding equation includes no allowance for slack in the wires, and holds when the stress is within the elastic limit. Braid wires are subject to corrosion. As a result of the experience gained for the main engines (RS-25) of the Space Shuttle, the braid materials for the flexible hoses used in those engines have been nickel-base alloys.

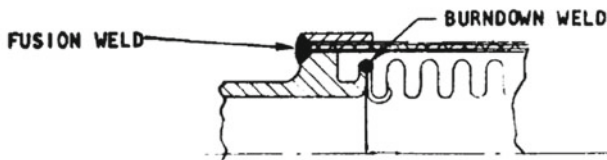
There are two principal types of end construction used for flexible hoses of small diameter:

- (a) a welded-and-brazed type, used at temperatures from cryogenic to 478 K; and
- (b) an all-welded type, used at temperatures above 478 K.

These two types are shown in the following figure, adapted from [1].



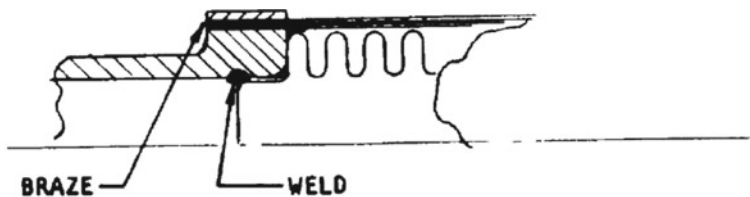
(a) End construction for small-diameter braided metal hose
(temperatures from cryogenic to 478 K)



(b) End construction for small-diameter braided metal hose
(temperatures above 478 K)

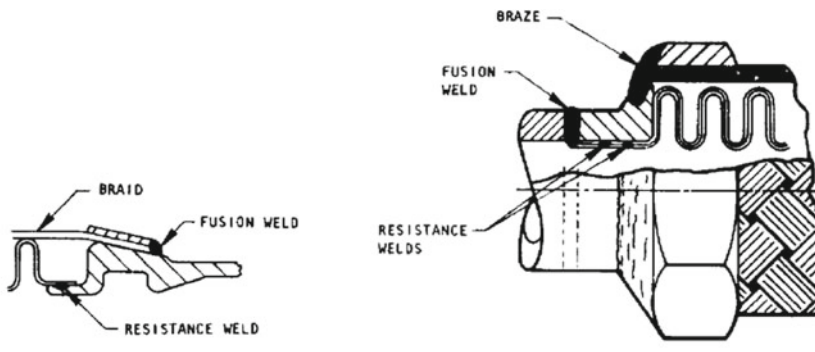
By end construction we mean a juncture of inner core, tube adapter, and braid. The all-welded type is required at high temperatures, because of the loss of strength of the braze material at such temperatures. These two types have been used for flexible hoses up to 76.2 mm in diameter [1].

In case of tubes whose internal diameter (ID) exceeded 76.2 mm, another type of end construction has been used at temperatures from cryogenic to 478 K. This type (c) is shown in the following figure, adapted from [1].



(c) End construction for braided metal hose 76.2 mm ID and over (temperatures from cryogenic to 478 K)

The type of construction illustrated in the preceding figure has been used in hoses of large inner diameters (88.9 and 101.6 mm) developed for the gimbaling feed systems of the engines of the Atlas and Thor rocket vehicles. In such engines, the internal diameter of the tube was large enough to permit a lap weld of the pressure-carrier neck to the tube adapter [1]. Two further examples of end construction are shown in the following figure, adapted from [1].



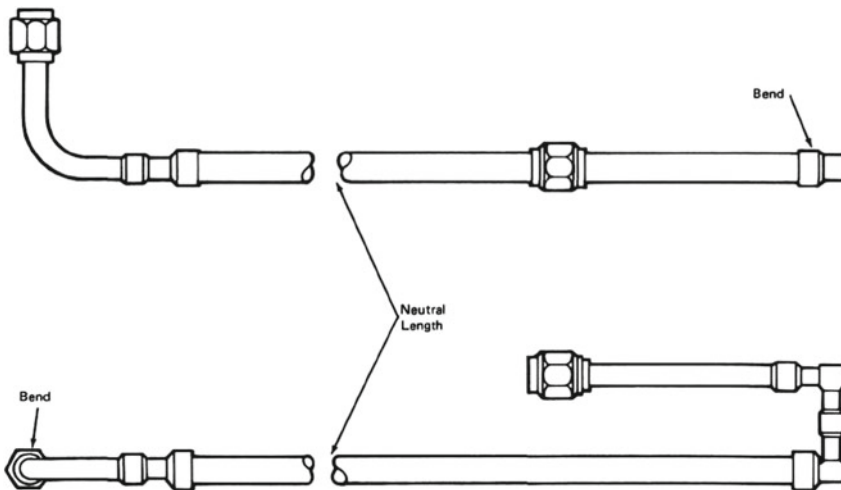
(a) ALL-WELDED CONFIGURATION

(b) WELDED AND BRAZED CONFIGURATION

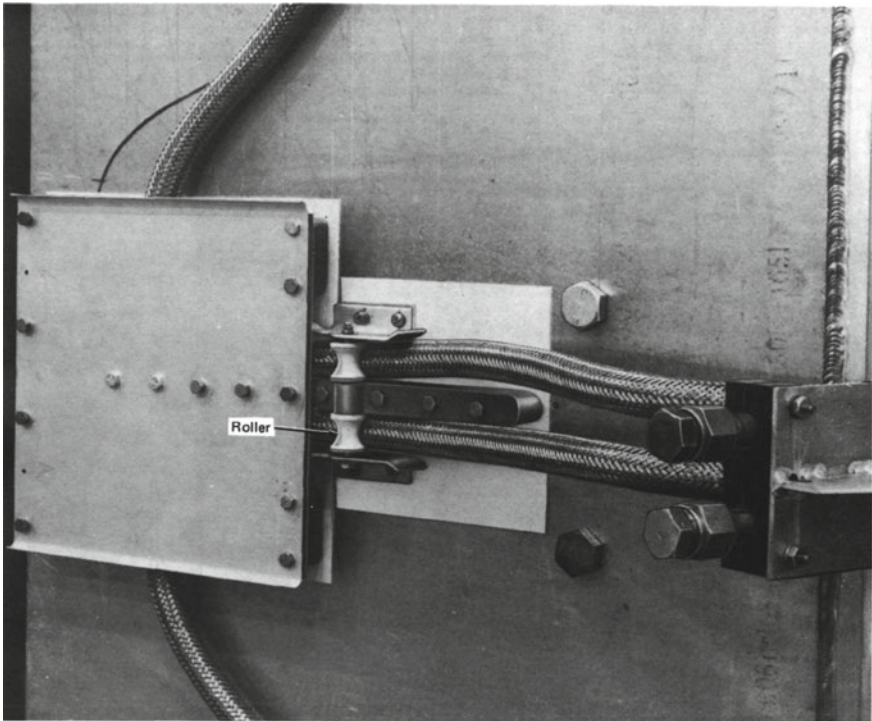
The moments required to deflect braided metallic hoses depend on numerous parameters, such as inner diameter, outer diameter, thickness of the inner core, number of plies, live length, number of layers of braid, number of wires and their diameters, and operating pressure. Data on the bending moments can be obtained from the manufacturers of flexible hoses or by test. Some typical values can be found in [1].

A guide enables a flexible hose to bend, move, and operate in more than one plane without twisting, in order for the hose to have a longer service life. This guide has proved successful under severe conditions. Two independent bends are curved one

in a horizontal plane, and the other in the vertical plane. The guide provides a neutral length of hose which separates the bends and prevents interactions between them, as shown in the following figure, due to the courtesy of NASA [15].



Determination of the minimal neutral distance required for proper operation led to the identification of a single theoretical point of inflection, where the hose becomes free of the guide. A roller, for each hose in the assembly, is placed in this point. The inherent stiffness of the hose makes this point the point of inflection between the horizontal bend and the vertical bend. Each bend is curved in a single plane with no components of rotation or twist along the axis of the hose. The arrangement shown in the following figure, due to the courtesy of NASA [15], can be modified for other motions of the hose.



7.9 Filters

As has been shown in paragraph 1, filters are often installed in fluid-carrying ducts of rocket engines to retain solid particles of contaminants which may be contained in the fluids. Downstream of filters, the size of the remaining solid particles is reduced to such an extent as not to affect the performance of components sensitive to contaminants. Examples of such components are valves and actuators. According to Buckingham and Winzel [16], contaminating particles existing in fluid-carrying ducts of rocket engines are due to three principal causes, which are:

- residual manufacturing debris in the tanks and in other parts of a fluid system;
- contaminating particles in the on-loaded fluids; and
- particles generated by the wear of components in normal operation.

Generally speaking, as has been shown by Howell and Weathers [2], there are two techniques of filtration, which are briefly described below.

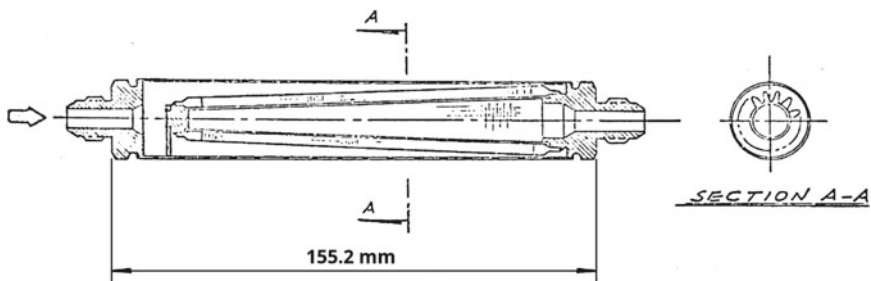
One of them, called surface filtration, is accomplished by impingement and retention of solid particles on a matrix of pores placed in a single planar or curved surface. Filtration occurs only at that surface, and the particles which are not stopped there

pass through the filtering medium with no further change in direction. This technique of filtration is effective in collecting particles larger than the sizes of the pores, but not effective in collecting fibres and particles smaller than the sizes of the pores. Its capability of retaining solid particles is limited by the area of the surface which can be provided within a given envelope. Examples of surface filtration media are single-layer mesh screens, stacked washers, wound metallic ribbons, and sheets of perforated metals.

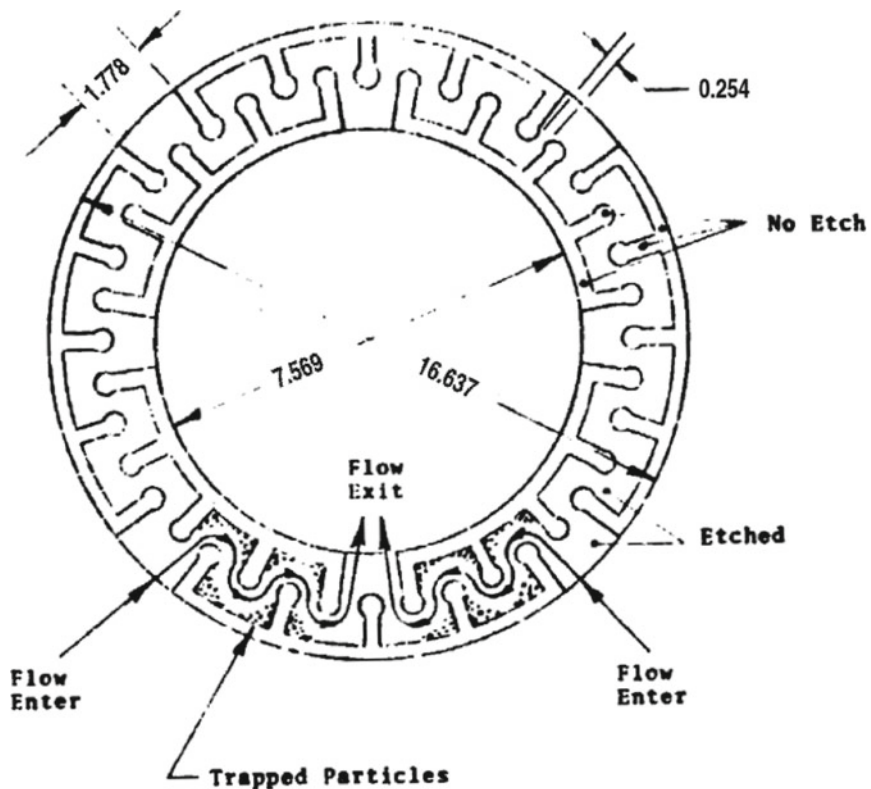
The other technique, called depth filtration, is accomplished by impingement and retention of solid particles in a matrix of pores placed in depth. Sand is a typical example of a depth filtering medium, in which the filtering action consists of absorption and entrapment of solid particles at random. Solid particles are retained not only at the surface, but also throughout the thickness of the filtering medium. The particles which pass through a matrix of pores are forced to change direction in a tortuous path. Depth filters are effective in collecting solid particles larger than the maximum size of the pores and fibres. They can also collect a portion of solid particles smaller than the largest size of the pores, depending on the type and on the thickness of the filtering medium. Their capability per unit area of retaining solid particles is large, because the particles are retained not only on the surface but also throughout the depth of the filtering medium. Examples of depth filtration media are multiple layers of mesh, wounded wire cylinders, stacked discs of paper, sintered granulated materials, multiple layers of cloth, compressed or matted organic or inorganic fibres, stacked discs of etched metallic sheet, materials of elastic foam with open pores, and stacked membranes [2].

In the particular case of filters used in fluid-carrying ducts of rocket engines, most surface filters are made of woven wire cloth, and most depth filters are made of stacked etched metallic discs.

In a filter made of woven wire cloth, the filtering medium is woven from strands of metal. A type of weave is plain square wave, in which the strands pass over and under each other in alternating sequence. Another type is twilled square wave, in which the strands pass “over two, under two” in a staggered pattern. In both cases, the resultant openings are square-shaped [16]. Woven wire cloth, also known as woven wire mesh, is woven on looms, by using a process similar to that used to weave clothing. The mesh uses one or another of various crimping pattern for the interlocking segments. Square mesh, described above, is the most common type of mesh. The plain weave is the most common weave for woven wire cloth with a square opening in the plain weave. Materials used are austenitic and ferritic stainless steels. This type of filter is suitable for non-critical hydraulic, pneumatic, and propellant feed applications [2]. The following figure, adapted from [16], shows a wire cloth pleated conical filter.



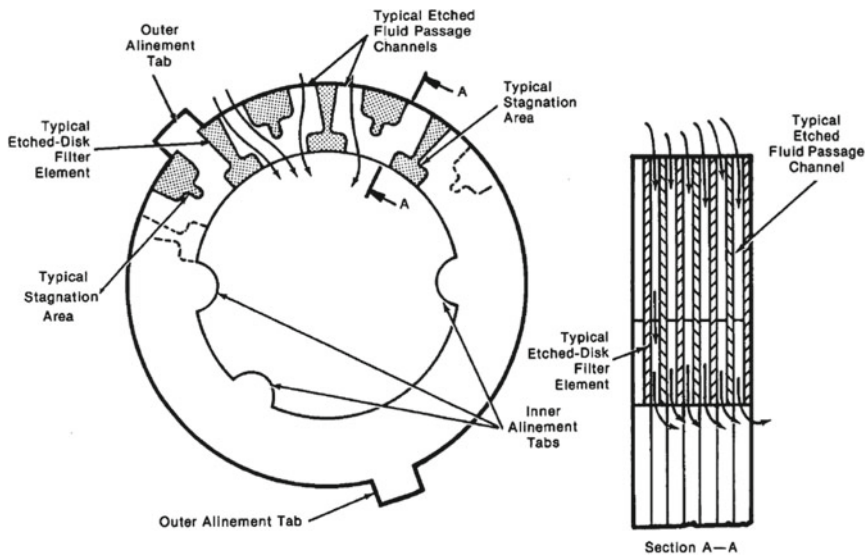
An etched-disc filter is a stack of segments resembling thin washers. Each segment has one face chemically etched to provide a desired flow path, as shown in the following figure, adapted from [16], where all dimensions are expressed in millimetres.



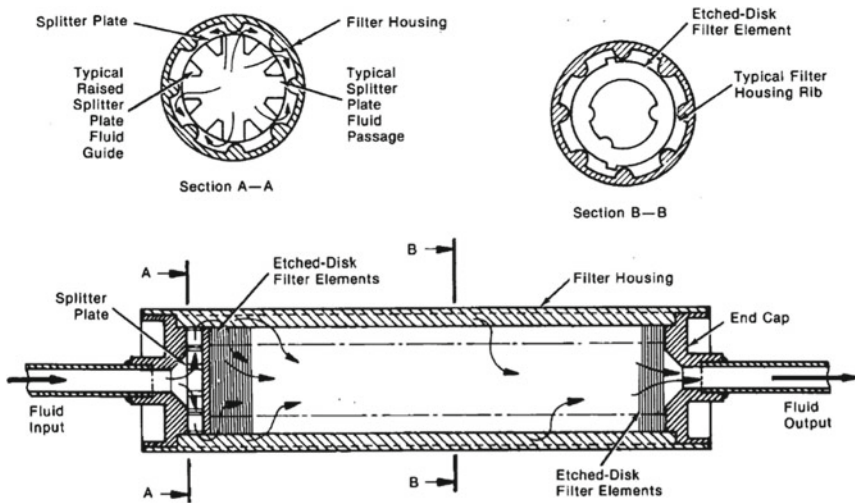
The non-etched face of each segment in the stack is in contact with the etched face of the next adjacent segment, so that the etched areas form minute passages for the flow. The stack of segments is held rigidly by a supporting cage and is tightly compressed. The depth property of an etched disc filter is obtained by compelling

the solid particles to cross the surface of each segment through a tortuous path. An etched disc filter can be cleaned by releasing the compression on the segments and back-flushing. This type of filter is suitable for critical hydraulic, pneumatic, and propellant feed applications. Recent advances in wire cloth filter technology have broadened the field of choice for critical applications. However, the etched disc filter remains the only filter made only of metal which can be used for filtering particles below 8×10^{-6} m [2].

A full-flow etched-disc filter, developed by Caltech/JPL [17], has fluid passageways in a configuration which allows very low restriction of flow and has also stagnation areas for the collection of impurities. A filter housing without a central post has also been developed to improve the flow characteristics. The full-flow etched-disc filter produces a zero reversal of flow and a very low drop of pressure. A permanently sealed (welded) filter housing without a central post has improved the flow characteristics. The following figure, due to the courtesy of NASA [17], shows an etched-disc filter element consisting essentially of a thin metallic disc with shallow, radially-disposed, etched, fluid channels incorporating stagnation areas located away from the main flow streams.



Fluid may flow in either direction. The discs have inner alignment tabs, which ensure proper front-to-back orientation, and outer alignment tabs, which keep the discs aligned within a housing. The following figure, also due to the courtesy of NASA [17], shows: (above) how the discs are oriented, front-to-back, so that the non-etched surfaces are adjacent to the aligned etched channels; and (below) the assembled etched-disc filter.

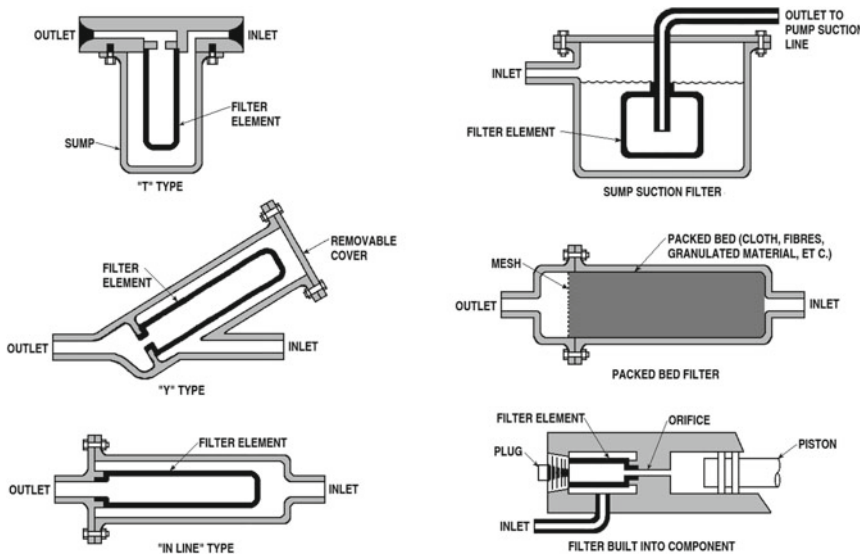


Of various metals used for filters, stainless steel is the most common. Filters of the wire-mesh type have, in comparison with those made of stacked etched discs, the advantages of:

- greater surface area with lower weight; and
- capability of handling higher flow rates.

Filters and filter elements are covered by the military standards MIL-F-5504B [18] and MIL-F-8815D [19].

Some standard filter elements and filter cases used in hydraulic systems for aircraft are illustrated in the following figure, re-drawn from [2]. As shown in this figure, filter cavities can also be machined in the body of a component such as a servo-cylinder, a pump, or a regulator. A filter case provides structural support for a filter element. The design of a filter case takes account of space available, easiness of access and service, pressure loss, fluid compatibility, and pressure and temperature in operating conditions. The size and the shape of a filter case have influence on the capacity and the service life of the filter.



The choice of a type of filter case depends on requirements of accessibility. The in-line filter case is the least accessible type of filter. It requires the removal of the case from the piping system before a filter element can be removed. The T-type, also known as pot type, is designed so that the filter element can be removed by removing the filter pot. The Y-type is designed so that the filter element can be removed through one leg of the Y, by removing a blank flange or a cover plate.

The seal used for a filter is particularly important in case of mechanical vibrations. In critical propellant feed applications, internal seals should be avoided whenever possible, due to compatibility of materials and generation of particles during assembly.

Such devices as supporting cages, bolts, nuts, and O-rings are used to seal the filter element at its interface with the case. The seals or the locking devices used in filters are designed so as to avoid damages due to parts of filters which may migrate downstream.

Some filters have a pressure indicator which senses abnormal high differences in pressure across a filter element. This device may sometimes indicate a high difference in pressure where a liquid and a gas flow intermittently. This may happen in ducts carrying cryogenic fluids.

Some filters used in lubrication and hydraulic ducts have a built-in by-pass valve, which opens and by-passes the filter when the difference in pressure across it exceeds a given value. This device is incorporated in the filter, because it is better in some cases to keep a fluid-carrying duct working with a contaminated fluid than to have a complete failure due to lack of fluid when the filter becomes plugged. This device is rarely used in rocket engines which operate for a very brief period of time, and therefore the level of contamination in these filters cannot grow appreciably during their operating time.

A filter can be cleaned in one or more of the following manners:

- back-flushing;
- ultrasonic cleaning;
- flushing;
- purging; and
- initial cleaning.

A brief description of these methods is given below.

Back-flushing results from reversing the direction of flow through a filtering element, with consequent flushing of solid particles from the inlet side of the filter. This method removes loose particles, but not those which are tightly fixed within the porous medium. Therefore, back-flushing must be followed by other methods to restore a filter element to its original conditions of cleanliness.

Ultrasonic cleanliness consists in immersing a filter element in a tank containing a solvent solution, and applying ultrasonic waves to this solution by means of transducers mounted on or within the tank. The ultrasonic waves produce cavitation on the surface of the filter element immersed in the solution, and this in turn loosens solid particles on the filter element.

Flushing a filter element in the normal direction of flow, after applying back-flushing or ultrasonic cleaning, removes the solid particles which have previously been loosened and improves the degree of cleanliness.

Purging consists in using a pre-filtered dry gas, such as air or nitrogen, which passes through a filter element to dry it and to also remove residual solvent which may be left by previous cleaning processes. Purging a filter element is often less effective than ultrasonic cleaning and back-flushing.

Initial cleaning of a new filter element is necessary, because solid particles may have been introduced during manufacture and assembly of the filter into the filter element and also into the filter case.

Ultrasonic cleaning, flushing, and back-flushing may be combined together to reach a desired level of cleanliness in a filter element.

Cloth elements made of stainless steel can reach a higher degree of initial cleanliness by applying acid passivation after assembly, or by annealing the assembly in an environment of hydrogen [2].

The choice of a particular type of filter to be used for a specific application depends on:

- largest size of solid particles which can be tolerated by the components of a fluid-carrying duct;
- amount and type of solid particles which may be contained in a fluid during the service life of a given rocket engine;
- maximum loss of pressure due to the presence of a given filter; and
- space available within a fluid-carrying duct.

The maximum allowable size of solid particles in a given component (for example, a valve or a servo-actuator) can be determined by evaluating the clearances or the sizes of narrow passages in the given component which are sensitive to contaminants. For this purpose, it is necessary to determine the possible malfunctions of the given component caused by the entrapment of solid particles carried by the fluid.

The amount and the type of solid particles during service life is difficult to determine, because of uncertainties in the prediction of: (a) amount of solid particles which remain after cleaning a given component and its filter; (b) amount of solid particles which are carried by the fluid; and (c) fluids and temperatures in operational conditions, which may differ from those of the tests conducted in laboratories.

The maximum loss of pressure due to a given filter and the space available within the given duct can result from a system analysis and a trade-off study to determine whether it is more advantageous to install a filter mounted externally to the component to be protected or a filter forming an integral part of the component itself.

The largest size of solid particles which can be transmitted through a filter is expressed by a parameter known as filter rating. This parameter measures the degree of protection which a filter provides for downstream components.

Several types of filter rating are specified by filters manufacturers.

One of them is the maximum particle size rating (MPR), which is the longest dimension, in microns, of any solid particle allowed downstream of a filter.

Another type of filter rating is the absolute rating, also known as glass bead rating (GBR), which is the size, in microns, of the largest hard spherical particle (i.e., glass bead) which would be removed by the filter under steady flow conditions [16]. In other words, the definition of absolute filter rating considers all solid particles to have spherical shape, and requires a filter to retain all solid particles whose diameter is greater than or equal to a specified value. Therefore, the absolute rating takes account only of the second largest dimension of any solid particle which can be transmitted through a filter.

Still another type of filter rating is the nominal rating, which assesses the ability of a filter to remove a specified percentage (in either count or weight) of spherical solid particles or graded dust whose size is equal to or greater than the value defined by its absolute rating. Therefore, the nominal rating of a given filter is always less than its absolute rating.

The maximum particle size rating can be determined by test. The test is conducted by using a readily identifiable contaminant with particles of various sizes and shapes. A procedure for determining the maximum particle size rating is described in [16].

The absolute rating of a filter also can be determined by test. A test is conducted by filtration of an artificial contaminant (glass beads) under specified conditions, as described in [19].

The nominal average rating of a filter can be determined by means of a mercury intrusion test, which is described in [20].

Maximum particle size tests are not practical for acceptance testing of production filters. The glass bead test is a destructive type of test, and therefore is never used as an acceptance test. However, correlation of a glass bead test with a non-destructive bubble-point test permits verification of absolute rating for production filters [1]. The bubble-point test is based on the fact that, for a given liquid and for a given size of pores with a constant wetting, the pressure necessary to force a bubble of air through a pore is inversely proportional to the diameter of the pore. In other words, the diameter of the largest pore in a filter can be measured by wetting the filter element with a liquid and then measuring the pressure at which the first stream of bubbles is emitted from the upper surface of the filter element, when air is introduced to the open end. The pressure at which the first stream of bubbles emerges is taken as a measure of the diameter of the largest pore. The value of the constant of inverse proportionality between pressure and diameter is determined experimentally. Further information on the bubble-point test can be found, for example, in [16, 21]. The bubble-point test is covered by the standards ISO 4003:1977 [22] and ARP 901A [23].

As has been shown above, a filter is necessary to reduce the size of solid particles carried in suspension by an operating fluid to a level which cannot cause damage to critical components of a duct. The determination of the filter area required for this purpose is based on an accurate prediction of the amount of contaminant which can be expected for any given application. The problem of accurately predicting the actual degree of contamination is still open. So far, there appears to be no correlation between the actual and the predicted amounts, sizes, and types of contamination [1]. The reason of this may be the variation in techniques used in manufacturing and building components and assemblies.

In this state of things, for the purpose of demonstrating that a filter of sufficient area has been provided for a given application, a specified amount of contaminant is required to be retained by the filter, without exceeding some maximum difference of pressure between its inlet and outlet. The contaminants most frequently used are AC-Fine and AC-Coarse dusts. These test dusts are Natural Arizona Dusts supplied by General Motors Phoenix Laboratory and classified to specific particle-size distributions by the AC Spark Plug Division of General Motors Corporation [1]. Further information on AC-Fine and AC-Coarse dusts can be found in [24]. The two dusts named above provide a baseline material for evaluating the ability of a filter to retain particles on its upstream side under flow conditions. Buckingham and Winzen [16] gives further information on tests which were conducted to determine the tolerance of various filter materials to contaminants for both gaseous and liquid flow.

Residual contaminants, that is, contaminants remaining in a filter after cleaning, may slough off and pass downstream of the filter. As has been shown above, such contaminants may accumulate in a filter during its manufacturing process, or be introduced there by the operating fluid, or be generated by the wear of mechanical components.

A cleaning of a filter removes a part of contaminants from the filter, the amount of this part depending on the accuracy of the cleaning process. Since this process is expensive, sometimes more expensive than the manufacturing process, then it is desirable to reduce the amount of contaminants which accumulate during fabrication, assembly, and testing.

It is also desirable to reduce media migration, that is, the presence in the operating fluid of contaminants coming from either the filter element or the filter-supporting structure. Filter materials subject to media migration are sintered porous metals, pressed paper, matted fibres, glass fibres, sintered plastic, fired porcelain, bonded carbon, and bonded stone [1, 2].

One of the most common tests for media migration combines thermal shock with vibration. In this test, a filter is exposed to its highest service temperature for a period of time and then to its lowest service temperature for an equal period. This procedure is repeated several times. After this thermal shock, the filter is caused to vibrate at frequencies of service for a given period of time. After testing, the filter is flushed with a given amount of fluid (usually 500 ml of either Freon TF or some ozone-friendly substitute for it), and the fluid is collected and passed through a $0.45\ \mu$ membrane pad. The membrane pad is then analysed for particles identifiable as material coming from either the filter element or the filter-supporting structure. When all of the particles are non-metallic and the filter is made entirely of metal, then no media migration has occurred. When some of the particles are metallic, then further analysis is required, and the filter material must be distinguished from residual contaminants [1]. Individual particles taken from a representative sample of the pad can be identified by microscopic examination.

The problem of determining the loss of pressure Δp through a filter as a function of its volumetric flow rate q is difficult to solve. In case of a filter element of the surface type, the pressure loss across the filter medium for either fine or coarse mesh is small in comparison with the pressure loss at filter entrance or exit.

In practice, the problem indicated above can be solved by tests which make it possible to plot curves of pressure loss against volumetric flow rate.

One of the formulae which can be used for determining the properties of a filter is known as the Kozeny-Carman equation [25], which is briefly discussed below.

The Kozeny-Carman equation expresses the pressure loss Δp (N/m^2) of a fluid which passes through a porous material, such as a packed bed of solids. This equation, which holds only in case of laminar flow ($Re \leq 1$), can be expressed as follows

$$\frac{\Delta p}{L} = -\frac{180\mu}{\phi_s^2 D_p^2} \frac{(1-\varepsilon)^2}{\varepsilon^3} u = -\frac{180\mu}{\phi_s^2 D_p^2} \frac{(1-\varepsilon)^2}{\varepsilon^3} \frac{q}{A}$$

where L (m) is the total height of the bed, μ ($\text{kg m}^{-1} \text{ s}^{-1}$) is the coefficient of dynamic viscosity of the fluid, ϕ_s is the sphericity (see below) of the particles in the packed bed, D_p (m) is the diameter of the volume equivalent spherical particle, ε is the porosity (the fraction of the volume of voids over the total volume) of the bed, μ (m/s) is the mean velocity of the fluid at right angles to the layers of the bed,

q (m^3/s) is the volumetric flow rate of the fluid through the bed, and A (m^2) is the cross-sectional area of a layer (the cross-sectional area of the solids plus the cross-sectional area of the pores) of the bed. The minus sign in front of the right-hand side of the preceding equation takes account of the loss of pressure with increasing mean velocity or volumetric flow rate.

By sphericity ϕ_s of a particle in a packed bed we mean the ratio of the surface area of a sphere having the same volume V_p as the given particle to the surface area A_p of the particle, as follows

$$\phi_s = \frac{\pi^{\frac{1}{3}}(6V_p)^{\frac{2}{3}}}{A_p}$$

According to this definition, the sphericity of a spherical particle is unity, and the sphericity of any non-spherical particle is less than unity.

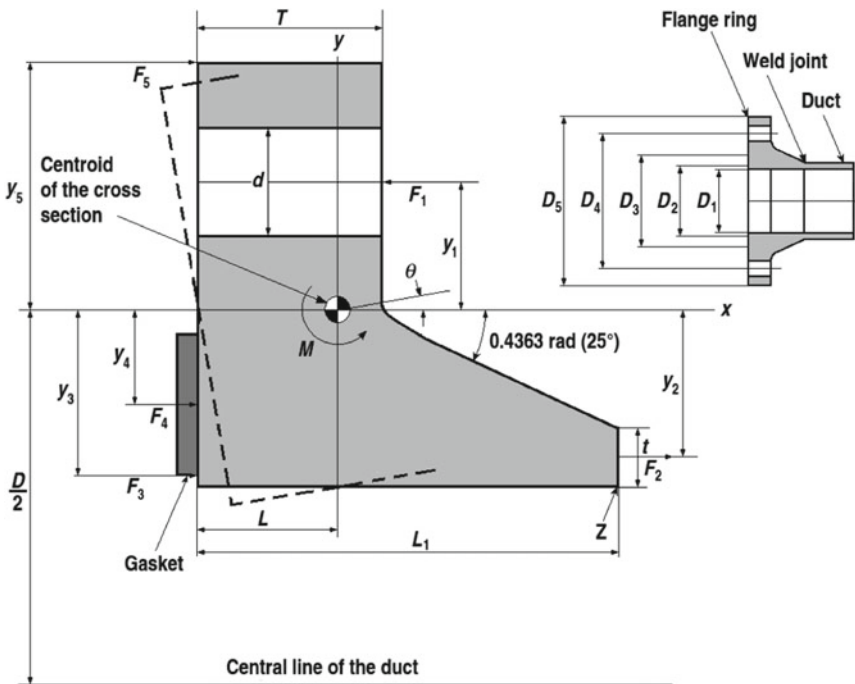
A derivation of the Kozeny-Carman equation and worked examples for its application can be found in [26].

Other equations (Darcy-Weisbach and Hagen-Poiseuille) found experimentally to determine the loss of pressure through a filter as a function of its volumetric flow rate are discussed in [16]. The equations cited above provide an excellent means for evaluating filter area requirements. However, they do not consider pressure losses at entrance and exit [1].

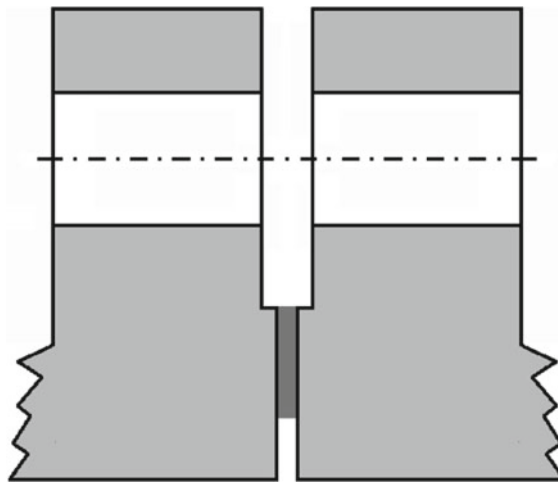
Filters are not tested for acceptance with the same fluids as the propellants used by rocket engines, because of difficulties due to testing with cryogenic or toxic or corrosive propellants. Some fluids used for tests are Freon TF, hydraulic oil, trichloroethylene, water, isopropyl alcohol, and methylated ethanol [1].

7.10 Design of a Flange Joint

A flange joint of a type frequently used for a rocket engine is shown in the following figure, re-drawn from [3].



Under various conditions of loads, the flange ring is subject to bending moments M , which cause the ring to rotate. The dashed line in the preceding figure indicates exaggeratedly the counter-clockwise direction of rotation of the flange ring illustrated in the preceding figure. Some flange joints of the raised-face type shown in Sect. 7.4 and also in the following figure, re-drawn from [28], have a small gap to eliminate or reduce stresses in the peripheral part of the flange ring. A flange joint of this type is sealed by the bolt force which squeezes the gasket. Seals used for flange joints will be described in Sect. 7.11.



The stresses resulting from the bending moments reach their maximum value at the point Z , where the flange connects with the wall of the inner cylindrical surface of the duct. The bolts used for a flange joint are frequently pre-stressed in tension, in order for a compressive stress to act on the gasket. This compression seals effectively the joint and avoids leakage.

Let us consider an arc of circle of unit length (1 m) passing through the centroid of the flange cross section. According to Huzel and Huang [3], the relations between the forces acting on this arc of circle and the minimum loads acting on the bolts can be written as follows

$$F_1 = F_2 + F_3 + F_4 + F_5$$

$$F_2 = \frac{pD_1^2}{4D} + \frac{W_e}{\pi D}$$

$$F_3 = \frac{p(D_2^2 - D_1^2)}{4D}$$

$$F_4 = \frac{\sigma_g(D_3^2 - D_2^2)}{4D}$$

$$\sigma_g = mp$$

$$F_5 = nF_1$$

$$W_b = F_1\pi D$$

where D (m) is the diameter of the circle passing through the centroid of the cross section of the flange ring, D_1 (m) is the inside diameter of the flange and of the duct, D_2 (m) is the inside diameter of the gasket, D_3 (m) is the outside diameter of the gasket, p (N/m^2) is the maximum pressure of the fluid in working conditions, F_1 (N/m) is the force per unit length of the flange ring due to the bolt loading, F_2 (N/m) is the force per unit length of the flange ring due to the longitudinal tension in the duct, F_3 (N/m) is the force per unit length of the flange ring due to the internal pressure, F_4 (N/m) is the force per unit length of the flange ring due to the gasket loading or seal loading, F_5 (N/m) is the force per unit length of the flange ring due to the compressive load at the outside of the flange, σ_g (N/m^2) is the average compressive stress on the gasket required for proper seating against an internal pressure p of the fluid, m is a gasket factor which depends on the gasket design and whose value (to be determined experimentally) ranges from 0.8 to 10, n is a flange factor which depends on the configuration and on the rigidity of the flange and whose value ranges from 0.1 to 0.8, W_e (N) are the end loads on the duct due to inertial and thermal effects (tension or compression), and W_b (N) is the minimum required bolt loading.

As an example of application [3] of the equations given above, the following data are known for a flexible duct at the discharge of the oxidiser pump used in a rocket engine: pressure in normal operating conditions $1.038 \times 10^7 \text{ N/m}^2$, maximum pressure in transient conditions $1.207 \times 10^7 \text{ N/m}^2$, inner diameter of the duct $D_1 = 0.2032 \text{ m}$, inner diameter of the gasket $D_2 = 0.2032 \text{ m}$, outer diameter of the gasket $D_3 = 0.2159 \text{ m}$, end loads in the duct due to thermal contraction $W_e = 1.068 \times 10^4 \text{ N}$, gasket factor $m = 0.8$, and flange factor $n = 0.3$. It is required to determine the minimum loading needed for the bolts of the flange joint.

By using the maximum value of pressure, we set $p = 1.207 \times 10^7 \text{ N/m}^2$. After substituting this value and $m = 0.8$ in the equation $\sigma_g = mp$, we find

$$\sigma_g = 0.8 \times 1.207 \times 10^7 = 0.9656 \times 10^7 \text{ N/m}^2$$

By substituting $F_5 = nF_1$ into $F_1 = F_2 + F_3 + F_4 + F_5$ and solving for F_1 , there results

$$F_1 = \frac{F_2 + F_3 + F_4}{1 - n}$$

By substituting this expression of F_1 and the following expressions

$$F_2 = \frac{pD_1^2}{4D} + \frac{W_e}{\pi D}$$

$$F_3 = \frac{p(D_2^2 - D_1^2)}{4D}$$

$$F_4 = \frac{\sigma_g(D_3^2 - D_2^2)}{4D}$$

into $W_b = F_1 \pi D$, there results

$$W_b = \frac{\pi p D_1^2 + 4W_e + \pi p(D_2^2 - D_1^2) + \pi \sigma_g(D_3^2 - D_2^2)}{4(1-n)}$$

After substituting $p = 1.207 \times 10^7 \text{ N/m}^2$, $D_1 = D_2 = 0.2032 \text{ m}$, $W_e = 1.068 \times 10^4 \text{ N}$, $D_3 = 0.2159 \text{ m}$, $\sigma_g = 0.9656 \times 10^7 \text{ N/m}^2$, and $n = 0.3$ in the preceding equation, we find the following value of the minimum loading needed for the bolts

$$W_b = \frac{3.1416 \times 1.207 \times 10^7 \times 0.2032^2 + 4 \times 1.068 \times 10^4}{4 \times (1 - 0.3)} + \frac{3.1416 \times 0.9656 \times 10^7 \times (0.2159^2 - 0.2032^2)}{4 \times (1 - 0.3)} = 6.321 \times 10^5 \text{ N}$$

After the minimum loading needed for the bolts has been determined as has been shown above, the following empirical relation can be used to determine the maximum circumferential spacing P_s (m) between two bolts required for a tight joint

$$P_s = 2d + T$$

where, with reference to the preceding figures, d (m) is the nominal diameter of each bolt, and T (m) is the thickness of the flange.

With reference to the preceding figures, the following empirical relations [3] can be used for the general proportions of a flange joint

$$T = At$$

$$L_1 = Bt$$

where T (m) is the thickness of the flange, t (m) is the thickness of the wall of the duct (depending on the circumferential stress σ_2 acting in the wall, as has been shown in Chap. 6), L_1 (m) is the overall axial length of the flange ring, and A and B are design factors, such that $4 \leq A \leq 8$, and $10 \leq B \leq 14$. The hub portion of the flange ring has a taper angle whose value is usually 0.4363 rad (25°).

With reference to the preceding figures, the following equations of [3] can be used to compute approximately the maximum stresses and strains in a flange ring

$$M = F_1y_1 + F_2y_2 + F_3y_3 + F_4y_4 - F_5y_5$$

$$y_1 = \frac{D_4 - D}{2}$$

$$y_2 = \frac{D - D_1 - t}{2}$$

$$y_3 = \frac{2D - D_2 - D_1}{4}$$

$$y_4 = \frac{2D - D_3 - D_2}{4}$$

$$y_5 = \frac{D_5 - D}{2}$$

$$\theta = \frac{MD^2}{4EI}$$

$$\sigma_z = \frac{MD^2(L_1 - L)}{2D_1 I}$$

where, with reference to the preceding figures, M (Nm/m) is the magnitude of the resultant bending moment per unit length of the flange ring, D_4 (m) is the diameter of the bolt circle, D_5 (m) is the outer diameter of the flange ring, y_1 (m), y_2 (m), y_3 (m), y_4 (m), and y_5 (m) are the distances between the centroid of the cross section of the flange ring and the forces per unit length respectively F_1 (N/m), F_2 (N/m), F_3 (N/m), F_4 (N/m), and F_5 (N/m), I (m^4) is the moment of inertia of the cross section of the flange ring about an axis perpendicular to the plane of the sheet, E (N/m^2) is the Young modulus of the material of which the flange is made, θ (rad) is the angle of rotation of the flange ring under maximum working pressure and loads, and σ_z (N/m^2) is the maximum tensile stress which occurs at the point Z of the flange ring in the circumferential direction.

With the same data as those of the preceding example, we want to design the flange for a flexible duct at the discharge of the oxidiser pump used in a rocket engine, with the following materials and related data: Inconel® alloy 718 [27] for flange and duct, minimum yield strength $\sigma_y = 1.172 \times 10^9 \text{ N}/\text{m}^2$, minimum ultimate strength $\sigma_u = 1.379 \times 10^9 \text{ N}/\text{m}^2$, Young modulus $E = 2.041 \times 10^{11} \text{ N}/\text{m}^2$, duct weld efficiency $e_w = 0.75$, bolt diameter $d = 7.938 \times 10^{-3} \text{ m}$, bolt head diameter $1.336 \times 10^{-2} \text{ m}$, A-286 stainless steel, ultimate bolt load $4.565 \times 10^4 \text{ N}$.

In order to determine the design limit pressure, we multiply the value $1.207 \times 10^7 \text{ N}/\text{m}^2$ of the maximum transient pressure by the safety factor 1.1, and obtain

$$1.1 \times 1.207 \times 10^7 = 1.328 \times 10^7 \text{ N}/\text{m}^2$$

Then, we determine the yield pressure p_y as follows

$$p_y = 1.1 \times 1.328 \times 10^7 = 1.461 \times 10^7 \text{ N}/\text{m}^2$$

and use this value to calculate the thickness t of the wall of the duct, as follows

$$t = \frac{p_y D_1}{2\sigma_y e_w} = \frac{1.461 \times 10^7 \times 0.2032}{2 \times 1.172 \times 10^9 \times 0.75} = 0.001689 \text{ m}$$

We determine the ultimate pressure p_u as follows

$$p_u = 1.5 \times 1.328 \times 10^7 = 1.992 \times 10^7 \text{ N/m}^2$$

and use this value to calculate again the thickness t of the wall of the duct, as follows

$$t = \frac{p_u D_1}{2\sigma_u e_w} = \frac{1.992 \times 10^7 \times 0.2032}{2 \times 1.379 \times 10^9 \times 0.75} = 0.001957 \text{ m}$$

We use the higher value (0.001957 m) of t , and round it to 0.002 m (2 mm), which value we choose for the thickness t of the wall.

We assume the values $A = 6$ and $B = 12.2$ for the flange design factors. By using the equation $T = At$, the thickness of the flange can be computed as follows

$$T = At = 6 \times 0.002 = 0.012 \text{ m} = 12 \text{ mm}$$

Likewise, by using the equation $L_1 = Bt$, the overall axial length of the flange ring results

$$L_1 = Bt = 12.2 \times 0.002 = 0.0244 \text{ m} = 24.4 \text{ mm}$$

The following values are given in [3] for the quantities D_4 , D_5 , L , D , and I : $D_4 = 0.2286 \text{ m}$, $D_5 = 0.2443 \text{ m}$, $L = 0.009398 \text{ m}$, $D = 0.2184 \text{ m}$, and $I = 1.136 \times 10^{-8} \text{ m}^4$. By solving the equation $W_b = F_1 \pi D$ for F_1 , we find

$$F_1 = \frac{W_b}{\pi D} = \frac{6.321 \times 10^5}{3.1416 \times 0.2184} = 9.213 \times 10^5 \text{ N/m}$$

Likewise, we compute F_2 as follows

$$\begin{aligned} F_2 &= \frac{p D_1^2}{4D} + \frac{W_e}{\pi D} = \frac{1.207 \times 10^7 \times 0.2032^2}{4 \times 0.2184} + \frac{1.068 \times 10^4}{3.14 \times 0.2184} \\ &= 5.860 \times 10^5 \text{ N/m} \end{aligned}$$

F_3 results from

$$F_3 = \frac{p(D_2^2 - D_1^2)}{4D} = 0 \text{ N/m}$$

because, in the present case, $D_1 = D_2$

F_4 results from

$$F_4 = \frac{\sigma_g(D_3^2 - D_2^2)}{4D} = \frac{0.9656 \times 10^7 \times (0.2159^2 - 0.2032^2)}{4 \times 0.2184} \\ = 0.5883 \times 10^5 \text{ N/m}$$

F_5 results from

$$F_5 = nF_5 = 0.3 \times 9.213 \times 10^5 = 2.764 \times 10^5 \text{ N/m}$$

The distance y_3 is of no interest, because $F_3 = 0$. The distances y_1, y_2, y_4 , and y_5 result from

$$y_1 = \frac{D_4 - D}{2} = \frac{0.2286 - 0.2184}{2} = 0.0051 \text{ m}$$

$$y_2 = \frac{D - D_1 - t}{2} = \frac{0.2184 - 0.2032 - 0.001689}{2} = 0.006756 \text{ m}$$

$$y_4 = \frac{2D - D_3 - D_2}{4} = \frac{2 \times 0.2184 - 0.2159 - 0.2032}{4} = 0.004425 \text{ m}$$

$$y_5 = \frac{D_5 - D}{2} = \frac{0.2443 - 0.2184}{2} = 0.01295 \text{ m}$$

By using the equation $M = F_1y_1 + F_2y_2 + F_3y_3 + F_4y_4 - F_5y_5$ with $F_3y_3 = 0$, the magnitude of the bending moment per unit length of the flange ring results

$$M = (9.213 \times 0.0051 + 5.86 \times 0.006756 + 0.5883 \\ \times 0.004425 - 2.764 \times 0.01295) \times 10^5 \\ = 5339 \text{ Nm/m}$$

The angle of rotation of the flange ring under maximum working pressure and loads results from

$$\theta = \frac{MD^2}{4EI} = \frac{5339 \times 0.2184^2}{4 \times 2.041 \times 10^{11} \times 1.136 \times 10^{-8}} = 0.02746 \text{ rad}$$

The maximum tensile stress, which occurs at the point Z of the flange ring in the circumferential direction, results from

$$\sigma_z = \frac{MD^2(L_1 - L)}{2D_1I} = \frac{5339 \times 0.2184^2 \times (0.0244 - 0.009398)}{2 \times 0.2032 \times 1.136 \times 10^{-8}} \\ = 8.275 \times 10^8 \text{ N/m}^2$$

The yield load stress at the same point results from

$$1.1 \times 1.1 \times 8.275 \times 10^8 = 1.001 \times 10^9 \text{ N/m}^2$$

The value computed above is less than the minimum yield strength ($\sigma_y = 1.172 \times 10^9 \text{ N/m}^2$) of the material chosen.

The ultimate load stress at the same point results from

$$1.5 \times 1.1 \times 8.275 \times 10^8 = 1.365 \times 10^9 \text{ N/m}^2$$

The value computed above is less than the minimum ultimate strength ($\sigma_u = 1.379 \times 10^9 \text{ N/m}^2$) of the material chosen.

Therefore, the design resulting from the preceding calculation is acceptable.

The maximum spacing between the bolts is computed by using the following equation

$$P_s = 2d + T = 2 \times 0.007938 + 0.012 = 0.02788 \text{ m}$$

The required number N of bolts results from the following equation

$$N P_s = \pi D_4$$

which, solved for N , yields

$$N = \frac{\pi D_4}{P_s} = \frac{3.1416 \times 0.2286}{0.02788} = 25.76 \approx 26$$

The minimum required value of the bolt loading ($W_b = 6.321 \times 10^5 \text{ N}$) has been computed above by using the maximum transient pressure ($p = 1.207 \times 10^7 \text{ N/m}^2$). The required ultimate bolt loading can be computed as follows

$$1.5 \times 1.1 \times 6.321 \times 10^5 = 1.043 \times 10^6 \text{ N}$$

Consequently, the ultimate loading on each bolt is

$$\frac{1.043 \times 10^6}{26} = 4.012 \times 10^4 \text{ N}$$

This value is smaller than the ultimate bolt load ($4.565 \times 10^4 \text{ N}$).

The required pre-load on each bolt is

$$\frac{W_b}{N} = \frac{6.321 \times 10^5}{26} = 2.431 \times 10^4 \text{ N}$$

The preceding description and the related examples of calculation refer to a common type of flange joint, but not to all types. Other types of flange joints have been illustrated in Sect. 7.4. Methods of calculation for such types of joints are described, for example, in [28, 29].

7.11 Gaskets and Other Seals for Flange Joints

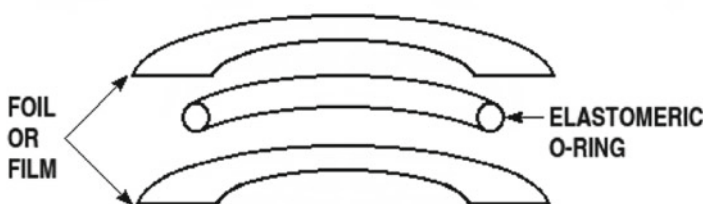
Gaskets are used as static seals. The following types of gaskets are generally used for flange joints:

- annular-ring gaskets;
- pressure-actuated gaskets; and
- full-face gaskets.

Gaskets of the annular-ring type are the most widely used for bolted flanges. Pressure-actuated gaskets use the internal pressure of the fluid as an aid to the sealing action. Full-face gaskets generally require higher bolt loads than is the case with annular-ring gaskets. Full-face gaskets are scarcely tolerant to thermal gradients, and have a tendency to concentrate the loads at the bolt holes and at the portion of the gasket outside the bolt circle. These gaskets are largely used for non-critical service conditions, but rarely used for service conditions involving either high (above 505 K) or cryogenic (below 122 K) temperatures, or relative pressures above 2.068 MPa [2].

A gasket used for a flange joint should be thick enough to provide adequate conformity to the surfaces of the metallic parts of the joint, because thicker gaskets are generally better suited to conform to surface scratches and to compensate for sealing waviness. However, the same gasket should be thin enough to provide stability to the joint and to prevent blow-out when residual stresses are low and internal pressures are high [2].

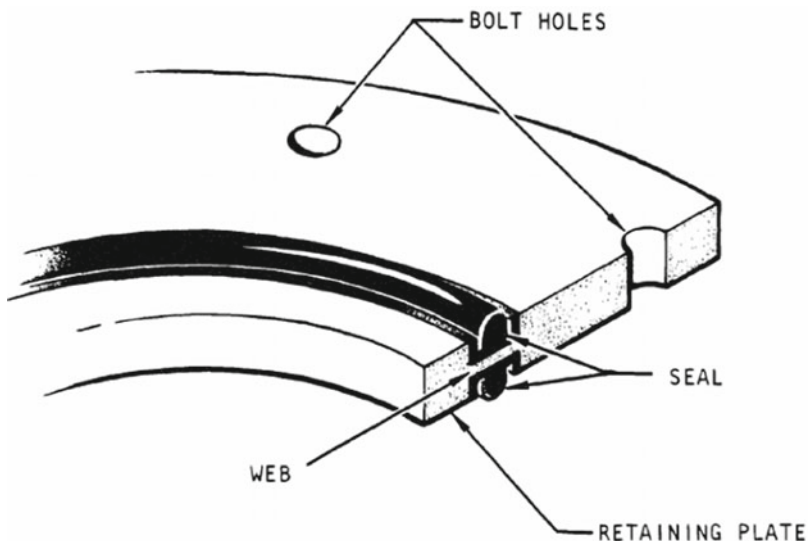
Gaskets of a common type have O-rings made of elastomeric materials, which are natural or synthetic rubbers. They are used over a temperature range going from 211 to 505 K for long periods of time, and at higher temperatures for shorter periods of time [11]. At low temperatures, the elastomeric O-ring is installed between thin foil films, or is coated with indium, which remains ductile at such temperatures, as shown in the following figure, re-drawn from [2].



The initial seal is obtained by compressing the elastomer to the desired position of installation. The pressure on the flange ring in service causes the elastomer to conform completely to the flange at the leak path.

Elastomeric O-ring gaskets can be used over a wide range of pressures and are highly reliable when installed properly. Incorrect installation can cause damage or improper squeeze or extrusion to the elastomer, with consequent leakage. The squeeze required to prevent damage while at the same time preventing leakage due to insufficient pressure ranges from 8 to 32%. O-ring extrusion and consequent nibbling of the elastomer occur when the clearance between the retaining members permits the elastomer to be forced into the clearance. When the elastomer becomes trapped, it is nibbled or sheared off when the pressure decays. Extrusion can be prevented by combining proper clearances and hard elastomers [11].

Elastomeric materials for flanges can also be used in moulded-in-place seals, which are flat plates having elastomeric inserts moulded into machined grooves, as shown in the following figure, due to the courtesy of NASA [11].



In these devices, the initial sealing action is due to the compression of the elastomer, and the subsequent sealing action is due to the pressure in service, which forces the elastomer against the flange at the leak path.

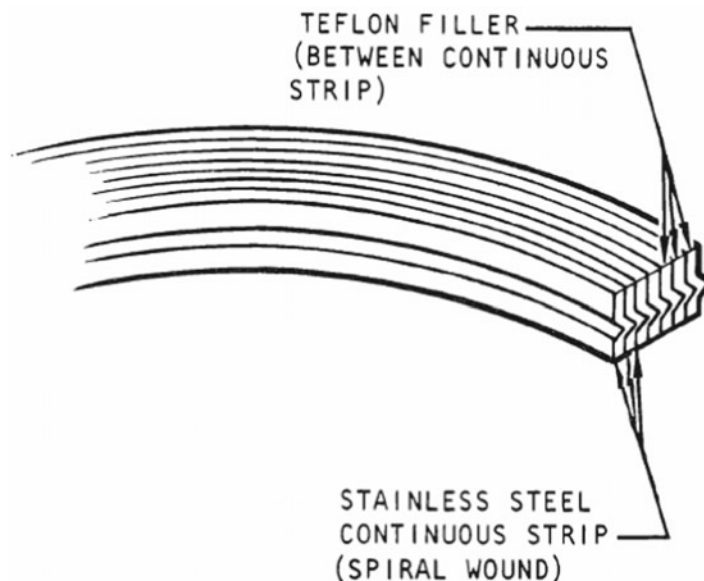
A moulded-in-place seal has the following advantages over a conventional O-ring:

- the thickness of the metal plate controls the amount of squeeze on the elastomeric portion of the seal, thereby permitting the use of flat-faced flanges on both sides of the seal, and making it unnecessary to machine an O-ring groove in one of the flanges; and
- it is easier to install in large and cumbersome hardware, because it can be installed laterally between two flanges.

Moulded-in-place seals have been used successfully in the fuel system of the F-1 rocket engine [11].

Metallic gaskets can be used at both cryogenic and high temperatures. These gaskets require high seating loads and are scarcely apt to follow flange deflection. Metallic O-rings are used in rocket engines particularly where the flanges or the mating surfaces are very rigid and connected with ample bolting [11]. Metallic O-ring perform satisfactorily in these conditions and offer the advantage of small cross sections where space is limited. They can be either Teflon®-coated for use at cryogenic temperatures or soft-metal plated for use at high or cryogenic temperatures.

Spiral-wound gaskets (see Chap. 5, Sect. 5.8) are made of a V-shaped ribbon of stainless steel wrapped spirally with a soft filler of either graphite or Teflon® between the turns, as shown in the following figure, adapted from [11].

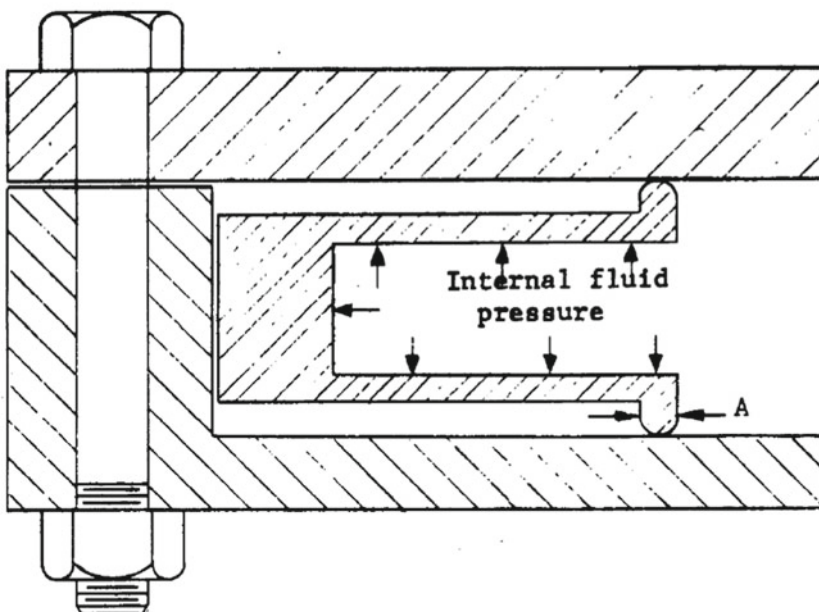


These gaskets were used extensively in rocket engines for both cryogenic and high (up to 811 K) temperatures. They need heavy, rigid flanges and high bolt loads (of the order of magnitude of $5 \times 10^5 - 7 \times 10^5$ N per metre of circumference). The high loads at the edges of the steel ribbon caused marring of the mating flanges and reduced the possibility of achieving a good seal when the joint was re-assembled [11]. Spiral-wound gaskets are still used today where leakage is tolerable, which happens in isolate engine locations and in large diameters, where they have a cost advantage over more sophisticated machined seals.

Pressure-actuated seals were originally developed for cryogenic temperatures. Later on, they were modified for hot gases. They have been used extensively in the J-2 and F-1 rocket engines. Their range of use includes cryogenic fluids at temperatures

as low as 20 K and pressures as high as 27.56 MPa, and hot gases at temperatures up to 1033 K and pressures up to 10.34 MPa [11].

Pressure-actuated seals are more complex to manufacture and more expensive than those using elastomeric materials, and therefore are used only when those of the latter type cannot meet the requirements. The cross section of a pressure-actuated seal expands due to the internal pressure exerted by the fluid carried in the duct, and this expansion generates the seal. The deflection of the sealing face is larger than the deflection permissible in an elastomeric material. Therefore, a flange using a pressure-actuated seal can be less rigid and heavy than one using an elastomeric seal. A pressure-actuated seal of the cantilever (U-shaped) type is shown in the following figure, due to the courtesy of NASA [28].

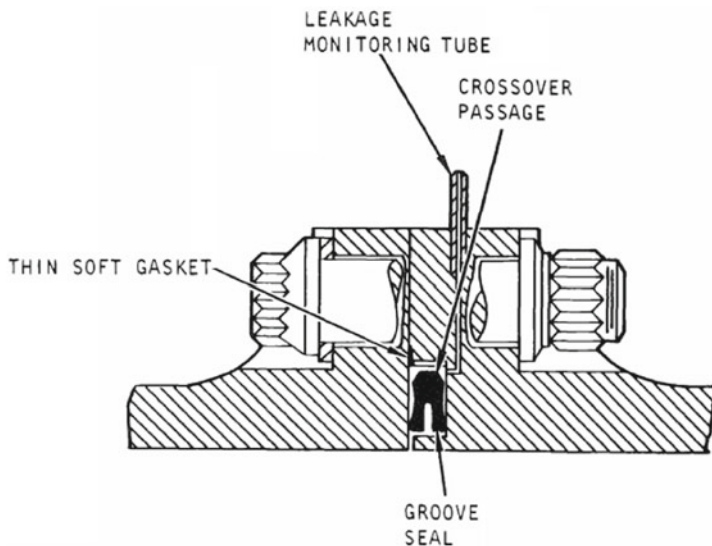


The U-shaped seal sits in a recess of the flange. The cross section of this seal has a web and two legs, each of which has a small tip at its end. The U-shaped seal is supported at the lips and at the outer surface of the web. The internal pressure of the fluid pushes the lips toward the inner surfaces of the flange, thereby exerting the sealing action. The dimensions of the cross-section of the seal are usually much smaller than the inside radius of the seal, and the legs of the seal are much more flexible than the web [28]. The cross section of a pressure-actuated seal may also be C-shaped (open O-ring) instead of U-shaped.

According to [28], pressure-actuated seals have the following advantages over elastomeric or metallic O-rings:

- high resiliency in seal and low clamping pressures, which result in lightweight flanges;
- high localised sealing stress;
- external load taken by other components of the connector;
- use of available pressure to increase sealing; and
- reduction of negative effects of extreme temperatures, due to the ability of the seal to “follow through”.

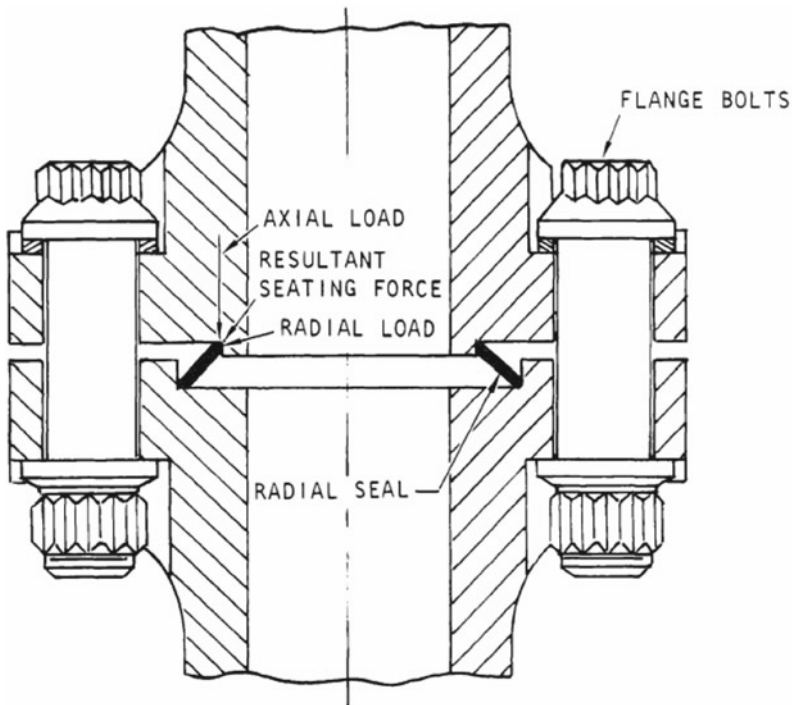
Pressure-actuated seals used for ducts carrying cryogenic fluids are generally coated with Teflon® or with metallic plates. Metallic pressure-actuated seals have been employed in the RS-25 engines of the Space Shuttle. They have been used for cryogenic fluids at temperatures as low as 20 K and pressures up to 62.05 MPa, and also for hot gases at temperatures up to 1255 K and pressures up to 42.75 MPa. The metallic seals have been made of Inconel® 718 plated with silver or gold to provide a soft sealing material at the interface [11]. A groove-type seal, shown in the following figure, adapted from [11], is used to save weight and provide a small envelope.



Plastic spring-loaded seals have been developed for fluids at cryogenic temperatures. Such seals are made of a jacket of plastic material, usually Teflon®, which covers a core of metallic spring. The spring provides the force required for the initial seal and also the forces necessary to compensate for dimensional changes resulting from thermal expansions and contractions. These seals are pressure-actuated, and therefore the sealing load increases with pressure.

Plastic spring-loaded seals are less reliable than metallic pressure-actuated seals at cryogenic temperatures, and are therefore used principally in rocket engines fed with storable propellants, when elastomeric materials are not compatible with such propellants.

A seal of the radial type used for a flange is shown in the following figure, due to the courtesy of NASA [11].

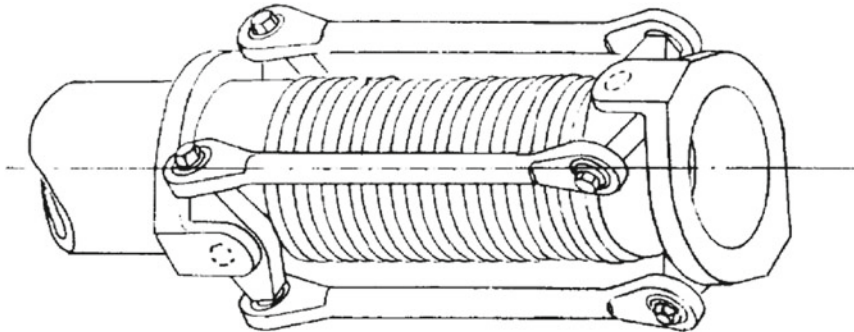


In this seal, the axial load acting on the flange is converted to a radial load acting on the interface through a toggle action within the structure of the seal. The two pieces of the flange joint are designed to confine the outer diameter of the seal, so that radial interference occurs and plastic flow of the seal takes place when an axial load is applied to the joint during installation. The plastic flow makes the seal not re-usable, but the two pieces of the joint are re-usable after installation of new seals. The magnitude of the axial load per unit length required to install a radial seal ranges from 87500 to 105000 N per metre of circumference.

A type of radial seal, the Conoseal® (described in [30]), has been used in some rocket engines (such as the M-1 engine and the Titan engines) and for some rocket vehicles (such as the upper stages S-IV and S-IVB) to seal flange joints for ducts carrying cryogenic propellants, storable propellants, and hot gases [11].

7.12 Design of a Bellows Joint for a Flexible Duct

In the present paragraph, we consider a bellows joint with restraining linkage for a flexible duct at the discharge of the oxidiser pump used in a rocket engine. The bellows joint is shown in the following figure, adapted from [1].



The equations considered below use the following symbols: C_t is the correction factor of the bellows wall-thinning; C_p is the ply inter-reaction factor (whose values are 1.00 for one-ply bellows, 0.90 for two-ply bellows, and 0.85 for three-or-more ply bellows); d_o (m) is the outside diameter of the bellows; d_i (m) is the outside diameter of the convolution root of the bellows; $d_m = [(d_i^2 + d_o^2)/2]^{1/2}$ (m) is the root-mean-square diameter of the bellows; d_d (m) is the mean diameter of the duct; E (N/m²) is the Young modulus of the material of which the bellows is made; e_a (m) is the axial deflection of the bellows; e_b (m) is the equivalent axial deflection of the bellows due only to bending; e_p (m) is the equivalent axial deflection of the bellows due to parallel offset; e_s (m) is the equivalent axial deflection of the bellows due only to shear; F_s (N) is the shear load; F_p (N) is the pressure separating load; G (N/m²) is the shear modulus of elasticity of the material of which the bellows is made; $h = (d_o - d_i)/2$ (m) is the mean height of the convolutions of the bellows; L (m) is the axial length of a convolution of the bellows; $L_a = (N_c - \frac{1}{2})L + N_p t$ (m) is the free axial length of the bellows; N_c is the number of convolutions of the bellows; N_p is the number of plies; t (m) is the thickness of the wall of the bellows; L_b (m) is the axial length of the rigid duct; M (Nm) is the bending moment; p (N/m²) is the internal or external pressure of the fluid; p_{cr} (N/m²) is the critical pressure for stability of the bellows; R_a (N/m) is the axial spring constant of the bellows; R_b (N/m) is the bending spring constant of the bellows; R_p (N/m) is the parallel offset spring constant of the bellows; R_s (N/m) is the shear spring constant of the bellows; R_t (Nm/rad) is the torsional spring constant of the bellows; σ_b (N/m²) is the bulging (meridian) stress of the bellows; σ_h (N/m²) is the hoop (circumferential) stress of the bellows; σ_m (N/m²) is the motion stress of the bellows; σ_s (N/m²) is the shear stress of the bellows; σ_t (N/m²) is the torsion stress of the bellows; T (Nm) is the torsional moment; T_{cr} (Nm) is the critical stability torsional moment of the bellows; v is the

Poisson ratio of the material of which the bellows is made; y (m) is the transverse deflection of the bellows; θ (rad) is the bending angle of rotation; and ϕ (rad) is the torsional angle of rotation.

Bellows are formed by applying hydraulic pressure to tubes of the same diameter d_i as the bellows diameter at the root of the convolution. The thinning process of the wall of a bellows starts at the original thickness of the material at the root of the convolution, and reduces approximately linearly the thickness to its minimum value at the outside diameter d_o of the convolution. The amounts of thinning range from 10% to 40% [3]. The effects of thinning are taken into account by applying the thinning correction factor to the bellows design.

For the bellows design, we use the following equations indicated by Huzel and Huang [3].

For steel and nickel alloys, the axial spring constant R_a (N/m) is expressed by

$$R_a = \frac{1.49C_t C_p N_p E d_i t^3}{N_c h^3}$$

For aluminium alloys, the axial spring constant R_a (N/m) is expressed by

$$R_a = \frac{1.23C_t C_p N_p E d_i t^3}{N_c h^3}$$

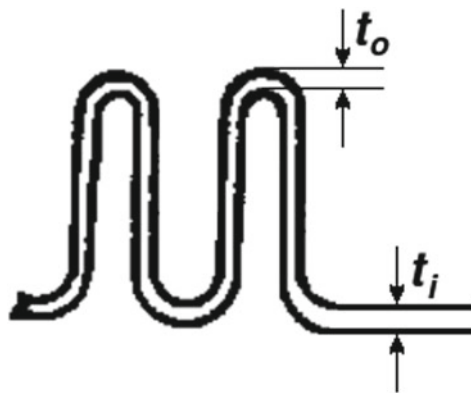
The value of the correction factor C_t in the two preceding equations can be determined by substituting the value of the percent thinning x , relating to the bellows of interest, in the following polynomial

$$C_t(x) = -0.0001333x^2 - 0.01133x + 1$$

The percent thinning x is defined as follows

$$x = \left(\frac{t_i - t_o}{t_i} \right) 100$$

where the thicknesses t_i and t_o are shown in the following figure.



Bulging (meridian) stresses σ_b (N/m^2) are the radial bending stresses induced in the side walls of the bellows by internal or external pressure. They are expressed by

$$\sigma_b = \frac{C_t p h^2}{2 N_p t^2}$$

The value of the correction factor C_t in the preceding equation can be determined by substituting the value of the percent thinning x , relating to the bellows of interest, in the following polynomial

$$C_t(x) = 0.0004 x^2 + 0.01 x + 1$$

The values of σ_b should be kept below those given in the following table, adapted from [3], which indicates mechanical properties of some materials used for bellows.

Material	Yield strength, MPa	Limiting bulging stresses, MPa		Allowable motion stresses, MPa		
		$t \leq 0.3048 \text{ mm}$	$t \geq 0.3302 \text{ mm}$	1000 cycles	10,000 cycles	100,000 cycles
321 and 347 stainless steels	269	965	827	1430	1030	634
19-9DL	607	965	827	1430	1030	634
A-2S6	1240	1310	1030	1100	1030	951
Inconel 718	1170	1310	1030	1100	1030	951
Inconel X-750	676	1310	1030	1100	1030	951
6061-T6 aluminum alloy	276	448	448	731	469	193

Bellows are subject to separating loads, because they are loaded by pressure and also by the axial force acting along the duct. The pressure separating loads F_p (N)

are expressed by

$$F_p = \frac{p(d_m^2 - d_d^2)\pi}{4}$$

The hoop (circumferential) stresses σ_h (N/m²) in a bellows are calculated as follows

$$\sigma_h = \frac{p d_m}{2 N_p t \left(\frac{\pi}{2} - 1 + \frac{2h}{L} \right)}$$

The values of these stresses should be kept below the yield and ultimate strengths of the bellows material by a given margin.

Motion stresses σ_m (N/m²) due to axial deflection of the bellows are caused by bending of the side walls of the bellows. For steel and nickel alloys, motion stresses due to axial deflection are expressed by

$$\sigma_m = \frac{1.40 C_t E t e_a}{N_c h^2}$$

For aluminium alloys, motion stresses due to axial deflection are expressed by

$$\sigma_m = \frac{1.78 C_t E t e_a}{N_c h^2}$$

The value of the correction factor C_t in the preceding equation can be determined by substituting the value of the percent thinning x , relating to the bellows of interest, in the following polynomial

$$C_t(x) = 0.000067x^2 - 0.0023x + 1.02$$

Allowable motion stresses for bellows materials, depending on their design cycle life, are given in the preceding table.

Motions of the bellows due to other causes than axial deflection (for example, angular motion and parallel offset motion) can be converted into an equivalent axial deflection of the bellows. By so doing, the two preceding equations expressing σ_m can also be used to calculate the corresponding motion stresses, as will be shown below.

In case of bellows subject to pure bending, the corresponding motion stresses σ_m can be computed by using the following equations

$$R_b = \frac{M}{\theta} = \frac{d_m^2 R_a}{8}$$

$$e_b = \frac{1}{2} d_m \sin \theta$$

$$\sigma_m = \frac{1.40C_t E t e_b}{N_c h^2} \quad \text{for steel and nickel alloys}$$

$$\sigma_m = \frac{1.78C_t E t e_b}{N_c h^2} \quad \text{for aluminium alloys}$$

where the value of the correction factor C_t in the preceding equations can be determined by substituting the value of the percent thinning x , relating to the bellows of interest, in the following polynomial

$$C_t(x) = 0.000067x^2 - 0.0023x + 1.02$$

In case of bellows subject to pure shear, the corresponding motion stresses σ_m can be computed by using the following equations

$$R_s = \frac{F_s}{y} = \frac{3d_m^3 R_a}{8L_a^2}$$

$$\theta = \frac{4F_s L_a}{R_a d_m^2}$$

$$e_s = \frac{3d_m y}{2L_a}$$

$$\sigma_m = \frac{1.40C_t E t e_s}{N_c h^2} \quad \text{for steel and nickel alloys}$$

$$\sigma_m = \frac{1.78C_t E t e_s}{N_c h^2} \quad \text{for aluminium alloys}$$

where the value of the correction factor C_t in the preceding equations can be determined by substituting the value of the percent thinning x , relating to the bellows of interest, in the following polynomial

$$C_t(x) = 0.000067x^2 - 0.0023x + 1.02$$

In case of bellows subject to parallel offset, the corresponding motion stresses σ_m can be computed by using the following equations

$$R_s = \frac{F_s}{y} = \frac{3d_m^2 R_a}{2L_a^2}$$

$$M = \pm \frac{F_s L_a}{2} = \pm \frac{3d_m^2 y R_a}{4L_a^2}$$

$$e_p = \frac{3d_m y}{2L_a}$$

$$\sigma_m = \frac{1.40C_t E t e_p}{N_c h^2} \quad \text{for steel and nickel alloys}$$

$$\sigma_m = \frac{1.78C_t E t e_p}{N_c h^2} \quad \text{for aluminium alloys}$$

where the value of the correction factor C_t in the preceding equations can be determined by substituting the value of the percent thinning x , relating to the bellows of interest, in the following polynomial

$$C_t(x) = 0.000067x^2 - 0.0023x + 1.02$$

In case of parallel offset of articulated bellows (two bellows, each of which L_a in free length, separated by a rigid duct L_b in length), the corresponding motion stresses σ_m can be computed by using the following equations

$$R_s = \frac{F_s}{y} = \frac{3d_m^2 R_a}{2(4L_a^2 + 6L_a L_b + 3L_b^2)}$$

$$M = \pm \frac{F_s(2L_a + L_b)}{2} = \pm \frac{3d_m^2(2L_a + L_b)yR_a}{4(4L_a^2 + 6L_a L_b + 3L_b^2)}$$

$$e_p = \frac{3d_m(2L_a + L_b)y}{4L_a^2 + 6L_a L_b + 3L_b^2}$$

$$\sigma_m = \frac{1.40C_t E t e_p}{N_c h^2} \quad \text{for steel and nickel alloys}$$

$$\sigma_m = \frac{1.78C_t E t e_p}{N_c h^2} \quad \text{for aluminium alloys}$$

where the value of the correction factor C_t in the preceding equations can be determined by substituting the value of the percent thinning x , relating to the bellows of interest, in the following polynomial

$$C_t(x) = 0.000067x^2 - 0.0023x + 1.02$$

The torsional stresses σ_t (N/m^2) in a bellows are calculated by using the following equation

$$\sigma_t = \frac{2T}{N_p \pi d_i^2 t}$$

and the torsional spring constant R_t (Nm/rad) of the bellows is

$$R_t = \frac{T}{\phi} = \frac{\pi G d_i t N_p}{4(2h + 0.57L)N_c}$$

A restrained bellows, if pressurised internally beyond a critical value p_{cr} (N/m²), is subject to an instability failure of the same type as a buckling column. The critical value of internal pressure results from

$$p_{cr} = \frac{5.02 R_a}{L_a \frac{d_o}{d_i}}$$

A bellows, if pressurised externally beyond a critical value p_{cr} (N/m²), is subject to buckling in the same manner as a thin cylinder. The critical value of external pressure results from

$$p_{cr} = \frac{4E t N_p h^3}{(1 - \nu^2) d_m^3 e_b}$$

A bellows, if loaded by pure torsion, buckles in some manner as one loaded by internal pressure. The critical value T_{cr} (Nm) of the torsional moment results from

$$T_{cr} = \frac{1}{2} \pi d_m^2 R_a$$

The critical pressure p_{cr} and the critical torsional moment T_{cr} have smaller values than those resulting from the preceding equations, in case of bellows under angular and offset deflections. The values of the correction factor to be applied are determined experimentally. These values range from 0.2 to 0.9 [3].

In case of bellows operating at high temperatures due to the flow of hot gases, working stresses used for bellows materials should be adjusted accordingly. An internal liner is generally provided to protect a bellows from high-velocity, high-temperature gases.

A bellows design depends on the forming process. The following geometric limits are generally used for bellows having up to three plies: maximum value of the ratio $d_o/d_i = 1.35$; and maximum value of the axial length of a convolution as a function of thickness $L = (8 + 2N_p)t$.

As an example of application of the concepts discussed above, it is required to design a bellows joint with restraining linkage for a flexible duct at the discharge of the oxidiser pump used in a rocket engine, with the following data: pressure in normal operating conditions 1.038×10^7 N/m², maximum pressure in transient conditions 1.207×10^7 N/m², and inner diameter of the duct $d_i = 0.2032$ m.

We use Inconel 718® for the material of which the bellows is made. This material has the following properties: minimum yield strength $\sigma_y = 1.172 \times 10^9$ N/m², minimum ultimate strength $\sigma_u = 1.379 \times 10^9$ N/m², and Young modulus $E = 2.041 \times 10^{11}$ N/m².

Since the inner diameter of the duct is $d_i = 0.2032$ m, then the outside diameter of the convolution root of the bellows is also $d_i = 0.2032$ m.

We also know that the percent thinning of the wall of the bellows is $x = 20\%$, the maximum value of the free axial length of the bellows is $L_a = 0.1778$ m, the angle of rotation of the bellows is $\theta = \pm\pi/60$ rad ($\pm 3^\circ$), and the life of the bellows is equal to 10000 cycles. In addition to the dimensions, it is also required to determine the axial spring constant R_a (N/m) of the bellows, the magnitude M (Nm) of the bending moment at the angle $\theta = \pm\pi/60$ rad, and the necessary restraining load F (N) due to the linkage at the maximum pressure in transient conditions 1.207×10^7 N/m².

As has been shown above, the bulging (meridian) stress σ_b (N/m²) is expressed by the following equation

$$\sigma_b = \frac{C_t p h^2}{2N_p t^2}$$

where the value of the correction factor C_t of the bellows wall-thinning can be determined by substituting 20 for x in the following polynomial

$$C_t(x) = 0.0004x^2 + 0.01x + 1$$

By so doing, we find $C_t = 1.36$.

From the table on the properties of materials given above, we take the value $\sigma_b = 1030$ MPa = 1.03×10^9 N/m² for the limiting bulging stress relating to Inconel 718® with a life of 10000 cycles and a thickness greater than or equal to 0.3302 mm. From the data of the present example, we also obtain the design limit pressure of the duct as follows

$$1.1 \times 1.207 \times 10^7 = 1.328 \times 10^7 \text{ N/m}^2$$

where 1.1 is the value of the safety factor. We also choose a three-ply bellows, such that $N_p = 3$.

After substituting $C_t = 1.36$, $p = 1.328 \times 10^7$ N/m², $\sigma_b = 1.03 \times 10^9$ N/m², and $N_p = 3$ in the following equation

$$\sigma_b = \frac{C_t p h^2}{2N_p t^2}$$

and solving for h/t , we find

$$\frac{h}{t} = \left(\frac{2N_p \sigma_b}{C_t p} \right)^{\frac{1}{2}} = \left(\frac{2 \times 3 \times 1.03 \times 10^9}{1.36 \times 1.328 \times 10^7} \right)^{\frac{1}{2}} = 18.50$$

We choose a thickness $t = 0.56$ mm = 5.6×10^{-4} m for the wall of the bellows, and consequently the mean height of the convolutions of the bellows results

$$h = 5.6 \times 10^{-4} \times 18.50 = 0.01036 \text{ m} \approx 0.0104 \text{ m}$$

Since $h = (d_o - d_i)/2 = 0.0104 \text{ m}$, $d_i = 0.2032 \text{ m}$, and $h = 0.0104 \text{ m}$, then the outside diameter of the bellows results

$$d_o = d_i + 2h = 0.2032 + 2 \times 0.0104 = 0.2240 \text{ m}$$

and the root-mean-square diameter of the bellows results

$$d_m = \left(\frac{d_i^2 + d_o^2}{2} \right)^{\frac{1}{2}} = \left(\frac{0.2032^2 + 0.2240^2}{2} \right)^{\frac{1}{2}} = 0.2136 \text{ m}$$

The equivalent axial deflection of the bellows due to pure bending results from the following equation

$$e_b = \frac{1}{2} d_m \sin \theta = 0.5 \times 0.2136 \times \sin\left(\frac{\pi}{60}\right) = 0.005589 \text{ m}$$

Again, from the table on the properties of materials given above, we take an allowable motion stress of $1030 \text{ MPa} = 1.03 \times 10^9 \text{ N/m}^2$ for Inconel 718® with a life of 10,000 cycles. However, we use a fraction of this value, that is,

$$0.36 \times 1.03 \times 10^9 = 3.708 \times 10^8 \text{ N/m}^2$$

to improve stability.

The number of convolutions N_c of the bellows can be determined by using the following equation

$$\sigma_m = \frac{1.40 C_t E t e_b}{N_c h^2}$$

where $\sigma_m = 3.708 \times 10^8 \text{ N/m}^2$, $e_b = 0.005589 \text{ m}$, and the value of the correction factor C_t of the bellows wall-thinning can be determined by substituting 20 for x in the following polynomial

$$C_t(x) = 0.000067 x^2 - 0.0023 x + 1.02$$

By so doing, we find $C_t = 1$. Therefore, N_c results from

$$N_c = \frac{1.40 C_t E t e_b}{h^2 \sigma_m} = \frac{1.40 \times 1 \times 2.041 \times 10^{11} \times 0.00056 \times 0.005589}{0.0104^2 \times 3.708 \times 10^8} = 22.3 \approx 22$$

The axial length of a convolution of the bellows results from

$$L = (8 + 2N_p)t = (8 + 2 \times 3) \times 5.6 \times 10^{-4} = 0.00784 \text{ m}$$

The free axial length of the bellows results from

$$L_a = (N_c - 1/2)L + N_p t = (22 - 0.5) \times 0.00784 + 3 \times 0.00056 = 0.1702 \text{ m}$$

The axial spring constant of the bellows is expressed by the following equation

$$R_a = \frac{1.49 C_t C_p N_p E d_i t^3}{N_c h^3}$$

where the correction factor C_t results from substituting 20 for x in the following polynomial

$$C_t(x) = -0.0001333 x^2 - 0.01133 x + 1$$

Hence, $C_t(20) = 0.72$. Therefore, the axial spring constant of the bellows is

$$\begin{aligned} R_a &= \frac{1.49 \times 0.72 \times 0.85 \times 3 \times 2.041 \times 10^{11} \times 0.2032 \times 0.00056^3}{22 \times 0.0104^3} \\ &= 8.051 \times 10^5 \text{ N/m} \end{aligned}$$

The critical value of internal pressure for the bellows (without angulation) results from

$$p_{cr} = \frac{5.02 R_a}{L_a \frac{d_o}{d_i}} = \frac{5.02 \times 8.051 \times 10^5}{0.1702 \times \frac{0.2240}{0.2032}} = 2.154 \times 10^7 \text{ N/m}^2$$

This value, divided by the value ($1.207 \times 10^7 \text{ N/m}^2$) of the maximum pressure in transient conditions, indicates a safety factor of 1.785, which allows for bellows stability in the presence of angulation.

As has been shown in paragraph 10, the yield pressure p_y and the ultimate pressure p_u result from

$$\begin{aligned} p_y &= 1.1 \times 1.1 \times 1.207 \times 10^7 = 1.461 \times 10^7 \text{ N/m}^2 \\ p_u &= 1.1 \times 1.5 \times 1.207 \times 10^7 = 1.992 \times 10^7 \text{ N/m}^2 \end{aligned}$$

The yield hoop (circumferential) stress σ_{hy} results from substituting $p_y = 1.461 \times 10^7 \text{ N/m}^2$ into the following equation

$$\sigma_h = \frac{p d_m}{2 N_p t \left(\frac{\pi}{2} - 1 + \frac{2h}{L} \right)}$$

By so doing, we find

$$\sigma_{hy} = \frac{1.461 \times 10^7 \times 0.2136}{2 \times 3 \times 0.00056 \times \left(\frac{3.1416}{2} - 1 + \frac{2 \times 0.0104}{0.00784} \right)} = 2.881 \times 10^8 \text{ N/m}^2$$

This value is less than the yield strength ($1.170 \times 10^9 \text{ N/m}^2$) of Inconel® 718, resulting from the preceding table.

The ultimate hoop (circumferential) stress of the bellows results from

$$\sigma_{hu} = 2.881 \times 10^8 \times \frac{1.992 \times 10^7}{1.461 \times 10^7} = 3.928 \times 10^8 \text{ N/m}^2$$

This value is less than the ultimate strength ($1.375 \times 10^9 \text{ N/m}^2$) of Inconel® 718.

Summarising, the following results have been found in the preceding calculation: $d_i = 0.2032 \text{ m}$, $d_o = 0.2240 \text{ m}$, $d_m = 0.2136 \text{ m}$, $t = 0.00056 \text{ m}$, $N_p = 3$, $h = 0.0104 \text{ m}$, $N_c = 22$, $L = 0.00784 \text{ m}$, $L_a = 0.1702 \text{ m}$, and $R_a = 8.051 \times 10^5 \text{ N/m}$.

The angular spring constant of the bellows results from the following equation

$$R_b = \frac{d_m^2 R_a}{8} = \frac{0.2136^2 \times 8.051 \times 10^5}{8} = 4592 \text{ Nm/rad}$$

The magnitude of the bending moment on the duct, at an angle $\theta = \pi/60 \text{ rad}$, is

$$M = R_b \theta = 4592 \times \frac{3.1416}{60} = 240.4 \text{ Nm}$$

The pressure separating load acting on the bellows results from

$$F_p = \frac{p(d_m^2 - d_d^2)\pi}{4}$$

Therefore, the necessary restraining load acting on the link at the maximum pressure in transient conditions ($p = 1.207 \times 10^7 \text{ N/m}^2$), considering the axial force, is

$$F = F_p + \frac{pd_d^2\pi}{4} = \frac{pd_m^2\pi}{4} = \frac{1.207 \times 10^7 \times 0.2136^2 \times 3.1416}{4} = 4.325 \times 10^5 \text{ N}$$

Further information on the structural calculation of bellows can be found in [31, pages 92–94].

References

1. Daniels CM, Keller RB Jr (eds) (1977) Liquid rocket lines, bellows, flexible hoses, and filters, NASA SP-8123, April 1977, 189 p. Web site <https://ntrs.nasa.gov/archive/nasa/casi.ntrs.nasa.gov/19780008146.pdf>
2. Howell GW, Weathers TM (eds) (1970) Aerospace fluid component designers' handbook, volume I, Revision D, Report No. RPL-TDR-64-25, TRW Systems Group, One Space Park, Redondo Beach, California, USA, February 1970. Web site <https://apps.dtic.mil/dtic/tr/fulltext/u2/874542.pdf>
3. Huzel DK, Huang DH (1967) Design of liquid propellant rocket engines, 2nd edn. NASA SP-125, NASA, Washington, DC, 472 p. Web site <https://ntrs.nasa.gov/archive/nasa/casi.ntrs.nasa.gov/19710019929.pdf>
4. Anonymous, Space Shuttle main engine orientation, Boeing-Rocketdyne Propulsion & Power, Presentation BC98-04, June 1998, 105 p. Web site http://large.stanford.edu/courses/2011/ph240/nguyen1/docs/SSME_PRESENTATION.pdf
5. Kolowith R (1966) Saturn IB Program, Test report for flexible hose, 1/4 in, 3000-PSIG, Chrysler Corporation, Space Division, 20 December 1966. Web site <https://ntrs.nasa.gov/archive/nasa/casi.ntrs.nasa.gov/19670019497.pdf>
6. Burcham RE, Keller RB Jr (eds) (1978) Liquid rocket engine turbopump rotating-shaft seals, NASA SP-8121, February 1978, 168 p. Web site <https://ntrs.nasa.gov/archive/nasa/casi.ntrs.nasa.gov/19780022641.pdf>
7. Anonymous, Saturn V flight manual SA 503, Technical Manual MSFC-MAN-503, NASA TM X-72151, 243 pages, November 1968. Web site <https://ntrs.nasa.gov/archive/nasa/casi.ntrs.nasa.gov/19750063889.pdf>
8. NASA, Saturn V news reference, J-2 engine fact sheet, December 1968. Web site https://www.nasa.gov/centers/marshall/pdf/499245main_J2_Engine_fs.pdf
9. Sabin AJ, Bissell WR, Keller RB Jr (eds) (1974) Turbopump systems for liquid rocket engines, NASA SP-8107, August 1974, 168 p. Web site <https://ntrs.nasa.gov/archive/nasa/casi.ntrs.nasa.gov/19750012398.pdf>
10. Anonymous, Cryogenic materials data handbook, U.S. Department of Commerce, National Bureau of Standards, 1960, 58 p. Web site <https://apps.dtic.mil/dtic/tr/fulltext/u2/a286675.pdf>
11. Stuck DE, Keller RB Jr (eds) (1976) Liquid rocket disconnects, couplings, fittings, fixed joints, and seals, NASA SP-8119, 164 p. Web site <https://ntrs.nasa.gov/archive/nasa/casi.ntrs.nasa.gov/19770017247.pdf>
12. Kazakov NF (ed) (1985) Diffusion bonding of materials. Pergamon Press, Oxford. ISBN 0-08-032550-5
13. Anonymous (2009) Standard welding terms and definitions including terms for adhesive bonding, brazing, soldering, and thermal spraying, AWS A3.0 M/A3.0:2010, American Welding Society, 12th edn. ISBN: 978-0-87171-763-4
14. Anderson RV, Jaquay KR (1975) Flexible piping joints for large-scale breeder reactor primary loop applications, Phase I, Technical summary, report, 12 November 1975, United States of America. Web site <https://digital.library.unt.edu/ark:/67531/metadc1195050/>
15. French EA, George H (1976) Flexible hose guide for multiplane kinematics. In: Fluid handling equipment—a compilation, NASA SP-5976 (03):25. Web site <https://ntrs.nasa.gov/archive/nasa/casi.ntrs.nasa.gov/19760013403.pdf>
16. Buckingham JR, Winzen J (1974) Shuttle filter study—final report, vol I, NASA technical report CR-140386, June 1974, 158 p. Web site <https://ntrs.nasa.gov/archive/nasa/casi.ntrs.nasa.gov/19750005841.pdf>
17. Toth LR, Hagler R Jr (1975) Full-flow fluid filter, NASA Tech Brief, B74-10277, January 1975. Web site <https://ntrs.nasa.gov/archive/nasa/casi.ntrs.nasa.gov/19740000277.pdf>
18. Filters and filter elements, fluid pressure, hydraulic micronic type, Military specification MIL-F-5504B, 17 October 1958. Web site http://everyspec.com/MIL-SPECS/MIL-SPECS-MIL-F/MIL-F-5504B_20463/

19. Filter and filter elements, fluid pressure, hydraulic line, 15 micron absolute and 5 micron absolute, type II systems, Military specification MIL-F-8815D, 27 September 1976. Web site http://everyspec.com/MIL-SPECS/MIL-SPECS-MIL-F/MIL-F-8815D_38187/
20. Howell GW, Weathers TM (eds) (1970) Aerospace fluid component designers' handbook, volume II, Revision D, Report No. RPL-TDR-64-25, TRW Systems Group, One Space Park, Redondo Beach, California, USA, February 1970. Web site <https://ntrl.ntis.gov/NTRL/dashboard/searchResults/titleDetail/AD874543.xhtml>
21. Scott Laboratories, Bubble point test, Appalachian State University. Web site <https://wine.appstate.edu/sites/wine.appstate.edu/files/Bubble%20Point%20Test.pdf>
22. ISO 4003:1977, Permeable sintered metal materials—determination of bubble test pore size. Web site <https://www.iso.org/standard/9678.html>
23. SAE International, Bubble-point test method ARP901A. Web site <https://www.sae.org/standards/content/arp901a/>
24. Filtration Group, Glossary of filtration terms. Web site https://dm.energy/sites/default/files/Glossary%20of%20Filtration%20Terms_20190619.pdf
25. Kozeny J (1927) Über kapillare Leitung des Wassers im Boden, Sitzungsberichte der Akademie der Wissenschaften, Wien, 136(2a):271–306. Web site https://www.zobodat.at/pdf/SBAWW_136_2a_0271-0306.pdf
26. Anonymous, Freestudy, Free tutorials on engineering and science, Fluid mechanics, Tutorial No. 4, Flow through porous passages. Web site <http://www.freestudy.co.uk/fluid%20mechanics/t4203.pdf>
27. Special Metals Corporation, Inconel® alloy 718, Pub. No. SMC-045. Web site http://www.specialmetals.com/assets/smc/documents/inconel_alloy_718.pdf
28. Anonymous (1979) Modern flange design, Bulletin 502, Edition VII, Taylor Forge Engineered Systems, Inc., 47 p. Web site <https://www.steeltank.com/Portals/0/docs/Modern%20Flange%20Design%20-%20Taylor%20Forge%20Engineered%20Products.pdf>
29. Rathbun FO Jr (ed) (1964) Separable connector design handbook (tentative), General Electric Company, NASA CR-64944, December 1964, 269 p. Web site <https://ntrs.nasa.gov/archive/nasa/casi.ntrs.nasa.gov/19740079014.pdf>
30. Aeroquip Corporation, Aerospace Engineering Bulletin, AEB 197A, 1980. Web site <https://www.herbaircraft.com/pdf/117Cat/Clamps/AEB197A.pdf>
31. Anderson WF (1964) Analysis of stresses in bellows, Part 1, Design criteria and test results, Report NAA-SR-4527 (Pt. 1), United States of America, Atomic Energy Commission, Division of Technical Information, 15 October 1964. Web site <https://www.osti.gov/servlets/purl/4676097>